Cell Journal (Yakhteh)

Guide for Authors

Aims and Scope: The "Cell Journal (Yakhteh)" is a peer review and monthly English publication of Royan Institute of Iran. The aim of the journal is to disseminate information by publishing the most recent scientific research studies based on medical and developmental biology including cell therapy and regenerative medicine, stem cell biology reproductive medicine, medical genetics, immunology, oncology, clinical biochemistry, neuroscience, and tissue engineering. **Cell J**, has been certified by the Ministry of Culture and Islamic Guidance since 1999 and accredited as a scientific and research journal by HBI (Health and Biomedical Information) Journal Accreditation Commission since 2000 which is an open access journal. **This journal holds the membership of the Committee on Publication Ethics (COPE).**

1. Types of articles

The articles in the field of Cellular and Molecular can be considered for publications in **Cell J.** These articles are as below:

A. Original articles

Original articles are scientific reports of the original research studies. The article consists of English Abstract (structured), Introduction, Materials and Methods, Results, Discussion, Conclusion, Acknowledgements, Author's Contributions, and References **(Up to 40).**

B. Review articles

Review articles are the articles written by well experienced authors and those who have excellence in the related fields. The corresponding author of the review article must be one of the authors of at least three published articles appearing in the references. The review article consists of English Abstract (unstructured), Introduction, Conclusion, Author's Contributions, and References **(Up to 70).**

C. Systematic Reviews

Systematic reviews are a type of literature review that collect and critically analyzes multiple research studies or papers. The Systematic reviews consist of English Abstract (unstructured), Introduction, Materials and Methods, Results, Discussion, Conclusion, Acknowledgements, Author's Contributions, and References **(Up to 70).**

D. Short communications

Short communications are articles containing new findings. Submissions should be brief reports of ongoing researches. The short communication consists of English Abstract (unstructured), the body of the manuscript (should not hold heading or subheading), Acknowledgements, Author's Contributions, and References **(Up to 30).**

E. Case reports

Case reports are short discussions of a case or case series with unique features not previously described which make an important teaching point or scientific observation. They may describe novel techniques or use equipment, or new information on diseases of importance. It consists of English Abstracts (Unstructured), Introduction, Case Report, Discussion, Acknowledgements, Author's Contributions, and References **(Up to 30).**

F. Editorial

Editorials are articles should be written in relevant and new data of journals' filed by either the editor in chief or the editorial board.

G. Imaging in biology

Images in biology should focus on a single case with an interesting illustration such as a photograph, histological specimen or investigation. Color images are welcomed. The text should be brief and informative.

H. Letter to the editors

Letter to the editors are in response to previously published **Cell J** articles, and may also include interesting cases that do not meet the requirement of being truly exceptional, as well as other brief technical or clinical notes of general interest.

I. Debate

Debates are articles which show a discussion of the positive and negative view of the author concerning all aspect of the issue relevant to scientific research.

2. Submission process

It is recommended to see the guidelines for reporting different kinds of manuscripts. This guide explains how to prepare the

manuscript for submission. Before submitting, we suggest authors to familiarize themselves with **Cell J** format and content by reading the journal via the website (www.celljournal.com). The corresponding author ensures that all authors are included in the author list and agree with its order, and they must be aware of the manuscript submission.

A. Author contributions statements

It is essential for authors to include a statement of responsibility in the manuscript that specifies the contribution of every one of them. This participation must include conception and design of the manuscript, data acquisition or data analysis and interpretation, drafting of the manuscript and/or revising it for critically important intellectual content, revision and final approval of the manuscript and statistical analysis, obtaining funding, administrative, technical, or material support, or supervision. Authors who do not meet the above criteria should be acknowledged in the **Acknowledgments section.**

B. Cover letter and copyright

Each manuscript should be accompanied by a cover letter, signed by all authors specifying the following statement: "The manuscript has been seen and approved by all authors and is not under active consideration for publication. It has neither been accepted for publication nor published in another journal fully or partially (except in abstract form). **Also, no manuscript would be accepted in case it has been pre-printed or submitted to other websites.** I hereby assign the copyright of the enclosed manuscript to **Cell J.**" Corresponding author must confirm the proof of the manuscript before online publishing. Also, it is needed to suggest three peer reviewers in the field of their manuscript.

C. Manuscript preparation

Authors whose first language is not English encouraged to consult a native English speaker in order to confirm his manuscripts to American or British (not a mixture) English usage and grammar. It is necessary to mention that we will check the plagiarism of your manuscript by iThenticate Software. The manuscript should be prepared in accordance with the "International Committee of Medical Journal Editors (ICMJE)". Please send your manuscript in two formats word and PDF (including: title, name of all the authors with their degree, abstract, full text, references, tables and figures) and also send tables and figures separately in the site. The abstract and text pages should have consecutive line numbers in the left margin beginning with the title page and continuing through the last page of the written text. Each abbreviation must be defined in the abstract and text when they are mentioned for the first time. Avoid using abbreviation in the title. Please use the international and standard abbreviations and symbols

It should be added that an essential step toward the integration and linking of scientific information reported in published literature is using standardized nomenclature in all fields of science and medicine. Species names must be italicized (*e.g., Homo sapiens*) and also the full genus and species written out in full, both in the title of the manuscript and at the first mention of an organism in a paper.

It is necessary to mention that genes, mutations, genotypes, and alleles must be indicated in italics. Please use the recommended name by consulting the appropriate genetic nomenclature database, e.g., HUGO for human genes. In another words; if it is a human gene, you must write all the letters in capital and italic (*e.g., OCT4, c-MYC*). If not, only write the first letter in capital and italic (*e.g., Oct4, c-Myc*). **In addition, protein designations are the same as the gene symbol but are not italicized.**

Of note, Cell J will only consider publishing genetic association study papers that are novel and statistically robust. Authors are advised to adhere to the recommendations outlined in the STREGA statement (http://www.strega-statement.org). The following criteria must be met for all submissions:

1. Hardy-Weinberg Equilibrium (HWE) calculations must be carried out and reported along with the P-values if applicable [see Namipashaki et al. 2015 (Cell J, Vol 17, N 2, Pages: 187-192) for a discussion].

2. Linkage disequilibrium (LD) structure between SNPs (if multiple SNPs are reported) must be presented.

3. Appropriate multiple testing correction (if multiple independent SNPs are reported) must be included.

Submissions that fail to meet the above criteria will be rejected before being sent out for review.

Each of the following manuscript components should begin in the following sequence:

Authors' names and order of them must be carefully considered (full name(s), highest awarded academic degree(s), email(s), and institutional affiliation(s) of all the authors in English. Also, you must send mobile number and full postal address of the corresponding author).

Changes to Authorship such as addition, deletion or rearrangement of author names must be made only before the manuscript has been accepted in the case of approving by the journal editor. In this case, the corresponding author must explain the reason of changing and confirm them (which has been signed by all authors of the manuscript). If the manuscript has already been published in an online issue, an erratum is needed.

Title is providing the full title of the research (do not use abbreviations in title).

Running title is providing a maximum of 7 words (no more than 50 characters).

Abstract must include Objective, Materials and Methods, Results, and Conclusion (no more than 300 words).

Keywords, three to five, must be supplied by the authors at the foot of the abstract chosen from the Medical Subject Heading (MeSH). Therefore; they must be specific and relevant to the paper.

The following components should be identified after the abstract:

Introduction: The Introduction should provide a brief background to the subject of the paper, explain the importance of the study, and state a precise study question or purpose.

Materials and Methods: It includes the exact methods or observations of experiments. If an apparatus is used, its manufacturer's

name and address should be stipulated in parenthesis. If the method is established, give reference but if the method is new, give enough information so that another author can perform it. If a drug is used, its generic name, dose, and route of administration must be given. Standard units of measurements and chemical symbols of elements do not need to be defined.

Statistical analysis: Type of study and statistical methods should be mentioned and specified by any general computer program used.

Ethical considerations*:* Please state that informed consent was obtained from all human adult participants and from the parents or legal guardians of minors and include the name of the appropriate institutional review board that approved the project. It is necessary to indicate in the text that the maintenance and care of experimental animals complies with National Institutes of Health guidelines for the humane use of laboratory animals, or those of your Institute or agency.

Clinical trial registration: All of the Clinical Trials performing in Iran must be registered in Iranian Registry of Clinical Trials (www.irct.ir). The clinical trials performed abroad, could be considered for publication if they register in a registration site approved by WHO or www.clinicaltrials.gov. If you are reporting phase II or phase III randomized controlled trials, you must refer to the CONSORT Statement for recommendations to facilitate the complete and transparent reporting of trial findings. Reports that do not conform to the CONSORT guidelines may need to be revised before peer-reviewing.

Results: They must be presented in the form of text, tables, and figures. Take care that the text does not repeat data that are presented in tables and/or figures. Only emphasize and summarize the essential features of the main results. Tables and figures must be numbered consecutively as appeared in the text and should be organized in separate pages at the end of the manuscript while their location should be mentioned in the main text.

Tables and figures: If the result of your manuscript is too short, it is better to use the text instead of tables & figures. Tables should have a short descriptive heading above them and also any footnotes. Figure's caption should contain a brief title for the whole figure and continue with a short explanation of each part and also the symbols used (no more than 100 words). All figures must be prepared based on cell journal's guideline in color (no more than 6 Figures and Tables) and also in TIF format with 300 DPI resolution.

Of Note: Please put the tables & figures of the result in the results section not any other section of the manuscript.

Supplementary materials would be published on the online version of the journal. This material is important to the understanding and interpretation of the report and should not repeat material within the print article. The amount of supplementary material should be limited. Supplementary material should be original and not previously published and will undergo editorial and peer review with the main manuscript. Also, they must be cited in the manuscript text in parentheses, in a similar way as when citing a figure or a table. Provide a caption for each supplementary material submitted.

Discussion: It should emphasize the present findings and the variations or similarities with other researches done by other researchers. The detailed results should not be repeated in the discussion again. It must emphasize the new and important aspects of the study.

Conclusion: It emphasizes the new and important aspects of the study. All conclusions are justified by the results of the study.

Acknowledgements: This part includes a statement thanking those who contributed substantially with work relevant to the study but does not have authorship criteria. It includes those who provided technical help, writing assistance and name of departments that provided only general support. You must mention financial support in the study. Otherwise; write this sentence "There is no financial support in this study".

Conflict of interest: Any conflict of interest (financial or otherwise) and sources of financial support must be listed in the Acknowledgements. It includes providers of supplies and services from a commercial organization. Any commercial affiliation must be disclosed, regardless of providing the funding or not.

Of Note: If you have already any patent related to the subject of your manuscript, or you are going to apply for such a patent, it must be mentioned in this part.

References: The references must be written based on the Vancouver style. Thus the references are cited numerically in the text and listed in the bibliography by the order of their appearance. The titles of journals must be abbreviated according to the style used in the list of Journals Indexed in PubMed. Write surname and initials of all authors when there are six or less. In the case of seven or more authors, the names of the first six authors followed by "et al." must be listed. You can download Endnote file for Journal references style: endnote file

The reference of information must be based on the following order:

Article:

Surname(s) and first letter of name &middle name(s) of author(s) .Manuscript title. Journal title (abbr).publication date (year); Volume & Issue: Page number.

Example: Manicardi GC, Bianchi PG, Pantano S, Azzoni P, Bizzaro D, Bianchi U, et al. Presence of endogenous nicks in DNA of ejaculated human spermatozoa and its relationship to chromomycin A3 accessibility. Biol Reprod. 1995; 52(4): 864-867.

Book:

Surname(s) and first letter of name & middle name(s) of author(s).Book title. Edition. Publication place: publisher name; publication date (year); Page number.

Example: Edelman CL, Mandle CL. Health promotion throughout the lifespan. 2nd ed. ST Louis: Mosby; 1998; 145-163.

Chapter of book:

Surname(s) and first letter of name & middle name(s) of author(s).Chapter title. In: Surname(s) and first letter of name & middle name(s) of editor(s), editors. Book title. Edition. Publication place: publisher name; publication date (year); Page number.

Example: Phillips SJ, Whisnant JP. Hypertension and stroke. In: Laragh JH, Brenner BM, editors. Hypertension: pathophysiology, diagnosis, and management. 2nd ed. New York: Raven Press; 1995; 465-478.

Abstract book:

Example: Amini rad O.The antioxidant effect of pomegranate juice on sperm parameters and fertility potential in mice. Cell J. 2008;10 Suppl 1:38.

Thesis:

Name of author. Thesis title. Degree. City name. University. Publication date (year).

Example: Eftekhari Yazdi P. Comparison of fragment removal and co-culture with Vero cell monolayers on development of human fragmented embryos. Presented for the Ph.D., Tehran. Tarbiyat Modarres University. 2004.

Internet references

Article:

Example: Jahanshahi A, Mirnajafi-Zadeh J, Javan M, Mohammad-Zadeh M, Rohani M. Effect of low-frequency stimulation on adenosineA1 and A2A receptors gene expression in dentate gyrus of perforant path kindled rats. Cell J. 2008; 10 (2): 87-92. Available from: http://www.celljournal.org. (20 Oct 2008).

Book:

Example: Anderson SC, Poulsen KB. Anderson's electronic atlas of hematology.[CD-ROM]. Philadelphia: Lippincott Williams & Wilkins; 2002.

D. Proofs are sent by email as PDF files and should be checked and returned within 72 hours of receipt. It is the authors' responsibility to check that all the text and data as contained in the page proofs are correct and suitable for publication. **We are requested to pay particular attention to author's names and affiliations as it is essential that these details be accurate when the article is published.**

E. Pay for publication: Publishing an article in **Cell J** requires Article Processing Charges (APC) that will be billed to the submitting author following the acceptance of an article for publication. For more information please see www.celljournal.org.

F. Ethics of scientific publication: Manuscripts that have been published elsewhere with the same intellectual material will refer to duplicate publication. If authors have used their own previously published work or work that is currently under review, as the basis for a submitted manuscript, they are required to cite the previous work and indicate how their submitted manuscript offers novel contributions beyond those of the previous work. Research and publication misconduct is considered a serious breach of ethics.

The Journal systematically employs iThenticate, plagiarism detection and prevention software designed to ensure the originality of written work before publication. Plagiarism of text from a previously published manuscript by the same or another author is a serious publication offence. Some parts of text may be used, only where the source of the quoted material is clearly acknowledged.

3. General information

A. You can send your manuscript via online submission system which is available on our website. If the manuscript is not prepared according to the format of **Cell J**, it will be returned to authors.

B. The order of article appearance in the Journal is not demonstrating the scientific characters of the authors.

C. Cell J has authority to accept or reject the manuscript.

D. The received manuscript will be evaluated by associate editor. **Cell J** uses a single-blind peer review system and if the manuscript suits the journal criteria, we select the reviewers. If three reviewers pass their judgments on the manuscript, it will be presented to the editorial board of **Cell J.** If the editorial board has a positive judgment about the manuscript, reviewers' comments will be presented to the corresponding author (the identification of the reviewers will not be revealed). The executive member of journal will contact the corresponding author directly within 3-4 weeks by email. If authors do not receive any reply from journal office after the specified time, they can contact journal office. Finally, executive manager will respond promptly to authors' request.

The Final Checklist

The authors must ensure that before submitting the manuscript for publication, they have to consider the following parts:

1. The first page of manuscript should contain title, name of the author/coauthors, their academic qualifications, designation & institutions they are affiliated with, mailing address for future correspondence, email address, phone, and fax number.

2. Text of manuscript and References prepared as stated in the "guide for authors" section.

3. Tables should be on a separate page. Figures must be sent in color and also in JPEG (Jpg) format.

4. Cover Letter should be uploaded with the signature of all authors.

5. An ethical committee letter should be inserted at the end of the cover letter.

The Editor-in-Chief: Ahmad Hosseini, Ph.D.

Cell Journal *(Yakhteh)*

P.O. Box: 16635-148, Iran

Tel/Fax: + 98-21-22510895

Emails: info@celljournal.org

journals@celljournal.org

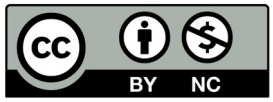

Dr. Saeed Kazemi Ashtiani

IN THE NAME OF GOD

Gone But not Forgotten

In the memory of the late Director of Royan Institute, Founder of Stem Cells Research in Iran and Chairman of ***Cell Journal*** *(Yakhteh)*. May he rest in peace.

PUBLISHED & SPONSORED BY:
Publication of Royan Institute (ACECR)

Indexed in:
1. Thomson Reuters (ISI)
2. PubMed
3. PubMed Central (PMC)
4. National Library Medicine (NLM)
5. Biosis Preview
6. Index Medicus for the Eastern Mediterranean Region (IMEMR)
7. Regional Information Center for Sciences and Technology (RICeST)
8. Index Copernicus International
9. Cambridge Scientific Abstract (CSA)
10. EMBASE
11. Scopus
12. Cinahl Database
13. Google Scholar
14. Chemical Abstract Service (CAS)
15. Proquest
16. Directory of Open Access Journals (DOAJ)
17. Open Academic Journals Index (OAJI)
18. Directory of Research Journals Indexing (DRJI)
19. Scientific Information Database (SID)
20. Iranmedex
21. Islamic World Science Citation Center (ISC)
22. Magiran
23. Science Library Index
24. Biological Abstracts
25. Essential Science Indicators
26. EuroPub

Editorial Office Address (Dr. Ahmad Hosseini):
Royan Institute, P.O.Box: 16635-148,
Tehran, Iran
Tel & Fax: (+9821)22510895
Website: www.celljournal.org
Emails: info@celljournal.org
journals@celljournal.org

Printing Company:
Naghshe e Johar Co.
No. 103, Fajr alley, Tehranpars Street,
Tehran, Iran.

Cell Journal(Yakhteh), Vol 24, No 12, December 2022, Serial Number: 107, Pages: 705-781

CONTENTS

Original Articles

Short Communication

Correction

Original Article

Differentiation of Human Adipose-Derived Mesenchymal Stromal/Stem Cells into Insulin-Producing Cells with A Single Tet-Off Lentiviral Vector System

Hiroyuki Moriyama, Ph.D.[1#*], Mariko Moriyama, Ph.D.[1#], Toshiyuki Ozawa, Ph.D.[2], Daisuke Tsuruta, Ph.D.[2], Takao Hayakawa, Ph.D.[1]

1. Pharmaceutical Research and Technology Institute, Kindai University, 3-4-1 Kowakae, Higashi-Osaka, Osaka 577-8502, Japan
2. Department of Dermatology, Graduate School of Medicine, Osaka Metropolita University, 1-4-3 Asahimachi, Abeno-Ku, Osaka 545-8585, Japan

#These authors equally contributed to this work.

*Corresponding Address: Pharmaceutical Research and Technology Institute, Kindai University, 3-4-1 Kowakae, Higashi-Osaka, Osaka 577-8502, Japan
Email: moriyama@phar.kindai.ac.jp

Received: 10/July/2022, Accepted: 16/August/2022

Abstract

Objective: Human adipose-derived mesenchymal stromal/stem cells (hASC) constitute an attractive source of stem cells for cell-based therapies in regenerative medicine and tissue engineering as they are easy to acquire from lipoaspirate, expansion, and genetic modification *ex vivo*. The combination of Pdx-1, MafA, and NeuroD1 has been indicated to possess the ability to reprogram various types of cells into insulin-producing cells. The aim of this study is to investigate whether MafA and NeuroD1 would cooperate with Pdx-1 in the differentiation of hASC into insulin-producing cells.

Materials and Methods: In this experimental study, we generated polycistronic expression vectors expressing Pdx1 and MafA/NeuroD1 with a reporter from a human EF-1α promoter using 2A peptides in a single tet-off lentiviral vector system. Briefly, hASC were transduced with the lentiviral vectors and allowed to differentiate into insulin-producing cells *in vitro* and *in vivo.* Thereafter, RNA expression, dithizone staining, and immunofluorescent analysis were conducted.

Results: Cleaved transcriptional factors from a single tet-off lentiviral vector were functionally equivalent to their native proteins and strictly regulated by doxycycline (Dox). Insulin gene expression in hASC transduced with Pdx1, Pdx1/MafA, and Pdx1/NeuroD1 in differentiation medium were successfully increased by 1.89 ± 0.39, 4.81 ± 0.98, 5.51 ± 0.63, respectively, compared to venus-transduced, control hASC. These cells could form dithizone-positive cell clusters *in vitro* and were found to express insulin *in vivo*.

Conclusion: Using our single tet-off lentiviral vector system, Pdx-1 and MafA/NeuroD1 could be simultaneously expressed in the absence of Dox. Further, this system allowed the differentiation of hASC into insulin-producing cells.

Keywords: Adipose-Derived Mesenchymal Stromal/Stem Cells, Doxycycline, Insulin-Producing Cells, Gene Expression Regulation, Genetic Vectors

Cell Journal(Yakhteh), Vol 24, No 12, December 2022, Pages: 705-714

Citation: Moriyama H, Moriyama M, Ozawa T, Tsuruta D, Hayakawa T. Differentiation of human adipose-derived mesenchymal stromal/stem cells into insulin-producing cells with a single tet-off lentiviral vector system. Cell J. 2022; 24(12): 705-714. doi: 10.22074/CELLJ.2022.557533.1063.

Introduction

Type 1 diabetes mellitus is characterized by the destruction of insulin-producing beta cells through autoimmune responses. Although insulin therapy has been used to treat diabetes, insulin administration via injection causes suffering and is inconvenient for patients with diabetes. Islet transplantation has been used to replace insulin therapy in patients with type 1 diabetes; however, donor shortage restricts the broad use of this therapy. Recent developments in stem cell biology have offered the exciting potential for generating islet β-cells from various cell types, including embryonic stem cells (ESCs) or induced pluripotent stem cells (iPSCs). However, ESCs and iPSCs may result in teratoma formation after transplantation. ESCs are also limited by ethical issues regarding the use of human embryos, as their retrieval requires the destruction of the embryo.

Mesenchymal stem/stromal cells (MSCs) can differentiate into various types of cells, including adipocytes, chondrocytes, osteoblasts (1), and possibly, though controversially, other non-mesodermal cells, such as keratinocytes (2), and neuronal cells (3). In addition, owing to their hypoimmunogenicity and immunomodulatory effects, MSCs are expected to be stem cell products for therapeutic purposes. Unlike other MSCs, human adipose-derived mesenchymal stromal/stem cells (hASC) can be easily and safely obtained in large quantities from a lipoaspirate from any person at any time and can be grown *ex vivo* under appropriate culture conditions. Furthermore, Strem et al. (4) reported that adipose tissue yields approximately 5 to 50 times more stem cells than bone marrow. In addition, compared to other types of stem cells, including hematopoietic stem cells, hASC can be readily transduced with all major clinically prevalent viral vector systems, including adenovirus (5),

murine retroviruses (6), lentiviruses (7), and adeno-associated viral vectors (8). Thus, hASC constitutes an attractive source of stem cells for autologous cell-based therapies in regenerative medicine and tissue engineering. Direct reprogramming of ASCs into pancreatic lineage cells has recently been reported (9-11). In addition, MSCs have been reported to express a variety of pancreas or islet progenitor genes by forced expression of pancreatic duodenal homeobox 1 (Pdx-1) (12, 13), a key transcription factor required for pancreatic development and insulin gene transcription (14). However, sequential expression of specific transcription factors, including Pdx-1, is also required for pancreatic endocrine differentiation. NeuroD1 is a class B basic helix-loop-helix transcription factor critical for pancreatic endocrine cell differentiation (15). In addition, MafA is a member of the basic leucine zipper family that is clearly expressed in the final stage of β cell differentiation and regulates insulin gene expression by binding to the insulin promoter in the C1box (16). Therefore, ectopic expression of Pdx-1, MafA, and/or NeuroD1 has been utilized to induce insulin production in mouse ESCs (17), mouse bone marrow MSCs (18), and mouse exocrine pancreatic cells *in vivo* (19). Although this approach is beneficial, there are two significant limitations to this approach. One is the inadequate efficiency of gene delivery when several genes are simultaneously transferred to the target cells and the other is the transfer of genes that stimulate differentiation to undifferentiated cells, which generally results in the inhibition of active cell proliferation, ultimately hindering the expansion of the cells required for transplantation. Solving these issues is thus inevitable for establishing the use of insulin-producing cells differentiated from autologous mesenchymal stem cells for cell regeneration therapy in the clinical.

To resolve these problems, we previously established a single tet-off lentiviral vector system, which allows for the tightly regulated and homogenous expression of genes of interest. This vector combines a modified tetracycline (tet)-response element composite promoter and a multi-cistronic strategy to express an improved version of the tet-controlled transactivator and the blasticidin resistance gene under the control of the elongation factor 1 a (EF-1a) promoter (7). In the present study, we generated polycistronic expression vectors that would express multiple transcription factors with a reporter from a single promoter using "self-cleaving" 2A peptides in our single tet-off lentiviral vector system. Using this revolutionary system, multiple transgene expression is strictly repressed in the presence of doxycycline (Dox) in undifferentiated cells during *in vitro* expansion, thereby overcoming the aforementioned limitation.

Here, we aimed to investigate whether MafA and NeuroD1 would cooperate with Pdx-1 in the differentiation of hASC into insulin-producing cells.

Materials and Methods

Animals

In this experimental study, a total of 60 male immunodeficient (C.B-17/IcrHsd-Prkdc^{scid}) mice (weight, 24-26 g; age, eight weeks) were purchased from Japan SLC, Inc. (Kyoto, Japan). All mice were housed in standard plastic cages and provided food and water ad libitum at Kindai University at 24˚C with a 12 hours light/dark cycle. The experimental procedures for the mice were approved by the Kindai University Animal Care and Use Committee (approval no. KAPR-2021-001), and the study was performed in compliance with the ARRIVE guidelines (20). Mice were anesthetized by inhalation of isoflurane (3% induction and 1% maintenance) using the SomnoSuite Small Animal Anesthesia System (Kent Scientific Corporation, Torrington, CT, USA). Before the experiment, the animals were acclimated to the facility for one week. After the completion of the experiment, the animals were euthanized using carbon dioxide at a flow rate of 30% of the chamber volume per minute in their home cages. Death was verified by the cessation of respiratory and cardiovascular movements by observation at room air for at least 10 minutes.

Adipose tissue samples

Subcutaneous adipose tissue samples (10-50 g each) were collected from a discarded tissue resected during plastic surgery for skin graft in ten subjects (four men and six women, 53 ± 5 years of age (mean ± SEM); range 30-76 years, non-obese, non-diabetic individuals). The study protocol was ethically coded and approved by the Review Board for Human Research of Osaka City University Graduate School of Medicine and the Kindai University Pharmaceutical Research and Technology Institute (reference number: 15-074). All participants provided written informed consent.

Cell culture

The hASC were isolated as previously reported (7, 21) and maintained in Dulbecco's modified Eagle's medium (DMEM) (Nacalai tesque, Kyoto, Japan) containing 10% fetal bovine serum (FBS, Nichirei Bioscience, Osaka, Japan), 1× GlutaMAX (Thermo Fisher Scientific, Waltham, MA, USA), and 10 ng/mL epidermal growth factor (PeproTech, Rocky Hill, NJ, USA). The cells were plated at a density of 4×10^3 cells/cm^2 on cell culture dishes, and the medium was replaced every two days.

Plasmid construction

The gene encoding Venus was a kind gift from Dr. Atsushi Miyawaki at the Brain Science Institute, RIKEN, Japan; this gene was subcloned into a pENTR11 vector (Thermo Fisher Scientific, USA), to create an entry vector, pENTR11-Venus. The pENTR11-PDX1-2A-Venus

was created according to the following outline: PDX1-T2A and Venus were amplified using polymerase chain reaction (PCR) using PDX1-2A F and R, or Venus F and R primers (Table 1), respectively. PDX1-T2A and Venus were digested with EcoRI and ApaI, or ApaI and XbaI, respectively, and sub-cloned into the EcoRI and XbaI sites of the pENTR11 vector. To create pENTR11-PDX1-E2A-MAFA-T2A-Venus (hereafter PM-2A-Venus) and pENTR11-PDX1-P2A-NEUROD1-T2A-Venus (hereafter PN-2A-Venus), E2A-MAFA was amplified using PCR using 2A-MAFA F and R, or 2A-NEUROD1 F and R primers (Table S1, See Supplementary Online Information at www.celljournal.org), respectively. Thereafter, the E2A-MAFA or P2A-NEUROD1 fragment was digested with BamHI and subcloned into the BamHI site of the pENTR11-PDX1-2A-Venus vector. The entry vectors pENTR11-Venus, pENTR11-PDX1-2A-Venus, pENTR11-PM-2A-Venus, or pENTR11-PN-2A-Venus, and pTRE-RfA-EF-tTA-2A-Bsd (third-generation, self-inactivating lentiviral vector) (7) were incubated with LR clonase II enzyme mix (Thermo Fisher Scientific, USA) to generate pTRE-Venus-EF-tTA-2A-Bsd, pTRE-PDX1-2A-Venus-EF-tTA-2A-Bsd, pTRE-PM-2A-Venus-EF-tTA-2A-Bsd, or pTRE-PN-2A-Venus-EF-tTA-2A-Bsd, respectively. INS-Luc, a plasmid containing the luciferase (Luc) gene controlled by the human insulin gene promoter, was generated by subcloning the insulin promoter fragment (-342 to +6) into the pGV-B2 vector (TOYO B-net, Osaka, Japan).

Lentivirus production

Lentiviral vector particles were packaged as previously reported (7). Briefly, a 100 mm dish of non-confluent 2.5×10^6 HEK 293T cells (RIKEN BioResource Center, Tsukuba, Japan) was transfected with 10.2 µg of pCAG-HIVgp (kindly provided by Dr. Miyoshi, RIKEN BioResource Center), 10.2 µg of pCMV-VSVG-RSV-Rev (kindly provided by Dr. Miyoshi), and 18 µg of lentiviral vector plasmid (pTRE) mixed with 50 µL of 2.5M $CaCl_2$, and then mixed with 500 µL of 2×HBS (50 mM HEPES, 280 mM NaCl, 1.5 mM Na_2HPO_4, pH=7.05) and incubated at room temperature for 15 minutes. The calcium phosphate-DNA solution was then added to partially confluent HEK 293T cells for 12 hours at 37˚C in 5% CO_2. The supernatant medium, which contained lentiviral vectors, was collected two days after transduction and concentrated by centrifugation (6000 × g, 15 hours, 4˚C). Viral titers were determined using the Lenti-X qRT-PCR Titration Kit (Clontech, Mountain View, CA, USA). To obtain hASC with the tetracyclin-controlled expression of Venus, PDX1/Venus, PM-2A-Venus, or PN-2A-Venus, 1×10^5 cells of hASC at passage 3 were seeded into a 6-well plate in growth media. The next day, the lentiviral vector at a multiplicity of infection (MOI) of 250 (7) was added to each well. Then, the spinfection protocol (800 × g, 1 hour, 30˚C) was applied for efficient lentiviral vector transduction. After 24 hours, the medium was changed and cultured with 4 µg/mL blasticidin and 1 µg/mL Dox at 37˚C in 5% CO_2 for 14 days.

Western blot analysis

Whole-cell extracts were prepared by washing the cells with ice-cold phosphate-buffered saline (PBS) and lysing them with M-PER Mammalian Protein Extraction Reagent (Thermo Scientific Pierce, Rockford, IL, USA) according to the manufacturer's instructions. Equal amounts of proteins were separated using sodium dodecyl sulfate-polyacrylamide gel electrophoresis (SDS-PAGE), transferred to polyvinylidene fluoride (PVDF) membranes (Immobilon-P; Merck Millipore, Billerica, MA, USA), and probed with antibodies against GFP (1:1000, cat. no. A11122; Thermo Fisher Scientific, USA), and PDX1 (1:1000, cat. no. 2437, Cell Signaling Technology, Danvers, MA, USA), MAFA (1:2000, cat. no. A300-611A, BETHYL Laboratories, Montgomery, TX, USA) and NEUROD1 (1:2000, cat. no. ab109188, Abcam, Cambridge, UK), and actin (1:10000; cat. no. MAB1501, Merck Millipore). Horseradish peroxidase (HRP)-conjugated anti-mouse or anti-rabbit IgG antibodies (1:5000, cat. no. 7074, Cell Signaling Technology) were used as secondary antibodies, and immunoreactive bands were visualized using an Immobilon Western Chemiluminescent HRP substrate (Merck Millipore). The band intensities were measured using the ImageJ software.

Luciferase assay

hASC transduced with INS-Luc and pGL4.74 (Promega, Madison, WI, USA) were further transfected with pTRE-Venus-EF-tTA-2A-Bsd, pTRE-PDX1-2A-Venus-EF-tTA-2A-Bsd, pTRE-PM-2A-Venus-EF-tTA-2A-Bsd, or pTRE-PN-2A-Venus-EF-tTA-2A-Bsd. Three days after transfection, according to the manufacturer's protocol, Firefly and Renilla luciferase activities were determined using a Dual-Luciferase Reporter Assay System (Promega).

Induction of hASC differentiation into insulin-producing cells

Induction of hASC differentiation into insulin-producing cells was performed as previously described, with some modifications (22, 23). Before differentiation, hASC were cultured in a normal growth medium with 1 µg/mL Dox for five days. The cells were also cultured in serum-free low-glucose DMEM containing 1% dimethyl sulfoxide (DMSO) for three days and incubated with DMEM: F12(1:1) containing 1% B27 supplement (Thermo Fisher Scientific, USA), 0.5% N2 supplement (Thermo Fisher Scientific, USA), 10 mM nicotinamide (Calbiochem, San Diego, CA, USA), 10 nM exendin-4 (Sigma-Aldrich, St. Louis, MO, USA), and 10 nM Activin A (Peprotech) for 15 days. Finally, the cells were incubated with high-glucose DMEM containing 1% DMSO and 10% FBS for nine days. The medium was replaced every three days.

RNA extraction, complementary DNA generation, and quantitative polymerase chain reaction

Total RNA extraction, complementary DNA (cDNA) synthesis, and quantitative polymerase chain reaction (qPCR) analysis were performed as previously described (21) and were performed according to the Minimum

Information for Publication of Quantitative Real-Time PCR Experiments (MIQE) guidelines (24). Briefly, reactions were performed using a CFX96 real-time PCR system (Bio-Rad, Hercules, CA, USA). The relative expression of each gene was calculated using the ΔΔCt method, and the most reliable reference gene was identified from the eight genes (*ACTB, B2M, GAPDH, GUS, H6PD, UBC, UBE2D2*, and *UBE4A*) using the genormPLUS module in qbasePLUS software (Biogazelle, Zwijnaarde, Belgium). Details of the primers used in these experiments are listed in Table S2 (See Supplementary Online Information at www.celljournal.org).

Dithizone staining

Dithizone was purchased from Sigma-Aldrich. Staining was performed in a culture medium containing 0.01% dithizone at 37˚C for 15 minutes. After three rounds of rinsing with HBSS, the cells were examined under an inverted microscope.

Transplantation of hASC cells

Hyperglycemia was induced in adult male C.B-17/IcrHsd-Prkdc^{scid} mice via an intraperitoneal injection of 50 mg/kg of streptozotocin (STZ, Sigma-Aldrich) for five consecutive days. Blood glucose levels were determined using a blood glucose meter (Freestyle Freedom Lite; NIPRO, Osaka, Japan). Mice with blood glucose levels >300 mg/dl were determined as diabetic . Mice were randomly assigned to four study groups: Venus-hASC, PDX1-2A-Venus-hASC, PM-2A-Venus-hASC, and PN-2A-Venus-hASC transplanted (n=15). Under general anesthesia, mice received a renal subcapsular transplant of 2.0×10^5 cells in the right subcapsular renal space. Blood glucose levels were monitored every two days after transplantation for five weeks. All experimental procedures were approved by the Kindai University Animal Care and Use Committee and were carried out according to institutional animal experimentation regulations.

Histology

Kidneys were fixed in 4% paraformaldehyde, embedded in an optimal cutting temperature compound, frozen, and cut into 10-µm-thick sections. The sections were then subjected to immunohistochemical analysis, as previously described (25). The sections were stained with guinea pig polyclonal antibody against insulin (1:100; cat. no. ab7842, Abcam). After the sections were washed with Tris-buffered saline, they were incubated at 4˚C for 3 hours with a Cy3 conjugated-donkey polyclonal antibody against guinea pig IgG (1:1000, cat. no. 706-165-148; Jackson ImmunoResearch). Images were obtained using a fluorescence microscope (BZ-9000; Keyence, Osaka, Japan) and analyzed with the BZ Analyzer software (Keyence).

Statistical analysis

The values are expressed as mean ± SE. Statistical differences were determined using one-way analysis of variance (ANOVA) followed by Tukey's test using GraphPad Prism software (GraphPad Software, Version 9, La Jolla, CA, USA). Differences were considered statistically significant at $P<0.05$. Data are presented as the mean ± SEM from three or four independent experiments.

Results

Generation and validation of the single tet-off lentiviral vectors carrying PDX1, MAFA, and NeuroD1

To increase the efficiency of hASC differentiation into insulin-producing cells, we first generated single tet-off lentiviral vectors carrying PDX1 (pTRE-PDX1-2A-Venus-EF-tTA-2A-Bsd), PDX1, and MAFA (pTRE-PM-2A-Venus-EF-tTA-2A-Bsd), and PDX1 and NeuroD1 (pTRE-PN-2A-Venus-EF-tTA-2A-Bsd) (Fig.1). EF-1α promoters drive the mRNA expression of advanced tTA linked to the *Bsd* gene by the Thosea asigna virus 2A (T2A) peptide sequence. This single transcript was then translated and cleaved into two proteins: tTA, which carries the 2A tag at the C-terminus (tTA-2A), and Bsd. In the absence of Dox, tTA-2A binds to TRE-tight and activates the transcription of the gene of interest to a very high level. However, tTA-2A cannot bind to TRE-Tight in a tet-responsive promoter in the presence of Dox. As a result, the system is inactive (7).

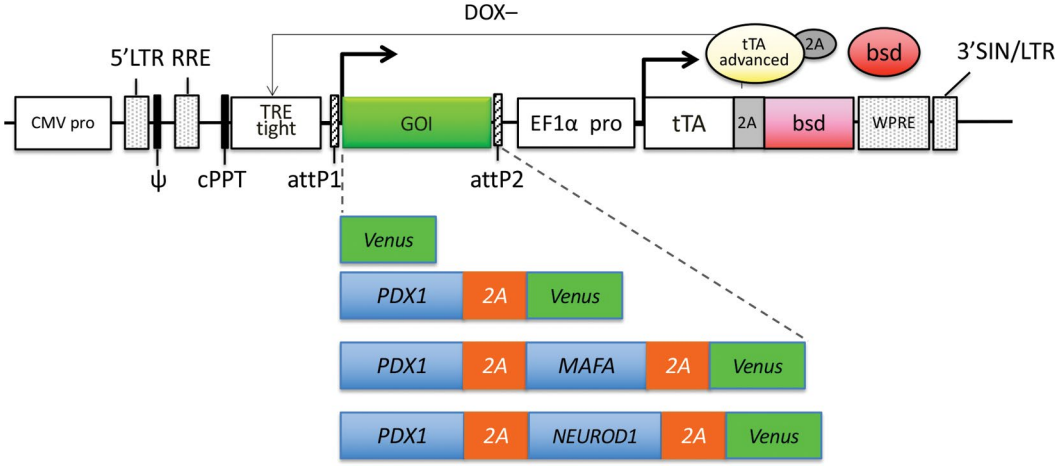

Fig.1: Schematic drawings of the single lentiviral vectors for the tet-off system used in this work.

The lentiviral vector, pTRE-EF-tTA-2A-Bsd, has an improved version of the tetracycline-controlled transactivator (tTA) linked to the blasticidin resistance (*Bsd*) gene by the Thosea asigna virus 2A (2A) peptide sequence, whose expression is regulated by the EF-1α promoter. In the absence of doxycycline (Dox), tTA-2A binds to the TRE-Tight promoter and activates the transcription of genes of interest (Venus, PDX1-2A-Venus, PDX1-2A-MAF1-2A-Venus, or PDX1-2A-NEUROD1-2A-Venus). CMV pro, CMV promoter; LTR, long terminal repeats; ψ, packaging signal; RRE, rev response elements; cPPT, central polypurine tract; TRE, tet-responsive element; GOI, gene of interest; tTA, tetracycline-controlled transactivator; Bsd, blasticidin resistance; WPRE, woodchuck hepatitis virus post-transcriptional control element; SIN, self-inactivating.

Various vectors were individually and transiently transduced into hASC to investigate the usefulness of these lentiviral vectors. As shown in Figure 2, we detected the cleaved immunoblot bands of Venus (~27 kDa), PDX1 (~46 kDa), MAFA (~40 kDa), and NeuroD1 (~50 kDa) at appropriate molecular sizes. Thereafter, we evaluated the functions of these cleaved transcription factors on the human insulin promoter. PDX1 (pCMV-PDX1-IresGFP) caused a ~2.3-fold higher enhancement of insulin promoter activity than the control (pTRE-Venus-EF-tTA-2A-Bsd) (Fig.2B). Moreover, the addition of MAFA (pCMV-MAFA-IresGFP) or NeuroD1 (pCMV-NeuroD1-IresGFP) to PDX1 (pCMV-PDX1-IresGFP) significantly upregulated the insulin promoter (i.e., ~8.5-fold) relative to the control, as previously reported (26) (Fig.2C, D). Intriguingly, transduction of pTRE-PDX1-2A-Venus-EF-tTA-2A-Bsd, pTRE-PM-2A-Venus-EF-tTA-2A-Bsd, or pTRE-PN-2A-Venus-EF-tTA-2A-Bsd resulted in the activation of the insulin gene promoter at the same levels as pCMV-PDX1-IresGFP, pCMV-PDX1-IresGFP, pCMV-MAFA-IresGFP, or pCMV-PDX1-IresGFP and pCMV-NeuroD1-IresGFP (Fig.2B-D), respectively. Such findings demonstrate that the activity of these cleaved transcriptional factors (carrying the 2A tag at the C-terminus) is functionally equivalent to that of their native protein.

Generation of hASC that express PDX1, MAFA, and NeuroD1 in a Dox-dependent manner

The single tet-off lentiviral vectors (pTRE-Venus-EF-tTA-2A-Bsd, pTRE-PDX1-2A-Venus-EF-tTA-2A-Bsd, pTRE-PM-2A-Venus-EF-tTA-2A-Bsd, and pTRE-PN-2A-Venus-EF-tTA-2A-Bsd) were transduced into hASC to generate PDX1-2A-Venus-hASC, PM-2A-Venus-hASC, and PN-2A-Venus-hASC. As shown in Figure 3, the expression of Venus, PDX1, MAFA, and NeuroD1 in the absence of Dox could be confirmed through western blot analysis. As these expression levels were strictly suppressed in the presence of Dox, we confirmed that gene expression was strictly regulated by these vector constructs (Fig.3).

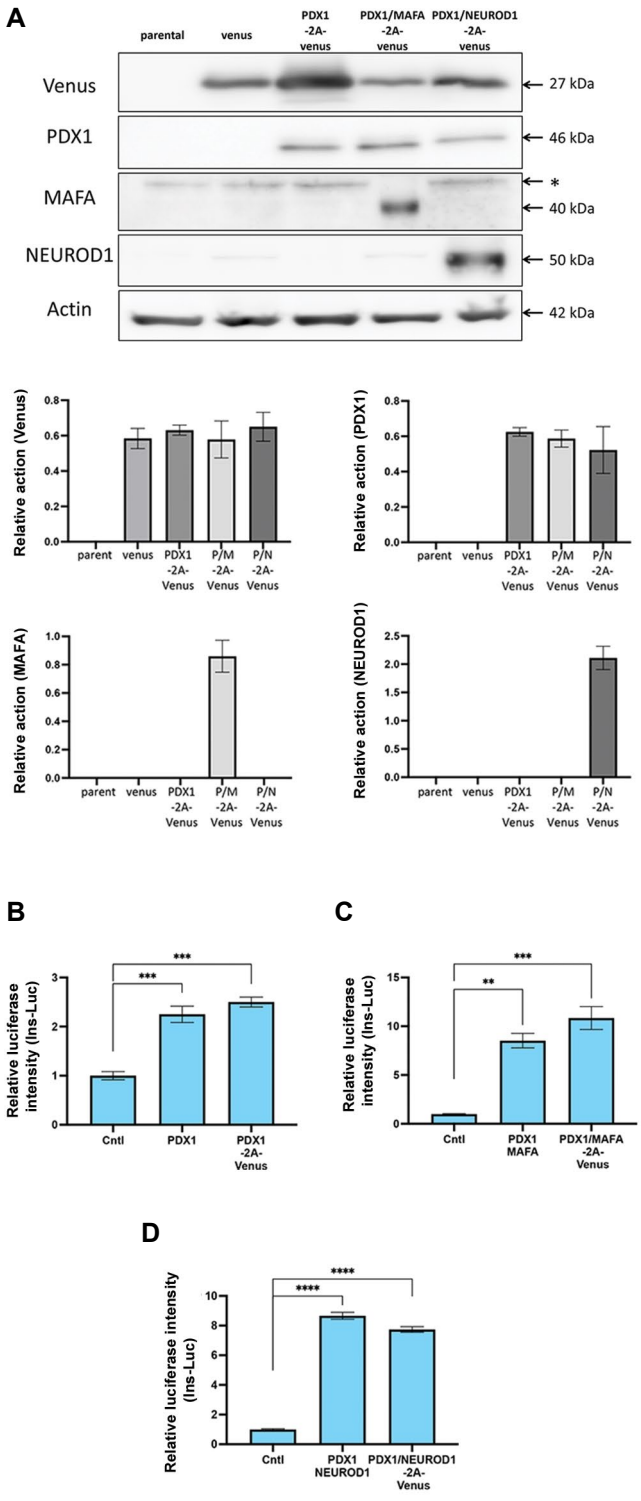

Fig.2: Evaluation of the functions of cleaved transcriptional factors. **A.** The plasmids pTRE-Venus-EF-tTA-2A-Bsd, pTRE-PDX1-2A-Venus-EF-tTA-2A-Bsd, pTRE-PM-2A-Venus-EF-tTA-2A-Bsd, or pTRE-PN-2A-Venus-EF-tTA-2A-Bsd were transiently transduced into hASC, and whole cell extract from the cells was subjected to western blot analysis. The asterisk indicates a non-specific band. The graphs indicate the mean ± SEM values from three independent experiments. **B.** The plasmids, pTRE-PDX1-2A-Venus-EF-tTA-2A-Bsd of pCMV-PDX1-IresGFP, **C.** pTRE-PM-2A-Venus-EF-tTA-2A-Bsd, or pCMV-PDX1-IresGFP and pCMV-MAFA-IresGFP, or **D.** pTRE-PN-2A-Venus-EF-tTA-2A-Bsd or pCMV-PDX1-IresGFP and pCMV-NeuroD1-IresGFP, were transiently transduced with plasmids insulin promoter-Luc and pGL4.74 into hASC. Thereafter, the effects of PDX1, MAFA, and/or NEUROD1 overexpression on INS(−342)-luc expression were evaluated. Data are presented as mean ± SEM from three independent experiments. ****; P<0.0001, ***; P<0.001, and **; P<0.01.

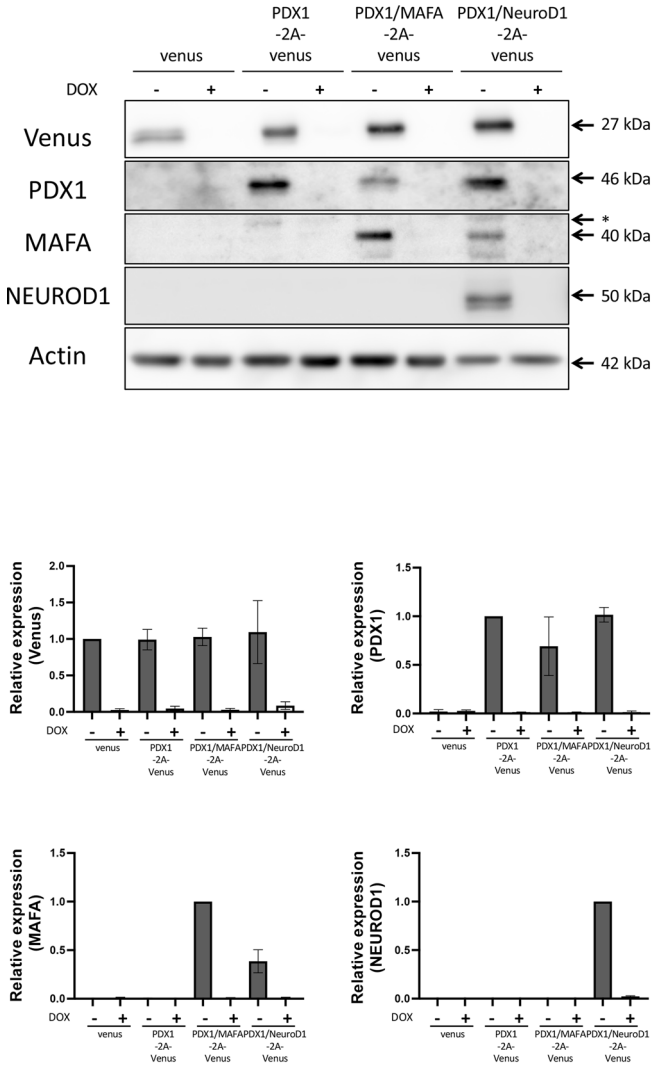

Fig.3: Evaluation of hASC that express PDX1, MAFA, and NeuroD1 in a Dox-dependent manner. hASC were transduced with pTRE-Venus-EF-tTA-2A-Bsd, pTRE-PDX1-2A-Venus-EF-tTA-2A-Bsd, pTRE-PM-2A-Venus-EF-tTA-2A-Bsd, or pTRE-PN-2A-Venus-EF-tTA-2A-Bsd at an MOI of 250. The cells were treated with 4 µg/mL blasticidin and 1 µg/mL Dox for two weeks. Thereafter, the cells were cultured in the absence (Dox –) or presence (Dox +) of 1 µg/mL Dox for four days and subjected to western blot analysis. The asterisk indicates a non-specific band. The graphs indicate mean ± SEM values from three independent experiments. hASC; Human adipose-derived mesenchymal stromal/stem cells and MOI; Multiplicity of infection.

In vitro differentiation of hASC into insulin-producing cells

Venus-hASC, PDX1-2A-Venus-hASC, PM-2A-Venus-hASC, and PN-2A-Venus-hASC were differentiated into insulin-producing cells *in vitro* (Fig.4A). After 5–7 days in the differentiation medium, the cells became round, and cell clusters appeared; however, undifferentiated hASC remained adherent and displayed a normal fibroblast-like shape. After 12 days in the differentiation medium, a qPCR analysis was performed to determine whether the gene encoding insulin (INS) expression was upregulated in the differentiated cells. As shown in Figure 4B, *INS* expression in PDX1-2A-Venus-hASC was upregulated relative to that in Venus-hASC. Furthermore, *INS* expression levels in PM-2A-Venus-hASC and PN-2A-Venus-hASC were significantly higher than those in Venus-hASC and PDX1-2A-Venus-hASC (Fig.4B). At the end of differentiation, the extent of hASC differentiation into insulin-producing cells was evaluated via DTZ staining. DTZ specifically binds to zinc ions in insulin molecules, which allows for identifying clusters with insulin-producing cells. As shown in Figure 4C, cell aggregates in Venus-hASC were observed to be DTZ-positive, as previously reported (11); however, the number and size of the aggregates were small. The DTZ-positive cell clusters in PDX1-2A-Venus-hASC were larger than those in Venus-hASC. Moreover, markedly larger clusters that were positive for DTZ staining could be found in PM-2A-Venus-hASC and PN-2A-Venus-hASC. In contrast, none of these cells formed DTZ-positive aggregates without induction of differentiation (Fig.4D), demonstrating that transducing the transcription factors alone is insufficient for the differentiation of hASC into insulin-producing cells *in vitro*.

In vivo differentiation of hASC into insulin-producing cells

Despite failing to fully differentiate into insulin-producing cells without induction of differentiation, we noticed that PN-2A-Venus hASC spontaneously upregulated MAFA expression (Fig.3), suggesting that PM-2A-Venus and PN-2A-Venus hASC may spontaneously and partially differentiate into insulin-producing cells without inducing differentiation. Previous studies have reported that partially differentiated PDX1-MSC could differentiate into insulin-producing cells *in vivo* (12, 13, 27). We decided to transplant undifferentiated Venus-hASC, PDX1-2A-Venus-hASC, PM-2A-Venus-hASC, and PN-2A-Venus-hASC into the renal subcapsular region of immunodeficient STZ-induced diabetic model mice to alter the external environment of the cells. Unfortunately, the blood glucose levels of the hyperglycemic mice that received Venus-hASC, PDX1-2A-Venus-hASC, PM-2A-Venus-hASC, and PN-2A-Venus-hASC did not exhibit a significant reduction (data not shown). However, a small proportion of cells expressing insulin was observed in the renal tissue sections transplanted with PM-2A-Venus-hASC and PN-2A-Venus-hASC (Fig.5). These findings indicate that the transplanted PM-2A-Venus-hASC and PN-2A-Venus-hASC could differentiate into insulin-producing cells in the kidneys of STZ-treated mice. Thus, PM-2A-Venus-hASC and PN-2A-Venus-hASC, but Pdx1-ASCs, seemed competent to differentiate into insulin-producing cells *in vivo*.

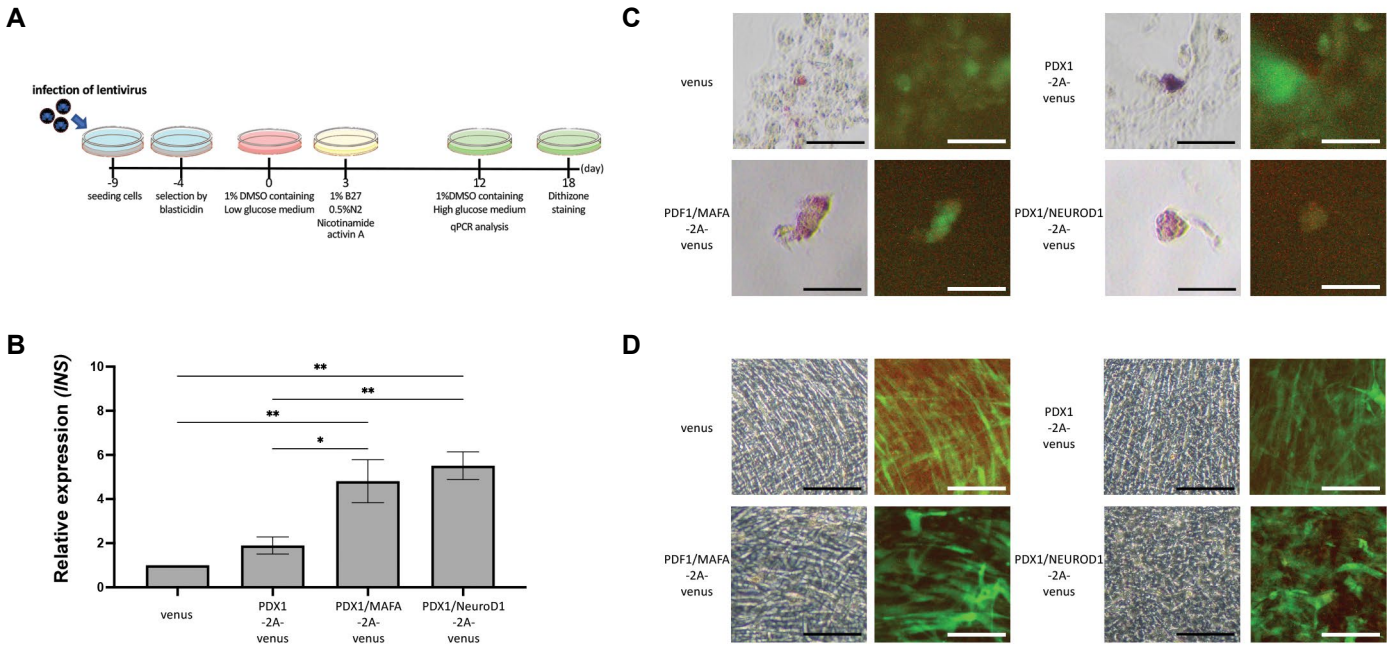

Fig.4: Evaluation of the capacities of hASC to differentiate into insulin-producing cells *in vitro*. Venus-hASC, PDX1-2A-Venus-hASC, PM-2A-Venus-hASC, and PN-2A-Venus-hASC were differentiated into insulin-producing cells *in vitro*. **A.** Schematic illustration of the methods for differentiation of hASC into insulin-producing cells. **B.** qPCR analysis of insulin mRNA expression on day 12 of hASC differentiation was performed. Each expression value was calculated using the ΔΔCt method, with B2M as an internal control. Data represent mean ± SEM of four independent experiments. **C.** The cells were stained with dithizone (DTZ) after 18 days of differentiation. **D.** The cells were grown in a maintenance medium for 18 days (undifferentiated control) and stained with DTZ. An image of the same field of cells captured using brightfield (left) and fluorescence (right) microscopy. Venus expression was also observed to confirm the exogenous expression (right panel, scale bars: 200 µm). hASC; Human adipose-derived mesenchymal stromal/stem cells, qPCR; Quantitative polymerase chain reaction, **; P<0.01, and *; P<0.05.

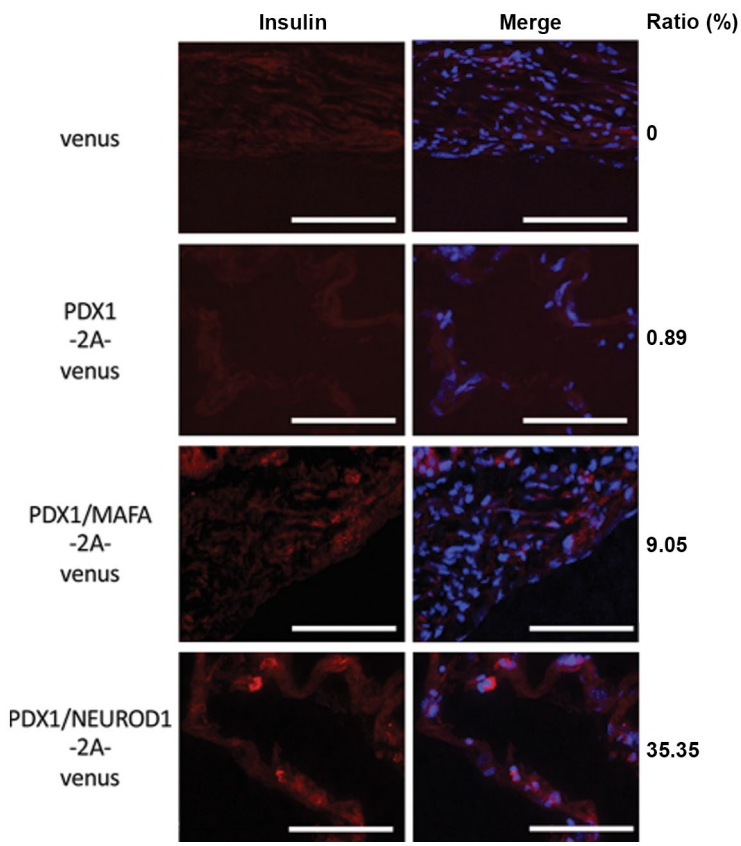

Fig.5: Evaluation of the capacities of hASC to differentiate into insulin-producing cells *in vivo*. Venus-hASC, PDX1-2A-Venus-hASC, PM-2A-Venus-hASC, and PN-2A-Venus-hASC were transplanted into the right subcapsular renal space in STZ-treated diabetic mice. Three months after transplantation, the grafts were removed and subjected to immunofluorescence staining for insulin (red). The nuclei were stained with DAPI (scale bars: 100 µm). The numbers on the right side of the images indicate the percentage of insulin-positive cells. hASC; Human adipose-derived mesenchymal stromal/stem cells, STZ; Streptozotocin, and DAPI; 4',6-diamidino-2-phenylindole.

Discussion

Current attempts to generate functional insulin-producing cells include direct differentiation of MSCs, iPSCs, and fibroblasts (28). In this study, we demonstrated that the forced expression of PDX1 enhanced the ability of hASC to differentiate into insulin-producing cells *in vitro*. In addition, simultaneous expression of PDX1 in combination with MAFA or NEUROD1 in hASC markedly induced the differentiation of insulin-producing cells both *in vitro* and *in vivo*.

Recently, several researchers have attempted to induce the differentiation of MSCs into pancreatic lineage cells (9-11). One of the strategies is the forced expression of a single or a combination of transcription factors, including Pdx1, NeuroD1, and/or MafA, which play essential roles in promoting the development of pancreatic β cells (12-14). Kajiyama et al. (13) reported that human PDX1 gene-transduced murine ASCs acquire a functional β-cell phenotype *in vivo.* Other researchers have also demonstrated that PDX1 transduction by non-integrated lentivirus could successfully induce the differentiation of human ASCs into insulin-producing cells (12). However, our present study revealed that insulin-producing β cells were derived from PDX1-2A-Venus-hASC *in vitro* but not *in vivo*. Consistent with our present study, several researchers have found that single transduction of PDX1 could induce the expression of insulin; however, the effect elicited in MSCs was weak compared to that obtained with the combination of several factors (17, 29). PDX1 transduction has also been reported to cause severe hepatitis, as exocrine differentiation is also induced by the transduction of PDX1. Therefore, strategies using transcription factors that induce β cell differentiation without inducing the exocrine lineage should be assessed to derive an ideal system for pre-clinical applications. Kojima et al. (30) found that the combination of NeuroD1 and betacellulin induced islet neogenesis in the liver without producing hepatitis. MafA is another good candidate/therapeutic target for diabetes owing to its potent activator of insulin gene transcription (16). In the present study, NeuroD1 or MafA together with PDX1 resulted in increased insulin expression *in vitro* and *in vivo*, demonstrating that transduction of PDX1 with NeuroD1/MafA in hASC is crucial for differentiation into insulin-producing cells. To verify these results, some researchers have demonstrated that combining these three factors efficiently induces insulin gene promoter and pancreatic β cell differentiation from non-β cells (17, 18, 31, 32). As endogenous MAFA expression was observed in PN-2A-Venus-hASC, PDX1 and NEUROD1 might be a better combination than PDX1 and MAFA. However, the differentiation potential of PN-2A-Venus-hASC and PM-2A-Venus-hASC into β cells was almost identical in this study, which might be due to insufficient expression of MAFA in PN-2A-Venus-hASC. A lentiviral vector simultaneously expressing PDX1, NEUROD1, and MAFA was constructed for further experiments.

We transplanted undifferentiated hASC that were transduced with a lentiviral vector because several groups have previously demonstrated that partially differentiated PDX1-MSC [NeuroD1^{+}Insulin^{-} cells (27), Nkx2.2^{+}NeuroD1^{-}Insulin^{-} cells (13), and Ngn3^{+} glucagon^{-} cells (12)] could differentiate into insulin-producing cells *in vivo*. In addition, several researchers have shown further differentiation of MSCs into insulin-producing cells after cell transplantation under the renal capsule (33-35). Gabr et al. (33) reported that the proportion of insulin-producing cells at the end of the *in vitro* differentiation of human bone marrow-derived MSCs was relatively low (ranging between 0.12% and 3.4%) but had increased significantly (approximately 20 times) after transplantation under the kidney capsule. These data suggest that further differentiation of partially differentiated MSCs occurred after transplantation under the influence of favorable microenvironmental conditions. In the present study, neither PDX1-2A-Venus, PM-2A-Venus, or PN-2A-Venus hASC formed DTZ-positive aggregates without induction of differentiation. However, we shows that PN-2A-Venus hASC spontaneously upregulated MAFA expression, suggesting that PM-2A-Venus and PN-2A-Venus hASC may spontaneously and partially differentiate into insulin-producing cells without inducing differentiation. Consistent with our prediction, Limbert et al. (36) demonstrated that transduction of NGN3- and/or PDX1 into hMSC-TERT cell lines was sufficient to differentiate the cells into insulin-producing cells. Therefore, we assume that PM-2A-Venus and PN-2A-Venus hASC were partially differentiated and thus could differentiate into the insulin-producing cells *in vivo*.

In the present study, we did not observe a decline in the blood glucose levels of hyperglycemic mice administered either Venus-hASC, PDX1-2A-Venus-hASC, PM-2A-Venus-hASC, or PN-2A-Venus-hASC, despite their potential to differentiate into insulin-producing cells. A recent study by Gerace et al. (37) showed that *ex vivo* expansion of MSCs resulted in the impairment of differentiation into pancreatic β cells. In the present study, hASC were cultured for at least two weeks for selection with blasticidin before differentiation. The problem might be alleviated by using puromycin-resistant genes instead of blasticidin-resistant genes, as puromycin has a fast mode of action, which results in a rapid selection of transgene-positive cells compared to blasticidin. Adenovirus vectors might also aid in resolving this issue as adenoviral vectors enable high levels of protein expression and are easily amplified to high concentrations, which allows for the efficient preparation of large numbers of cells for transplantation. Notably, adenovirus vectors can contribute to a risk-benefit assessment of biosafety as they are rarely integrated into genomic DNA. However, our present lentivirus system was constructed to be compatible with the Gateway cloning technology; therefore, we can easily and rapidly transfer the insulin-inducing transcription factors to Gateway-compatible adenoviral vectors. Altogether, further experiments, including glucose-induced insulin secretion assay *in vitro* and proliferation assay of transplanted cells

in vivo, are required to address this issue. In addition, the limitation of the present study is the differentiation of hASC into only β cells because glucagon-producing α cells have been reported to be essential to maintain β cell proliferation and survival (38, 39). Therefore, the development of strategies for differentiation into not only β cells but also other pancreatic cell types might-be advantageous for the survival and proliferation of transplanted β cells. Recently, Xiao et al. (40) reported that transcription factors Pdx-1 and MafA were delivered *in vivo* with an adeno-associated virus to the mouse pancreas to reprogram α cells into functional β cells. Thus, our vector system could also be useful for this strategy. Our attractive vector system has shown some progress in increasing the efficiency of hASC differentiation into insulin-producing cells, which is an attractive cell source for clinical use. However, several improvements are required to achieve an ideal gene expression system for preclinical studies. Further improvement and fine-tuning of the present vector systems are needed to overcome the accompanying problems and reach our goals.

Conclusion

Using our single tet-off lentiviral vector system, Pdx-1 and MafA/NeuroD1 could be simultaneously expressed in the absence of Dox, and allowed the differentiation of hASC into insulin-producing cells. Although further solutions are required to overcome these limitations, the present study's findings might contribute to the development of novel cellular therapies for patients with type I diabetes.

Acknowledgments

We thank C. Sone and J. Uda for their technical assistance and Dr. Hiroyuki Miyoshi for the pCMV-VSVG-RSV-Rev and pCAG-HIVg/p plasmids. We also thank Editage for English language editing. This work was supported by JSPS KAKENHI (Grant Number JP17K11559) awarded to H.M. We also received grants from the Japan Agency for Medical Research and Development (AMED). The authors declare that there are no conflicts of interest regarding the publication of this article.

Authors' Contributions

H.M., M.M., T.O.; Performed the experiments. H.M., M.M., T.H.; Designed the study and interpreted the data. T.O., D.T.; Provided the samples. H.M., M.M.; Contributed to the funding for this study. H.M., M.M., T.H.; Wrote the manuscript. All authors read and approved the final manuscript.

References

1. Ashton BA, Allen TD, Howlett CR, Eaglesom CC, Hattori A, Owen M. Formation of bone and cartilage by marrow stromal cells in diffusion chambers in vivo. Clin Orthop Relat Res. 1980; (151): 294-307.
2. Tamai K, Yamazaki T, Chino T, Ishii M, Otsuru S, Kikuchi Y, et al. PDGFRalpha-positive cells in bone marrow are mobilized by high mobility group box 1 (HMGB1) to regenerate injured epithelia. Proc Natl Acad Sci USA. 2011; 108(16): 6609-6614.
3. Leu S, Lin YC, Yuen CM, Yen CH, Kao YH, Sun CK, et al. Adipose-derived mesenchymal stem cells markedly attenuate brain infarct size and improve neurological function in rats. J Transl Med. 2010; 8: 63.
4. Strem BM, Hicok KC, Zhu M, Wulur I, Alfonso Z, Schreiber RE, et al. Multipotential differentiation of adipose tissue-derived stem cells. Keio J Med. 2005; 54(3): 132-141.
5. Bosch P, Stice S L. Adenoviral transduction of mesenchymal stem cells. Methods Mol Biol. 2007; 407: 265-274.
6. Doering CB. Retroviral modification of mesenchymal stem cells for gene therapy of hemophilia. Methods Mol Biol. 2008; 433: 203-212.
7. Moriyama H, Moriyama M, Sawaragi K, Okura H, Ichinose A, Matsuyama A, et al. Tightly regulated and homogeneous transgene expression in human adipose-derived mesenchymal stem cells by lentivirus with tet-off system. PLoS One. 2013; 8(6): e66274.
8. Stender S, Murphy M, O'Brien T, Stengaard C, Ulrich-Vinther M, Soballe K, et al. Adeno-associated viral vector transduction of human mesenchymal stem cells. Eur Cell Mater. 2007; 13: 93-99; discussion 99.
9. Gabr MM, Zakaria MM, Refaie AF, Abdel-Rahman EA, Reda AM, Ali SS, et al. From human mesenchymal stem cells to insulin-producing cells: comparison between bone marrow- and adipose tissue-derived cells. Biomed Res Int. 2017; 2017: 3854232.
10. Karaoz E, Okcu A, Unal ZS, Subasi C, Saglam O, Duruksu G. Adipose tissue-derived mesenchymal stromal cells efficiently differentiate into insulin-producing cells in pancreatic islet microenvironment both in vitro and in vivo. Cytotherapy. 2013; 15(5): 557-570.
11. Moshtagh PR, Emami SH, Sharifi AM. Differentiation of human adipose-derived mesenchymal stem cell into insulin-producing cells: an in vitro study. J Physiol Biochem. 2013; 69(3): 451-458.
12. Boroujeni ZN, Aleyasin A. Insulin producing cells established using non-integrated lentiviral vector harboring PDX1 gene. World J Stem Cells. 2013; 5(4): 217-228.
13. Kajiyama H, Hamazaki TS, Tokuhara M, Masui S, Okabayashi K, Ohnuma K, et al. Pdx1-transfected adipose tissue-derived stem cells differentiate into insulin-producing cells in vivo and reduce hyperglycemia in diabetic mice. Int J Dev Biol. 2010; 54(4): 699-705.
14. Hui H, Perfetti R. Pancreas duodenum homeobox-1 regulates pancreas development during embryogenesis and islet cell function in adulthood. Eur J Endocrinol. 2002; 146(2): 129-141.
15. Naya FJ, Stellrecht CM,Tsai MJ. Tissue-specific regulation of the insulin gene by a novel basic helix-loop-helix transcription factor. Genes Dev. 1995; 9(8): 1009-1019.
16. Kataoka K, Han SI, Shioda S, Hirai M, Nishizawa M, Handa H. MafA is a glucose-regulated and pancreatic beta-cell-specific transcriptional activator for the insulin gene. J Biol Chem. 2002; 277(51): 49903-49910.
17. Xu H, Tsang KS, Chan JC, Yuan P, Fan R, Kaneto H, et al. The combined expression of Pdx1 and MafA with either Ngn3 or NeuroD improves the differentiation efficiency of mouse embryonic stem cells into insulin-producing cells. Cell Transplant. 2013; 22(1): 147-158.
18. Guo QS, Zhu MY, Wang L, Fan XJ, Lu YH, Wang ZW, et al. Combined transfection of the three transcriptional factors, PDX-1, NeuroD1, and MafA, causes differentiation of bone marrow mesenchymal stem cells into insulin-producing cells. Exp Diabetes Res. 2012; 2012: 672013.
19. Zhou Q, Brown J, Kanarek A, Rajagopal J, Melton DA. In vivo reprogramming of adult pancreatic exocrine cells to beta-cells. Nature. 2008; 455(7213): 627-632.
20. Percie du Sert N, Ahluwalia A, Alam S, Avey MT, Baker M, Browne WJ, et al. Reporting animal research: explanation and elaboration for the ARRIVE guidelines 2.0. PLoS Biol. 2020; 18(7): e3000411.
21. Moriyama H, Moriyama M, Ozawa T, Tsuruta D, Iguchi T, Tamada S, et al. Notch signaling enhances stemness by regulating metabolic pathways through modifying p53, NF-kappaB, and HIF-1alpha. Stem Cells Dev. 2018; 27(13): 935-947.
22. Kim SJ, Choi YS, Ko ES, Lim SM, Lee CW, Kim DI. Glucose-stimulated insulin secretion of various mesenchymal stem cells after insulin-producing cell differentiation. J Biosci Bioeng. 2012; 113(6): 771-777.
23. Oh SH, Muzzonigro TM, Bae SH, LaPlante JM, Hatch HM,Petersen BE. Adult bone marrow-derived cells trans-differentiating into insulin-producing cells for the treatment of type I diabetes. Lab Invest. 2004; 84(5): 607-617.
24. Bustin SA, Benes V, Garson JA, Hellemans J, Huggett J, Kubista M, et al. The MIQE guidelines: minimum information for publication of quantitative real-time PCR experiments. Clin Chem. 2009; 55(4):

611-622.
25. Nishimura EK, Jordan SA, Oshima H, Yoshida H, Osawa M, Moriyama M, et al. Dominant role of the niche in melanocyte stem-cell fate determination. Nature. 2002; 416(6883): 854-860.
26. Kaneto H, Matsuoka TA, Katakami N, Matsuhisa M. Combination of MafA, PDX-1 and NeuroD is a useful tool to efficiently induce insulin-producing surrogate beta-cells. Curr Med Chem. 2009; 16(24): 3144-3151.
27. Prabakar KR, Dominguez-Bendala J, Molano RD, Pileggi A, Villate S, Ricordi C, et al. Generation of glucose-responsive, insulin-producing cells from human umbilical cord blood-derived mesenchymal stem cells. Cell Transplant. 2012; 21(6): 1321-1339.
28. Zhu S, Russ HA, Wang X, Zhang M, Ma T, Xu T, et al. Human pancreatic beta-like cells converted from fibroblasts. Nat Commun. 2016; 7: 10080.
29. Li HT, Jiang FX, Shi P, Zhang T, Liu XY, Lin XW, et al. In vitro reprogramming of rat bmMSCs into pancreatic endocrine-like cells. In Vitro Cell Dev Biol Anim. 2017; 53(2): 157-166.
30. Kojima H, Fujimiya M, Matsumura K, Younan P, Imaeda H, Maeda M, et al. NeuroD-betacellulin gene therapy induces islet neogenesis in the liver and reverses diabetes in mice. Nat Med. 2003; 9(5): 596-603.
31. Liu XD, Ruan JX, Xia JH, Yang SL, Fan JH, Li K. The study of regulatory effects of Pdx-1, MafA and NeuroD1 on the activity of porcine insulin promoter and the expression of human islet amyloid polypeptide. Mol Cell Biochem. 2014; 394(1-2): 59-66.
32. Wang L, Huang Y, Guo Q, Fan X, Lu Y, Zhu S, et al. Differentiation of iPSCs into insulin-producing cells via adenoviral transfection of PDX-1, NeuroD1 and MafA. Diabetes Res Clin Pract. 2014; 104(3): 383-392.
33. Gabr MM, Zakaria MM, Refaie AF, Khater SM, Ashamallah SA, Ismail AM, et al. Differentiation of human bone marrow-derived mesenchymal stem cells into insulin-producing cells: evidence for further maturation in vivo. Biomed Res Int. 2015; 2015: 575837.
34. Karnieli O, Izhar-Prato Y, Bulvik S, Efrat S. Generation of insulin-producing cells from human bone marrow mesenchymal stem cells by genetic manipulation. Stem Cells. 2007; 25(11): 2837-2844.
35. Xin Y, Jiang X, Wang Y, Su X, Sun M, Zhang L, et al. Insulin-producing cells differentiated from human bone marrow mesenchymal stem cells in vitro ameliorate streptozotocin-induced diabetic hyperglycemia. PLoS One. 2016; 11(1): e0145838.
36. Limbert C, Path G, Ebert R, Rothhammer V, Kassem M, Jakob F, et al. PDX1- and NGN3-mediated in vitro reprogramming of human bone marrow-derived mesenchymal stromal cells into pancreatic endocrine lineages. Cytotherapy. 2011; 13(7): 802-813.
37. Gerace D, Martiniello-Wilks R, Habib R, Ren B, Nassif NT, O'Brien BA, et al. Ex vivo expansion of murine MSC impairs transcription factor-induced differentiation into pancreatic beta-cells. Stem Cells Int. 2019; 2019: 1395301.
38. Kilimnik G, Kim A, Steiner DF, Friedman TC, Hara M. Intraislet production of GLP-1 by activation of prohormone convertase 1/3 in pancreatic alpha-cells in mouse models of ss-cell regeneration. Islets. 2010; 2(3): 149-155.
39. Liu Z, Stanojevic V, Avadhani S, Yano T, Habener JF. Stromal cell-derived factor-1 (SDF-1)/chemokine (C-X-C motif) receptor 4 (CXCR4) axis activation induces intra-islet glucagon-like peptide-1 (GLP-1) production and enhances beta cell survival. Diabetologia. 2011; 54(8): 2067-2076.
40. Xiao X, Guo P, Shiota C, Zhang T, Coudriet GM, Fischbach S, et al. Endogenous reprogramming of alpha cells into beta cells, induced by viral gene therapy, reverses autoimmune diabetes. Cell Stem Cell. 2018; 22(1): 78-90. e74.

Original Article

Assessment of Adiponectin and Sperm Function Parameters in Obese and Non-Obese: A Comprehensive Study

Marziyeh Pooladi, M.Sc.[1], Mohammadreza Sharifi, Ph.D.[2], Gholam Reza Dashti, Ph.D.[1, 3*]

1. Department of Anatomical Sciences, School of Medicine, Isfahan University of Medical Sciences, Isfahan, Iran
2. Department of Genetics and Molecular Biology, School of Medicine, Isfahan University of Medical Sciences, Isfahan, Iran
3. Saint Maryam Fertility and Infertility Center, Shahid Beheshti Hospital, Isfahan University of Medical Sciences, Isfahan, Iran

**Corresponding Address: P.O.Box: 8174673461, Department of Anatomical Sciences, School of Medicine, Isfahan University of Medical Sciences, Isfahan, Iran*
Email: dashti@med.mui.ac.ir

Received: 05/February/2022, Accepted: 14/June/2022

Abstract

Objective: The role of adiponectin in sperm function is inconclusive and there is a paucity of evidence. Obesity shows an ambiguous influence on sperm motility, and male subfertility. The aim of this study was to compare the role of adiponectin and sperm functional parameters among obese and non-obese men.

Materials and Methods: In this comprehensive study, 64 male patients were included, and were classified as non-obese [body mass index (BMI)< 24.9 kg/m^2, n=32] and obese (BMI >25 kg/m^2, n=32) groups. Sperm analysis, was conducted using World Health Organization (WHO) 2010 standards. Real-time polymerase chain reaction (PCR) and enzyme-linked immunosorbent assay (ELISA) were used for the analysis of adiponectin gene expression and protein levels, respectively. Sperm viability was assessed using the 3-(4, 5-dimethylthiazol-2-yl)-2, 5-diphenyl tetrazolium bromide (MTT test), Acridine orange (AO) test was utilized to detect DNA denaturation, and sperm chromatin dispersion (SCD) technique was used to investigate the fragmentation of DNA.

Results: In obese men, adiponectin gene expression (P<0.0001) and protein levels (P<0.001) were significantly lower compared to the non-obese group. Additionally, sperm motility, was significantly lower in the obese group. The rapid progressive (RP) motility was less in obese men in comparison to the non-obese group (P<0.001). Sperm count and morphology were not significantly different in the two groups. DNA denaturation and DNA fragmentation were significantly more frequent in the obese group than in non-obese men (P<0.05) and (P<0.01), respectively. The obese men showed significantly lower sperm viability compared to the non-obese group (P<0.05).

Conclusion: This study showed no significant correlation between the evaluated variables (sperm parameter, sperm viability, DNA fragmentation and integrity), and obesity in men. Based on these results, adiponectin may potentially play positive role in sperm function for acquiring fertility.

Keywords: Adiponectin, Chromatin, Obesity, Sperm, Viability

Cell Journal(Yakhteh), Vol 24, No 12, December 2022, Pages: 715-722

Citation: Pooladi M, Sharifi M, Dashti GR. Assessment of adiponectin and sperm function parameters in obese and non-obese: a comprehensive study. Cell J. 2022; 24(12): 715-722. doi: 10.22074/CELLJ.2022.557337.1044.

Introduction

Adipose tissue has a complex system, consisting of adipocytes, pre-adipocytes, fibroblasts, endothelial cells, immune cells such as macrophages, dendritic cells, and T cells, which secrete fat metabolites, cytokines, and adipokines. It maintains energy homeostasis by preserving proteins, controlling energy balance, fertility, and inducing an increase in immunological response. However, excess fat causes imbalance with a detrimental effect on health. Adipose tissue is a toxic depot of triglycerides, and is a vital endocrine organ releasing adipokines, whose actions of mechanism have paucity of evidence (1). The role of adipokines is to preserve energy homeostasis, having other endocrine axes with direct influences on various organs, which are emerging with the advent of research in these realms (2). Metabolic disorders, like obesity, can jeopardized adipose tissue hormonal milieu, effecting health factors (3).

Obesity is a serious global health problem including multifactorial diseases, like atherosclerosis, hypertension, diabetes, cardiovascular disease (CVD), stroke, infertility, and cancer, potentially leading to one´s death (4-6). The body mass index (BMI) is indicative of the state of body weight (7). BMIs of 25-30 kg/m^2 and values higher than 30 kg/m^2 are considered as obese. Over the past decades, obesity has become a public health priority in both genders in Iran (8), with a risk of male-factor infertility, suggesting prevention and management due to the comorbidities, oxidative stress (OS), and complications (9). The evidence of decreased male fertility ,has encouraged researchers to unveil the link between metabolic disorders like obesity and male fertility (10). The issue of male infertility has become a global public health problem, indicating the important effects of obesity on sperm functions (11). In a previous study, non-obese men showed higher sperm function, and lower DNA fragmentation index (DFI) (12) than obese men. Obesity has shown to decrease adiponectin levels, serum and intra-testicular levels of follicle stimulating hormone (FSH), luteinising hormone and testosterone, sperm count, motility, viability and normal morphology, but increase serum leptin, epididymal malondialdehyde level and sperm DNA fragmentation (13).

Adipose tissue, produces many bioactive polypeptides called adipokines, inducing metabolic disorders and infertility (14), suggesting the missing link between obesity and infertility (15). Adiponectin is a specific adipokines, found in adipose tissue (16). Unlike other adipokines, serum adiponectin levels shows an inverse relationship with visceral fat and body mass (17). Adiponectin and its receptors (AdipoR1 and AdipoR2) have been reported in various male genital cells of different species, like chickens, mice, rams, cattle and humans (18). It has been reported that diet-induced obesity in mice, leads to changes in serum levels of the hormone adiponectin, but does not lead to epigenetic changes in a high-fat diet mouse (19).

The exact role of adiponectin in diagnosis of male fertility is inconclusive at this point, but there is a clear association. Previous studies have investigated the function of adiponectin receptors on testicular cells. However, to our knowledge, no study has reported the role of adiponectin on sperm molecular factors and DNA integrity in men. Similarly, the correlation between seminal adiponectin concentration and sperm function parameters in patients in Isfahan, Iran, has not been reported. Thus, there is a need to explore the adverse effects of obesity and the possible role of adiponectin in sperm function in our population. Consequently, this study was considered as a basis of novelty to explore the impact of adiponectin on normal reproductive sperm function and its possible role on infertility. To test these hypotheses, we studied the *adiponectin* gene expression and protein level in human semen, and its relationship with sperm function in obese and non-obese normozoospermic men.

Materials and Methods

Study population

This comprehensive study, was approved by the Institutional Ethics Committee of Isfahan University of Medical Sciences (IR.MUI.MED.REC.1398.568). Informed permission was acquired from all normozoospermic men referred to the Andrology Unit of Hazrat-e-Maryam Fertility and Infertility Center of Shahid Beheshti Hospital, Isfahan University of Medical School, Isfahan, Iran. According to World Health Organization (WHO) criteria published in 2010 (20), sperm samples were classed as normozoospermic. Based on the BMI values, sperm and blood samples of 64 men were collected and separated into two groups: obese and non-obese normozoospermic males.

Inclusion criteria

The age of the participants was between 25 to 55 years. The BMI values ranging from 24.8 to 18.9 kg/m^2 were considered as non-obese men, and those higher than 25 kg/m^2 were classified as obese men. The participants were told to refrain from sexual activity for at least 3 to 4 days before the experiment.

Exclusion criteria

Individuals with a history of cryptorchidism, varicocele, vasectomy, drug abuse and usage of exogenous hormones (replacement therapy of testosterone) were excluded from the study. Biochemical variables, like normal serum inhibin B<50 ng/ml, HBA1c ≥ 6.5%, normal weight with triglycerides> 2.3 mmol/ml, and FSH level>12.4 IU/ml were also excluded.

Fertility assessment

Fertility was evaluated through sperm analysis, blood sampling, physical examination and a general questionnaire. The questionnaire included the body weight, height, medical history, lifestyle variables, use of cigarettes and other narcotics, alcohol, drugs and any nutritional supplements. Fresh semen samples were collected by masturbation in sterile containers and were evaluated using computer-assisted sperm analysis (CASA) in accordance with WHO (2010) criteria (21).

Sperm preparation and analysis

After liquefaction, semen samples obtained in sterile containers were analyzed for the volume as well as, sperm morphology, and motility, according to the WHO (2010) guidelines. The sperm count, morphology, and motility were evaluated using a CASA-system (CASA, VT-Sperm Test.2.3 model-company of Video Test-Finland) guidelines. Each semen sample was washed twice and re-suspended in modified Hams F10 with 5% human serum albumin (Irvine Scientific, Santa Ana. California) (22). Sperm viability was determined using the MTT Test. DNA fragmentation and denaturation were assessed by means of the sperm chromatin dispersion (SCD) technique and the AO test. The adiponectin level was assessed by ELISA and RNA isolation for gene expression analysis was performed using real-time quantitative reverse transcription-polymerase chain reaction (RT-PCR).

Sperm motility assessment

The percentage of motile spermatozoa was studied in obese and non-obese samples by evaluation of the samples under a light microscope (Olympus, Tokyo, Japan) equipped with CASA system (CASA, VT-Sperm Test, 2.3 model- Company of Video Test-Finland). Percentage of rapid progressive (RP), progressive (P), non-progressive (NP) and immotile spermatozoa (IM) were assessed in both groups. FP sperm cells are those that swim forward in a straight line. SP sperm swim forward, but either in linear or curved line. NP sperm move their tails but do not move forward and IM sperm do not move at all. The results of sperm motility were evaluated compared between two groups of sperm samples (23).

Gene expression by real-time polymerase chain reaction

Total human sperm RNA was extracted as per the

manufacturer's protocol of Super RNA extraction kit (Thermo-Fisher, USA). Sperm samples were stored at -80˚C until RNA extraction. Briefly, 800 µl of lysis buffer was added to the sperm sample and vortexed. Next, 300 µl of chloroform (Merck, Germany) was added to the sample and vortexed for an additional 15 seconds. After that, it was incubated for 5 minutes at room temperature. The sample was centrifuged at 12,000 rpm at 4˚C for 5 minutes, forming three phases in the microtube. The supernatant fluid was removed, and 300 µl of sperm cell precipitate was added and vortexed. The sperm cells were transferred to the column, and again centrifuged at 12,000 rpm for 30 secs at room temperature. 700 µl of PBS was added and centrifuged at 12,000 rpm for 90 seconds at room temperature. The column was then placed in a new sterile microtube and 35-45 µl of elution buffer was added, then placed in thermomixer at 65˚C temperature for 3 minutes, and centrifuged at 12,000 rpm for 2 minutes at room temperature. The final concentration and RNA purity were measured at 260 nm using a spectrophotometer (Nano-drop, Eppendorf, Germany). Subsequently, total RNA was reverse transcribed to complement deoxyribonucleic acid (cDNA) using cDNA Synthesis Kit (Anacell, Iran), according to manufacturer's instructions. The primers, which are summarized in Table 1, were designed on the National Center for Biotechnology Information (NCBI) site and certified by Blast Primer software. Each primer's final concentration was 1 µM. Real time polymerase chain reaction (PCR) was run on Life Cycler 96 system (Roche Diagnostics, Gmblt, Germany) by the use of SYBR green PCR kit (Anacell, Iran). The PCR conditions included 95˚C for 15 minutes followed by 40 cycles at 95˚C for 20 seconds, 60˚C for 30 seconds and 72˚C for 30 seconds. Finally, for data acquisition, the samples were placed at 72ºC-95ºC temperature for 0.5ºC/0.05 seconds. Glyceraldehyde-3-phosphate dehydrogenase *(GAPDH)* gene was used as the housekeeping gene. The relative expression of messenger RNA (mRNA) was specified via the $2^{-\Delta\Delta CT}$ method.

The concentration of adiponectin by ELISA method

The adiponectin concentration in 32 obese and 32 non-obese samples was evaluated by human adiponectin enzyme-linked immunosorbent assay (ELISA) kit (Mediagnost human Adiponectin ELISA kit, E09), which was performed per the protocol of the manufacturer. Quality control and semen were diluted 200 times with dilution buffer before testing, ideally in two phases. The coefficients of inter-and intra-assay variation were determined to be less than 6.7 and 4.7%, respectively. Within 30 minutes, absorbances were measured at 450 nm using an ELISA Microplate Reader RT-6000, lorderan with >590 nm as the reference wavelength.

Sperm viability by MTT method

Using the MTT test, we determined sperm viability in 32 obese and 32 non-obese samples. This experiment was done through a technique outlined by Mosmann (24). In summary, 10 µl of MTT (Sigma, USA) stock solution (5 mg/ml ham's F10) was poured into each tube of sperm suspension. The tubes were then put in an incubator for 1 hour at 37˚C. After the tubes were centrifuged for 6 minutes at 6000 rpm, the precipitate was dissolved in a solution of 200 µl dimethyl sulfoxide (DMSO), which was centrifuged for 4 minutes at 4000 rpm. 100 µl of the purple solution was poured into a 96-well plate, and its absorbance rate was measured at 505 nm through an ELISA reader (RT-6000 | lorderan). The sample's optical density was then utilized to specify the percentage of viable sperm (25).

Acridine orange test

The Acridine orange (AO) stain is used to measure the rate of DNA denaturation. The smears of 32 obese and 32 non-obese samples were produced and air-fixed for 20 minutes before being fixed in a Carnoy's solution (methanol/glacial acetic acid at a ratio of 3:1) at 4˚C for at least 2 hours. The prepared samples were then stained with a newly produced AO solution (at a 0.19 mg/ml concentration in Mc Ilvain phosphate citrate buffer (pH=4). On the same day, each smear was examined through a fluorescencet microscope, with a 460 nm filter. 200 spermatozoa were analyzed in each slide, and the percentage of healthy sperm cells that had double-stranded DNA (normal green fluorescent) was determined while single-stranded DNA was detected through red fluorescence (abnormal cells) (26, 27).

Table 1: Sequence of primers used to synthetize the studied genes

Oligo gene	Primer sequence (5´-3´)	Tm (˚C)	MW (g/mol)	GC content (%)
ADIPONECTIN	F: ACTGCAGTCTGTGGTTCTGA	57.3	6139	50
	R: GAGTCGTGGTTTCCTGGTCA	59.4	6155	55
GAPDH	F: AAGCTCATTTCCTGGTATG	52.4	5794	42.1
	R: CTTCCTCTTGTGCTCTTG	53.7	5398	50

Tm; Temperature and MW; Molecular weight.

Sperm chromatin dispersion method for DNA fragmentation detection

SCD test was employed to detect DNA fragmentation by using a halo sperm kit (Idevarzan-e-Farda Co., Tehran, Iran). The 32 obese and 32 non-obese sperm samples were evaluated according to manufacturer's protocol. Each sample was washed twice in phosphate-buffered saline (PBS), before adding 50 µl of the samples to the agarose. Then placed 30 microliters of the samples on a glass slide, wrapped in foil, and refrigerated for 5 minutes. Denaturation and slip solutions were applied to the slides. Before dehydrating with a rising gradient of ethanol (70%, 90%, and 100%), each sample was rinsed with distilled water for 5 minutes. The samples were washed and dried. On each plate, 200 sperm cells were inspected under a light microscope for halo analysis (1000x magnification). Sperms without, or with small, halos were taken as having fragmented DNA while sperms with medium/large halos were thought to have intact DNA (28).

Statistical analysis

SPSS (version 20, IBM Corporation, Armonk, NY) was used for conducting statistical analysis. Kolmogorov–Smirnov test was used to check the normality of the data. The student t test was utilized to compare the acquired results between the non-obese and obese groups. Pearson's correlation test was used to study the relationship between variables. Data were analyzed as the means and standard deviation (mean ± SD), and $P<0.05$ was considered as statistically significant.

Results

The comparison of sperm parameters by CASA

Sperm rapid progression (fast motility) in obese group (11.70 ± 6.99) was significantly different from non-obese group (18.25 ± 6.69, $P<0.001$, Fig.1A, B) and sperm progression (slow motility) in the control group (35.94 ± 8.55), was not significantly different from the obese group (32.0 ± 7.57). Additionally, sperm morphology in the non-obese group (4.83 ± 0.89) compared to the obese group (4.78 ± 0.73) was not significantly different ($P>0.05$). Similarly, the sperm count in the non-obese group (122.1 ± 34.13) compared to the obese group (115.0 ± 33.21) was not significantly different ($P>0.05$, Fig.1C, D).

Comparison of adiponectin levels in obese and non-obese individuals

The seminal fluid adiponectin levels in the obese group (5.42 ± 0.21 ng/ml) was significantly different from non-obese group (6.13 ± 0.76 ng/ml, $P<0.001$, Fig.2A).

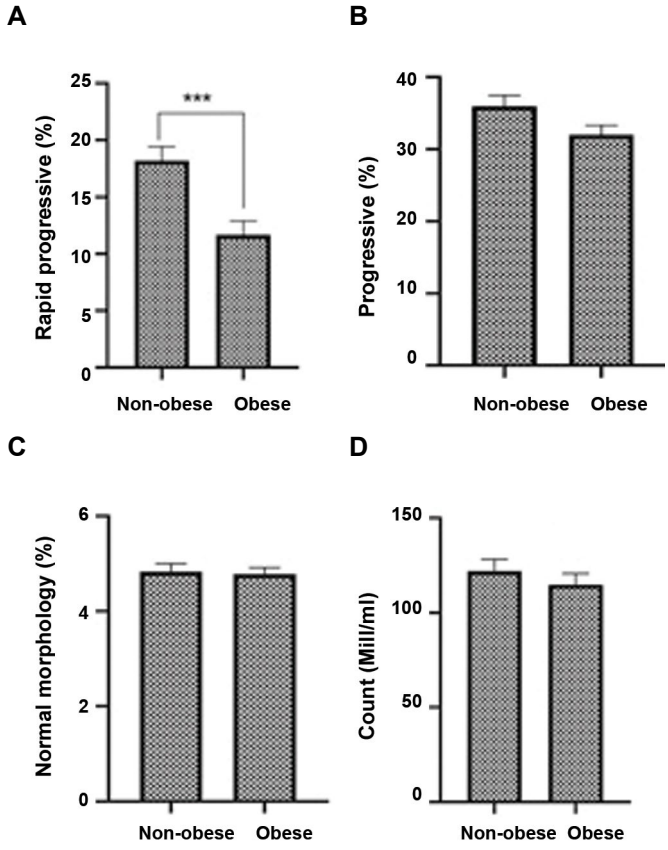

Fig.1: Percentage of sperm parameters (mean ± standard deviation) in non-obese and obese groups. Sperm motility, **A.** Rapid progressive and **B.** Progressive. **C.** Sperm morphology and **D.** Count percentages. ***; $P<0.001$.

Comparison of *ADIPONECTIN* gene expression in obese and non-obese individuals

The expression level of *ADIPO* gene was evaluated in seminal specimens taken from non-obese and obese patients. The obese group (0.44 ± 0.060) was significantly different from the non-obese group (1 ± 0, $P<0.0001$, Fig.2B).

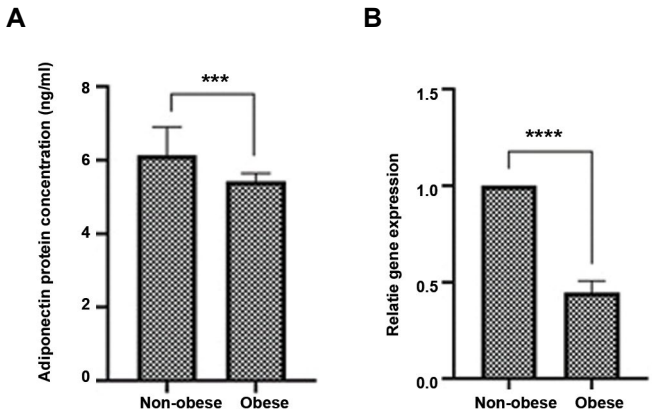

Fig.2: Evaluation of semen adiponectin protein concentration and relative gene expression (mean ± standard deviation) in obese and non-obese groups. **A.** Adiponectin protein and **B.** Gene expression. ***; $P<0.001$ and ****; $P<0.0001$.

MTT assay

Sperm viability was analyzed by MTT assay. The proportion of viability in the obese group (0.48 ± 0.27) was significantly lower from the non-obese group (0.65 ± 0.17, P<0.05. Fig.3A).

Acridine orange test

According to our findings, the rate of sperm DNA denaturation in the non-obese group (52.00 ± 15.85) was significantly lower from the obese group (67.35 ± 24.05, P<0.05, Fig.3B).

Evaluation of DNA fragmentation

Using the SCD technique, we discovered that the proportion of sperm with fragmented DNA in the non-obese group (17.91 ± 9.96) was significantly different from the obese group (25.83 ± 9.56, P≤0.01, Fig.3C). The SCD method revealed that obesity has a detrimental effect on the integrity level of sperm DNA, while the non-obese group compensates for obesity's negative effect on the DNA of sperm (Fig.4).

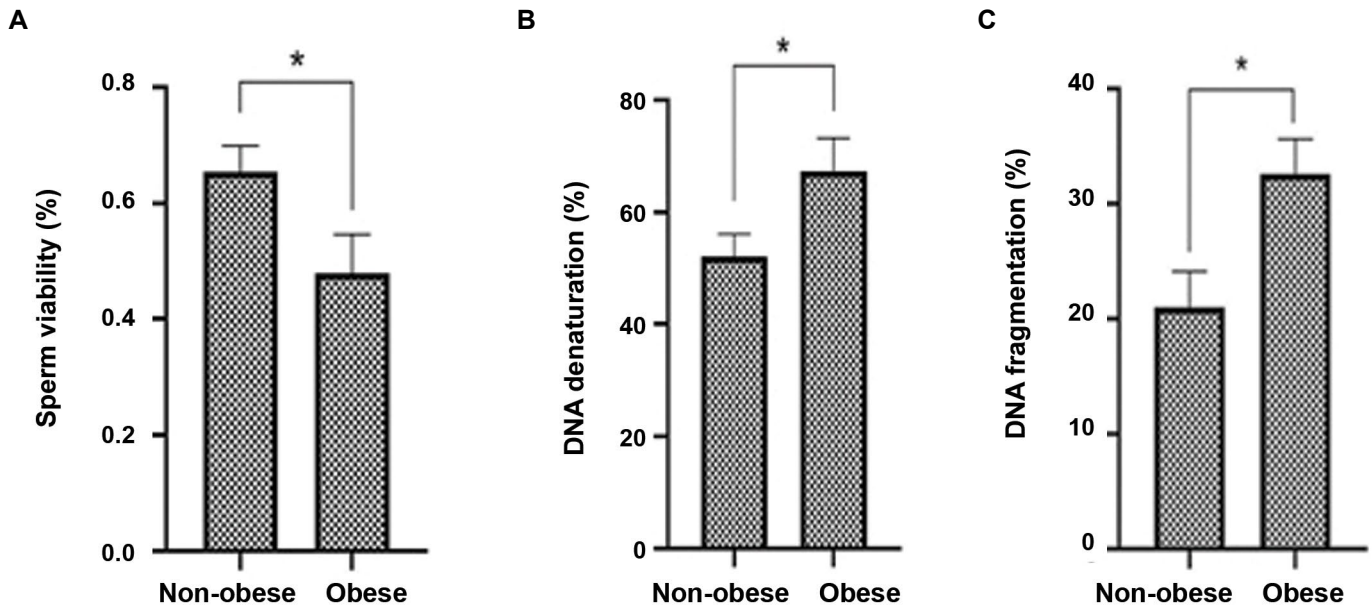

Fig.3: Percentage of sperm viability, DNA denaturation and DNA fragmentation (mean ± standard deviation) in obese and non-obese groups. **A.** Sperm viability, **B.** DNA denaturation (*; P<0.05), and **C.** DNA fragmentation (*; P≤0.01).

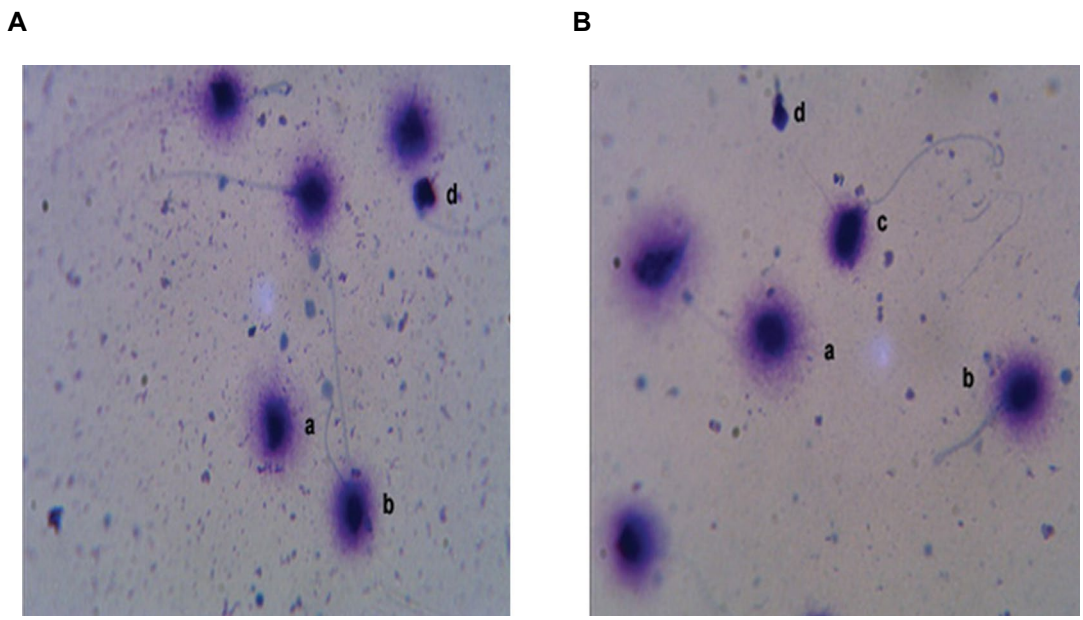

Fig.4: Percentage SCD test. Large halo sperm (a), medium halo sperm (b), small halo sperm (c), and no halo sperm (d). Sperm cells with large/medium halos have healthy DNA, sperm with small or absent halos had damaged DNA (light microscopy, magnification 1000x). **A.** Non-obese men and **B.** Obese men (n=32).

Correlation of variables

Pearson's correlation analysis revealed no significant relationship between adiponectin and sperm parameters, viability, fragmentation, and denaturation of DNA in the obese or non-obese group (Table 2).

Table 2: Pearson's correlation coefficient between research variables

Variable	Obese (n=32)	Non-obese (n=32)
Sperm count	r=-0.256	r=-0.212
	P=0.196	P=0.356
Morphology	r=0.277	r=-0.033
	P=0.297	P=0.886
Progressive	r=-0.061	r=0.248
	P=0.819	P=0.278
Rapid progressive	r=0.116	r=0.161
	P=0.562	P=0.483
Viability	r=-0.130	r=0.022
	P=0.628	P=0.935
Acridine orange	r=-0.052	r=0.016
	P=0.845	P=0.953
SCD test	r= 0.409	r=-0.126
	P=0.058	P=0.584

Discussion

Obesity was shown to have a deleterious influence on critical sperm parameters and DNA integrity in normozoospermic individuals in this research. Nevertheless, we did not discover any statistically significant correlation between adiponectin and the study factors. Obesity has more than tripled among men of childbearing age in the last 30 years, which may be a reason for the increased infertility and decreased sperm parameters.

On the other hand, the relationship between an increased BMI and sperm functions have been hypothesized extensively, yet there is a paucity of experimental evidence about these observations. In a study on 1558 males, 23.9% of men showed decreased sperm count when BMI was more than 25 kg/m^2 (29). Another study, reported a decreased motility of sperm in obese men compared to the group with normal BMI. The average value for sperm motility was 51.4% in non-obese men, while it was 46.6%, in men with BMIs higher than 30 kg/m^2 (30). A previous study reported that obesity was associated with lower number of motile sperms, and higher incidence of abnormal morphology. Our findings are in agreement with that study, suggesting a negative correlation between obesity and sperm quality and viability. However, in contrast to our results, another study did not find that obesity has detrimental influence on sperm morphology (31). It is reported that obesity could influence sperm quality, but the putative mechanism of action of this pathogenesis remains unclear. A causal impact of the adipokines profile that changes during obesity, can be the link between obesity and infertility (15). One study has found that the concentration of seminal adiponectin in ram sperm is related to sperm motility (32). In humans, it seems that seminal adiponectin concentrations is directly related to both sperm count and morphology (33), as overweight individuals show lower levels of adiponectin. As a result of the decreased level of adiponectin in these patients, the sperm count, motility, morphology and viability are found to be affected in obese men (34). Similarly, in our study, non-obese men had higher levels of *ADIPONECTIN* gene expression and protein than the obese individuals, showing the correlations of adiponectin with BMI, which is in agreement with previous findings (35).

Sperm cell viability showed a direct relationship with sperm fertility (36). In our study, the proportion of sperm viability in the non-obese men was significantly higher than the obese men, which is in line with a previous research study (37). Our study found that obesity, sperm parameters and viability can affect sperm function, as the non-obese men had significantly lower mean rates of sperm DNA denaturation and fragmentation compared to the obese group. Similar to our study, increased adiponectin levels in Holstein bulls, was reported to have an increased DNA fragmentation in another study (18). Our results, regarding the role of adiponectin, are in agreement with the above observation of adiponectin levels. Hypersensitivity of sperm to reactive oxygen species (ROS) and OS, induces DNA damage (38, 39). Sperm DNA denaturation and fragmentation was reported in obese people with high ROS levels. Sperm DNA damage, was reported to be associated with morphology and motility (39, 40). In our research, sperm motility in the non-obese group (RP and progressive) was greater than the obese group, which may be due to higher level of *ADIPONECTIN* gene expression and protein in the non-obese group confirming the beneficial effect of adiponectin. We observed that especially RP sperms in the non-obese men were significantly higher than those in the obese group. However, no significant relationship was seen between the count and sperm morphology, as the determined values were located within the standard range of WHO criteria. It was reported that damage to sperm DNA is not necessarily associated with change in sperm parameters. Finally, we found no significant correlation between adiponectin levels and viability of sperm cells, denaturation and fragmentation of DNA, or molecular characteristics of the sperm cells in the obese and non-obese groups.

Conclusion

Our results showed that obesity can play an important

role in male infertility as well as in has influence on sperm motility, viability, and DNA integrity in normozoospermic men. Although, we did not discover any statistically significant correlation between adiponectin and the research variables. However, further research is required to unveil more accurate information on the extent to which adiponectin may mediates sperm functions, to reduce the risk of male infertility. Such potential treatment may especially be useful in cases where infertility is related to obesity and metabolic syndromes. In light of the current knowledge, adiponectin could be suggested as a marker for sperm function, which can be determined in further research.

Acknowledgements

This study was funded by Isfahan University of Medical Sciences, Isfahan, Iran. We thank Mrs. Shahla Ishaqi, Andrology Unit of Saint Maryam Fertility and Infertility Center of Shahid Beheshti Hospital, for her generous technical assistance. The authors declare that they have no conflict of interest in this study.

Author' Contributions

G.R.D.; Contributed to concept and design of the study, and final approval of the manuscript, and responsible for overall supervision. G.R.D., M.P., M.Sh.; Performed all the experiments, analyzed the data and interpreted them. G.R.D., M.P.; Drafting the manuscript. All authors read, and approved the final version of the manuscript.

References

1. Trayhurn P, Beattie JH. Physiological role of adipose tissue: white adipose tissue as an endocrine and secretory organ. Proc Nutr Soc. 2001; 60(3): 329-339.
2. Sengupta P, Dutta S, Tusimin M, Karkada I. Orexins and male reproduction. Asian Pac J Reprod. 2019; 8(5): 233-238.
3. Darbandi M, Darbandi S, Agarwal A, Sengupta P, Durairajanayagam D, Henkel R, et al. Reactive oxygen species and male reproductive hormones. Reprod Biol Endocrinol. 2018; 16(1): 87.
4. Flegal KM, Kit BK, Orpana H, Graubard BI. Association of all-cause mortality with overweight and obesity using standard body mass index categories: a systematic review and meta-analysis. JAMA. 2013; 309(1): 71-82.
5. Hammoud AO, Gibson M, Peterson CM, Meikle AW, Carrell DT. Impact of male obesity on infertility: a critical review of the current literature. Fertil Steril. 2008; 90(4): 897-904.
6. Vatandoust N, Rami F, Salehi AR, Khosravi S, Dashti G, Eslami G, et al. Novel high-fat diet formulation and streptozotocin treatment for induction of prediabetes and type 2 diabetes in rats. Adv Biomed Res. 2018; 7: 107.
7. Leisegang K, Sengupta P, Agarwal A, Henkel R. Obesity and male infertility: mechanisms and management. Andrologia. 2021; 53(1): e13617.
8. Jafari-Adli S, Jouyandeh Z, Qorbani M, Soroush A, Larijani B, Hasani-Ranjbar S. Prevalence of obesity and overweight in adults and children in Iran; a systematic review. J Diabetes Metab Disord. 2014; 13: 121.
9. Meldrum DR, Morris MA, Gambone JC. Obesity pandemic: causes, consequences, and solutions-but do we have the will? Fertil Steril. 2017; 107(4): 833-839.
10. Sengupta P, Borges E Jr, Dutta S, Krajewska-Kulak E. Decline in sperm count in European men during the past 50 years. Hum Exp Toxicol. 2018; 37(3): 247-255.
11. Nguyen RH, Wilcox AJ, Skjaerven R, Baird DD. Men's body mass index and infertility. Hum Reprod. 2007; 22(9): 2488-2493.
12. Kort HI, Massey JB, Elsner CW, Mitchell-Leef D, Shapiro DB, Witt MA, et al. Impact of body mass index values on sperm quantity and quality. J Androl. 2006; 27(3): 450-452.
13. Suleiman JB, Nna VU, Othman ZA, Zakaria Z, Bakar ABA, Mohamed M. Orlistat attenuates obesity-induced decline in steroidogenesis and spermatogenesis by up-regulating steroidogenic genes. Andrology. 2020; 8(5): 1471-1485.
14. Leal Vde O, Mafra D. Adipokines in obesity. Clin Chim Acta. 2013; 419: 87-94.
15. Elfassy Y, McAvoy C, Fellahi S, Dupont J, Fève B, Levy R, et al. Seminal plasma adipokines: involvement in human reproductive functions. Eur Cytokine Netw. 2017; 28(4): 141-150.
16. Paasch U, Grunewald S, Kratzsch J, Glander HJ. Obesity and age affect male fertility potential. Fertil Steril. 2010; 94(7): 2898-2901.
17. Fève B, Bastard JP. Adiponectine et carcinogenèse mammaire: rôle physiopathologique et intérêt thérapeutique. Obésité. 2014; 9(3): 191-196.
18. Kasimanickam VR, Kasimanickam RK, Kastelic JP, Stevenson JS. Associations of adiponectin and fertility estimates in Holstein bulls. Theriogenology. 2013; 79(5): 766-77. e1-3.
19. Meneghini MA, Galarza RA, Flores Quiroga JP, Faletti AG. Diet-induced maternal obesity and overnutrition cause a decrease in the sperm quality of the offspring. J Nutr Biochem. 2022; 103: 108966.
20. Cooper TG, Noonan E, von Eckardstein S, Auger J, Baker HW, Behre HM, et al. World Health Organization reference values for human semen characteristics. Hum Reprod Update. 2010; 16(3): 231-245.
21. World Health O. WHO laboratory manual for the examination and processing of human semen. 5th ed. Geneva: World Health Organization; 2010.
22. Dashti GR, Nateghian Z, Golshan Iranpour F. Effect of preservation of human semen sample at 4-6 and 25 ˚C on sperm motility. Cell Tissue Bank. 2018; 19(4): 653-658.
23. Golshan Iranpour F, Fazelian K, Dashti GR. Thymoquinone as a natural spermostatic substance in reproductive medicine: An experimental study. Int J Reprod Biomed. 2017; 15(10): 641-648.
24. Mosmann T. Rapid colorimetric assay for cellular growth and survival: application to proliferation and cytotoxicity assays. J Immunol Methods. 1983; 65(1): 55-63.
25. Buranaamnuay K. The MTT assay application to measure the viability of spermatozoa: a variety of the assay protocols. Open Vet J. 2021; 11(2): 251-269.
26. Ghasemi N, Dashti GR, Amoozgar F, Vaez SA. Effect of cholesterol, iron and vitamin E on protamine deficiency and DNA fragmentation of male rabbit sperm. J Isfahan Med Sch. 2014; 31(259): 1769-1778.
27. Golshan Iranpour F, Nateghian Z, Henkel R, Dashti GR. Effects of temperature and storage time on the motility, viability, DNA integrity and apoptosis of processed human spermatozoa. Andrologia. 2020; 52(2): e13485.
28. Rarani FZ, Golshan-Iranpour F, Dashti GR. Correlation between sperm motility and sperm chromatin/DNA damage before and after cryopreservation and the effect of folic acid and nicotinic acid on post-thaw sperm quality in normozoospermic men. Cell Tissue Bank. 2019; 20(3): 367-378.
29. Jensen TK, Andersson AM, Jørgensen N, Andersen AG, Carlsen E, Skakkebaek NE. Body mass index in relation to semen quality and reproductive hormonesamong 1,558 Danish men. Fertil Steril. 2004; 82(4): 863-870.
30. Martini AC, Tissera A, Estofán D, Molina RI, Mangeaud A, de Cuneo MF, et al. Overweight and seminal quality: a study of 794 patients. Fertil Steril. 2010; 94(5): 1739-1743.
31. Stewart TM, Liu DY, Garrett C, Jørgensen N, Brown EH, Baker HW. Associations between andrological measures, hormones and semen quality in fertile Australian men: inverse relationship between obesity and sperm output. Hum Reprod. 2009; 24(7): 1561-1568.
32. Kadivar A, Khoei HH, Hassanpour H, Golestanfar A, Ghanaei H. Correlation of adiponectin mRNA abundance and its receptors with quantitative parameters of sperm motility in rams. Int J Fertil Steril. 2016; 10(1): 127-135.
33. Thomas S, Kratzsch D, Schaab M, Scholz M, Grunewald S, Thiery J, et al. Seminal plasma adipokine levels are correlated with functional characteristics of spermatozoa. Fertil Steril. 2013; 99(5): 1256-1263. e3.
34. Bieniek JM, Kashanian JA, Deibert CM, Grober ED, Lo KC, Brannigan RE, et al. Influence of increasing body mass index on semen and reproductive hormonal parameters in a multi-

institutional cohort of subfertile men. Fertil Steril. 2016; 106(5): 1070-1075.
35. Jonas MI, Kurylowicz A, Bartoszewicz Z, Lisik W, Jonas M, Domienik-Karlowicz J, et al. Adiponectin/resistin interplay in serum and in adipose tissue of obese and normal-weight individuals. Diabetol Metab Syndr. 2017; 9: 95.
36. Eskandari F, Momeni HR. Protective effect of silymarin on viability, motility and mitochondrial membrane potential of ram sperm treated with sodium arsenite. Int J Reprod Biomed. 2016; 14(6): 397-402.
37. Cui X, Jing X, Wu X, Yan M. Protective effect of resveratrol on spermatozoa function in male infertility induced by excess weight and obesity. Mol Med Rep. 2016; 14(5): 4659-4665.
38. Hammadeh M, Radwan M, Al-Hasani S, Micu R, Rosenbaum P, Lorenz M, et al. Comparison of reactive oxygen species concentration in seminal plasma and semen parameters in partners of pregnant and non-pregnant patients after IVF/ICSI. Reprod Biomed Online. 2006; 13(5): 696-706.
39. Golshan Iranpour F, Zamani Rarani Z, Dashti GR. Effect of chromatin condensation on frozen-thawed sperm DNA integrity in normozoospermic men. Sci J Kurd Univ Med Sci. 2019; 24(3): 34-42.
40. Elbashir S, Magdi Y, Rashed A, Ibrahim MA, Edris Y, Abdelaziz AM. Relationship between sperm progressive motility and DNA integrity in fertile and infertile men. Middle East Fertil Soc J. 2018; 23(3): 195-198.

Original Article

Mutant Allele of CD44 (rs8193C>T) and Pum2 Regulatory Element as A Prognosis Factor of Prostate Neoplasms: A Case-Control and In Silico Studies

Mohammadkazem Heydari, M.Sc.[1], Abasalt Hosseinzadeh Colagar, Ph.D.[1]*, Emadoddin Moudi, Ph.D.[2]

1. Department of Molecular and Cell Biology, Faculty of Science, University of Mazandaran, Babolsar, Iran
2. Department of Urology, Babol University of Medical Sciences, Babol, Iran

Corresponding Address: P.O.Box: 47416-95447, Department of Molecular and Cell Biology, Faculty of Science, University of Mazandaran, Babolsar, Iran
Email: ahcolagar@umz.ac.ir

Received: 13/February/2022, Accepted: 08/June/2022

Abstract

Objective: Expression of CD44 variant 6 (CD44v6) as a homing-associated cell adhesion molecule (HCAM), has proved to change most cancer cells. Aim of the study is the effect of mutant allele of *CD44* (rs8193C>T) and Pum2 regulatory element as a prognosis factor of prostate neoplasms: a case-control and in silico studies in the Mazandaran province-Iran.

Materials and Methods: In a case-control study, CD44-rs8193C>T genotyping of the 420 prostate neoplasms (210 benign prostatic hyperplasia (BPH) patients and 210 prostate cancer patients) and 150 healthy samples are performed by the touchdown polymerase chain reaction with confronting two-pair primers (PCR-CTPP) method. The T mutant allele effects on the mRNA structure and cell pathways were also investigated in silico methods.

Results: Our results showed that the increase of T mutant allele frequency was significantly associated with BPH compared with prostate cancer. Furthermore, results showed TT genotype was significantly associated with BPH [odds ratio (OR)=0.572 and P=0.015], and also influenced the CD44v6 transcript secondary structure, miRNA binding, and regulatory element-binding site for Pum2 protein. Attachment of Pum2 to standard CD44 transcript may lead to transcript isoform-switching and shift-expression to a variety of CD44 isoforms, which can trigger some of the cell signaling pathways, such as Nanog-Stat, PKC-Nanog, and PKC-Twist.

Conclusion: Based on this, the presence of the T mutant allele of CD44 (rs8193C>T) in the populations may create a regulatory element-binding site for Pum2. So, it could be known as a prognosis factor and prediction of prostate neoplasms. However, more comprehensive studies in different populations (with various ethnicities and large population sizes), and also CD44v6 gene expression studies in protein and transcript levels are required to confirm our data.

Keywords: CD44, Neoplasm, Prostate, Pum2

Cell Journal(Yakhteh), Vol 24, No 12, December 2022, Pages: 723-731

Citation: **Heydari M, Hosseinzadeh Colagar A, Moudi E. Mutant allele of CD44 (rs8193C>T) and Pum2 rgulatory element as a prognosis factor of prostate neoplasms: a case-control and in silico studies. Cell J. 2022; 24(12): 723-731. doi: 10.22074/cellj.2022.8468.**

Introduction

The prostate neoplasm or tumor refers to a group of cells with unregulated growth and cell proliferation. There are two types of prostate tumors: benign prostatic hyperplasia (BPH) and malignant tumor, malignant tumor generally known as prostate cancer (1). Prostate cancer is known as the second most frequent cancer in men and the worldwide fifth leading cause of death. There are several risk factors for prostate cancer including age, ethnicity, family history, genetic disorders, or genetic risk factors (2). The gene risk factors occur as a chromosome and nucleotide-level genomic instability. The chromosome instability may happen due to the change of number (aneuploidy), structure (e.g., translocation, inversion, or duplication), or both. However, nucleotide-level genomic instability includes single nucleotide variations (SNVs) and small insertion/deletions (3). Single-nucleotide polymorphisms (SNPs) are one of the SNVs by redundancy upper than 1%. They happen in a variety of genes, correlated to prostate neoplasm e.g., *HPC1*, *HPC2* (4), *MSMB*, *KLK2-3* (5), *HNF1B* (6), and *CD44* (7).

CD44 is an integral cell surface protein that has been referred to as a homing-associated cell adhesion molecule (HCAM), phagocytic glycoprotein-1 (Pgp-1), Hermes antigen, lymphocyte homing receptor, extracellular matrix receptor III (ECMRIII) (8), and HUTCH-1. CD44 is a mouse IgG2a mAb derived from the fusion of NS-1 myeloma cells to spleen cells from a BALB/c mouse immunized with whole macaque peripheral blood mononuclear cell/PBMC (9). In humans, its protein-coding gene is located on chromosome 11p13 with about 443500 base pairs and 20 exons. Its largest variant CDS has a 5437 bp with 19 exons because exon 19 is normally spliced out (10).

CD44 protein contains four domains: two N-terminal extracellular regions (globular- and stem), a helical transmembrane domain, and a cytoplasmic domain (10). The globular- extracellular region, which is glycosylated and acts as a ligand-binding site, is encoded by exons 1 to 5, stem- the extracellular region is encoded by exons 6 to 17, the helical domain is encoded by exon 18, and cytoplasmic domain (C-terminal) is encoded by exon 20 (8). Alternative splicing of hnRNA-CD44 transcripts led to CD44 different isoforms (CD44v), which named CD44v1 to CD44v10. These CD44vs may have individual or incorporations

sequences encoded by exons 6-15 (also named CD44v1-CD44v10), inserted in the stem in the extracellular region (10). When all variable exons (v1-v10 in humans) are spliced out it is called standard CD44 (CD44s).

Some researchers commented that CD44 isoforms may have interplay with a variety of cell signaling pathways so, it is considered to be a signaling hub and interact with several ligands. Some of these ligands are protein receptors including EGF, TGF-β (11), etc., and extracellular martial including serglycin, osteopontin, collagen (12), etc. These interactions can lead to proliferation, adhesion, migration, and invasion of cells (13). On the other hand, researchers emphasized that *CD44* gene variants can lead to various diseases (14, 15).

Previous researchers reported that CD44 receptors, as CAMs, play an important role in metastasis and homing of cells (16). Also, their expressions inhibit tumor growth (17), so their gene modification is associated with several cancers (15). On the other hand, some researchers reported that two isoforms of CD44 (CD44s and CD44v6) are very important when they are expressed by alternative splicing of a single mRNA in the prostate neoplasm (18). These researchers showed that expression of CD44s in prostate adenocarcinoma is lost and may predict a poor prognosis independent of stage and grade. Heider et al. (19) also characterized a high-affinity monoclonal antibody specific for CD44v6, which is a candidate for immunotherapy of squamous cell carcinomas. Certain CD44 isoforms, especially CD44v6 have been implicated in tumorigenesis, tumor cell invasion, and metastasis (20).

We hypothesize that single nucleotide mutations in populations alter transcription factors or create new locations for regulatory factors on the gene transcripts, which are the shift expression of these protein isoforms. Previous studies showed the correlation of the CD44 SNPs (21) to several cancers including breast- (22), prostate- (7), and bladder- (23) cancers. For example, rs187115T>C of CD44 is associated with non-small cell lung cancer/ NSCLC risk (24). Also, rs353639T>G of CD44 may have a risk for bladder cancer (23), and rs8193C>T, which is located in the 3′UTR area of all variants except for CD44v8, is statistically associated with the risk of gastric cancer (25).

In this study, the association of the CD44-rs8193C>T mutant allele with prostate neoplasms (BPH and prostate cancers) (North of Iran), as well as its probable effects on CD44v6 structure and cell signaling pathways have been studied in Mazandaran province.

Materials and Methods

Samples collection

The intravenous blood of 570 samples including two case groups of BPH (210 patients) and prostate cancers (210 patients) without any cancer treatments such as prostatectomy, radiotherapy, and chemotherapy and 150 healthy men, without any history of prostate cancer, as a control group was included in this case-control study. The patients were histologically verified for BPH and prostate cancer, and control groups without any history of prostate cancer. Five milliliters of the case and control blood from the same geographical origin (Mazandaran, Iran) were collected into tubes containing $EDTA_{Na2}$ as an anticoagulant. All samples were prepared from some Mazandaran hospitals (Nimeh-e-Shaban, Sari; Babol Clinic and Rhohani Hospital of Babol, Iran) from September 2018 to March 2020.

This study is approved by the Ethics Committees of Mazandaran University of Medical Science (IR.UMZ.REC.1400.001) and all subjects signed an informed consent form before entering the study.

Genotyping by touchdown PCR-CTPP

Genomic DNA is extracted by the phenol-chloroform DNA extraction method from white blood cells (26). The CD44 genotypes were detected with the PCR-confronting two-pair primers (PCR-CTPP) method, as DNA fragments of the SNP (rs8198C>T) were amplified with four primers (Table 1). Touchdown PCR-CTPP fragment lengths are shown in Figure 1. Touchdown PCR program was used for amplification of DNA fragments, under Table 1 conditions in 25 µl of PCR total volume, by DNA thermal cycler (Master Cycler Gradient, Eppendorf Co., Germany).

Table 1: PCR conditions and oligomers used as primers

Primers names	Oligomers (5′-3′)*	PCR conditions	Cycles and thermal conditions	Twin primers: PCR products (bp)
C8193T-OF	TGTATTCCTGATCGCCAACCTTTC	0.25 U, Taq polymerase; 0.2 mM, mix dNTP;0.35 µM each of forward and reverse primers; 4 mM, $MgCl_2$; 7.5%, DMSO; 0.1 mg/ml, BSA; 2.5 µl of 10X AMS buffer (750 mM, Tris-Cl, pH=8.8; 200 mM, $(NH4)_2SO_4$; 0.1% Tween 20); and ~30 ng of t-DNA	4 minutes at 94˚C; 2 cycles (45 secods at 94˚C, 30 seconds at 64˚C, 30 seconds 72 ˚C); 2 cycles (45 seconds at 94˚C, 30 seconds at 63˚C, 30 seconds 72 ˚C); 2 cycles (45 seconds at 94˚C, 30 seconds at 62˚C, 30 seconds 72 ˚C); 2 cycles (45 seconds at 94˚C, 30 seconds at 61˚C, 30 seconds 72 ˚C); 25 cycles (45 seconds at 94˚C, 30 seconds at 60˚C, 30 seconds 72 ˚C); Final exten:10 minutes at 68-72˚C	*C8193T-OF / -OR*: 533
C8193T-OR	ATGAGATTTGGCTGAGTGGGTC			*C8193T-IF / -OR*: 427
C8193T-IF	GCCTAATCCCTGGGCATTGT			*C8193T-OF / -IR*: 147
C8193T-IR	CCCCAACCTCAGTGGAAAG			

PCR; Polymerase chain reaction, * Oligomers; Synthesized by CinnaClon Co, Iran, bp; Base pair, t-DNA; Template DNA, OF; Outer forward, IF; Inter forward, OR; Outer revers, and IR; Inter revers.

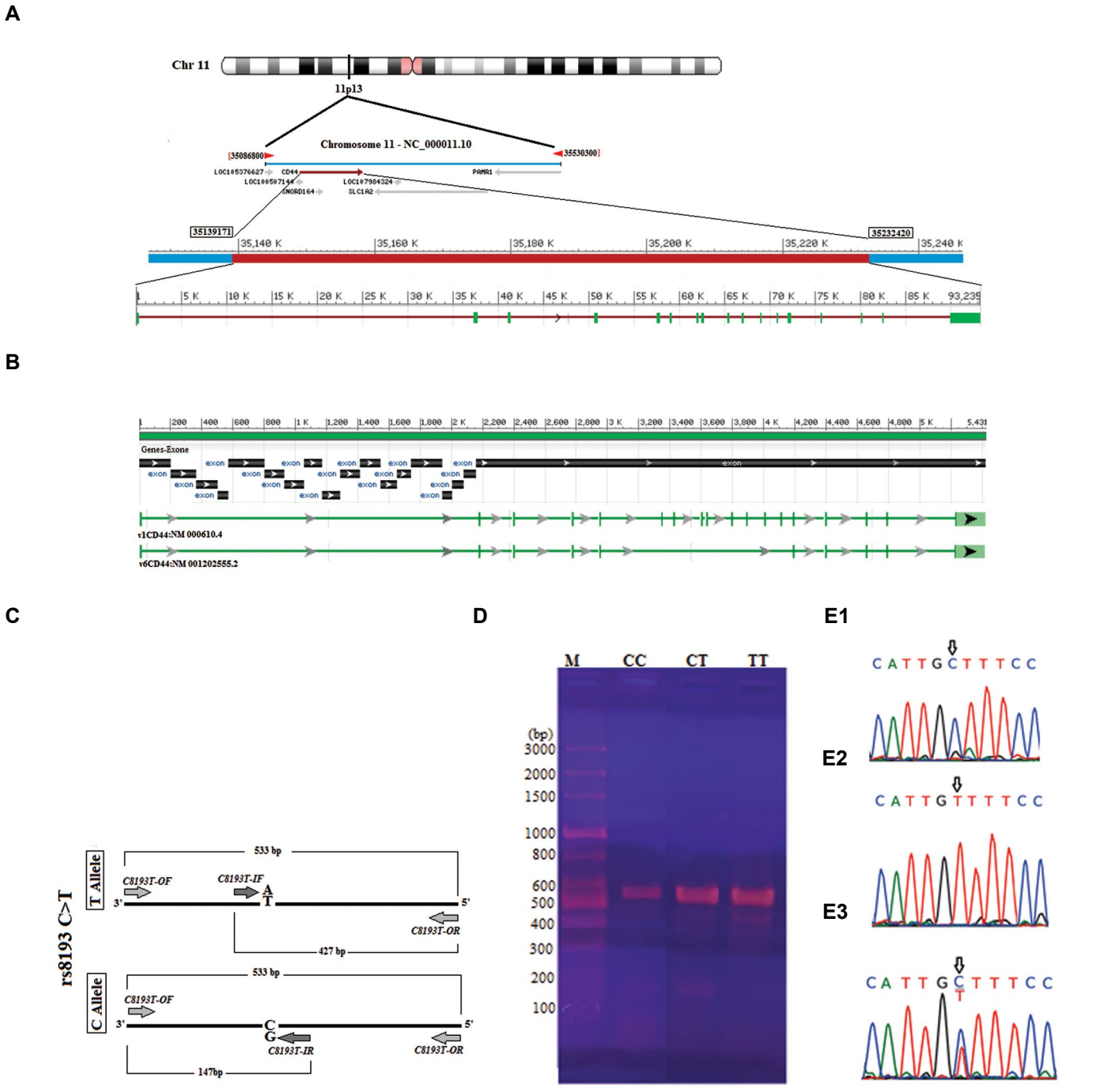

Fig.1: Schematic drawing of the *CD44* gene region on chromosome 11, and Touchdown PCR-CTPP mapping. **A.** Map of *CD44* gene with 93249 bp, retrieved from NCBI database # NC:000011.10. **B.** mRNA transcript of CD44v1 with 18 exons and 5431 bp, as the longest transcript, and CD44v6 transcript with 10 exons and 4492 bp, which studied in this paper. **C.** Touchdown PCR-CTPP diagrammatic map and its products length, that performed by four primers for diagnostic T allele and C allele of the rs8193C>T. **D.** PCR product pattern in the 1.5% agarose gel electrophoresis, which stained by 0.1 µg/ml ethidium bromide. CC, TC, and TT lanes are genotypes, M; Mid-range DNA ladder (Jena Bioscience JmbH Co. Germany), **E1.**, **E2.** and **E3.** Electropherogram results of PCR direct sequence of CC, TT, and TC genotypes, respectively. PCR-CTPP; Touchdown polymerase chain reaction with confronting two-pair primers.

All PCR reactants and chemical materials were purchased from SinnaClon Co (Iran) and Merck Co. (Germany), respectively. PCR fragments were electrophoresed in 1.5% agarose gel, stained in the 1 µg/ml of ethidium bromide solution, and observed by UV-transilluminator (ProteinSimple Red SA-01587, Co, USA). Then, at least three PCR product samples from any genotypes were sequenced by Bioneer Co. (Korea) for confirmation of PCR-CTPP results. Subsequently, electropherograms of the sequences were analyzed by Chromas ver 2.0 software.

Data sources for in silico analysis

The bioinformatics analysis used for SNPs selection is based on the information of the NCBI (https://www.ncbi.

nlm.nih.gov) data bank. To investigate and influences of rs8193C>T on the stability of the CD44 (mRNA) RNAsnp web server was used (https://rth.dk/resources/rnasnp). RegRNA2.0 (http://regrna2.mbc.nctu.edu.tw) is used for UTR motifs and their regulatory transcription factors. For the presence or absence of microRNAs (miRNAs), the miRNA SNP-v3 database (http://bioinfo.life.hust.edu.cn/miRNASNP) is used by targets gain/loss by SNP in miRNA seed modules, which provides the effect of SNPs in miRNA seed regions. In this module, at first miRNA wild sequence and SNP allele sequence were given. Then, two target prediction tools Targetscan (http://www.targetscan.org/vert_72/) and Miranda (http://www.microrna.org/microrna/home.do) web servers were used for the prediction of target sites, respectively. If one target shows in both SNP Targetscan (ST) and SNP Miranda (SM) web servers but not in either Wild Targescan (WT) or Wild Miranda (WM) web servers, it is called the miRNA gained one target gene. Study of signaling pathway performed by Kyoto encyclopedia of genes and genomes (KEGG) database (https://www.genome.jp/kegg/pathway.html). *CD44* gene expression, both on the RNA transcript and protein levels, in the various human tissues, was done by the human protein atlas (HPA) data bank (https://www.proteinatlas.org/).

Post-transcriptional UTR regulatory motif elements of CD44v6-rs8193C>T were analyzed by scanning for motifs (SFM) free web server (http://crispr.otago.ac.nz/). In this web server regulatory elements calculate with a matching score <= 0.175 per thousand bases analysis from the Transterm database (http://crispr.otago.ac.nz/newTTDB/) and protein binding sites from RNA binding protein database (RBPDB) (http://rbpdb.ccbr.utoronto.ca/index.php), which frequency matrices are available with an E-value <= 1.

Statistical analysis

Statistical genotype and allele differences and frequencies between normal and BPH; normal and cancer groups were analyzed by a Chi-squared ($\chi 2$) test so odds ratios (ORs) and 95% confidence interval (95% CI) were calculated for various alleles and genotypes. A two-tailed $P<0.05$ was considered statistically significant. All statistical analyses were performed by SPSS ver. 19 (SPSS Inc., IBM Corp Armonk, NY, USA).

Results

In silico analysis of CD44-SNPs

In the preliminary of the CD44-SNPs, we found that this gene contains 156 SNPs loci with allele frequency (MAF) ≥ 0.1 (https://www.ncbi.nlm.nih.gov). From these SNPs, 12 were intron-SNPs (rs7116432A>G, rs7110737T>A, rs379410T>C, rs3794109A>G, rs3794105G>A, rs353647C>G, rs353637A>T, rs353630G>A, rs353623G>A, rs353618T>C, rs353612G>A and rs112762C>T) which associated with clinical patients (https://www.ncbi.nlm.nih.gov/clinvar/), and five of them are 3'UTR-SNPs (rs7116432A>G, rs11607862C>T, rs7116739G>C, rs13347C>T and rs8193C>T). Three SNPs (rs7116432A>G, rs11607862C>T, rs7116739G>C) are in the 3'UTR region of variant 8 of CD44 (CD44v8), but other variants (CD44v1-CD44v10) were in intron regions. Furthermore, two SNPs (rs13347C>T and rs8193C>T), which are located in the 3'UTR area, were found in other variants (including CD44v6) except CD44v8. On the other hand, MAF of rs8193C>T (0.35 and 0.65 for C- and T- alleles, respectively), which have been reported in South Asian populations in the 1000 Genomes project, was selected in this study in Mazandaran province (North of Iran) populations.

Studying the effects of rs8193C>T on the stability of the CD44v6 transcript using the RNAsnp server showed that these SNPs loci have no significant effect on the stability of the CD44v6 transcript (P=0.2969). While there is a slight change in the structure of the CD44v6 transcript in both the mutant and wild forms in rs8193C>T, which is associated with a change in free energy from -109.30 to -111.30 (Fig.2A1-4).

Analysis of the post-transcriptional regulatory elements analysis of CD44v6 -rs8193C>T showed that the wild allele of this variant (C-allele) matches to P-element somatic inhibitor (Psi), embryonic lethal, abnormal vision- like 1 (ELAV1) and Y box binding protein 1 (YBX1) but T-mutant allele of CD44v6-rs8193C>T match to ELAV1, Pumilio homolog 2 (Pum2), and Psi (Fig.2B). The effects of rs8193C>T variants on affinity CD44v6 transcript with miRNAs were analyzed using the miRNA SNP-v3 database. As a result, the CD44v6 transcript gains four miRNAs and a loss of six miRNAs (Table 2). On the other hand, our study with the KEGG database showed that CD44 as a receptor can be bound to extracellular materials, especially hyaluronic acid (HA), and collaborated in at least six important pathways. These interactions are involved in angiogenesis, cell -growth, -survival, -differentiation, -invasion, and -migration. For example, it can result in "cell growth and survival" and "cell migration and invasion", by activating two downstream pathways with Nanog and Twist transcriptional factors.

The analysis of CD44 expression in two transcript and protein levels by the HPA databank showed that there is a significant difference between RNA transcript levels and protein levels in various tissues. So, it might be expressed in some tissues (e.g., stomach and liver) but its protein level is low or not enough for detection. Conversely, CD44-RNA may be

expressed at a lower level in some tissues (e.g., breast and prostate) but its protein expression is enough or at a high level for detection.

Genotyping

The rs8193C>T statistical analysis was performed between normal vs. BPH and normal vs cancer. These analyses showed that there is a significant difference in TT genotypes between normal and BPH groups (P=0.015) but not between normal and cancer groups (P=0.086). However, there is no significant difference in CT and CT+TT genotype between normal vs BPH and normal vs cancer groups. Also, results showed that the mutated allele (T- allele) with a frequency of 54% in the normal group, and 61.66% in the BPH group has a significant difference between normal and BPH (OR=0.730 and P=0.040). However, the T allele is not associated with prostate cancer (Table 3).

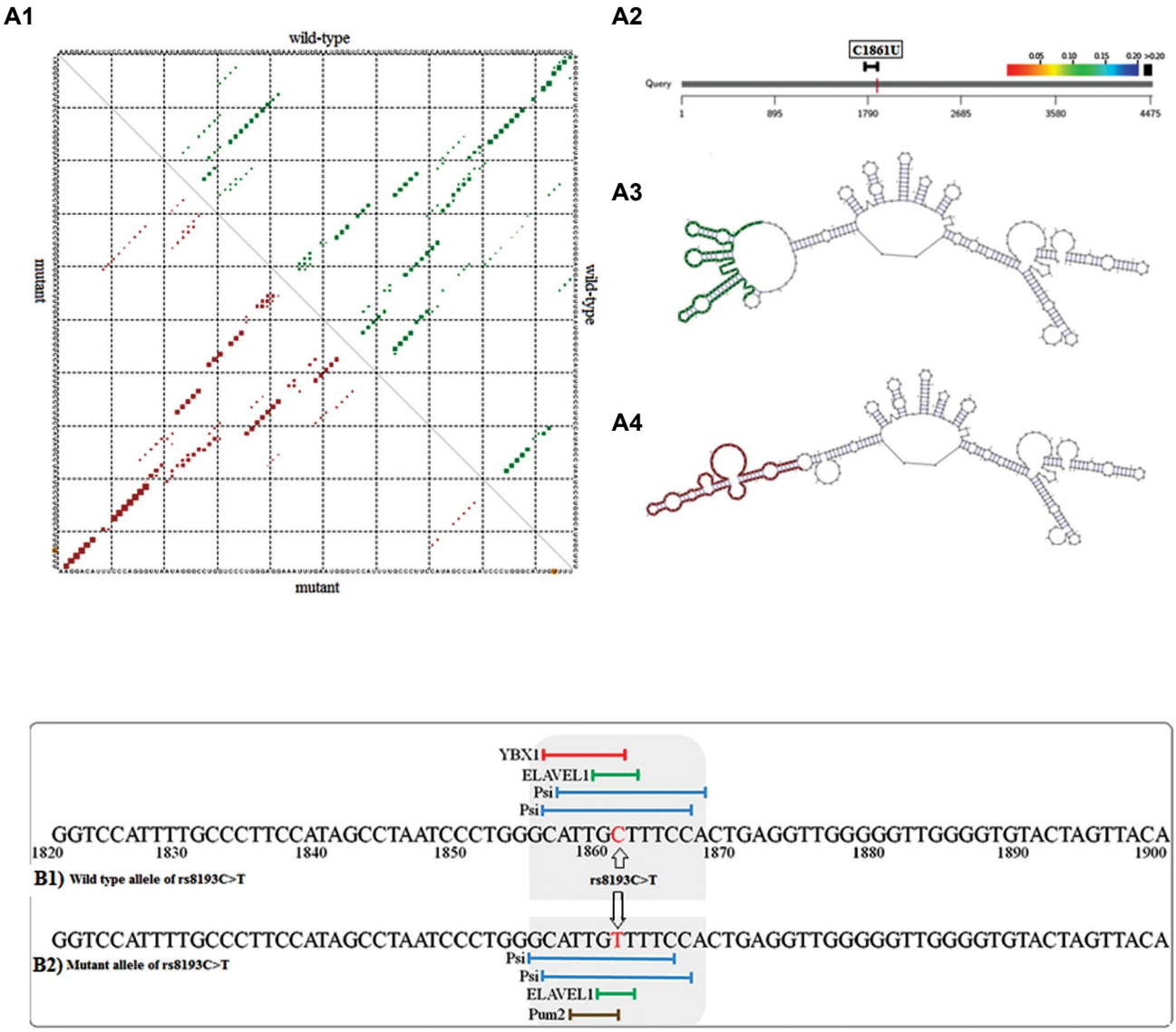

Fig.2: The result of in silico analysis. **A1-A4.** RNASNP analysis of rs8193C>T in the local region with maximum differences in wild-type and mutant mRNA. Base pair probabilities of the local region (1661-2061bp for rs8193C>T) were detected with maximum differences depicted. The upper and lower triangle of the matrix represents the base pair probabilities of wild-type and mutant sequences, respectively. **A1.** The mutated nucleotide is shown in yellow. **A2.** A graphic summary of the analysis. The SNP-affected region is colored in black since the P>0.2, which means not very significant change occurred in mRNA structure for rs8193C>T, and fewer than 0.2, which means very significant change occurred in mRNA structure for rs8198C>T with P value which is color direction. **A3.** The optimal secondary structure of global wild-type sequence (1661-2061 bp) depicted in green with the minimum free energy of -109.30 kcal/mol, and for rs8193C>T. **A4.** The optimal secondary structure of the global mutant sequence, 1661-2061bp, is shown in red with the minimum free energy equals to -111.30 kcal/mol for rs8193C>T; Retrieved from https://rth.dk/resources/rnasnp/results?jobid=579164-0212756279; 15 Feb 2020, 19:48 pm. **B.** Also, results of SFM webserver shown for **B1.** Wild type and **B2.** Mutant allele, respectively. SNP; single-nucleotide polymorphisms.

Table 2: In silico analysis rs8193C>T effects on the miRNA binding by miRNA SNP-v3 database

Gain/ Loss	miRNA	ΔG*duplex	ΔG binding	ΔG open	TargetScan score	AU content	Exact probability
Gain	hsa-miR-10523-5p	-9.70	-8.06	18.07	20.48	0.48	0.03
	hsa-miR-3148	-9.80	-10.11	18.15	21.97	0.47	0.05
	hsa-miR-570-3p	-8.90	-6.47	18.14	21.49	0.49	0.01
	hsa-miR-6124	-14.90	-15.13	18.15	23.47	0.47	0.05
Loss	hsa-miR-10527-5p	-16.20	-9.83	17.66	23.34	0.34	0.04
	hsa-miR-3908	-13.30	-11.47	17.66	21.38	0.38	0.01
	hsa-miR-3942-5p	-11.80	-6.69	17.66	20.42	0.42	0.02
	hsa-miR-4422	-11.20	-10.43	17.66	23.36	0.36	0.04
	hsa-miR-4703-5p	-11.60	-6.19	17.66	20.92	0.42	0.02
	hsa-miR-6835-3p	-10.30	-8.53	17.66	22.36	0.36	0.04

ΔG energy; kCal/mo, AU; Adenine and uracil, Gain; SNP in gene 3'UTR causes target gain, Loss; SNP in gene 3'UTR causes target loss, and SNP; Single-nucleotide polymorphisms.

Table 3: Genotype and allele frequencies of *CD44v6*-rs8193C>T were analyzed in case and control samples

Genotype	Normal (n=150)	BPH (n=210)	P value [OR (95% CI)]*	HWE	Cancer (n=210)	P value [OR (95% CI)]*	HWE
CC	30 (20)	36 (17.14)	Reference	0.395	42 (20)	Reference	0.465
CT	78 (52)	89 (42.38)	0.072 [1.473 (0.966-2.245)]	-	91 (43.33)	0.105 [1.417 (0.930-2.158)]	-
TT	42 (28)	85 (40.47)	0.015 [0.572 (0.364-0.897)]	-	77 (36.66)	0.086 [0.672 (0.427-1.057)]	-
CT+TT	120 (80)	174 (81.66)	0.490 [0.828 (0.484-1.417)]	-	168 (80)	0.912 [1.030 (0.611-1.736)]	-
C- allele	138 (46)	161 (38.33)	Reference	-	175 (41.66)	Reference	-
T- allele	162 (54)	259 (61.66)	0.040 [0.730 (0.540-0.985)]	-	245 (58.33)	0.248 [0.839 (0.622-1.130)]	-

Data are presented as n (%). OR; Odds ratio, CI; Confidence interval, HWE; P value for Hardy-Weinberg equilibrium, * OR (95% CI); OR (95% CI lower-upper).

SNP and isoform switching

Likely, the SNP of rs8193C>T led to the creation of a new regulatory element site, which is named the Pum2 protein binding site. This new regulatory element (Pum2) may cause translational inhibition and mRNA degradation. Also, it may lead to isoforms switch so, which results in overexpression of other variants or isoforms (Fig.3).

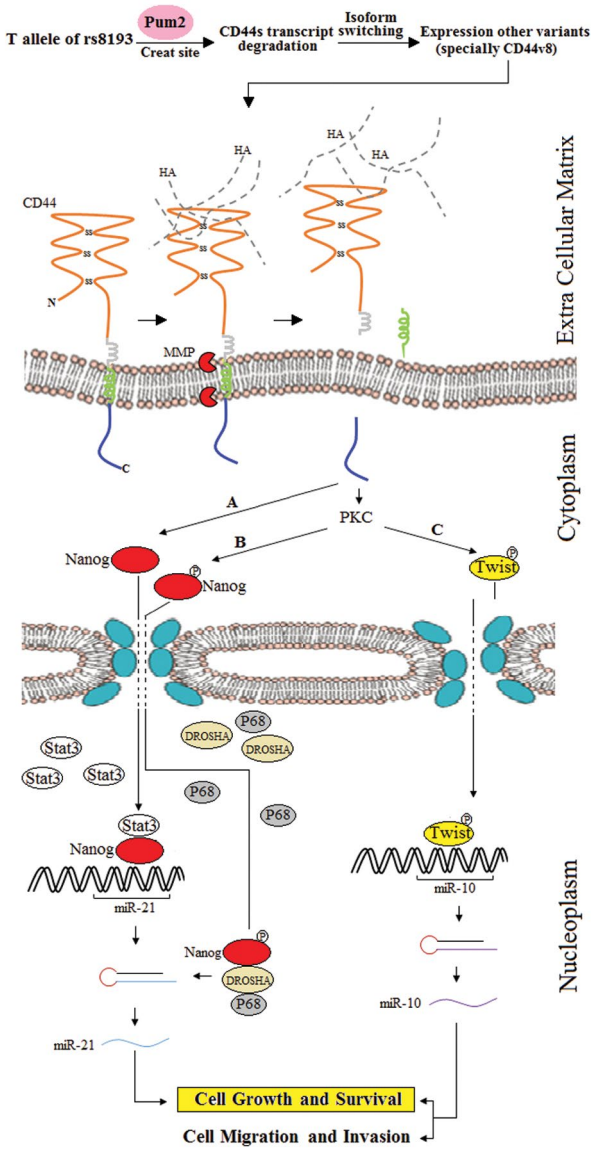

Fig.3: Effects of the CD44 rs8193C>T transition on its transcripts under mechanism of isoform switching. Pum2; Pumilio homolog 2, HA; Hyaluronic acid, CD44; Cluster of differentiation 44, MMP; Matrix metalloproteinases, PKC; Protein kinase C, Stat3; Signal transducer and activator of transcription 3, miR-21; MicroRNA-21, miR-10; MicroRNA-10, A; Nanog-Stat pathway, B; PKC-Nanog pathway, and C; PKC-Twist pathway.

Discussion

Prostate cancer is one of the most prevalent cancers among men. Risk factors of age, ethnicity, and family history could have an effect on the pathogenicity of prostate carcinogenesis (2). There are so many different genetic markers that have been reported to evaluate cancer susceptibility, including, *CD44* (7). All variant isoforms of CD44 are cell-surface glycoproteins, generated by alternative splicing and post-translational modifications (19). These CAMs are expressed in a variety of human tumors and play important roles in tumor progression, homing and metastasis (16), and inhibition of tumor growth (17). The study of its expression and gene modification has always been considered by researchers as a controversy. For instance, the correlation of SNPs of its different variants (CD44s and CD44v1-v10) (21), as a gene modification, was studied in a variety of cancers (22, 23). One of the SNPs of CD44v6, which was investigated by previous researchers is rs8193C>T. The effect of this SNP on the risk of gastric cancer (25), and colon cancer (27, 28) were studied before. The C/C genotype of CD44 rs8193C>T may be associated with higher transcriptional activity of this gene as predicted by F-SNP (29), but the analysis of the HPA data bank showed that the transcriptional activity and the level of protein produced were related to tissue types.

Previous studies showed that lncRNA-uc002kmd.1 known as a molecular decoy for miR211-3p and targets the degradation of CD44. Wu et al. (30) report that lncRNA-uc002kmd.1 mediated cell migration and proliferation in gastric cancer populations. But our study showed that there isn't any ncRNA, which matches rs8193C>T.

Gerger et al. (27) showed that the rs8193C>T variant represented a high-risk subgroup with time to tumor recurrence (TTR) in colon cancer patients, in the American population (California). Thus, patients carrying at least one T allele of CD44 rs8193C>T have longer TTR compared with patients with homozygous C/C (27). The study of Stremitzer et al. (28) in Southern California showed rs8193C>T associated with a higher radiological response rate so the C/C genotype is a lower rate compared with other genotypes, C/C 72%, any T 88%, P=0.033. Mokhtarian et al. (25) reported C allele of rs8193C>T is associated with the risk of malignancy, lymph node spread, and stage of gastric cancer, in the Iranian population (Esfahan province), while our result showed that the T allele of CD44 rs8193C>T was significantly associated with BPH with P=0.040 whereas prostate cancer with P=0.248. In addition, results showed that TT genotypes were significantly associated with BPH (P=0.015).

While Mokhtarian et al. (25) reported a correlation between rs8193C>T and gastric cancer, the results of Winder et al. (31) showed that there is no relation between rs8193C>T and gastric cancer. It seems that this difference is a result of different ethnicities.

Some researchers have reported that they did not observe any significant difference in rs8193C>T and susceptibility to breast cancer in Chinese women (32), gastric adenocarcinoma (31), and hepatocellular carcinoma (HCC) (33). However, this difference may be due to the different types of tissues and variety of the CD44 RNA and protein expression levels while our study also confirms that. Probably, rs8193C>T CD44v6 transition plays a different role in different ethnic populations and different cancer types.

The previous studies of CD44 isoform expression in the prostate neoplasm tissue showed it is different. For example, Noordzij et al. (18) showed that the expression of CD44v6 mRNA was present in 44% and 75% of the tumors and BPH samples, respectively. But Ni et al. (7) study showed that CD44v6 proteins are highly

expressed in this tissue. In silico analysis was performed the understanding the effect of rs8193C>T in populations on the altered transcription factors or the creation of new locations for transcripts regulatory factors. As shown rs8193C>T loci of CD44v6's, is located in the 3´UTR. Since, it may affect different cell functions, because 3´UTR of gene transcripts is a part of mRNA that is not translated and outright initiated from the translation termination codon, but it has important roles in the structure, function, stability, and expression of the transcript. Also, 3´UTR is mainly a site for the binding of microRNAs and ncRNAs, which regulated gene expression (34). The previous studies showed that the C allele of rs8193C>T might inflict its effect via destabilizing CD44 and miR-570 interaction (25). Whereas in silico studies showed that rs8193 C to T, gain four miRNAs and loss six miRNAs, probably. Also, results showed that rs8193C>T in CD44v6 transcript changed the RNA secondary structure and altered the expression level CD44v6 rs8193C>T transcript may be caused by RNA secondary structure or/and gain and loss of miRNAs.

Since rs8193C>T transition leads to the gain of a new regulatory element site, for Pum2 protein, and loss of YBX1, in the CD44s transcripts. Pum2 is a sequence-specific RNA-binding protein but YBX1 is a DNA- and RNA-binding protein. On the other hand, YBX1 binding to granulocyte-macrophage colony-stimulating factor/GM-CSF mRNA (GM-CSF is a cytokine that promotes eosinophil differentiation) and leads to the stabilization of mRNA and extends cell survival (35), and it can collaborate with ELAV like RNA binding protein 1/ELAVL1, which prevents mRNA decay (36). However, Pum2 mediates post-transcriptional repression of mRNAs via translational inhibition and mRNA degradation (37). Probably the attachment of Pum2 led to degradation of CD44s transcripts and stimulated switch isoforms with overexpression of other variants. The expression of CD44 isoforms affects the Nanog, in the two probably pathways. For example, i. In the Nanog-Stat pathway, Nanog translocates in the nucleus and is coupled with Stat3, and this complex arouses transcription of miR-21 resulting in cell growth and survival in cancer cells. ii. In the PKC-Nanog pathway, CD44 isoforms activate protein kinase C (PKC), and phosphorylated Nanog translocates to the nucleus. The nucleus, creates a ternary complex (p-Nanog, DROSHA, and P68) which affects miR-21 biogenesis. iii. In the PKC-Twist pathway, PKC activation cause Twist phosphorylation and translocation in the nucleus. The p-Twist binding to miR-10 and its transcription result in cell "growth and survival" and "migration and invasion" in cancer cells.

The previous studies showed the downregulation of CD44s in cancer diseases, especially in prostate cancer (38) and loss of CD44 expression was significantly associated with prostate tumor progression (7). Moura et al. (39) demonstrated that prostate neoplasm is caused by a change in the expression of CD44 isoforms which happens with a loss of CD44s and overexpression of all the other CD44 variants. Di Stefano et al. (40) showed that CD44v8-v10 overexpression might be a potential biomarker in gastric and prostate cancer, respectively. Thus, this transition affects the expression of other CD44 transcripts, under the mechanism of isoform switching. By this mechanism expression of CD44 from CD44s switches to CD44v, especially the CD44v8 isoform, because these SNPs are presented in all CD44 variants except for CD44v8.

Based on our findings, the increase of T mutant allele frequency is associated with BPH prostate neoplasm, with OR (0.572), 95% CI (0.364-0.897), and P=0.015. This transition has affected the CD44v6 transcript secondary structure (from -109.30 to -111.30 kcal/mol), miRNA binding sites (gain: four and loss: six for mutant allele), and gain of a new post-transcriptional regulatory element-binding site for Pum2 protein. It seems that the add-on of this site and this protein adjoin to standard CD44 transcript leads to degradation of this transcript, and stimulates switch-isoforms, with the overexpression of other variants. It triggers some of the cell signaling pathways such as Nanog-Stat, PKC-Nanog, and PKC-Twist which could run cell "growth and survival" and "migration and invasion" in cancer cells.

Conclusion

The presence of the T mutant allele in the populations probably can create a new location for regulatory factors on the gene transcripts, which is caused a shift in expression of this protein isoforms. Based on this study, the presence of the T mutant allele of CD44 (rs8193C>T) in the populations may affect transcripts isoform-switching. So, it is known as a prognosis factor and prediction of prostate neoplasms, probably. However, more comprehensive studies in different populations (with various ethnicities and large population sizes), and analysis of *CD44* gene expression in the protein and transcript levels, are required to confirm our data.

Acknowledgments

We would like to extend our thanks to the University of Mazandaran (Iran) for the financial support. There is no conflict of interest to declare.

Authors' Contributions

A.H.C.; Conceptualization, methodology, and software. M.H.; Data curation, writing and original draft preparation. E.M.; Sample preparing and data analysis. All authors were involved in writing this manuscript and approved the final manuscript.

Reference

1. Miah S, Catto J. BPH and prostate cancer risk. Indian J Urol. 2014; 30(2): 214-218.
2. Rawla, P. Epidemiology of prostate cancer. World J Oncol. 2019; 10(2): 63.
3. Lengauer C, Kinzler KW, Vogelstein B. Genetic instabilities in human cancers. Nature. 1998; 396 (6712): 643-649.
4. Wiklund F, Jonsson BA, Brookes AJ, Strömqvist L, Adolfsson J,

Emanuelsson M, et al. Genetic analysis of the RNASEL gene in hereditary, familial, and sporadic prostate cancer. Clin Cancer Res. 2004; 10(21): 7150-7156.
5. Lai J, Kedda MA, Hinze K, Smith RL, Yaxley J, Spurdle AB, et al. PSA/KLK3 AREI promoter polymorphism alters androgen receptor binding and is associated with prostate cancer susceptibility. Carcinogenesis. 2007; 28(5): 1032-1039.
6. Chen R, Ren S, Sun Y. Genome-wide association studies on prostate cancer: the end or the beginning? Protein Cell. 2013; 4(9): 677-686.
7. Ni J, Cozzi PJ, Hao JL, Beretov J, Chang L, Duan W, et al. CD44 variant 6 is associated with prostate cancer metastasis and chemo-/radioresistance. Prostate. 2014; 74(6): 602-617.
8. Goodison S, Urquidi V, Tarin D. CD44 cell adhesion molecules. J Mol Pathol. 1999; 52(4): 189-96.
9. Gallatin WM, Wayner EA, Hoffman PA, St John T, Butcher EC, Carter WG, et al. Structural homology between lymphocyte receptors for high endothelium and class III extracellular matrix receptor. Proc Natl Acad Sci. 1989; 86(12): 4654-4658.
10. Heldin P, Kolliopoulos C, Lin CY, Heldin, CH. Involvement of hyaluronan and CD44 in cancer and viral infections. Cell Signal. 2020; 65: 109427.
11. Bellerby R, Smith C, Kyme S, Gee J, Günthert U, Green A, et al. Overexpression of specific CD44 isoforms is associated with aggressive cell features in acquired endocrine resistance. Front Oncol. 2016; 6: 145.
12. Knutson JR, Iida J, Fields GB, McCarthy JB. CD44/chondroitin sulfate proteoglycan and alpha 2 beta 1 integrin mediate human melanoma cell migration on type IV collagen and invasion of basement membranes. Mol Biol Cell. 1996; 7(3): 383-396.
13. Günthert U, Hofmann M, Rudy W, Reber S, Zöller M, Haußmann I, et al. A new variant of glycoprotein CD44 confers metastatic potential to rat carcinoma cells. Cell. 1991; 65(1): 13-24.
14. Wang Q, Teder P, Judd NP, Noble PW, Doerschuk CM. CD44 deficiency leads to enhanced neutrophil migration and lung injury in Escherichia coli pneumonia in mice. Am J Pathol. 2002; 161(6): 2219-2228.
15. Jordan AR, Racine RR, Hennig MJ, Lokeshwar VB. The role of CD44 in disease pathophysiology and targeted treatment. Front Immunol. 2015; 6: 182.
16. Estess P, DeGrendele HC, Pascual V, Siegelman MH. Functional activation of lymphocyte CD44 in peripheral blood is a marker of autoimmune disease activity. J Clin Invest. 1998; 102(6): 1173-1182.
17. Jeyapalan Z, Deng Z, Shatseva T, Fang L, He C, Yang BB. Expression of CD44 3′-untranslated region regulates endogenous microRNA functions in tumorigenesis and angiogenesis. Nucleic Acids Res. 2011; 39(8): 3026-3041.
18. Noordzij MA, Van Steenbrugge GJ, Verkaik NS, Schröder FH, Van der kwast T. The prognostic value of CD44 isoforms in prostate cancer patients treated by radical prostatectomy. Clin Cancer Res. 1997; 3(5): 805-815.
19. Heider KH, Sproll M, Susani S, Patzelt E, Beaumier P, Ostermann E, et al. Characterization of a high-affinity monoclonal antibody specific for CD44v6 as candidate for immunotherapy of squamous cell carcinomas. Cancer Immunol Immunother. 1996; 43(4): 245-253.
20. Heider KH, Kuthan H, Stehle G, Munzer G. CD44v6: a target for antibody-based cancer therapy. Cancer Immunol Immunother. 2004; 53(7): 567-579.
21. Prochazka L, Tesarik R, Turanek J. Regulation of alternative splicing of CD44 in cancer. Cell Signal. 2014; 26(10): 2234-2239.
22. Rutnam ZJ, Yang BB. The non-coding 3′ UTR of CD44 induces metastasis by regulating extracellular matrix functions. J Cell Sci. 2012; 125(8): 2075-2085.
23. Verma A, Kapoor R, Mittal RD. Cluster of differentiation 44 (CD44) gene variants: a putative cancer stem cell marker in risk prediction of bladder cancer in north indian population. Indian J Clin Biochem. 2017; 32(1): 74-83.
24. Liu Y, Qing H, Su X, Wang C, Li Z, Liu S. Association of CD44 gene polymorphism with survival of NSCLC and risk of bone metastasis. Med Sci Monit. 2015; 21: 2694-2700.
25. Mokhtarian R, Tabatabaeian H, Saadatmand P, Azadeh M, Balmeh N, Yakhchali B, et al. CD44 gene rs8193 c allele is significantly enriched in gastric cancer patients. Cell J. 2020; 21(4): 451-458.
26. Sambrook J, Russell DW. Molecular cloning: a laboratory manual. 3th ed. New York: Cold Spring Harbor Laboratory; 2013.
27. Gerger A, Zhang W, Yang D, Bohanes P, Ning Y, Winder T, et al. Common cancer stem cell gene variants predict colon cancer recurrence. Clin Cancer Res. 2011; 17(21): 6934-6943.
28. Stremitzer S, Zhang W, Yang D, Ning Y, Stintzing S, Sunakawa Y, et al. Variations in genes involved in dormancy associated with outcome in patients with resected colorectal liver metastases. Annal Oncol. 2015; 26(8): 1728-1733.
29. Lee PH, Shatkay H. F-SNP: computationally predicted functional SNPs for disease association studies. Nucleic Acids Res. 2008; 36(Database issue): D820-D824.
30. Wu X, He X, Li S, Xu X, Chen X, Zhu H. Long non-coding RNA ucoo2kmd. 1 regulates CD44-dependent cell growth by competing for miR-211-3p in colorectal cancer. PLoS One. 2016; 11(3): e0151287.
31. Winder T, Ning Y, Yang D, Zhang W, Power DG, Bohanes P, et al. Germline polymorphisms in genes involved in the CD44 signaling pathway are associated with clinical outcome in localized gastric adenocarcinoma. Int J Cancer. 2011; 129(5): 1096-1104.
32. Lin X, You X, Cao X, Pan S. Association of single-nucleotide polymorphisms of CD44 gene with susceptibility to breast cancer in Chinese women. Med Sci Monit. 2018; 24: 3077-3083.
33. Deng Y, Chen ZJ, Lan F, He QT, Chen SY, Du YF, et al. Association of CD44 polymorphisms and susceptibility to HBV related hepatocellular carcinoma in the Chinese population. J Clin Lab Anal. 2019; 33(8): e22977.
34. Skeeles LE, Fleming JL, Mahler KL, Toland AE. The impact of 3′ UTR variants on differential expression of candidate cancer susceptibility genes. PLoS One. 2013; 8(3): e58609.
35. Capowski EE, Esnault S, Bhattacharya S, Malter JS. Y box-binding factor promotes eosinophil survival by stabilizing granulocyte-macrophage colony-stimulating factor mRNA. J Immunol. 2001; 167(10): 5970-5976.
36. Chen X, Li A, Sun BF, Yang Y, Han YN, Yuan X, et al. 5-methylcytosine promotes pathogenesis of bladder cancer through stabilizing mRNAs. Nat Cell Biol. 2019; 21(8): 978-990.
37. Van Etten J, Schagat TL, Hrit J, Weidmann CA, Brumbaugh J, Coon JJ, et al. Human Pumilio proteins recruit multiple deadenylases to efficiently repress messenger RNAs. J Biol Chem. 2012; 287(43): 36370-36383.
38. Lou W, Krill D, Dhir R, Becich MJ, Dong JT, Frierson HF Jr, et al. Methylation of the CD44 metastasis suppressor gene in human prostate cancer. Cancer Res. 1999; 59(10): 2329-2331.
39. Moura CM, Pontes J Jr, Reis ST, Viana NI, Morais DR, Dip N, et al. Expression profile of standard and variants forms of CD44 related to prostate cancer behavior. Int J Biol Markers. 2015; 30(1): e49-55.
40. Di Stefano C, Grazioli P, Fontanella RA, De Cesaris P, D'Amore A, Regno M, et al. Stem-like and highly invasive prostate cancer cells expressing CD44v8-10 marker originate from CD44-negative cells. Oncotarget. 2018; 9(56): 30905-30918.

Original Article

CTRP1 Aggravates Cardiac Fibrosis by Regulating The NOX2/P38 Pathway in Macrophages

Chenyu Li, M.D.[1], Shaozhen Ying, Ph.D.[2], Xiaolin Wu, M.D.[1], Tongjian Zhu, M.D.[1], Qing Zhou, M.D.[1], Yue Zhang, M.D.[1], Yongsheng Liu, M.D.[1], Rui Zhu, M.D.[1], He Hu, Ph.D.[1]*

1. Department of Cardiology, Xiangyang Central Hospital, Affiliated Hospital of Hubei University of Arts and Science, Xiangyang, Hubei, P.R. China
2. Department of Cardiology, Jiangxi provincial People's Hospital, Affiliated to Nanchang University, Nanchang, Jiangxi, China

***Corresponding Address: Department of Cardiology, Xiangyang Central Hospital, Affiliated Hospital of Hubei University of Arts and Science, Xiangyang, Hubei, P.R. China**
Email: 2012103020029@whu.edu.cn*

Received: 14/December/2021, Accepted: 11/October/2022

Abstract

Objective: C1q/TNF-related proteins 1 (CTRP1) is a recently identified adiponectin associated with obesity-linked disorders and adverse cardiovascular events. The effect of CTRP1 on cardiac fibrosis has not yet been fully elucidated; thus, we aimed to explore this association.

Materials and Methods: In this experimental study, a mouse model of cardiac fibrosis was established by administering isoproterenol (ISO) (subcutaneously injecting 10 mg/kg/day for 3 days and then 5 mg/kg/day for 11 days). Mice were also injected with recombinant CTRP1 protein (200 μg/kg) 14 days after the final ISO administration. Adult mouse fibroblasts were isolated and stimulated with transforming growth factor (TGF) β1, followed by treatment with recombinant CTRP1. Primary bone marrow-derived macrophages were isolated from C57BL/6J mice and treated with recombinant CTRP1 as well.

Results: CTRP1 level was increased in mouse plasma and heart tissue 2 weeks after ISO injection. Our findings indicated that recombinant CTRP1 injection aggravated ISO-induced cardiac fibrosis and dysfunction. However, recombinant CTRP1 did not alter TGFβ1-induced fibroblast proliferation and activation or collagen transcription. Recombinant CTRP1 exacerbated ISO-induced macrophage infiltration and inflammatory response. We determined that macrophages treated with recombinant CTRP1 showed increased pro-inflammatory cytokine release. Fibroblasts co-cultured with macrophages treated with recombinant CTRP1 showed increased proliferation and collagen transcription. We also found that CTRP1 upregulated the NADPH oxidase 2 (NOX2)/p38 pathway in macrophages. When we inhibited p38 signaling, the pro-inflammatory effect of CTRP1 on macrophages was counteracted. Fibroblasts co-cultured with macrophages treated with a p38 inhibitor also showed limited proliferation and collagen transcription.

Conclusion: Cardiac fibrosis was aggravated with the activation of the NOX2/p38 pathway in macrophages after CTRP1 treatment.

Keywords: Cardiac Fibrosis, CTRP1, Fibroblast, Macrophage, NOX2

Cell Journal(Yakhteh), Vol 24, No 12, December 2022, Pages: 732-740

Citation: Li Ch, Ying Sh, Wu X, Zhu T, Zhou Q, Zhang Y, Liu Y, Zhu R, Hu H. CTRP1 aggravates cardiac fibrosis by regulating the NOX2/P38 pathway in macrophages. Cell J. 2022; 24(12): 732-740. doi: 10.22074/CELLJ.2022.557327.1043.

Introduction

Cardiac fibrosis is a common pathological process in many cardiovascular diseases, including acute and chronic inflammation, myocardial ischemia, pressure overload (e.g., hypertension), aging, and genetic cardiomyopathies (1). Unlike other organs, the heart has a limited capacity to recover after injury because cardiomyocytes lack the ability to proliferate. After heart injury, fibrous tissue proliferates to maintain the integrity of heart structure and function (2). Nevertheless, many cells such as fibroblasts and macrophages play a critical role in this repair process (3). Despite this repair process which prevents myocardial dysfunction or even rupture, persistent fibrosis and inflammation hamper cardiomyocytes from accessing oxygen and nutrients, promoting adverse cardiac remodeling (1). This leads to reduced cardiac contraction and an increased arrhythmogenic risk (4). The currently available clinical drugs are not effective in treating cardiac fibrosis. Thus, finding new specific therapeutic targets for cardiac fibrosis is of great importance for improving cardiac function, reducing infarct size, and delaying incident heart failure.

Cardiac macrophages, derived from resident tissue macrophages and bone marrow progenitor cells, cooperate in the initiation and maintenance of fibrotic responses (3). In the first stage of tissue inflammation, macrophages undergo "M1-like" activation (5). M1-like macrophages aggravate the inflammatory response of the heart by releasing pro-inflammatory cytokines and promoting phagocytosis and proteolysis. At a later stage, macrophages switch to the "alternative activated" (M2-like) repair phenotype and produce anti-inflammatory cytokines, such as interleukin (IL)-10 and transforming growth factor (TGF)β1 (6). M2-like macrophages aggravate scar formation and

fibrosis by regulating the expression of extracellular matrix components and activating cardiac fibroblasts (7). Thus, targeting this "sterile" inflammation may be a useful therapeutic approach to inhibit the onset and progression of cardiac fibrosis.

CTRP1 is a member of a conserved family of secreted C1q/TNF-related proteins. Secreted hormones control energy metabolism via inter-organ crosstalk (8). Studies have reported both a protective and a deleterious effect of CTRP1 on cardiovascular diseases (9-12). Clinical studies have demonstrated that CTRP1 is a potential aggravating factor leading to adverse events. It was found that CTRP1 level was elevated in the plasma of hypertensive patients and was associated with subclinical target organ damage (11) and that increased serum CTRP1 levels increased adverse cardiovascular events in patients with coronary artery disease (13). Increased plasma CTRP1 levels were also observed in critically ill patients with sepsis and type 2 diabetes (10). Conversely, in an experimental animal model, CTRP1 seemed to have a cardioprotective effect. It was reported that CTRP1-deficient mice showed impaired glucose and lipid metabolism (14) and that CTRP1 can prevent sepsis-induced cardiomyopathy (9). These contradictory results on the role of CTRP1 still serve to indicate the close association of CTRP1 with cardiovascular disease. In the present study, we aimed to explore the functional role of recombinant CTRP1 in the mechanisms underlying cardiac fibrosis.

Materials and Methods

Animals

In this experimental study, C57BL6J male mice were purchased from Beijing Huafukang Biological Co. Ltd. (Beijing, China). The mice were divided into four groups: vehicle-NS (normal saline), CTRP1-NS, vehicle-isoproterenol (ISO), and CTRP1-ISO. Mice from the two ISO groups were injected subcutaneously with ISO (10 mg/kg/day for 3 days and then 5 mg/kg/day for 11 days). The mice in the two CTRP1 groups (n=12 for each group), following the last injection of ISO or NS, received 200 μg/kg recombinant CTRP1 full-length protein (ab151376, Abcam, Cambridge, UK) or vehicle solution for 2 weeks using an Alzet osmotic minipump (Durect, Cupertino, CA, USA). Animal experiments were performed per the guidelines of the National Institutes of Health Guidelines for the Care and Use of Laboratory Animals (NIH Publication No. 85-23, revised in 1996). All the animal experiments were reviewed and approved by Xiangyang Central Hospital's Animal Care and Use Committee.

Echocardiography measurements

Cardiac function was assessed using a Mylab30CV (ESAOTE) echocardiograph with an M-mode and pulse-Doppler 15-MHz probe. The left ventricular ejection fraction (LVEF), LV shortening fraction (LVFS), and E/A ratio were calculated.

Picrosirius red and immunohistochemical staining

The LV collagen fraction of six heart samples from each group was evaluated using Picrosirius red (PSR) staining. The images obtained were processed and analyzed using Image-Pro Plus 6.0. Immunohistochemical staining was used to detect the number of CD68-positive macrophages in the heart tissue. Anti-CD68 (Abcam) was used as the primary antibody, whereas anti-rabbit horseradish peroxidase (Gene Tech, Shanghai, China) was used as the secondary antibody. The DAB substrate kit was used for colorimetric development (Gene Tech) for visualization.

Detection of inflammatory cytokines using the enzyme-linked immunosorbent assay (ELISA)

The heart tissue and cell samples were lysed, and the levels of inflammatory cytokines, namely tumor necrosis factor α (TNFα), IL-1, IL-6, and TGFβ1, in the lysate were detected using ELISA kits (BioLegend). The ELISA kit for CTRP1 was purchased from Biovendor, Inc. (Czech Republic). After the color development using ELISA, the absorbance of the samples was measured using a microplate reader (BioTek, USA). The concentration of each inflammatory cytokine in the samples was estimated using the standard curve method.

Fibroblast isolation and culture

After removing the hearts of C57BL6J mice (4-6-week-old), the heart tissues were cut into small pieces and digested with 0.125% trypsin and collagenase five times. The samples were centrifuged and resuspended in a medium containing 10% fetal bovine serum (FBS). We used a 40-μm filter to remove large cell clumps. Then, we seeded the cells in a 10-cm dish for 90 minutes. Subsequently, non-adherent cells were removed, and α-SMA staining was used to verify that the isolated cells were fibroblasts, which were then stimulated with TGFβ1 (10 ng/μL). The control cells were treated with the same volume of phosphate-buffered saline (PBS) for 24 hours. Cells were then treated with 0, 1, 2, 4, or 8 μg/mL of CTRP1 diluted in PBS containing 0.1% bovine serum albumin (BSA) for 24 hours. The control group was treated with the same volume of PBS containing 0.1% BSA for 24 hours. A CCK-8 assay kit was used to detect cell proliferation.

Primary bone marrow-derived macrophage isolation and culture

Primary bone marrow-derived macrophages were extracted from the femur and tibia of C57BL6J male mice aged 6-8 weeks. The cells were cultured with DMEM-F12 containing 5% FBS, L-glutamine (5 mmol/L, Sigma), and recombinant macrophage colony-stimulating factor (MCSF, 25 ng/ml, Peprotech). MCSF and granulocyte-MCSF (Peprotech) were used at 25 ng/ml and 50 ng/

ml, respectively, to induce cell differentiation. Interferon (IFN)-γ (10 ng/ml, Peprotech) and lipopolysaccharides (LPS, 100 ng/ml, Sigma) were used to induce pro-inflammatory activation. Macrophages were then treated with CTRP1 (8 μg/mL) for 12 hours and co-cultured with fibroblasts. Macrophages were also treated with SB203580 (10 μM, MedChemExpress) for 12 hours to inhibit p38.

Western blot

Total proteins (50 μg/sample) were resolved using SDS-PAGE. The proteins were transferred to the Immobilon membrane and incubated with primary antibodies specific for NOX2, total p38, and p-p38 GAPDH (Cell Signaling Technology). Following incubation with the secondary antibody, a color reaction was carried out using the enhanced chemiluminescence (ECL) reagent (Bio-Rad, USA). We used a ChemiDoc MP imaging system (Bio-RAD) for color rendering.

Reverse transcription-polymerase chain reaction (RT-PCR)

The total mRNA of fibroblasts was extracted using the TRIzol reagent. A SmartSpec Plus spectrophotometer (Bio-Rad) was used to detect the ratio of OD260/OD280 to analyze mRNA purity. Two milligrams of mRNA was reverse transcribed to synthesize cDNA using a Roche Diagnostic Reverse Transcription Kit. The LightCycler 480 SYBR Green I Kit (Roche Diagnostics) was used for amplification. The PCR products were quantified using a LightCycler 480 SYBR® Green 1 Master Mix (04707516001, Roche Diagnostics). Following an initial 5 minutes denaturation step at 95˚C, a total of 42 primer-extension cycles were carried out. Each cycle consisted of a 10 seconds denaturation step at 95˚C, at 20 seconds annealing step at 60˚C, and a 20 seconds incubation at 72˚C for extension. Then a final extension step was performed at 72˚C for 10 minutes. The double standard curve was used to quantify the PCR results. The target gene expression was normalized to that of *GAPDH*, as the housekeeping gene. Primers used for RT-PCR listed as follow:

Collagen I-
F: 5′-AGGCTTCAGTGGTTTGGATG-3′
R: 5′- CACCAACAGCACCATCGTTA-3′

Collagen III-
F: 5′- AAGGCTGCAAGATGGATGCT -3′
R: 5′- GTGCTTACGTGGGACAGTCA -3′

α-SMA-
F: 5′- AACACGGCATCATCACCAAC -3′
R: 5′- ACCAGTTGTACGTCCAGAGG -3′

GAPDH-
F: 5′- ACTCCACTCACGGCAAATTC -3′
R: 5′- TCTCCATGGTGGTGAAGACA -3′

Immunofluorescence staining

Paraformaldehyde (4%) and Triton™ X-100 (0.1%) were used to fix and permeabilize the cells, respectively. The cells were incubated with anti-PCNA and anti-α-SMA (Abcam, 1:100 dilution) at 37˚C for 1 hour and then with an Alexa Fluor 568 goat anti-rabbit immunoglobulin IgG (Invitrogen Life Technologies, CA, USA) as the secondary antibody. The nuclei were stained with DAPI. Images were obtained using a fluorescence microscope.

Statistical analyses

Data are expressed as the mean ± standard deviation. Two-way way ANOVA and Tukey's post-hoc test were used to compare the four groups. An independent-sample t test was used for pairwise comparisons. Statistical significance was set at $P<0.05$.

Results

Recombinant CTRP1 aggravates ISO-induced cardiac fibrosis

The expression of CTRP1 was evaluated in the mouse plasma and heart tissues after ISO injection. As shown in Figures 1A and B, the expression of CTRP1 was sharply elevated in the plasma and heart tissue from the ISO group as compared to that from the NS group. The mice were then injected with the recombinant CTRP1 protein. The concentration of CTRP1 in the mouse plasma and heart tissue was also evaluated using an ELISA. After 14 days of consecutive recombinant CTRP1 injection, the concentration of CTRP1 increased significantly in the plasma and heart tissue of both ISO-injected and NS-control mice (Fig.1C, D). The collagen volume was detected using PSR staining. Notably, CTRP1 increased LV collagen volume in mice after ISO administration (Fig.1E). The expression of fibrosis markers, such as collagen I, collagen III, and TGFβ1, was increased in CTRP1-injected mice after ISO stimulation, as detected by using RT-PCR (Fig.1F). These data suggest that the CTRP1 protein may aggravate cardiac fibrosis.

Recombinant CTRP1 aggravates ISO-induced cardiac dysfunction

Cardiac function was assessed by echocardiography to determine the effect of CTRP1 on ISO-induced cardiac dysfunction. As shown in Figure 2A, heart rate increased in the ISO group as compared to that of the NS control group. CTRP1 injection did not affect heart rate compared with vehicle NS or ISO administration. However, similar to the ISO injection, CTRP1 injection reduced LVEF and LVFS, suggesting deteriorated systolic cardiac function (Fig.2B). ISO injection also caused a decrease in E/A value, as did CTRP1 injection, suggesting deteriorated diastolic cardiac function (Fig.2C). Taken together, recombinant CTRP1 protein contributes to cardiac fibrosis and aggravates ISO-induced cardiac dysfunction.

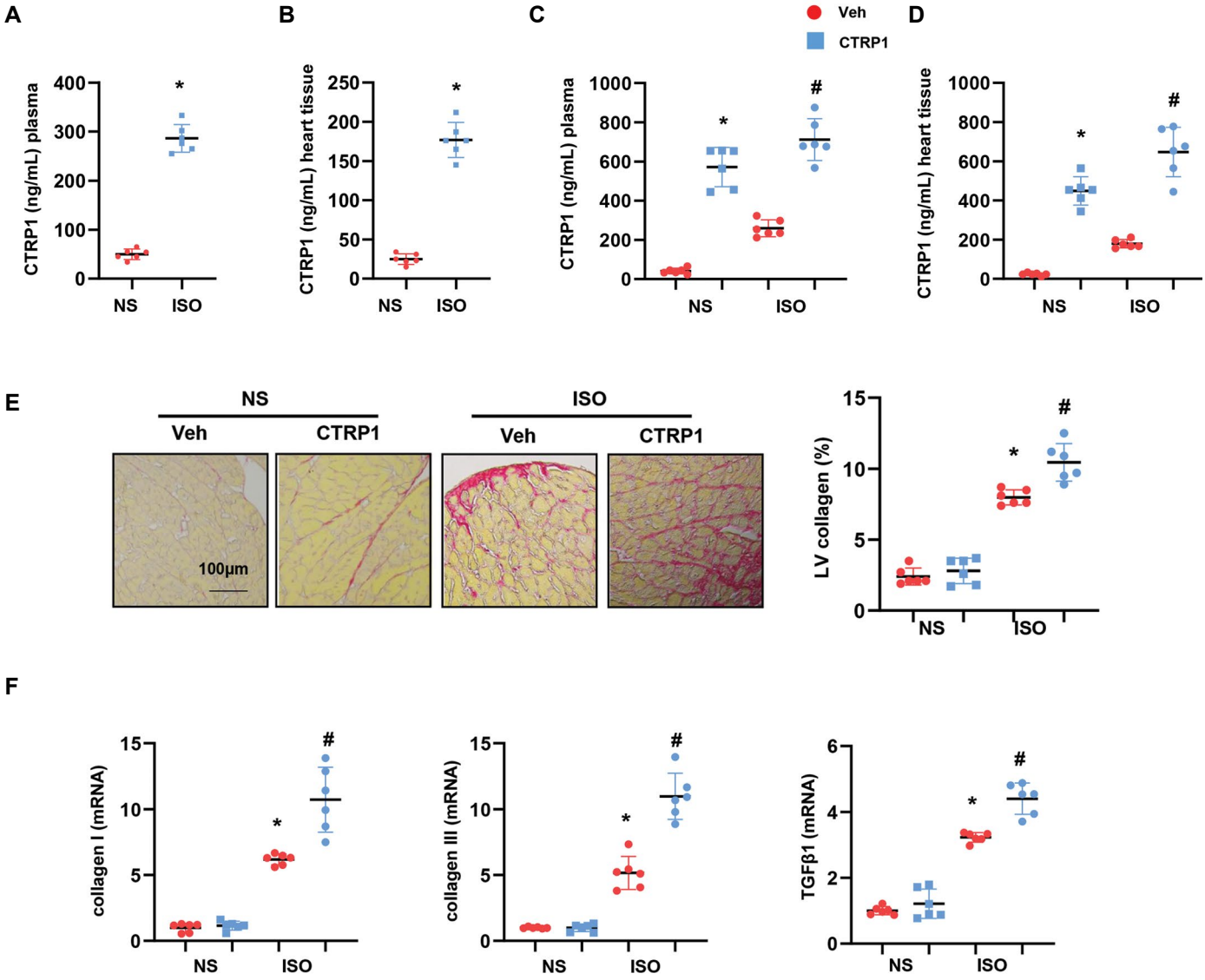

Fig.1: Recombinant CTRP1 aggravates cardiac fibrosis induced by isoproterenol (ISO)**. A.** The expression of CTRP1 in mouse plasma post-ISO injection (n=6) as detected by using enzyme-linked immunosorbent assay (ELISA). **B.** The expression of CTRP1 in mouse hearts post-ISO injection (n=6) detected by using ELISA. **C.** The expression of CTRP1 in mouse plasma post-recombinant CTRP1 injection (n=6) detected by using ELISA. **D.** The expression of CTRP1 in mouse hearts post-recombinant CTRP1 injection (n=6) detected by using ELISA. **E.** Representative image of picrosirius red (PSR) staining and quantification of left ventricular (LV) collagen volume (n=6). **F.** Transcription level of fibrosis markers in mouse hearts (n=6). *; P<0.05 vs. NS-Veh group, #; P<0.05 vs. ISO-Veh group, NS; Normal saline, and Veh; Vehicle.

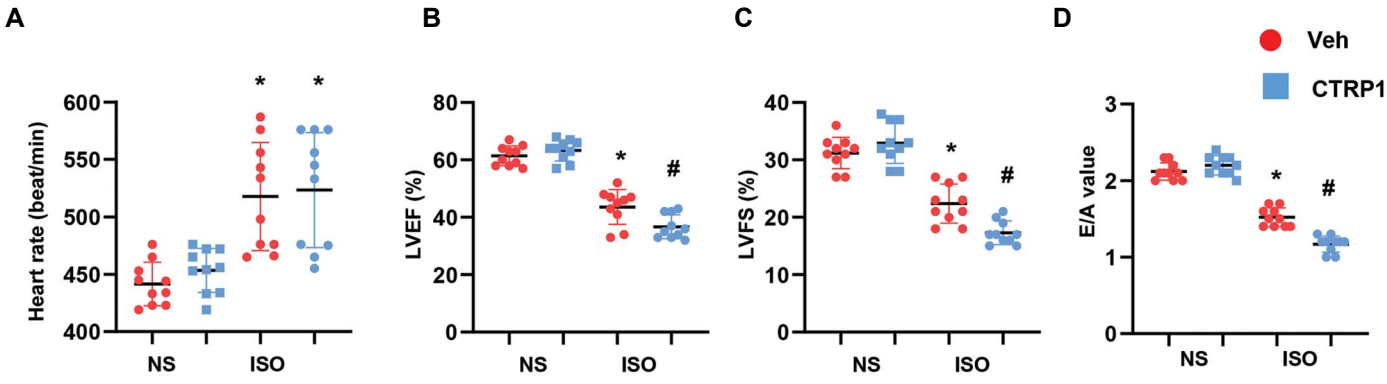

Fig.2: Recombinant CTRP1 aggravates cardiac dysfunction induced by ISO. Echocardiographic measurements in mouse hearts after recombinant CTRP1 injections (n=10). **A.** Heart rate, **B.** LV ejection fraction (LVEF) and LV fractional shortening (LVFS), and **C.** E/A ratio. ISO; Isoproterenol, LV; Left ventricular, and E/A; E value to A value.

The effect of CTRP1 on fibroblasts

We hypothesized that CTRP1 regulates cardiac fibrosis by affecting fibroblast function. We isolated cardiac fibroblasts from adult mice and stimulated them with TGFβ1. These fibroblasts were treated with different concentrations of CTRP1. However, the CCK-8 assay showed no significant difference in fibroblast proliferation between the CTRP1 and TGFβ1 groups (Fig.3A). We then selected a higher dose of CTRP1 to treat the fibroblasts. Staining results for proliferating cell nuclear antigen (PCNA), a proliferation marker, showed no significant difference between fibroblasts treated with CTRP1+TGFβ1 and fibroblasts treated with TGFβ1 alone (Fig.3B). Fibroblasts were also stained with α-SMA to detect fibroblast activation levels. Consistently, the expression of α-SMA was not significantly different between the CTRP1+TGFβ1 and TGFβ1 groups (Fig.S1A, See Supplementary Online Information at www.celljournal.org). The expression levels of fibrosis markers, such as collagen I, collagen III, and α-SMA, detected by using RT-PCR, were not different in the CTRP1+TGFβ1 and TGFβ1 groups (Fig.3C). These data suggest that other cell types may account for the regulatory effect of recombinant CTRP1 on cardiac fibrosis.

Recombinant CTRP1 increases macrophage-mediated inflammation *in vivo*

As immune cells, especially macrophages, play an essential role in cardiac fibrosis, we detected the effect of CTRP1 on macrophage infiltration and the inflammatory response in mice. Mouse hearts were stained with CD68 to label the cardiac macrophages. As shown in Figures 4A and B, the number of CD68-labeled macrophages increased remarkably in CTRP1-treated mice compared to that in the vehicle-treated mice. The release of inflammatory cytokines, such as TNFα, IL-1, IL-6, and TGFβ1, was sharply increased in ISO-injected mice. A similar significant increase was seen in CTRP1-injected mice (Fig.4C). Thus, CTRP1 may regulate cardiac fibrosis by targeting cardiac macrophages.

Recombinant CTRP1 enhances macrophage pro-inflammatory response and fibroblast activation

We evaluated the effects of CTRP1 on macrophages. CTRP1 treatment (8 μg/mL) of macrophages induced a remarkable increase in the release of inflammatory cytokines, such as TNFα, IL-1, IL-6, and TGFβ1 (Fig.5A). We co-cultured activated and CTRP1-treated macrophages with fibroblasts in a transwell dish and found that activated macrophages increased the proliferation and activation of fibroblasts. Similarly, CTRP1-treated macrophages increased fibroblast proliferation and activation, as evidenced by the results of the CCK-8 assay and the increased expression of collagen I, collagen III, and α-SMA (Fig.5B, C, Fig.S1B, See Supplementary Online Information at www.celljournal.org).

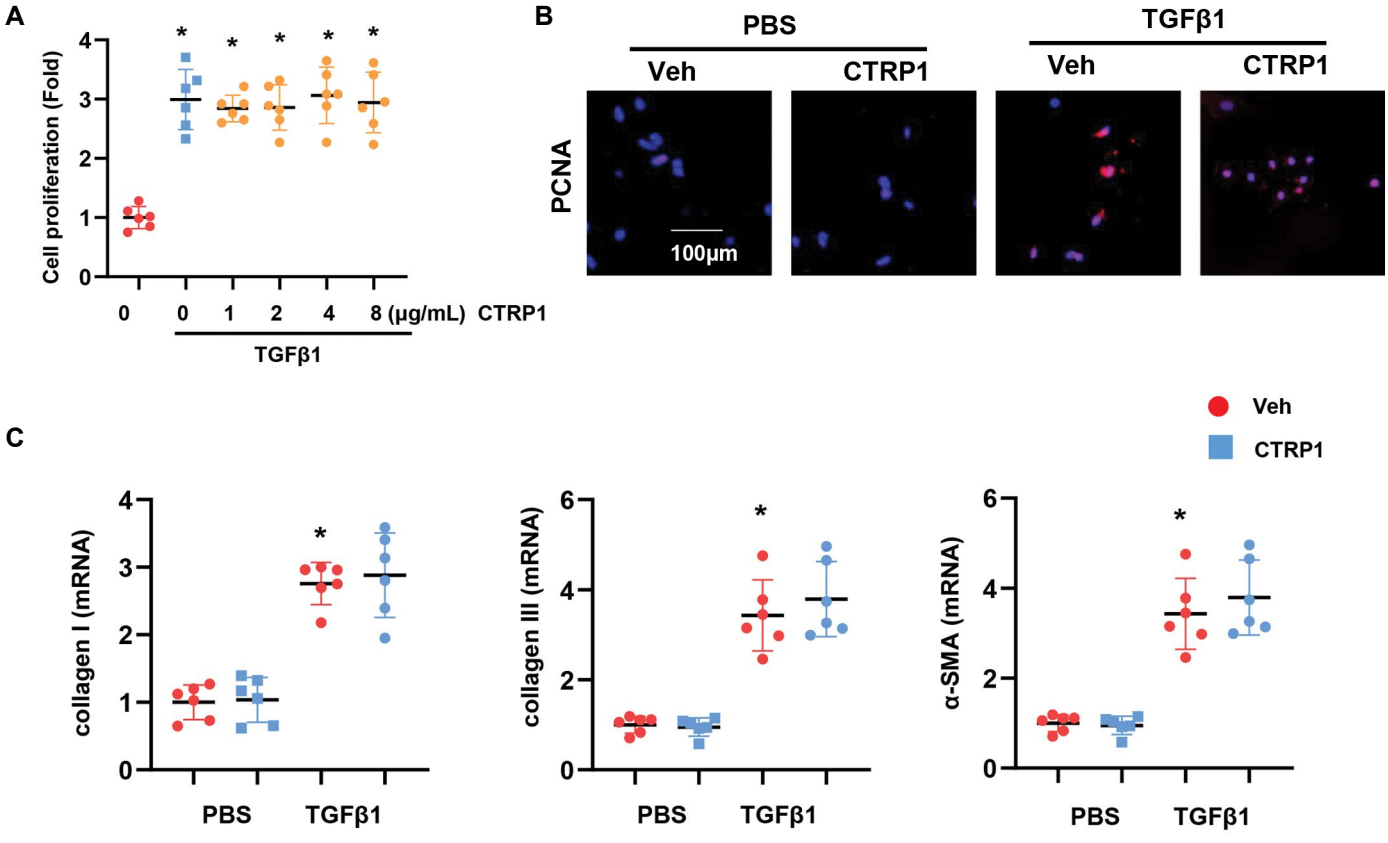

Fig.3: The effect of CTRP1 on fibroblasts. **A.** Cell proliferation was detected by using the CCK-8 assay for fibroblasts treated with recombinant CTRP1 (0, 1, 2, 4, 8 μg/mL) and TGFβ1. **B.** PCNA staining in fibroblasts treated with recombinant CTRP1 (8 μg/mL) and TGFβ1. **C.** Transcription level of fibrosis markers in fibroblasts (n=6). PBS; Phosphate balanced normal saline, TGFβ1; Transforming growth factor-β1, *; P<0.05 vs. PBS-Veh group, #; P<0.05 vs. TGFβ1-Veh group, and Veh; Vehicle.

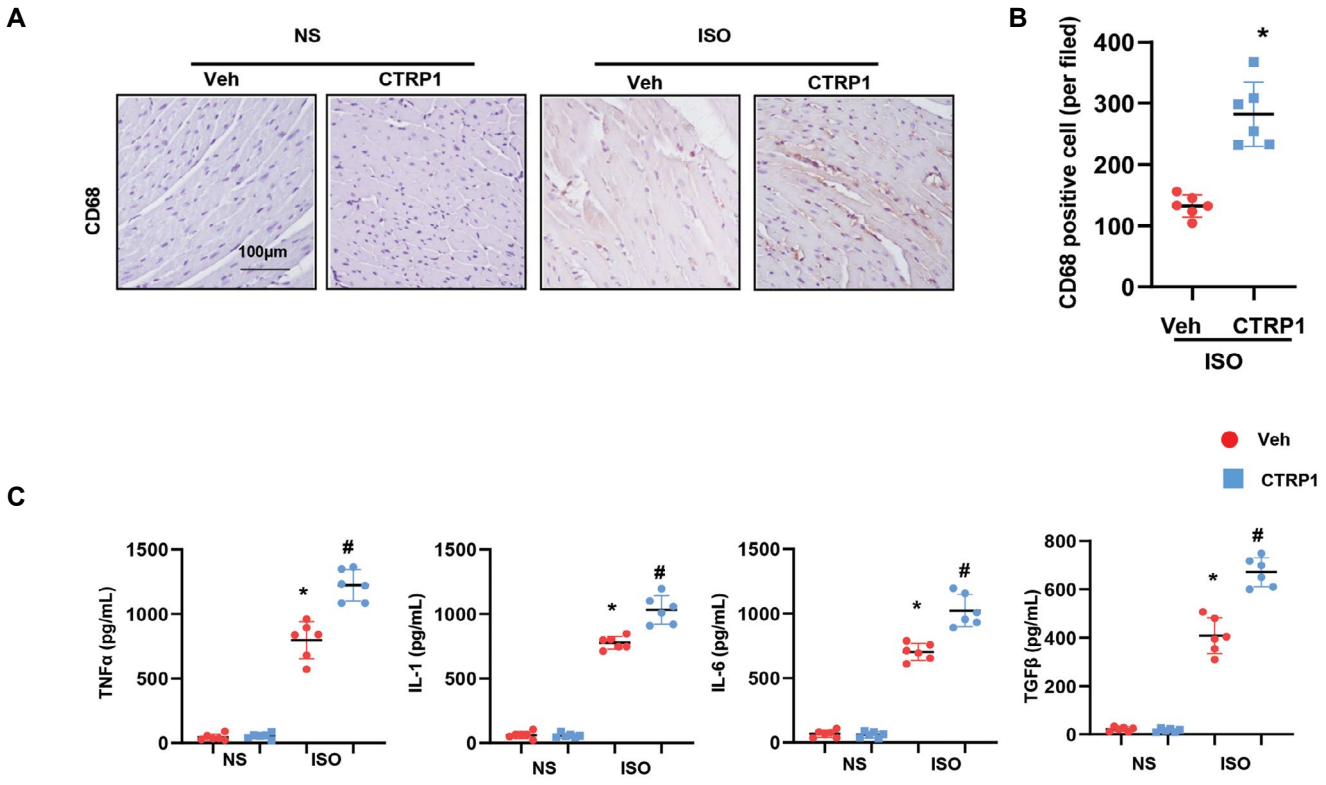

Fig.4: Recombinant CTRP1 increases macrophage-mediated inflammation *in vivo*. **A.** Representative image of CD68 staining, **B.** Quantification result of CD68-positive cell number (n=6). **C.** The release of pro-inflammatory cytokines in mouse hearts detected by using ELISA (n=6). ISO; Isoprenaline, *; P<0.05 vs. NS-Veh group, #; P<0.05 vs. ISO-Veh group, NS; Normal saline, and Veh; Vehicle.

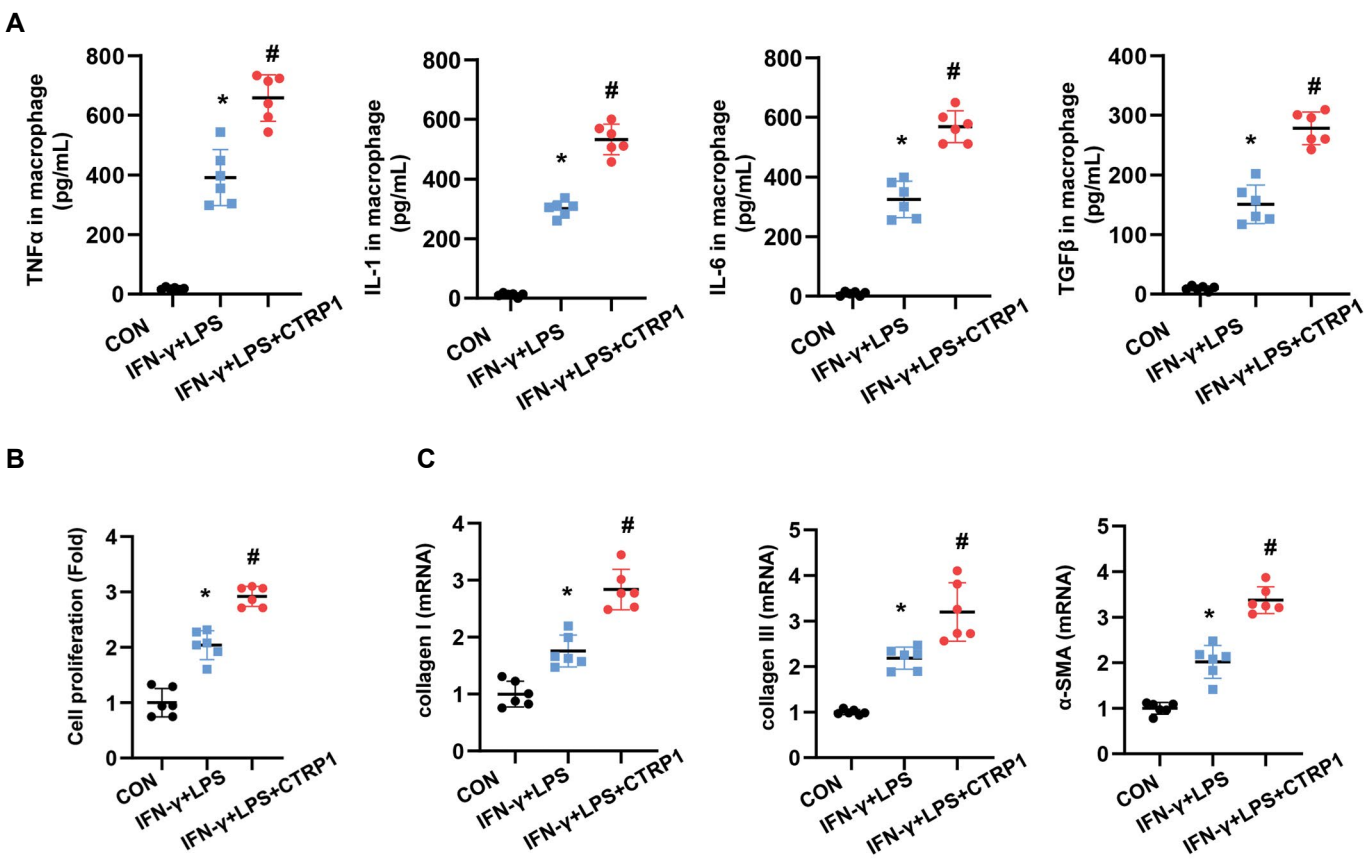

Fig.5: Recombinant CTRP1 enhances macrophage pro-inflammatory response and increases fibroblasts activation. **A.** The release of pro-inflammatory cytokines in macrophages activated by IFN-γ+LPS and treated with recombinant CTRP1 (8 μg/mL) (n=6), **B.** Fibroblasts were co-cultured with activated or CTRP1-treated macrophages. Fibroblast proliferation detected by using the CCK-8 assay (n=6). **C.** Transcription level of fibrosis markers in fibroblasts (n=6). TNF-α; Tumor necrosis factor-α, CON; Control, IFN-γ; Interferonγ, LPS; Lipopolysaccharide, *; P<0.05 vs. CON group, and #; P<0.05 vs. IFN-γ+LPS group.

NOX2/p38 mediates the effect of CTRP1 on macrophages

Next, we explored the mechanism by which CTRP1 affects macrophage function. We found that NADPH oxidase 2 (NOX2) expression increased in activated macrophages, with CTRP1 driving the enhancement of this expression. Downstream molecular p38 activation was also increased in CTRP1-treated macrophages (Fig.6A, B). We then used SB203580 to inhibit p38 in the activated macrophages, which caused a reduction in the release of TNFα, IL-1, IL-6, and TGFβ1. CTRP1 treatment did not induce the release of these pro-inflammatory cytokines in p38-inhibited macrophages (Fig.6C). We also co-cultured these p38-inhibited macrophages with fibroblasts. As shown in Figure 6D, fibroblast proliferation and activation were observed in the p38 inhibition condition, whereas CTRP1-treated macrophages did not enhance fibroblast proliferation and activation under the p38 inhibition condition. Collectively, CTRP1 promotes cardiac fibrosis by regulating the NOX2/p38 pathway in macrophages.

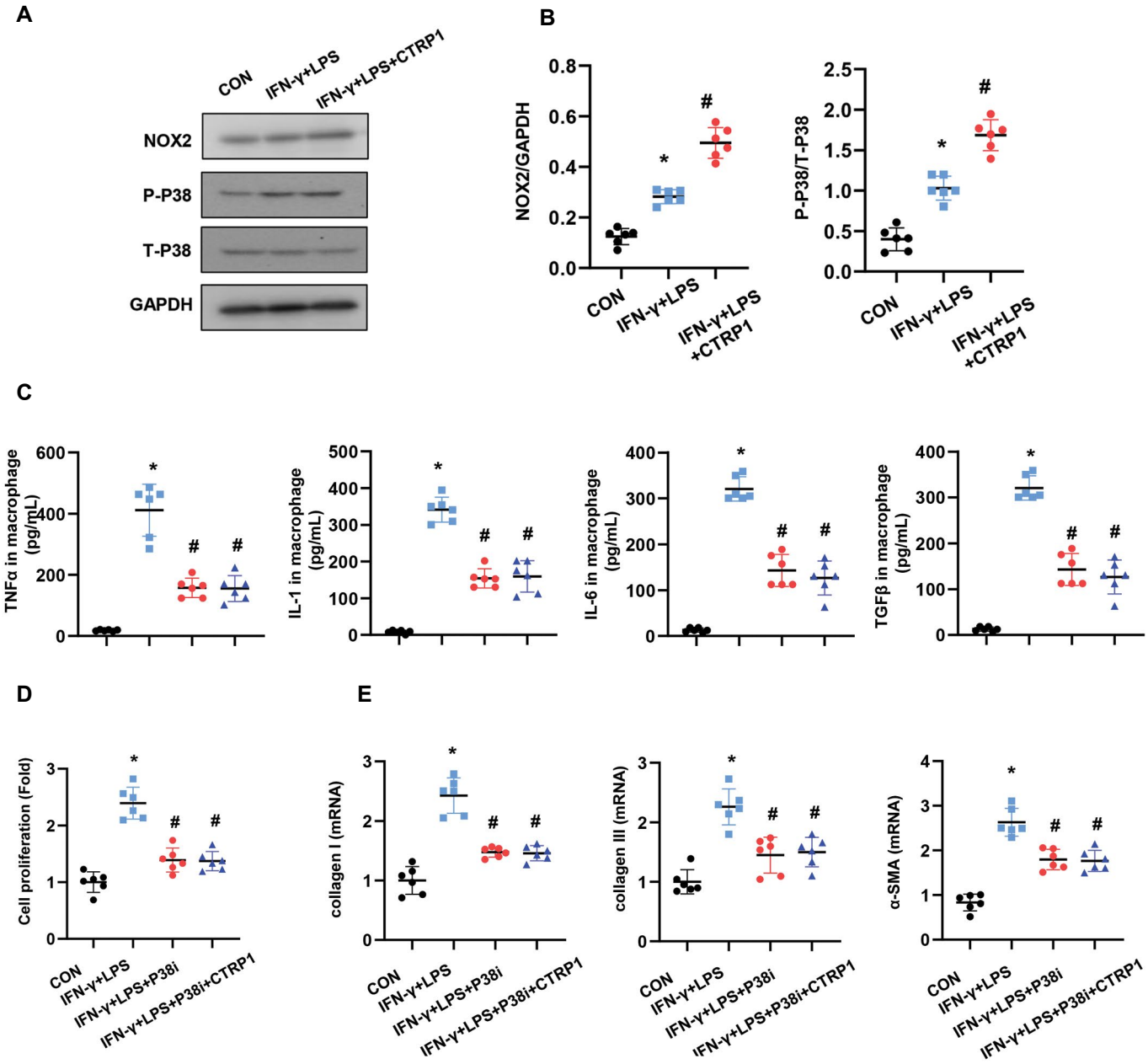

Fig.6: NOX2/p38 mediates the effect of CTRP1 on macrophages. **A, B.** Protein expression of NOX2, p-p38, and total p38 in activated or CTRP1-treated macrophages (n=6). **C.** Macrophages were activated by IFN-γ+LPS and treated with recombinant CTRP1 (8 μg/mL) and/or SB203580 (10 Mm). The release of pro-inflammatory cytokines in macrophages was detected using ELISA (n=6). **D, E.** Fibroblasts were co-cultured with activated CTRP1- and/or SB203580-treated macrophages. **D.** Fibroblast proliferation detected by using the CCK-8 assay (n=6). **E.** Transcription of fibrosis markers in fibroblasts (n=6). TNF-α; Tumor necrosis factor-α, CON; Control, IFN-γ; Interferonγ, LPS; Lipopolysaccharide, *; P<0.05 vs. CON group, and #; P<0.05 vs. IFN-γ+LPS group.

Discussion

CTRP1, a hormone that controls energy metabolism (8) has been reported to protect against cardiovascular diseases (9-12). However, we revealed the deleterious role of CTRP1 in cardiac fibrosis induced by ISO insult both *in vivo* and *in vitro*. We found that both recombinations of CTRP12 could aggravate ISO-induced cardiac fibrosis and dysfunction by exacerbating ISO-induced cardiac inflammation and macrophage dysfunction. These pro-inflammatory effects of CTRP1 lead to the proliferation and activation of myofibroblasts, resulting in aggravated fibrosis.

CTRP is a family of proteins similar to adiponectin, which plays an important role in immunity, development, and metabolism (8). As one of the members of CTRPs, CTRP1 has been reported to be associated with many diseases, including obesity, diabetes, renal fibrosis, and liver disease (8, 14-16). Recently, studies have found a close negative relationship between CTRP1 and cardiovascular diseases, such as coronary artery disease, hypertension, congestive heart failure, and atherosclerosis (11, 17, 18). CTRP1 recruits ERK1/2 and Jak-2 for aldosterone release and increases IL-6 release, thus acting in the pathogenesis of congestive heart failure (18). CTRP1 can increase the expression of adhesion molecules in endothelial cells and monocytes and aggravate atherosclerosis (17). However, some studies contradict these conclusions. CTRP1 has been reported to protect against sepsis-induced cardiomyopathy in mice (9) and attenuate doxorubicin-induced cardiac injury in mice (19). Additionally, CTRP1 attenuates angiotensin II-induced cardiac hypertrophy in a mouse model (20). These contradictory results raise the question of whether human CTRP1 has a different function from that of murine CTRP1. In this study, we used recombinant full-length CTRP1 and found that it exacerbates ISO-induced cardiac fibrosis and dysfunction in mice.

Another important question is whether CTRP1 directly affects fibroblasts. While previous studies found that CTRP1 could directly affect cardiomyocytes (19, 20) and protect against renal fibrosis (21), none of these studies explored the direct effect of CTRP1 on fibroblasts. In our study, we stimulated fibroblasts with TGFβ1, the most pro-fibrotic factor. However, we did not observe any pro- or anti-fibrotic effects of CTRP1 on fibroblasts. Thus, other cell types may be the targets of CTRP1.

Macrophages are the source of pro-inflammatory and pro-fibrotic cytokines such as TGFβ1, IL-1, and IL-6. TGF-β and IL-6 induce fibroblast activation and produce collagen I, collagen III, and fibronectin. IL-1 induces increased synthesis and production of metalloproteinases (22). It was found that recombinant CTRP1 increased macrophage infiltration in atherosclerotic plaques and enhanced inflammatory responses in endothelial cells (17). Consistent with these results, we found that recombinant CTRP1 protein increased macrophage infiltration in mouse hearts and led to macrophage M1-like activation, which subsequently induced fibroblast activation and proliferation. NOX is an important source of reactive oxygen species (ROS), and activated macrophages produce considerable amounts of ROS (23, 24). This respiratory burst in macrophages results in the activation of specific signaling pathways, such as MAPKs, leading to the expression of pro-inflammatory mediators (24). In our study, we found that recombinant CTRP1 increased the expression of NOX2 in macrophages and enhanced the activation of p38. When we inhibited p38 in macrophages, the pro-inflammatory effect of recombinant CTRP1 was counteracted. The effect of CTRP1-treated macrophages on fibroblasts was also counteracted by p38 inhibition. These results suggest that CTRP1 promotes cardiac fibrosis by regulating cardiac macrophages.

Conclusion

Recombinant CTRP1 can promote ISO-induced cardiac fibrosis and dysfunction. Recombinant CTRP1 exerts these effects by directly acting on macrophages via the NOX2/p38 pathways. Thus, targeting CTRP1 expression during cardiac fibrosis may be a new treatment strategy.

Acknowledgments

This work was funded by The Foundation of National Natural Science Foundation of China (81560409). There is no conflict of interest in this study.

Authors' Contributions

C.L., H.H.; Participated in study design, data collection and evaluation, drafting and statistical analysis. C.L., Sh.Y., X.W.; Conducted molecular experiments and RT-qPCR. T.Zh., Q.Zh., Y.Zh.; Conducted animal experiments and extensively in interpretation of the data and the conclusion. Y.L., R.Zh., H.H.; Wrote and critically revised the manuscript. All authors read and approved the final manuscript.

References

1. Spoladore R, Falasconi G, Fiore G, Di Maio S, Preda A, Slavich M, et al. Cardiac fibrosis: emerging agents in preclinical and clinical development. Expert Opin Investig Drugs. 2021; 30(2): 153-166.
2. Reichardt IM, Robeson KZ, Regnier M, Davis J. Controlling cardiac fibrosis through fibroblast state space modulation. Cell Signal. 2021; 79: 109888.
3. Zaidi Y, Aguilar EG, Troncoso M, Ilatovskaya DV, DeLeon-Pennell KY. Immune regulation of cardiac fibrosis post myocardial infarction. Cell Signal. 2021; 77: 109837.
4. Park S, Nguyen NB, Pezhouman A, Ardehali R. Cardiac fibrosis: potential therapeutic targets. Transl Res. 2019; 209: 121-137.
5. Hara H, Takeda N, Komuro I. Pathophysiology and therapeutic potential of cardiac fibrosis. Inflamm Regen. 2017; 37: 13.
6. Baci D, Bosi A, Parisi L, Buono G, Mortara L, Ambrosio G, et al. Innate immunity effector cells as inflammatory drivers of cardiac fibrosis. Int J Mol Sci. 2020; 21(19): 7165.
7. Frangogiannis NG. Cardiac fibrosis: cell biological mechanisms, molecular pathways and therapeutic opportunities. Mol Aspects Med. 2019; 65: 70-99.
8. Bai B, Ban B, Liu Z, Zhang MM, Tan BK, Chen J. Circulating C1q complement/TNF-related protein (CTRP) 1, CTRP9, CTRP12 and CTRP13 concentrations in Type 2 diabetes mellitus: in vivo regulation by glucose. PLoS One. 2017; 12(2): e0172271.
9. Jiang W, Li W, Hu X, Hu R, Li B, Lan L. CTRP1 prevents sepsis-

induced cardiomyopathy via Sirt1-dependent pathways. Free Radic Biol Med. 2020; 152: 810-820.
10. Yagmur E, Buergerhausen D, Koek GH, Weiskirchen R, Trautwein C, Koch A, et al. Elevated CTRP1 plasma concentration is associated with sepsis and pre-existing type 2 diabetes mellitus in critically Ill patients. J Clin Med. 2019; 8(5): 661.
11. Su Z, Tian S, Liang W. Circulating CTRP1 levels are increased and associated with the STOD in essential hypertension in Chinese patients. Cardiovasc Ther. 2019; 2019: 4183781.
12. Shen L, Wang S, Ling Y, Liang W. Association of C1q/TNF-related protein-1 (CTRP1) serum levels with coronary artery disease. J Int Med Res. 2019; 47(6): 2571-2579.
13. Muendlein A, Leiherer A, Saely C, Ebner J, Geiger K, Brandtner EM, et al. The novel adipokine ctrp1 is significantly associated with the incidence of major adverse cardiovascular events. Atherosclerosis. 2019; 286: 1-6.
14. Rodriguez S, Lei X, Petersen PS, Tan SY, Little HC, Wong GW. Loss of CTRP1 disrupts glucose and lipid homeostasis. Am J Physiol Endocrinol Metab. 2016; 311(4): E678-E697.
15. Han S, Kim JD, Lee S, Jeong AL, Park JS, Yong HJ, et al. Circulating CTRP1 levels in type 2 diabetes and their association with FGF21. Int J Endocrinol. 2016; 2016: 5479627.
16. Lei H, Wu D, Wang JY, Li L, Zhang CL, Feng H, et al. C1q/tumor necrosis factor-related protein-6 attenuates post-infarct cardiac fibrosis by targeting RhoA/MRTF-A pathway and inhibiting myofibroblast differentiation. Basic Res Cardiol. 2015; 110(4): 35.
17. Lu L, Zhang RY, Wang XQ, Liu ZH, Shen Y, Ding FH, et al. C1q/TNF-related protein-1: an adipokine marking and promoting atherosclerosis. Eur Heart J. 2016; 37(22): 1762-1771.
18. Yang Y, Liu S, Zhang RY, Luo H, Chen L, He WF, et al. Association between C1q/TNF-related protein-1 levels in human plasma and epicardial adipose tissues and congestive heart failure. Cell Physiol Biochem. 2017; 42(5): 2130-2143.
19. Chen H, Gao L, Huang Z, Liu Y, Guo S, Xing J, et al. C1qTNF-related protein 1 attenuates doxorubicin-induced cardiac injury via activation of AKT. Life Sci. 2018; 207: 492-498.
20. Wu L, Gao L, Zhang D, Yao R, Huang Z, Du B, et al. C1QTNF1 attenuates angiotensin II-induced cardiac hypertrophy via activation of the AMPKa pathway. Free Radic Biol Med. 2018; 121: 215-230.
21. Li W, Cheng F, Songyang YY, Wei J, Ruan Y. CTRP1 attenuates UUO-induced renal fibrosis via AMPK/NOX4 pathway in mice. Curr Med Sci. 2020; 40(1): 48-54.
22. Lu Z, Chang L, Du Q, Huang Y, Zhang X, Wu X, et al. Arctigenin induces an activation response in porcine alveolar macrophage through TLR6-NOX2-MAPKs signaling pathway. Front Pharmacol. 2018; 9: 475.
23. Kleniewska P, Piechota A, Skibska B, Gorąca A. The NADPH oxidase family and its inhibitors. Arch Immunol Ther Exp (Warsz). 2012; 60(4): 277-294.
24. Youn GS, Lee KW, Choi SY, Park J. Overexpression of HDAC6 induces pro-inflammatory responses by regulating ROS-MAPK-NF-kappaB/AP-1 signaling pathways in macrophages. Free Radic Biol Med. 2016; 97: 14-23.

Original Article

Left Ventricular Geometry and Angiogenesis Improvement in Rat Chronic Ischemic Cardiomyopathy following Injection of Encapsulated Mesenchymal Stem Cells

Negar Karimi Hajishoreh, Ph.D.[1], Nafiseh Baheiraei, Ph.D.[1]*, Nasim Naderi, M.D.[2]*, Mojdeh Salehnia, Ph.D.[3], Mehdi Razavi, Ph.D.[4]

1. Tissue Engineering and Applied Cell Sciences Division, Department of Anatomical Sciences, Faculty of Medical Sciences, Tarbiat Modares University, Tehran, Iran
2. Rajaie Cardiovascular, Medical, and Research Center, Iran University of Medical Sciences, Tehran, Iran
3. Department of Anatomical Sciences, Faculty of Medical Sciences, Tarbiat Modares University, Tehran, Iran
4. Biionix (Bionic Materials, Implants and Interfaces) Cluster, Department of Internal Medicine, College of Medicine, University of Central Florida, Orlando, Florida, United States

Corresponding Addresses: P.O.Box: 111-14115, Tissue Engineering and Applied Cell Sciences Division, Department of Anatomical Sciences, Faculty of Medical Sciences, Tarbiat Modares University, Tehran, Iran
P.O.Box: 1995614331, Rajaie Cardiovascular, Medical, and Research Center, Iran University of Medical Sciences, Tehran, Iran
Emails: n.baheiraei@modares.ac.ir, naderi@rhc.ac.ir

Received: 25/January/2022, Accepted: 14/June/2022

Abstract

Objective: Injection of hydrogel and cells into myocardial infarction (MI) patients is one of the emerging treatment techniques, however, it has some limitations such as a lack of electromechanical properties and neovascularization. We investigated the therapeutic potential of new electroactive hydrogel [reduced graphene oxide (rGO)/Alginate (ALG)] encapsulated human bone marrow mesenchymal stem cells (BMSCs).

Materials and Methods: The experimental study involved ligating the left anterior descending coronary artery (LAD) in rat models of chronic ischemic cardiomyopathy. Echocardiograms were analyzed at 4 and 8 weeks after MI treatment. In the eighth week after injection in the heart, the rats were sacrificed. Histological and immunohistochemical analyses were performed using Hematoxylin and Eosin (H&E) staining, Masson's trichrome staining and anti-CD31 antibody to analyze tissue structure and detect neovascularization.

Results: In comparison to the control and other treatment groups, MSCs encapsulated in rGO-ALG showed significant improvements in fractional shortening (FS), ejection fraction (EF), wall thickness and internal diameters ($P<0.05$). The morphological observation showed several small blood vessels formed around the transplantation site in all treated groups especially in the MSC-ALG-rGO group 8 weeks after the transplantation. Also, Masson's trichrome staining indicated an increased amount of collagen fibers in rGO-ALG-MSC. Microvessel density was significantly higher using MSC-ALG-rGO compared to controls ($P<0.01$).

Conclusion: This study demonstrates that intramyocardial injection of rGO/ALG, a bio-electroactive hydrogel, is safe for increasing LV function, neovascularization, and adjusting electrical characteristics following MI. The results confirm ALG promising capability as a natural therapeutic for cardiac regeneration.

Keywords: Alginates, Cell Therapy, Encapsulation, Graphene Oxide, Mesenchymal Stem Cells

Cell Journal(Yakhteh), Vol 24, No 12, December 2022, Pages: 741-747

Citation: Karimi Hajishoreh N, Baheiraei N, Naderi N, Salehnia M, Razavi M. Left ventricular geometry and angiogenesis improvement in rat chronic ischemic cardiomyopathy following injection of encapsulated mesenchymal stem cells. Cell J. 2022; 24(12): 741-747. doi: 10.22074/CELLJ.2022.557257.1040.

Introduction

Cardiovascular disease remains the main cause of death worldwide. In the United States, 86.2 million individuals had some type of cardiac disease in 2008, which is predicted to increase to 40.5 percent of the American population by 2030 (1).

Myocardial infarction (MI), made by blood flow blockage of the cardiac coronary arteries, is one of the most serious diseases with a high death ratio around the world (2). MI results in wall thinning, fibrosis, left ventricular (LV) dilation, and reduced cardiac function (3).The adult heart's inherent capacity to self-regenerate following myocardial damage is a major constraint in the treatment of cardiovascular disease. In the course of LV remodeling, structural and functional weakening of the LV occurs, leading to deteriorating clinical symptoms, exercise intolerance, and eventually death of the afflicted patient (4).

Despite advancements in pharmacological and interventional therapies, MI-related morbidity and mortality continue to increase (5). Transplantation of mesenchymal stem cells (MSCs) is a promising approach to repair damaged heart tissue after MI. Particularly, paracrine impacts of the transplanted MSCs play important roles in heart regeneration through the secretion of many growth factors and immune-modulatory cytokines.

Although cardiac cell injection has been shown to enhance heart function, there are still certain limitations that need to be addressed before their clinical application (6). Since the transplanted cells are subjected to high shear stress, caused by the injection and the harsh post-infarction

environment with high oxidative stress, their viability and efficacy remain low (7). One of the most significant issues associated with cell injection is the low engraftment rate as most of the cells are lost to the vasculature or leaking out of the injection site (8, 9). To overcome this problem, injected cells can be supported by being delivered with a biomaterial matrix. It has been stated that delivery of a proper material with cells or growth factors can be a more effective method to restore cardiac function compared with injecting materials or cells alone (6, 9, 10). In fact, injectable biopolymers allow the host body to perform as a bioreactor and recreate the injured tissue in situ (3).

Among biopolymers, which have been utilized for MI treatment, alginate (ALG) has been shown to improve LV function in animal models (3, 11). For example, it has been shown that intramyocardial injection of ALG in dogs with chronic heart failure could increase LV thickness and recover LV structure and function (11). Apart from decreasing wall stress that underlies the benefits of ALG therapy, an increase in LV wall thickness and reduction of LV size are other mechanisms, which can lead to a reduced end-diastolic length of the contractile element. Besides, ALG therapy can lessen cardiomyocyte hypertrophy induced by continuous LV enlargement and consequent augmentation of mechanical stretch (3). In chronic HF dogs, also, an ALG hydrogel implant enhanced LV function and halted progressive remodeling (11).

Electrical integration of the insulated hydrogels with the infarct myocardium can be delayed leading to arrhythmias. However, electroactive hydrogels could improve cell-cell electrical coupling and synchronous contractions of the cardiac cells; which is necessary for the effective integration with the host tissue (12, 13). Graphene-based nanomaterials, especially graphene oxide (GO) and its derivatives such as reduced GO (rGO), are likely to effectively reinforce materials to restore the ischemia in heart tissue due to their outstanding high mechanical and electrical properties. Also, rGO flakes could increase cell-ECM interactions by adsorption of ECM proteins such as fibronectin (FN) from cell culture serum (14). The potential of rGO application for MI treatment has been previously studied. It has been revealed that the combination of rGO flakes with MSC spheroids implanted into mouse-infarcted myocardium can successfully increase the expression of angiogenic growth factors and connexin 43, and improve MSC efficacy for MI treatment (15). Our group has previously demonstrated the in vitro assessment of ALG-rGO electroactive hydrogel for cardiac application. The presence of rGO, as an electroactive moiety, improved the physicochemical and biological properties of the ALG hydrogel (16). Here, we have further evaluated the therapeutic outcomes of ALG injection combined with human MSCs (hMSCs) and rGO in a rat model of chronic ischemic MI to improve cardiac function and induce neovascularization.

Materials and Methods

Experimental groups

Animal models were randomly categorized into seven experimental groups containing a sham group (surgical operation without any treatment) and the control group [receiving phosphate buffered saline (PBS) as treatment] (n=7/group).

Intramyocardial injection of hydrogel in Rat MI model

Twenty-eight days after left anterior descending artery (LAD) ligation, animals were anesthetized (isoflurane 1%) and underwent thoracotomy surgery. Then, intubation was done via mouth and inhaled anesthesia was continued and placed on mechanical ventilation. Identification of the infarct zone was detected via visual observation showing a darker area compared to other LV border zones near the anterior apex of the LV wall. Animals received an intramyocardial injection (28G insulin needle, 20 µl) in five parts of the infarct border zone. Each group that needed to get hBMSCs received 5×10^6 cells/µl. Simultaneously, a cross-linker ($CaCl_2$ 102 mM) was injected in the same site, in a separate syringe. The consent of each participant was aqcuired by filling out the informed Consent form and the code of National Committee of Ethics in Biomedicine Researches was approved in Tarbiat Modares University ID Number of Ethical Committee (IR.TMU.REC.1396.700).

Evaluation of cardiac function

Four and eight weeks after treatment, assessment of cardiac function was performed via transthoracic echocardiography in all animals by an echocardiologist with expertise in small animal echocardiography who was blinded to the study group allocations. Rats were positioned supine after the chest wall was shaved. Transthoracic two-dimensional (2D) echocardiography was performed using a 10-MHz linear array transducer connected to a Vivid 7 expert ultrasound system at a speed of 100 mm/s (General Electric-Vingmed Ultrasound, Horten, Norway), under low dose ketamine (10-20 mg/kg i.p) anesthesia. Parasternal M-mode and 2D short-axis views at the level of the papillary muscle were used to measure left ventricular internal diameter in systole (LVIDs), left ventricular internal diameter in diastole (LVIDd), left ventricular posterior wall thickness in diastole (LVPWd), and left ventricular posterior wall thickness in systole (LVPWs). Left ventricular ejection fraction percentage (LVEF %) was calculated using the following formula (Eq. 1):

$$\text{LVEF \%: } (LVIDd^2 - LVIDs^2)/LVIDd^2 \quad \text{(Eq. 1)}$$

To calculate the percentage of fractional shortening (FS%), the following formula (Eq. 2) was used (3, 17):

$$\text{FS\%: } [(LVIDd-LVIDs)/LVIDd] \times 100 \quad \text{(Eq. 2)}$$

Histology assessment

Eight weeks after MI treatments, rats were sacrificed with pentobarbital overdose (200 mg/kg). Their chest was opened and the hearts were removed and transferred immediately to paraformaldehyde 4% (Merck, Germany) for fixation. The paraffin-embedded blocks were sectioned at 5 µm thickness. Two sets of tissue sections (n=10) for each sample were collected and stained with hematoxylin and eosin (H&E) and Masson's trichrome (Merck, Germany) for morphological and collagen observation, respectively (18).

To evaluate neovascularization, immunohistochemistry was performed. After fixation with 4% paraformaldehyde for 24 hours, samples were permeabilized with 0.4% Triton X100 (Sigma-Aldrich, Germany) followed by being blocked in 10% goat serum (Sigma-Aldrich, Germany). Antigen retrieval processes were performed by sodium citrate buffer (10 mM for 20 minutes), then samples were blocked in 10% goat serum (Sigma-Aldrich, Germany). To quench endogenous peroxidase activity in samples, hydrogen peroxide (3wt.%) was applied for 10 minutes. The sections were then incubated with mouse monoclonal CD31 antibody (SC-376764, 1:100, Santa Cruz Biotechnology) for 2 hours at 37˚C followed by washing with PBS. Subsequently, samples were incubated with the secondary antibody (goat anti-mouse-HRP, 1:200, Sigma-Aldrich) for 3 hours. Hematoxylin was also used for counter-staining. Photomicrographs were taken with an Olympus microscope (Olympus Center Valy, PA) and Images were further quantified by ImageJ software (1.46r version, USA). The results were expressed as the mean number of vessels ± SDM. Negative control sections were obtained by omitting the primary antibody for CD31. Based on the acquired results on echocardiography, this evaluation was performed for MSC-ALG and MSC-ALG -rGO groups, and the results were compared with the control group.

Statistical analysis

Results were expressed as the mean ± standard deviation. We used SPSS (version 16.1, IBM, USA). One-way ANOVA analysis of variance was used to compare the means from multiple experimental groups, followed by a post hoc Tukey test. $P<0.05$ was considered statistically significant.

Results

Echocardiographic findings

Table 1 shows comparison of echocardiographic parameters in different groups at 4 and 8 weeks after the treatment. Compared to the control and other treatment groups, myocardial injection of rGO-ALG-MSC significantly improved ejection fraction, fractional shortening, wall thickness, and internal diameter ($P<0.05$). For example, 4 weeks after treatment, LVFS percentage in the MSC-ALG-rGO group increased from around 11 to 30 percent, whereas this value in ALG, ALG-MSC, and hBMSC was about 24, 25, and 27 percent respectively, compared to the control group.

Table 1: Echocardiographic data of experimental groups at 4 and 8 weeks post-treatment

Groups	Sham	MI (control)	ALG	ALG-MSC	hBMSC	MSC-ALG-rGO
			4 week after treatment			
LVPWs (mm)	2.6 ± 0.03	2 ± 0.01*†	2 ± 0.02	2.4 ± 0.05*	2.2 ± 0.02	2.6 ± 0.0†
LVPWd (mm)	1.6 ± 0.02	1.4 ± 0.03*†‡	1.4 ± 0.01	1.5 ± 0.03*	1.6 ± 0.03‡	1.6 ± 0.01†
LVIDs (mm)	3.2 ± 0.01	6.3 ± 0.11*†	5.2 ± 0.09	4.5 ± 0.08*	4.8 ± 0.07*	6.4 ± 0.1†
LVIDd (mm)	6.2 ± 0.050	7.4 ± 0.1*†	6.9 ± 0.12	6 ± 0.04*	6.6 ± 0.09	6.2 ± 0.07†
LVFS%	47.74 ± 3.24	11.56 ± 7.61*†	24.65 ± 2.59*	25.72 ± 8.81*	27.15 ± 7.43	30.13 ± 7.30†
LVEF%	84.05 ± 2.78	27.9 ± 16.53†*	54.59 ± 4.18*	55.45 ± 15.6*	58.05 ± 11.15*	62/6010/87 †
			8 weeks after treatment			
LVPws (mm)	2.6 ± 0.03	2 ± 0.01	2.6 ± 0.04	2.5 ± 0.05	2.3 ± 0.02	2.6 ± 0.01
LVPwd (mm)	1.6 ± 0.02	1.4 ± 0.03	1.6 ± 0.02	1.6 ± 0.02	1.5 ± 0.01	1.6 ± 0.01
LVIDs (mm)	3.2 ± 0.01	6.3 ± 0.11	4.6 ± 0.05*	4.8 ± 0.05*	4.3 ± 0.1*	6.3 ± 0.1
LVIDd (mm)	6.2 ± 0.050	7.4 ± 0.1	7.3 ± 0.08	6.8 ± 0.06*	6.5 ± 0.12	6.2 ± 0.07
LVFS%	47.74 ± 3.24	11.56 ± 7.61	33.0 ± 3.65*	29.4 ± 4.60	33.29 ± 0.54*	32.95 ± 6.12*
LVEF%	84.05 ± 2.78	26.9 ± 16.53*	63.33 ± 4.83*	60.06 ± 6.91*	62.59 ± 7.76*	67.85 ± 8.93*

LVPWs; Left ventricular posterior wall thickness at end-systole, LVPWd; Left ventricular posterior wall thickness at end-diastole, LVIDs; Left ventricular internal diameter end systole, LVIDd; Left ventricular internal diameter end diastole, LVFS; Left ventricular fractional shortening, LVEF; Left ventricular ejection fraction, MI; Myocardium infraction, ALG; Alginate, MSC; Mesenchymal stem cell, hBMSC; Human bone marrow-derived mesenchymal stromal cells, rGO; Reduced graphene oxide. One way ANOVA test showed MSC-rGO-ALG significantly improved echocardiographic parameters in the 4th and 8th weeks after treatment, and *, †, ‡, #; $P<0.05$.

Over the follow-up duration (from the 4th week to the 8th week of treatment), there was no change in echocardiographic parameters for the control group. However, in all treatment groups, LVEF parameters were significantly improved (P<0.05, Fig.1). Eight weeks after the treatment, in the MSC-ALG-rGO group, LVEF% was significantly higher when compared to the control group; at 26% and 66%, respectively (P<0.05).

Histological findings

The representative H&E staining images are presented in Figure 2. The morphological observation showed several small blood vessels formed around the transplantation site in all treated groups especially in the MSC-ALG-rGO group 8 weeks after the transplantation. Also, Masson's trichrome staining indicated an increased amount of collagen fibers in rGO-ALG-MSC.

Anti CD31 antibody was applied to detect neovascularization in three experimental groups (control, MSC-ALG, and MSC –ALG- rGO) and the results were further quantified by ImageJ software (Fig.3). More vessels were detected in the MSC –ALG- rGO group. The microvessel density in control, MSC-ALG, and MSC –ALG- rGO groups were 4.2 ± 1.3, 8.6 ± 2.0, and 19.6 ± 3.2 respectively per microscopic field, 8 weeks post-treatment. This value was significantly higher in the MSC-ALG-rGO treatment group compared with other groups (P<0.01). The angiogenesis index was also considerably higher in the MSC-ALG group compared to the control group (P<0.05).

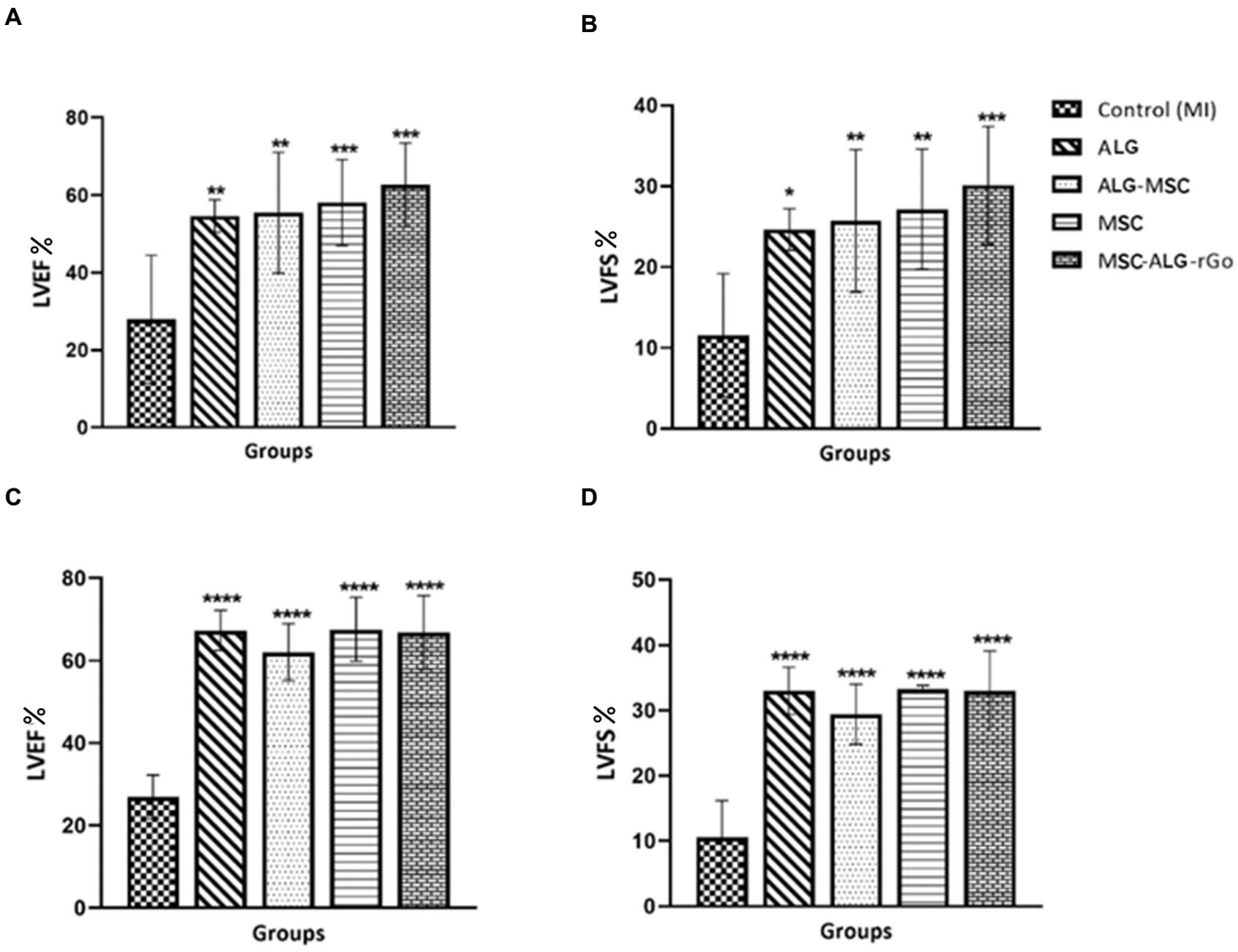

Fig.1: Effect of experimental groups on LV functions after treatment. **A.** LVEF% 4 weeks after treatment, **B.** LVFS% 4weeks after treatment, **C.** LVEF% 8 weeks after treatment, **D.** LVFS% 8 weeks after treatment. All of the treated groups showed significant increase in LVEF% and LVFS% compared to the control group (n=7/group, *; P<0.05, **; P<0.001, ***; P<0.0001, ****; P<0.00001). LVEF; Left ventricular ejection fraction, LVFS; Left ventricular fractional shortening, ALG; Alginate, MSC; Mesenchymal stem cell, and rGO; Reduced graphene oxide.

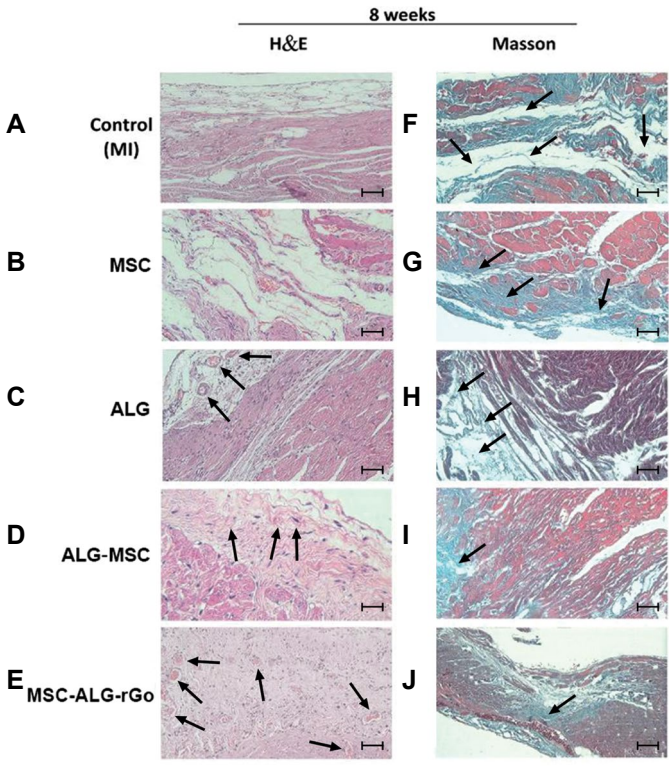

Fig.2: Histologic assessments 8 weeks after post-treatment. **A-E.** Effect of treatment on cardiac tissue remodeling 8 weeks after treatment. H&E staining to visualize myocyte and neovascularization. **F-J.** Masson's trichrome staining to distinguish collagen fibrils and scar tissues in the treated rats (magnification: 50x). MI; Myocardium infraction, ALG; Alginate, MSC; Mesenchymal stromal cell, and rGO; Reduced graphene oxide.

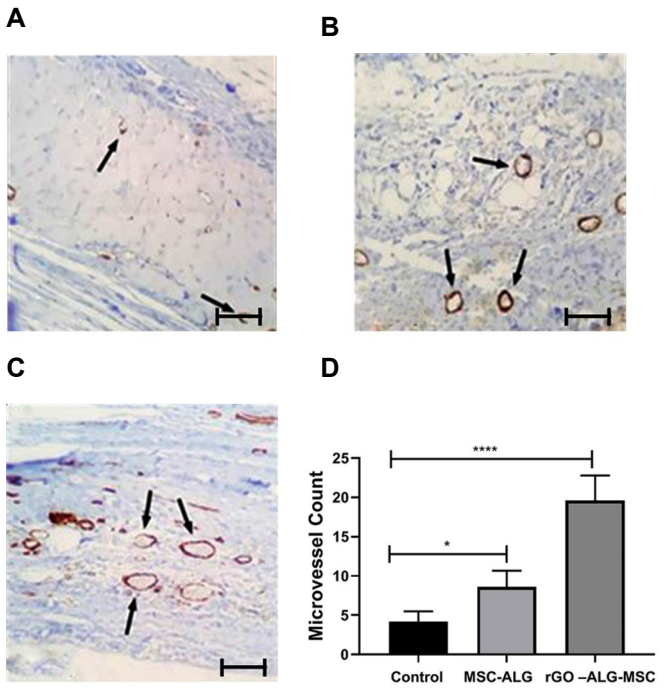

Fig.3: The immunohistochemistry images for CD31 marker to determine angiogenesis. The positive reaction for CD31 markers is shown with brown color and the arrows indicate several blood vessels. **A.** Control, **B.** MSC-ALG, **C.** MSC-ALG -rGO ($P<0.05$, $P<0.01$) (200x magnification). **D.** The results were further quantified by microvessel density defined by counting the positive staining for CD31 in five fields. MI; Myocardium infraction, ALG; Alginate, MSC; Mesenchymal stromal cells, and rGO; Reduced graphene oxide.

Discussion

Despite recent advances in treatment methods, the mortality rate from cardiovascular illnesses has increased significantly (19). Administration of stem cells with electroactive hydrogel could be a promising approach for recovery of effective signal transition and a cell-cell connection in the infarct area. Our experiment showed that injections of ALG hydrogel containing rGO/hMSCs in the free wall of the failing heart can improve LV function and promote the preservation of LV wall thickness. Our team previously demonstrated that the inclusion of rGO, an electroactive moiety, within ALG could improve hBM-MSC viability and offer a viable substrate for upregulation of cardiomyocyte gene expression, even without *in vitro* electrical stimulation (16). To assess the effect of rGO and/or hMSCs addition to ALG hydrogel on tissue regeneration, LV function was evaluated by echocardiography and dissected hearts were assessed for scarring and ventricular remodeling. A significant increase in LVPWs, LVPWd, LVIDs, and LVIDd was observed, all of which confirmed improvement in cardiac function following injection of ALG encapsulated hMSCs/rGO at week 8.

Over the past decade, ALG as a polysaccharide biomaterial has been considered the main candidate for cardiac regeneration (20). ALG implants might reduce LV dilatation while improving LV geometry, preventing electrical dispersion in HF patients (4). A recent study also demonstrated that an injectable hydrogel (Alginate/Dextran/β-Glycerophosphate) loaded with hMSCs is a promising strategy to improve the heart regeneration after MI. The authors achieved acceptable findings from ejection fraction, fibrosis, and vessel density with decreasing infraction size (21). The existence of injectable ALG in the infarct area created physical support for scar tissue by decreasing the stress of myofibers and inflammatory response in the microenvironment. Also, ALG assisted in inhibiting myocardial remodeling after MI (22).

The H&E staining and immunohistochemistry results showed the higher neovascularization and lower collagen fibrosis formation (indicating reduced scarring/collagen deposition) in rGO/ALG encapsulated hMSCs group compared to control groups. In a study performed on a model of MI in dogs, the alginate-treated group showed a significant increase in LV systolic and diastolic function and wall thickness compared to the control group; whereas LVEF and LV thickness in the control group decreased. Therefore, this investigation indicated that ALG could be considered as a promising biomaterial for the treatment of patients with advanced heart failure (11). According to our investigation, parameters such as EF and FS in the 4th and 8th weeks after treatments had a significant increase in the MSC-ALG-rGO group compared to the control group at 62, 67, and 30, 32%, respectively. These results indicate that MSC-ALG-rGO compositions have preventional effects on LV geometry and cardiac dysfunctionality after MI.

Graphene-based nanomaterials can effectively scavenge reactive oxygen species(ROS) providing antioxidant activities to the transplanted cells and MI tissues (23). The antioxidant activity of rGO has been previously considered as the reason to increase the survival and therapeutic efficacy of hMSCs delivered for MI treatment (7). In addition, the presence of rGO can improve the adhesion of MSC in the damaged area and consequently increase the paracrine action of angiogenic growth factors such as VEGF and FGF2. Ultimately, it increases the regeneration rate of damaged heart tissue (15) .The efficacy of ALG and hMSCs in preventing or reversing cardiac remodeling has been proved before (3, 24), but the injection of hMSCs along with rGO/ALG is a novel method to improve cardiac function and reverse cardiac remodeling.

As reported by a study, cardiomyocytes cultured on rGO-GelMA hydrogel sheets showed a stronger contraction, faster heartbeat rate, as well as improved electrical conductivity and mechanical properties, compared to that of cells cultured on GelMA hydrogels only. Therefore, rGO hybrid with a biocompatible hydrogel is an applicable strategy for the treatment of cardiac tissue engineering (25) .In a study by Choe et al. (7), the effect of rGO/ALG encapsulated human umbilical cord-derived MSCs was investigated. The results of Masson's Trichrome staining showed rGO/ALG containing MSCs have less fibrous tissue than the control group and alginate/GO, indicating a reduction in scar tissue and the presence of more collagen.

Based on the obtained results, we are assuming that the injected composition of rGO/hMSCs into the infarcted area could improve cardiac repair via the electrical conductivity of rGO as well as the ability to interact with ECM protein like FN which promoted the expression level of connexin 43 and angiogenic paracrine factors as has been previously proven (15). A recent study demonstrated that impaired propagation of electrical signals of the heart after MI could be improved by an applied anisotropic cardiac patch of rGO/silk fibroin composition. Increased pumping function, reduced susceptibility to arrhythmias, thickened LV walls, promoted angiogenesis of capillaries and better survival of cardiomyocytes were all considered the results of adding rGO to the silk patch via restoring the anisotropic electrical microenvironment in the infarcted myocardium (26). In summary, a combination of rGO, alginate, and hMSCs might be a viable approach for treating patients with MI.

Conclusion

Our experiments confirmed that the presence of rGO, as an electro-active moiety within ALG appears safe for intramyocardial injection, improving (LV) function and neovascularization. Applying this strategy provides a desirable electroactive hydrogel for stem cell therapy in patients with ischemic heart disease. However, more investigations are required to assess the safety of using rGO with ALG for the treatment of MI.

Acknowledgments

The authors acknowledge Dr. Behshid Gadrdoost for her technical assistance. The research was partially financially supported by Tarbiat Modares University, Tehran, Iran. There is no conflict of interest in this study.

Authors' Contributions

N.K.H.; Performed the experiments and wrote the main manuscript text, and performed data analysis. N.B.; Designed and supervised all experiments and manuscript writing. N.N.; Participated in the Eco cardiology investigation and participated in manuscript writing. M.S.; Data analysis and interpretation. M.R.; Data analysis and interpretation, and manuscript writing. All authors read, reviewed, and approved the manuscript.

References

1. Heidenreich PA, Trogdon JG, Khavjou OA, Butler J, Dracup K, Ezekowitz MD, et al. Forecasting the future of cardiovascular disease in the United States: a policy statement from the American Heart Association. Circulation. 2011; 123(8): 933-944.
2. Thygesen K, Alpert JS, White HD; Joint ESC/ACCF/AHA/WHF Task Force for the Redefinition of Myocardial Infarction. Universal definition of myocardial infarction. J Am Coll Cardiol. 2007; 50(22): 2173-2195.
3. Yu J, Christman KL, Chin E, Sievers RE, Saeed M, Lee RJ. Restoration of left ventricular geometry and improvement of left ventricular function in a rodent model of chronic ischemic cardiomyopathy. J Thorac Cardiovasc Surg. 2009; 137(1): 180-187.
4. Lee RJ, Hinson A, Bauernschmitt R, Matschke K, Fang Q, Mann DL, et al. The feasibility and safety of Algisyl-LVR™ as a method of left ventricular augmentation in patients with dilated cardiomyopathy: initial first in man clinical results. Int J Cardiol. 2015; 199: 18-24.
5. Chen J, Normand SL, Wang Y, Krumholz HM. National and regional trends in heart failure hospitalization and mortality rates for Medicare beneficiaries, 1998-2008. JAMA. 2011; 306(15): 1669-1678.
6. Nelson DM, Ma Z, Fujimoto KL, Hashizume R, Wagner WR. Intramyocardial biomaterial injection therapy in the treatment of heart failure: materials, outcomes and challenges. Acta Biomater. 2011; 7(1): 1-15.
7. Choe G, Kim SW, Park J, Park J, Kim S, Kim YS, et al. Anti-oxidant activity reinforced reduced graphene oxide/alginate microgels: Mesenchymal stem cell encapsulation and regeneration of infarcted hearts. Biomaterials. 2019; 225: 119513.
8. Müller-Ehmsen J, Whittaker P, Kloner RA, Dow JS, Sakoda T, Long TI, et al. Survival and development of neonatal rat cardiomyocytes transplanted into adult myocardium. J Mol Cell Cardiol. 2002; 34(2): 107-116.
9. Müller-Ehmsen J, Krausgrill B, Burst V, Schenk K, Neisen UC, Fries JW, et al. Effective engraftment but poor mid-term persistence of mononuclear and mesenchymal bone marrow cells in acute and chronic rat myocardial infarction. J Mol Cell Cardiol. 2006; 41(5): 876-884.
10. Zhang H, Song P, Tang Y, Zhang X-l, Zhao S-h, Wei Y-j, et al. Injection of bone marrow mesenchymal stem cells in the borderline area of infarcted myocardium: heart status and cell distribution. J Thorac Cardiovasc Surg. 2007; 134(5): 1234-1240.
11. Sabbah HN, Wang M, Gupta RC, Rastogi S, Ilsar I, Sabbah MS, et al. Augmentation of left ventricular wall thickness with alginate hydrogel implants improves left ventricular function and prevents progressive remodeling in dogs with chronic heart failure. JACC Heart Fail. 2013; 1(3): 252-258.
12. Roshanbinfar K, Hilborn J, Varghese OP, Oommen OP. Injectable and thermoresponsive pericardial matrix derived conductive scaffold for cardiac tissue engineering. RSC Adv. 2017; 7(51): 31980-31988.
13. Cui H, Liu Y, Cheng Y, Zhang Z, Zhang P, Chen X, et al. In vitro study of electroactive tetraaniline-containing thermosensitive hydrogels for cardiac tissue engineering. Biomacromolecules. 2014;

15(4): 1115-1123.
14. Lee WC, Lim CH, Shi H, Tang LA, Wang Y, Lim CT, et al. Origin of enhanced stem cell growth and differentiation on graphene and graphene oxide. ACS Nano. 2011; 5(9): 7334-7341.
15. Park J, Kim YS, Ryu S, Kang WS, Park S, Han J, et al. Graphene potentiates the myocardial repair efficacy of mesenchymal stem cells by stimulating the expression of angiogenic growth factors and gap junction protein. Adv Funct Mater. 2015; 25(17): 2590-2600.
16. Karimi Hajishoreh N, Baheiraei N, Naderi N, Salehnia M. Reduced graphene oxide facilitates biocompatibility of alginate for cardiac repair. J Bioact Compat Polym. 2020; 35(4-5): 363-377.
17. Naderi N, Hemmatinafar M, Gaeini AA, Bahramian A, Ghardashi-Afousi A, Kordi MR, et al. High-intensity interval training increase GATA4, CITED4 and c-Kit and decreases C/EBPβ in rats after myocardial infarction. Life Sci. 2019; 221: 319-326.
18. Shams Mofarahe Z, Ghaffari Novin M, Salehnia M. Folliculogenesis-associated genes expression in human vitrified ovarian tissue after xenotransplantation in γ-irradiated mice. Cell J. 2020; 22(3): 350-357.
19. Ye Z, Zhou Y, Cai H, Tan W. Myocardial regeneration: roles of stem cells and hydrogels. Adv Drug Deliv Rev. 2011; 63(8): 688-697.
20. Ruvinov E, Cohen S. Alginate biomaterial for the treatment of myocardial infarction: progress, translational strategies, and clinical outlook: from ocean algae to patient bedside. Adv Drug Deliv Rev. 2016; 96: 54-76.
21. Meng D, Diao C, Liang L. Engineering an alginate/β-glycerophosphate/dextran injectable hydrogel-delivery for cardiac therapies after acute myocardial infarctions. Mater Express. 2021; 11(6): 846-853.
22. Choy JS, Leng S, Acevedo-Bolton G, Shaul S, Fu L, Guo X, et al. Efficacy of intramyocardial injection of Algisyl-LVR for the treatment of ischemic heart failure in swine. Int J Cardiol. 2018; 255: 129-135.
23. Qiu Y, Wang Z, Owens AC, Kulaots I, Chen Y, Kane AB, et al. Antioxidant chemistry of graphene-based materials and its role in oxidation protection technology. Nanoscale. 2014; 6(20): 11744-11755.
24. Orlic D, Kajstura J, Chimenti S, Jakoniuk I, Anderson SM, Li B, et al. Bone marrow cells regenerate infarcted myocardium. Nature. 2001; 410(6829): 701-705.
25. Shin SR, Zihlmann C, Akbari M, Assawes P, Cheung L, Zhang K, et al. Reduced graphene oxide-gelma hybrid hydrogels as scaffolds for cardiac tissue engineering. Small. 2016; 12(27): 3677-3689.
26. Zhao G, Feng Y, Xue L, Cui M, Zhang Q, Xu F, et al. Anisotropic conductive reduced graphene oxide/silk matrices promote post-infarction myocardial function by restoring electrical integrity. Acta Biomater. 2022; 139: 190-203.

Original Article

Impact of Intraventricular Human Adipose-Derived Stem Cells Transplantation with Pregnenolone Treatment on Remyelination of Corpus Callosum in A Rat Model of Multiple Sclerosis

Mohammad Mardani, Ph.D.[1]*, Raosul Ganji, Ph.D.[1], Nazem Ghasemi, Ph.D.[1], Mohammad Kazemi, Ph.D.[2], Shahnaz Razavi, Ph.D.[1]*

1. Department of Anatomical Sciences, School of Medicine, Isfahan University of Medical Sciences, Isfahan, Iran
2. Department of Genetics, School of Medicine, Isfahan University of Medical Sciences, Isfahan, Iran

Corresponding Address: P.O.Box: 81746-73461, Department of Anatomical Sciences, School of Medicine, Isfahan University of Medical Sciences, Isfahan, Iran
Emails: mardani@med.mui.ac.ir, razavi@med.mui.ac.ir

Received: 11/August/2021, Accepted: 25/January/2022

Abstract

Objective: Multiple sclerosis (MS) is known as a nerve tissue disorder, which causes demyelination of central nervous system (CNS) fibers. Cell-based treatment is a novel strategy for the treatment of demyelinating diseases such as MS. Adipose-derived stem cells (ADSCs) have neuroprotective and neuroregenerative effects and pregnenolone as a neurosteroid has remarkable roles in neurogenesis. We intend to examine the impact of intraventricular transplantation of human ADSCs and systemic injection of pregnenolone on the remyelination of a rat model cuprizone-induced demyelination.

Materials and Methods: This experimental study was performed on 36 male Wistar rats that received a regular diet and a cuprizone diet for 3 weeks for M.S. induction. Through lipoaspirate surgery, human-ADSCs (hADSCs) were obtained from a patient. Six groups of rats (n=6): healthy, MS, sham, pregnenolone injection, ADSCs transplantation, and pregnenolone injection/ADSCs transplantation were included in this study. For assessment of remyelination, transmission electron microscopy (TEM), immunohistochemistry staining, real-time reverse transcription-polymerase chain reaction (RT-PCR), and enzyme-linked immunosorbent assay (ELISA) were performed.

Results: TEM outcomes revealed an increase in the thickness of the fibers myelin in the treatment groups (P<0.05). We also observed a significant upregulation of MBP, PDGFR-α, and MOG after treatment with hADSCs and pregnenolone compared to other study groups (P<0.001). These results were confirmed by immunostaining analysis. Moreover, there was no significant difference between the ADSCs/pregnenolone group and the control group regarding the level of MBP, A2B5, and MOG proteins in ELISA.

Conclusion: Our data implied that the remyelination and cell recovery were more improved by intraventricular ADSCs transplantation and pregnenolone injection after inducing a rat model of MS.

Keywords: Adipose-Derived Stem Cells, Intraventricular, Multiple Sclerosis, Pregnenolone

Cell Journal(Yakhteh), Vol 24, No 12, December 2022, Pages: 748-756

Citation: Mardani M, Ganji R, Ghasemi N, Kazemi M, Razavi Sh. Impact of intraventricular human adipose-derived stem cells transplantation with pregnenolone treatment on remyelination of corpus callosum in a rat model of multiple sclerosis. Cell J. 2022; 24(12): 748-756. doi: 10.22074/cellj.2022.8173.

Introduction

Multiple sclerosis (MS) is known as a nervous tissue disorder that causes demyelination of central nervous system (CNS) fibers. Degeneration of myelin sheath can create a complicated pattern of nervous system defects such as motor inability, visual problems, or mental disorders (1). The pathology of MS is described by lesions in CNS with perivascular inflammatory cell infiltration, demyelination, axonal destruction, neuronal decadence, and gliosis (2, 3).

MS is one of the most common neurological disorders in young adults worldwide. Overall, the prevalence of MS is 83 per 100000 individuals, and in women near two fold that of men (4, 5).

It is not yet clear what exactly causes MS, and there is currently no definitive cure for it; however, some treatments have been followed to reduce the number of *recurrence*s and slow the progression of the disease (6, 7). Cell-based treatment is a novel strategy for treating demyelinating diseases in CNS like MS (8).

In some studies, human embryonic stem cells, human bone marrow-derived mesenchymal stem cells (BM-MSCs), and human placental MSCs were used for transplantation in animal models of MS (9, 10). For example, a study on MSCs reported that they secrete various growth factors, especially facilitating oligodendrocyte differentiation (11).

hADSCs as a type of adult stem cells are able to differentiate into various cells and generate many identified neurotrophic factors, including brain-derived neurotrophic factor (BDNF), nerve growth factor (NGF), and glial cell line-derived neurotrophic factor (GDNF) (12, 13). Some studies have demonstrated that hADS are able to exert their effects by crossing the blood-brain barrier (BBB) (8, 11).

Transplantation of hADSCs in an animal model of MS could induce the regeneration of myelin sheaths and improve the complications of MS (8).

Pregnenolone is a cholesterol-derived neurosteroid synthesized in the central and peripheral nervous system, mainly in glial and neuron cells that other neurosteroids such as progesterone, estrogen, and cortisol are derived from it (14). It is demonstrated that pregnenolone and its related derivatives such as pregnenolone sulfate, allopregnanolone, and dehydroepiandrosterone (DHEA) enhance memory and learning and, relieve depression, and improve the conceptual functions of the brain (15). Also, pregnenolone and other neurosteroid have neuroprotective roles in some neuroinflammatory diseases, including MS and Alzheimer's disease (AD), and can benefit totreatment some disorders like schizophrenia, depression, and autism (16-18).

ADSCs, with a high proliferation rate for a long time, secrete neurotrophic factors (19) and may improve the remyelination process owing to the concomitant use of cell and pregnenolone.

In our previous study, the human ADSCs and pregnenolone were used for transplantation in an animal model in which demyelination induced by cuprizone and their efficacy in improving the histological structure and cell regeneration in demyelinated nerve tissue were examined. However, we found that ADSCs intravenously injected into rat MS model, were able to pass the BBB, and transplanting cells could improve remyelination. In this study, we aimed to transplant hADSCs into the cerebral ventricles with pregnenolone treatment, and the results of this procedure were compared with systemic injection.

Materials and Methods

Experimental design

This research was approved by the Ethical Committee of Isfahan University of Medical Sciences (IR.MUI.REC.1395.1.041) and was conducted at the Central Laboratory of this university in 2018.

Thirty-six, eight-week-old male Wistar rats weighing 200 ± 20 g were purchased from the Pasteur Institute, Tehran, Iran. Rats were maintained under 12 hours light/dark cycle, at basic room temperature, and had access to common food and water. The animals were randomly divided into six groups (six rats in each group) as follows: control group without any intervention (C), MS control group (demyelination was induced using cuprizone) (cup), sham group (demyelinated rats received culture medium intraventricular), the fourth group (rats underwent demyelination and injection of pregnenolone intraperitoneally) (Preg), the fifth group (demyelinated rats received PKH26-labeled hADSCs intraventricular), and the sixth group (demyelinated rats received pregnenolone intraperitoneally and hADSCs intraventricular simultaneously (ADS/Preg).

Induction of demyelination model

The demyelination lesion was induced using cuprizone (bis-cyclohexanone oxaldihydrazone, Sigma-Aldrich Inc C9012) a copper-chelating agent. To obtain the desired cuprizone model, we gavaged the rats for three weeks with 0.6% cuprizone, dissolved in corn oil. Three weeks after cuprizone feeding, a histological examination of the brain was done to verify the demyelination. Treatments led to oligodendrocyte apoptosis and demyelination of fibers which was examined in the corpus callosum (20).

Culture and labeling of human adipose-derived stem cells

After obtaining informed consent confirmed by the Ethic Committee of Isfahan University of Medical Sciences, adipose tissue was obtained by needle biopsy or liposuction aspiration from healthy adult donors during liposuction surgery. The obtained tissue was washed with phosphate-buffered saline (PBS, Sigma-Aldrich, UK, 806552-500ML). For the digestion of fat tissue, the 0.075% collagenase type I (Sigma-Aldrich, UK, SCR103) was added to the sample and incubated for 30 minutes at 37˚C, with 5% CO_2. This enzyme was prepared in PBS containing 2% penicillin/streptomycin (P/S, Bioidia, BI1036, Iran). The collagenase activity was then neutralized by DMEM/F12 (Bioidia, BI1027, Iran) containing 10% fetal bovine serum (FBS, Gibco, 10270106, US).

Afterward, the centrifuge was done for 10 minutes at 1400 rpm; and then the cell pellet was re-suspended in DMEM/F12, 10% FBS, and 1% P/S and cultured at 37˚C in a 5% CO_2 incubator. The medium was twice replaced over one week. When approximately 80% cell confluence was achieved, the cells were passaged. Detachment of cells was performed by 0.25% trypsin and 0.02% Ethylenediaminetetraacetic acid (EDTA). In the present study, passages 2-4 h-ADSCs were used for transplantation (12).

Before transplantation, the cells were labeled by PKH-26 based on instructions [(2 μmol of PKH26 for 1×10^7 cells) (Sigma-Aldrich, MINI26)]. Briefly, PKH26 was added to 1×10^6 cells/ml. After 1-5 minutes the labeling was stopped using 1% bovine serum albumin (BSA, Sigma-Aldrich A2153-10G, UK). To determine the percentage of labeled cells, hADSCs were assessed by fluorescent microscopy (Olympus BX51, Japan) after staining. Also, the survival of labeled cells was evaluated based on the culture of a portion of these cells (19).

Stereotaxic surgery, cell microinjection, and pregnenolone injection

Under deep anesthesia with an intraperitoneal injection (IP) of 10% ketamine (100 mg/kg) and 2% xylazine (10 mg/kg), the rats were positioned in a stereotaxic apparatus (Stoelting, USA). The scalp was dissected and the skull was cleaned. The lateral ventricles coordinates based on the Paxinos and Watson atlas (21) were as follows:

AP: -0.84 mm posterior to bregma; ML: ± 1.6 mm from the sagittal suture; and DV: 3-4 mm ventral from the skull surface.

Following a week of final cuprizone feeding for cell microinjections, 30-gauge stainless steel injector needles, connected to a Hamilton syringe by polyethylene tubing (PE-20), were stereo tactically proceeded to reach the lateral ventricles; subsequently, the solution was injected in a total volume of 5 ml/side containing 1×10^6 cell, over a 60 second period; the solution was then left in place for an extra 60s to facilitate the diffusion.

Also, pregnenolone sulfate (Pregnenolone sulfate sodium salt, Sigma-Aldrich, P162) was injected IP daily (2.5 mg) and dissolved in DMSO over the three weeks of cuprizone feeding.

Electron microscopic study

Rats were transcardially perfused with 1.6% glutaraldehyde (Sigma-Aldrich G5882, UK) in PBS (0.12 M, pH=7.4). The corpus callosum was detached and fixed by 1% osmium tetroxide (Sigma-Aldrich, UK, 75632) and embedded in epoxy resin after dehydration in graded ethanol. After embedding in resin, ultrathin 70 nm sections were prepared and stained with uranyl acetate and lead citrate and observed via a transmission electron microscopy (TEM, LEO 906 Germany, 100 kV). Images were taken from the corpus callosum after removing it from the rat brain. Pictures of the fibers cut in cross-section were taken and myelin status was assessed using ten images per specimen (×3000) analyzed by Digimizer Image Analysis Software 5.3.5 (copyright © 2005-2019 MedCalc software). The percentage of myelinated axons, axon diameter, myelin thickness, and G-ratio were measured using 50 fibers per sample. The G-ratio was calculated by the axon diameter/entire fiber diameter ratio. hence, a completely demyelinated fiber has a G-ratio of 1, whereas, in the myelinated fibers, the G-ratio is <1 (22).

Immunohistochemistry technique

The immunohistochemistry technique was accomplished to evaluate the myelin repair process and the rate of oligodendrocyte cell reproduction. For fixation of animals' brains, transcardial perfusion was done by 4% paraformaldehyde (PFA, Sigma, Germany) in 0.1 M PBS, pH=7.4, and post-fixation in the same fixative was followed overnight after brain removal. Then 3 µm-thick sections were prepared from Paraffin-embedded samples. After deparaffinization, rehydration, and heat unmasking, the samples were blocked with 10% normal goat serum, and then the samples were exposed overnight at 4˚C to the following primary antibodies: Mouse monoclonal Anti-MBP (1:1000; Abcam, Cambridge, MA, USA), Goat polyclonal Anti-MOG (1:1000; Abcam, Cambridge, MA, USA), Mouse monoclonal Anti-A2B5 (1:1000; Abcam, Cambridge, MA, USA. A2B5 is a cell surface ganglioside epitope expressed in oligodendrocyte progenitor cells.

The next day, the sections were washed by PBS and exposed to Goat anti-mouse and Anti-Goat (FITC) (1:500; Abcam, Cambridge, MA, USA)-conjugated secondary antibodies at room temperature for 1 hour. For cell nucleus staining we used 4',6-diamidino-2-phenylindole (DAPI) for 5 minutes. Finally, the number of MBP, MOG, and A2B5 positive cells in each section was counted using a fluorescence microscope (Olympus, BX51, Japan) (13).

Real-time reverse transcription-polymerase chain reaction analysis

The real-time reverse transcription-polymerase chain reaction (RT-PCR) method was used to evaluate the expression level of myelin basic protein (*MBP*), myelin oligodendrocyte glycoprotein (*MOG*), and platelet-derived growth factor receptor α (*PDGFR-α*) genes in the corpus callosum. Because there was no A2B5 primer, the *PDGFR-α* gene was employed to detect oligodendrocyte precursor cells. Total RNA was extracted from corpus callosum samples in all studied animals by Total RNA Prep Kit as stated in the manufacturer's protocol (BIOFACT, Korea). Reverse transcription of The RNA was performed by BioFact™ 5X RT Pre-Mix cDNA Synthesis Kit (BIOFACT) and oligo dT primers. To ensure that there is no DNA, the obtained RNA was treated with an RNase-free DNase kit (Qiagen, Germany).

The real-time RT-PCR was carried out by BIOFACT™ 2X Real-Time PCR Master Mix (BIOFACT) using the specifically mentioned primers and performed on a Step One Plus™ system (Applied Biosystems, US). The expression level of *MBP*, *MOG*, and *PGFRα* genes was assessed by quantitative real-time RT-PCR and compared to *β-actin* as a housekeeping gene (13). The PCR amplification conditions consisted of 15 minutes at 95˚C followed by 40 cycles of denaturation step at 95˚C for 20 seconds and annealing and extension for 1 minute at 60˚C. Melting curve analysis was used to determine the melting temperature of specific amplification products and primer. The comparative expression level of intended genes was calculated using the $2^{-\Delta\Delta ct}$ method. The primers were designed with Gene Runner 4.0 and tested by BLAST [http://blast. ncbi.nlm.nih.gov/Blast.cgi] to determine attachment to rats 'genome. The designed primers are presented in Table 1.

Enzyme-linked immunosorbent assay

The ELISA method was performed to evaluate the amount of MBP, MOG, and A2B5 protein. The rat's brain was stored at -70˚C after removal. When performing the ELISA process, corpus callosum separated from the brains and tissues was homogenized by a homogenizer. The homogenates were rotated at 6000 rpm for 10 minutes, and the pellets were resuspended in water at a pH of 3.0 for 1 hour. Then centrifuge at 10,000 rpm was done for 1 hour, and supernatants were stored at -20˚C at a pH of 8.8 by Tris-HCL buffer.

To perform the ELISA test, 50 µL of the sample was coated in each well, and on the next day after washing, 200 µL of blocking agent (5% BSA in PBS) was added

and incubated at 4˚C overnight. Next, washing was repeated 4 times, and 100 µL primary antibody was added as follows: anti-myelin basic protein (MBP) FITC antibody, anti-A2B5 FITC antibody, and anti-myelin oligodendrocyte glycoprotein (MOG) FITC antibody. The samples were incubated at 4˚C overnight. Then, after washing again, the plates were treated with the conjugated secondary antibody (goat anti-mouse HRP) for one hour. Then treatment by 100 µL tetramethylbenzidine (TMB) was done for 15 minutes at room temperature. Eventually, the ELISA reader measured optical density (OD) values of each sample at 450 nm and they were converted into concentration in pg/ml (23).

Statistical analysis

The results of the evaluation techniques were determined as mean± standard error of the mean (S.E.M). Data analysis was performed using SPSS 24 (IBM, US) software and the one-way analysis of variance (ANOVA), followed by the LSD post-hoc test. $P<0.05$ was defined for statistical significance.

Results

Transmission electron microscopy study

Transmission electron microscopic (TEM) images were applied to characterize myelin morphometric parameters, in the experimental groups. These photographs were obtained from the coronal sections of corpus callosum fibers and assessed by Digimizer Image Analysis Software to measure the myelinated axons percentage, axon diameter, thickness of myelin, and G-ratio. Three weeks after cuprizone feeding began the myelin of corpus callosum fibers degenerated. Myelin and axon degradation and also vacuole formation is seen in cuprizone and sham groups. In the treatment groups, especially the ADS/Preg group, myelination had been done relatively well (Fig.1A).

The mean of myelinated axons of the treatment groups was significantly increased compared with the cuprizone groups ($P<0.05$). Evaluation of TEM images showed a significant increase in the mean thickness of myelinated axons in the corpus callosum in the treatment groups compared with cuprizone and sham groups ($P<0.05$), but no significant difference with the control group was observed. Furthermore, a significant increase was observed in the mean of the G-ratio in cuprizone, and sham groups compared with the control group ($P<0.05$). On the other hand, in the treatment groups, the mean of this ratio was significantly reduced ($P<0.05$, Fig.1B).

Table 1: The designed both rat and human primers sequences for each gene

Gene	Primer sequences (5′-3′)	Annealing temperature (˚C)	PCR size bp
ACTB-H	F: GTTGTCGACGACGAGCG	60	93
	R: GCACAGAGCCTCGCCTT		
Actb-R	F: AGGCCCCTCTGAACCCTAAG	60	118
	R: CCAGAGGCATACAGGGACAA		
MBP-H	F: GGCCCCGTGGATGGA	60	76
	R: GAGGCGCGAAAGGAGATG		
Mbp-R	F: CACAGAAGAGACCCTCACAGCGAC	60	136
	R: CCGCTAAAGAAGCGCCCGATGGA		
MOG-H	F: ACCAGGCACCTGAATATCGG	60	195
	R: CAGGGCTCACCCAGTAGAAAG		
Mog-R	F: GAGGTTCTCGGATGAAGGAG	60	110
	R: CAGGGTTGATCCAGTAGAAGG		
PDGFR-H	F: TTGAAGGCAGGCACATTTACA	60	119
	R: GCGACAAGGTATAATGGCAGAAT		
Pdgfrα -R	F: AATGAAGGTGGCTGTGAAGATGC	60	102
	R: AGATGCGGTCCCAAGTGAGTC		

PCR; Polymerase chain reaction.

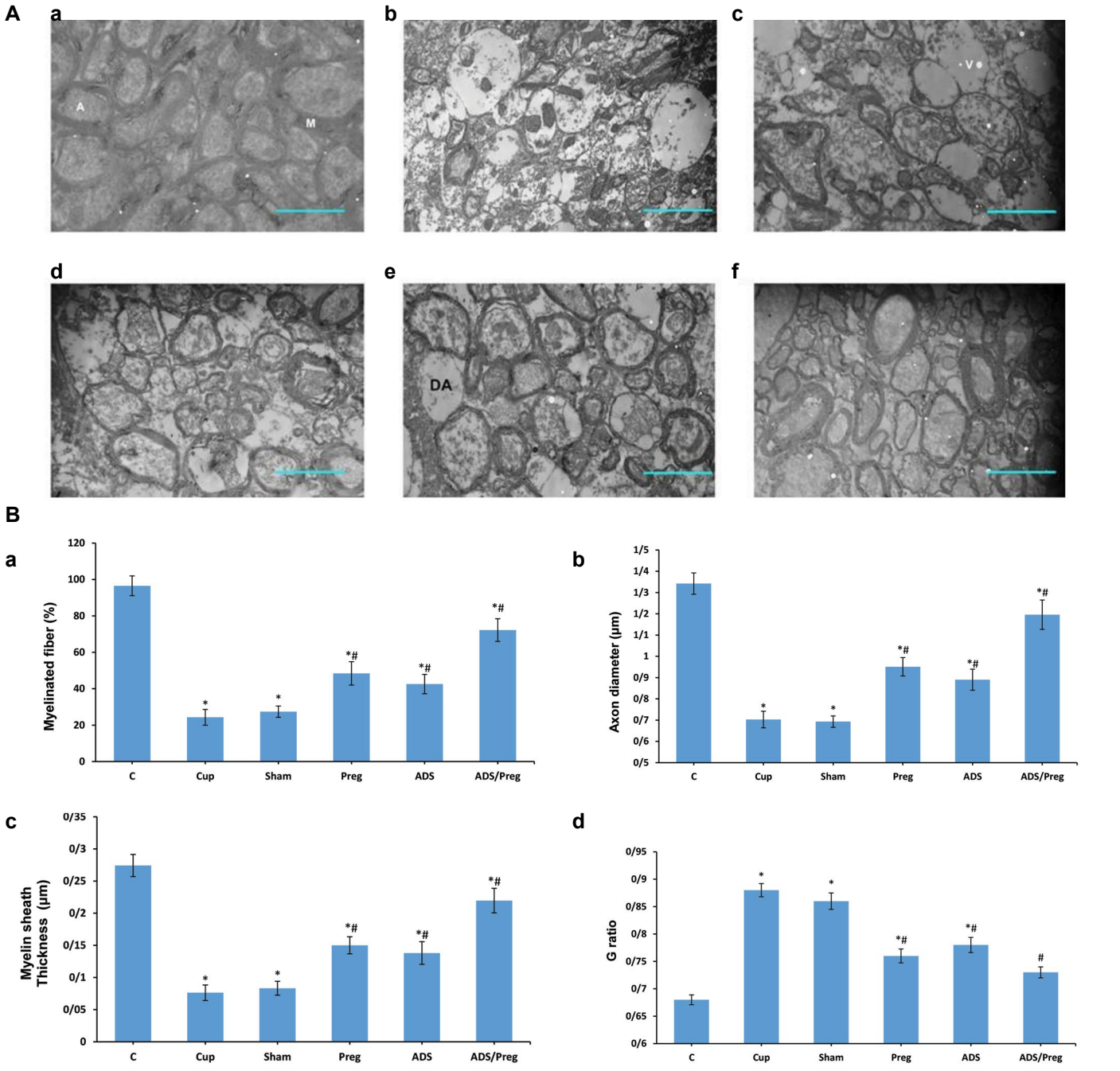

Fig.1: Transmission electron microscopic (TEM) study of the comparing groups. **A.** The TEM photos from the corpus callosum fibers of the rats' brains in the comparing groups**.** Demyelination of nerve fibers in the cuprizone and sham groups can be observed along with the destruction of demyelinated axons (DA) and vacuole formation (V). In ADS/Preg group, nerve fibers are properly remyelinated (TEM 2000x) (scale bar: 2 µm). **B.** Quantitative analysis of electron microscopy images**.** The mean percentage of myelinated fiber (a), axon diameter (b) and myelin thickness (c) in ADS/Preg group significantly increased compared with cuprizone and sham groups. Furthermore, the G-ratio (d) in the treatment groups, particularly ADS/Preg, was significantly reduced compared with cuprizone and sham groups. (mean ± SE) *; Significant difference with control group, #; Significant difference with cuprizone and sham group ($P<0.05$), C; Control group with any intervention, Cup; Cuprizone group, Sham; Sham group (received culture medium), Preg; Pregnenolone receiving group, ADS; hADSCs receiving group, and ADS/Preg; hADSCs and pregnenolone receiving group.

Real-time reverse transcription-polymerase chain reaction analysis

In this study, the source of ADSCs was from humans and examination was performed on rat corpus callosum to specify the level of myelination and oligodendrocyte retrieval; thus, rat and also human genes were analyzed. The results obtained from real-time RT-PCR showed that the injection of cuprizone significantly downregulated *Mbp*, *Mog*, and *PDGFR-α* genes in cuprizone and sham groups compared with the control group ($P<0.05$). However, *Mbp*, *Mog*, and *Pdgfr-α* expression significantly increased following treatment with hADSC and pregnenolone compared with cuprizone and sham groups. In the group simultaneously receiving hADSC and pregnenolone, the gene expression of *Mbp*, *Mog*, and *Pdgfr-α* increased even more than in healthy controls. Also, human *MBP, MOG* and *PDGFR-α* genes were significantly upregulated in ADS/Preg group in comparison to ADS group (Fig.2).

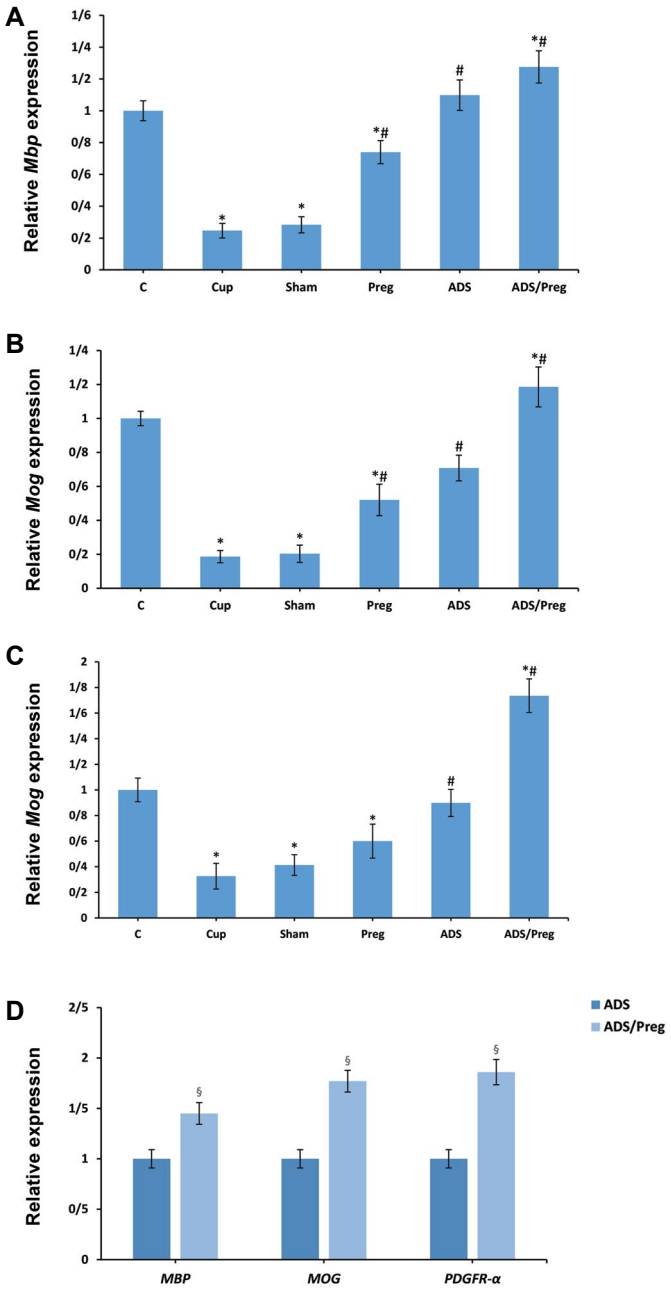

Fig.2: Comparison of the mean levels of *Mbp, Mog* and *Pdgfr-α* expression in corpus callusom of different groups using real time RT-PCR technique. **A.** The mean expression level of *Mbp* gene in ADS/Preg group significantly increased compared with other groups. **B.** The expression of *Mog* gene in ADS/Preg group significantly increased compared with other groups. **C.** The expression of *Pdgfr-α* gene in ADS/Preg group significantly increased compared with cuprizone, sham, and other treatment groups (mean ± SE). **D.** Human *MBP* and *MOG* and *PDGFR-α* genes were significantly upregulated in ADS/Preg group in comparison to ADS group. *; Significant difference with control group, #; Significant difference with cuprizone and sham group ((P<0.05), §: Significant difference between the ADS/Preg group and ADS and Preg groups, C; Control group with any intervention, Cup; Cuprizone group, Sham; Sham group (received culture medium), Preg; Pregnenolone receiving group, ADS; hADSCs receiving group, and ADS/Preg; hADSCs and pregnenolone receiving group.

Immunohistochemistry assay

After 3-4 cell passages of isolated hADSCs, the cells attached to the floor of the flasks had a homogenous morphology. The cells were then labeled by PKH26 and checked by fluorescent microscopy. The results showed that more than 85% of the isolated cells were labeled with PKH26.

Evaluation of the number of oligodendrocyte cells and remyelination in the corpus callosum was implemented by the IHC. Specific markers of immature oligodendrocyte (A2B5), mature oligodendrocyte (MOG), and myelination (MBP) were chosen for cell staining (Fig.3).

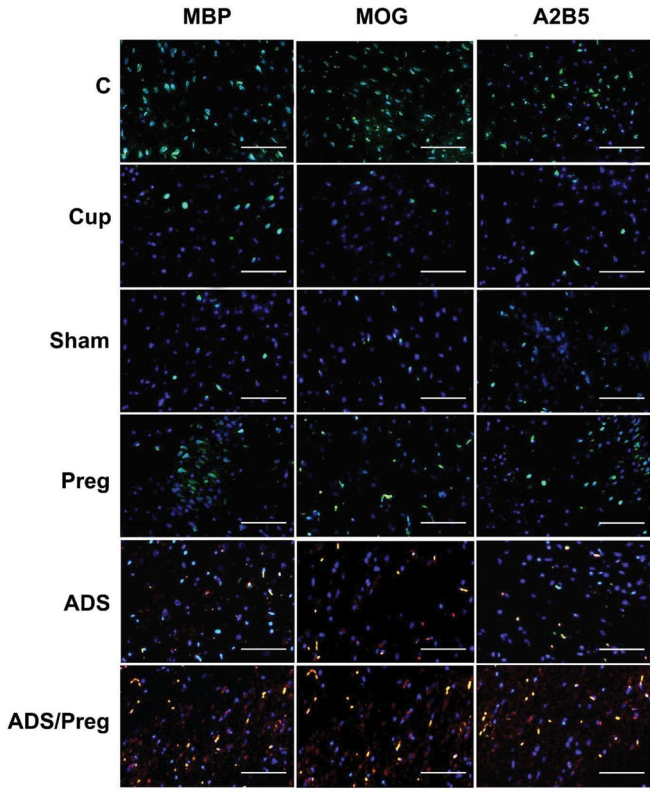

Fig.3: Immunohistochemistry images of paraffin section corpus callusom of studied groups for MBP, MOG and A2B5 four weeks after cell transplantation. The cells were depicted with a fluorescein isothiocyanate (FITC) (green), and 4' 6-diamidino-2-phenylindole (DAPI) (blue) for nuclear counterstaining. The PKH26 labeled cells (hADSCs) were red (scale bar: 50 µm). MBP; Myelin basic protein, MOG; Myelin oligodendrocyte glycoprotein, C; Control group with any intervention, Cup; Cuprizone group, Sham; Sham group (received culture medium), Preg; Pregnenolone receiving group, ADS; hADSCs receiving group, and ADS/Preg; hADSCs and pregnenolone receiving group.

Comparing the mean percentage of MBP, MOG, and A2B5 positive cells in different groups showed the mean percentage of MBP positive cells in all of the treated groups had a significant difference compared to the control group (P<0.05). Meanwhile, there was a significant increase in the Preg and ADS/Preg groups compared to the sham and cuprizone groups (P<0.05). Furthermore, the mean percentage of MOG-positive cells in treated groups showed a significant difference compared to the control group (P<0.05). However, the mean percentage of MOG-positive cells was significantly increased in the ADS and ADS/Preg groups compared to the sham and cuprizone groups (P<0.05). Similarly, the mean percentage of A2B5 positive cells showed a significant difference in all of the treated groups compared to the control group (P<0.05), but the ADS and ADS/Preg groups had a significant increase compared to sham and cuprizone groups (P<0.05, Fig.4).

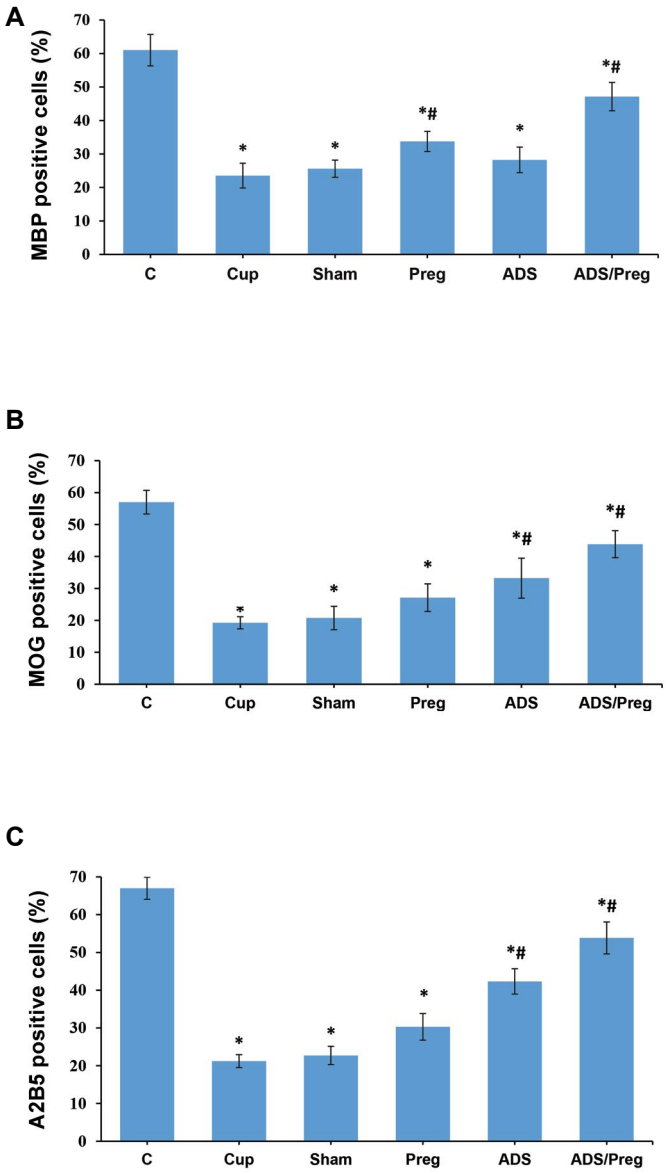

Fig.4: Comparison of the mean percentage of MBP, MOG and A2B5 positive cells in different groups. **A.** The mean percentage of myelin with MBP marker in all groups compared to the control group showed a significant difference (P<0.05). This percentage in the Preg and ADS/Preg treatment groups had a significant increase compared to the sham and cuprizone groups (P<0.05). **B.** The percentage of MOG positive cells in all groups compared to the control group showed a significant difference (P<0.05). This percentage had a significant increase in all treatment groups compared to sham and cuprizone groups (P<0.05). **C.** Similarly, the percentage of A2B5 positive cells in all groups compared to the control group showed a significant difference (P<0.05). This percentage in ADS and ADS/Preg treatment groups had a significant increase compared to sham and cuprizone groups. *; Significant difference with the control group, #; Significant difference with cuprizone and Sham groups (P<0.05), MBP; Myelin basic protein, MOG; Myelin oligodendrocyte glycoprotein, C; Control group with any intervention, Cup; Cuprizone group, Sham; Sham group (received culture medium), Preg; Pregnenolone receiving group, ADS; hADSCs receiving group, and ADS/Preg; hADSCs and pregnenolone receiving group.

Enzyme-linked immunosorbent assay

The protein level of MBP, MOG, and A2B5 significantly decreased in cuprizone, and sham groups compared to the control group (P<0.05), as presented in Figure 5. The protein levels of MBP, MOG, and A2B5 in the groups treated with hADSCs and pregnenolone were significantly higher than in the cuprizone and sham groups *(*P<0.05*)*. Treatment with hADSCs and pregnenolone in ADS/Preg increased the protein levels more than in other treatment groups, but no significant differences were observed (Fig.5).

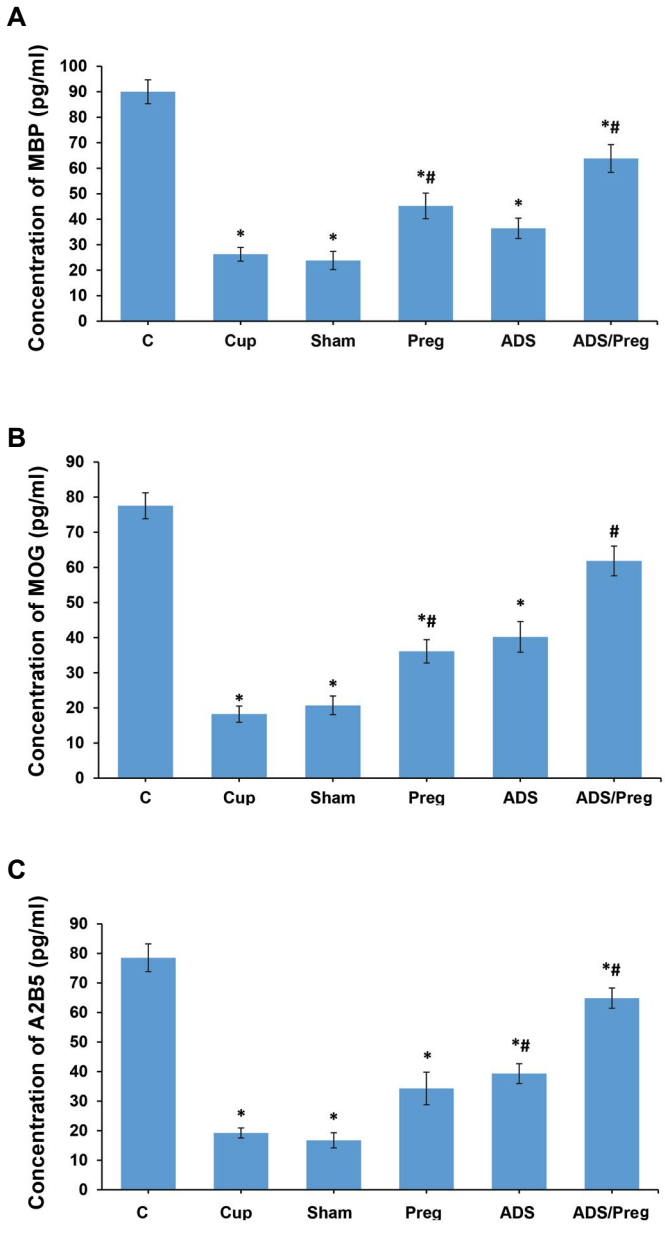

Fig.5: Comparison of the mean levels of MBP, MOG and A2B5 concentration in different groups using ELISA technique. The concentration of **A.** MBP, **B.** MOG and **C.** A2B5 proteins in groups reveals that the ADS/Preg and control group have no significant difference, but there is a significant increase in ADS/Preg group compared to the cuprizone and sham groups. *; Significant difference with control group, #; Significant difference with cuprizone and sham group (P<0.05), MBP; Myelin basic protein, MOG; Myelin oligodendrocyte glycoprotein, C; Control group with any intervention, Cup; Cuprizone group, Sham; Sham group (received culture medium), Preg; Pregnenolone receiving group, ADS; hADSCs receiving group, and ADS/Preg; hADSCs and pregnenolone receiving group.

Discussion

MS is a nerve tissue disorder specified by autoimmune and chronic inflammatory demyelination and degeneration of the CNS fibers (24).

Presently, some modulator drugs are used for treating MS, all of which influence the immune system (25), but there is no complete cure. Most medications have sedative and progress reduction aspects and remarkable drug efficacy is expected On the other hand, there are some side effects with them (26). Accordingly, it's essential to provide safer and complete treatments for this disorder.

Cell therapy is an interesting and effective strategy for treating neurodegenerative diseases; so far, different types of stem cells, for example, embryonic and MSCs, have been employed for this purpose. ADSCs have attracted the attention of many researchers because adipose tissues are abundant and have a large number of stem cells (27).

In this study, cuprizone was used orally to induce a model of MS in rats. Based on the obtained results, the MS model was induced effectively in the rats of the cuprizone-treated groups.

Cuprizone is a copper chelating agent that, when orally administrated, causes widespread demyelination in CNS fibers. After stopping cuprizone feeding, remyelination will resume, so this demyelination is dependent on the continuous feeding of cuprizone (20, 28). Corpus callosum is one of the main targets of cuprizone. Accumulation of microglia/macrophages in the corpus callosum is another effect of cuprizone (29).

Remyelination is the process of differentiation of oligodendrocytes from precursor cells, reconstruction of myelin sheaths on demyelinated fibers, prevention additional axonal damage, and re-establish saltatory conduction (30).

In our previous work, the human ADSCs and pregnenolone were used simultaneously through systemic injection in an animal model demyelination by cuprizone. We used behavior tests, histological examinations, real-time RT-PCR, and ELISA technique to evaluate functional status, remyelination progress, and myelin-producing cells recovery following 4 weeks. It was demonstrated that several ADSCs can migrate through blood circulation, cross the BBB and improve remyelination. Moreover, pregnenolone administration results in an increase in ADSCs differentiation into oligodendrocytes (31).

In the current study, to determine the effects of locally transplanted cells, near or at the site of injury, intraventricular transplantation of h-ADSCs and systemic injection of pregnenolone on remyelination in the corpus callosum of MS rat model induced by cuprizone.

Results of real-time RT-PCR and immunohistochemistry methods showed that transplantation of ADSCs into a model of MS leads to significant expression of some specific genes and markers of oligodendrocyte such as MOG, PDGFR-α, and A2B5 in ADS/Preg group than the other groups.

This process indicated an increase in the differentiation of oligodendrocytes from ADSCs, which was confirmed by increasing MBP expression by various methods. On the other hand, in this study, there was an increase in axon number and myelin thickness, which was confirmed by the TEM study. However, an increase in the amount and thickness of myelin suggests that differentiated oligodendrocytes may have the ability to regulate transcription of the major myelin genes that usually occur during active myelination (32). In addition, the increase in myelination by the ADS/Preg group may be due to the synergistic effect of the simultaneous use of ADSCs and pregnenolone.

Several studies have reported that the main mechanisms responsible for the therapeutic effects of stem cell transplantation are related to neurotrophic function and differentiation potential of stem cells in CNS (9, 10, 31).

The results of the current study were consistent with other studies. Aharonowiz et al. (33) found that human embryonic stem cell transplantation into the rat cerebral cortex had the potential to reduce the clinical signs in these models of MS and showed neuroprotective effects by suppressing the immune system. In addition, Burt et al. (34) showed that the use of hematopoietic stem cells incapable of producing myelin in patients with relapsing-remitting MS could reduce the disease progression and improve neurological symptoms.

In addition, the co-cell transplantation of hADSCs with neurotrophic factor secreting cells leads to more remyelination than transplantation of human ADSCs (19), and human ADSCs can differentiate into oligodendrocytes and enhance the remyelination process, possibly improving the motor functions (8).

We observed similar results given the fact that the number of positive cells for MBP, A2B5, and MOG significantly increased in the rats receiving ADSCs and pregnenolone as compared to other groups; this suggests that pregnenolone can have synergistic effects in the differentiation of ADSCs into oligodendrocyte.

Conclusion

Intraventricularly human ADSCs transplantation with pregnenolone injection can effectively improve remyelination of demyelinated nerve fibers in corpus callosum after inducing rat model of MS as compared to systemic transplantation of human ADSCs and pregnenolone treatment may be synergistic effects during differentiation of ADSCs into oligodendrocyte.

Acknowledgments

The author appreciates the Isfahan University of Medical Sciences for supporting this study (grant number: 195041). We would also like to thank the operating room of Alzahra Hospital for preparing the human adipose tissue. There is no conflict of interest in this study.

Authors' Contributions

M.M., R.G. Sh.R.; Contributed to conception and design. R.G.; N.Gh., M.K.; Contributed to all experimental work, data, and statistical analysis, and interpretation of data.

M.M., Sh.R.; Were responsible for overall supervision. R.G.; Drafted the manuscript, which was revised by Sh.R. All authors read and approved the final manuscript.

References

1. Ghasemi N, Razavi S, Nikzad E. Multiple sclerosis: pathogenesis, symptoms, diagnoses and cell-based therapy. Cell J. 2017; 19(1): 1-10.
2. Cohen JA, Imrey PB, Planchon SM, Bermel RA, Fisher E, Fox RJ, et al. Pilot trial of intravenous autologous culture-expanded mesenchymal stem cell transplantation in multiple sclerosis. Mult Scler. 2018; 24(4): 501-511.
3. Trapp BD, Nave KA. Multiple sclerosis: an immune or neurodegenerative disorder? Annu Rev Neurosci. 2008; 31: 247-269.
4. Kingwell E, Marriott JJ, Jetté N, Pringsheim T, Makhani N, Morrow SA, et al. Incidence and prevalence of multiple sclerosis in Europe: a systematic review. BMC Neurol. 2013; 13(1): 1-13.
5. Pugliatti M, Rosati G, Carton H, Riise T, Drulovic J, Vécsei L, et al. The epidemiology of multiple sclerosis in Europe. Eur J Neurol. 2006; 13(7): 700-722.
6. Boster A, Edan G, Frohman E, Javed A, Stuve O, Tselis A, et al. Intense immunosuppression in patients with rapidly worsening multiple sclerosis: treatment guidelines for the clinician. Lancet Neurol. 2008; 7(2): 173-183.
7. Stepien A, Dabrowska NL, Maciagowska M, Macoch RP, Zolocinska A, Mazur S, et al. Clinical application of autologous adipose stem cells in patients with multiple sclerosis: preliminary results. Mediators Inflamm. 2016; 2016: 5302120.
8. Ghasemi N, Razavi S, Mardani M, Esfandiari E, Salehi H, Esfahani SHZ. Transplantation of human adipose-derived stem cells enhances remyelination in lysolecithin-induced focal demyelination of rat spinal cord. Mol Biotechnol. 2014; 56(5): 470-478.
9. Bai L, Lennon DP, Eaton V, Maier K, Caplan AI, Miller SD, et al. Human bone marrow-derived mesenchymal stem cells induce Th2-polarized immune response and promote endogenous repair in animal models of multiple sclerosis. Glia. 2009; 57(11): 1192-1203.
10. Sharp J, Frame J, Siegenthaler M, Nistor G, Keirstead HS. Human embryonic stem cell-derived oligodendrocyte progenitor cell transplants improve recovery after cervical spinal cord injury. Stem Cells. 2010; 28(1): 152-163.
11. Constantin G, Marconi S, Rossi B, Angiari S, Calderan L, Anghileri E, et al. Adipose-derived mesenchymal stem cells ameliorate chronic experimental autoimmune encephalomyelitis. Stem Cells. 2009; 27(10): 2624-2635.
12. Razavi S, Mardani M, Kazemi M, Esfandiari E, Narimani M, Esmaeili A,et al. Effect of leukemia inhibitory factor on the myelinogenic ability of Schwann-like cells induced from human adipose-derived stem cells. Cell Mol Neurobiol. 2013 ; 33(2): 283-289.
13. Razavi S, Razavi MR, Kheirollahi-Kouhestani M, Mardani M, Mostafavi FS. Co-culture with neurotrophic factor secreting cells induced from adipose-derived stem cells: promotes neurogenic differentiation. Biochem Biophys Res Commun. 2013; 440(3): 381-387.
14. Agís-Balboa R C, Pinna G, Zhubi A, Maloku E, Veldic M, Costa E, et al. Characterization of brain neurons that express enzymes mediating neurosteroid biosynthesis. Proc Natl Acad Sci USA. 2006; 103(39): 14602-14607.
15. Vallée M, Mayo W, Le Moal M. Role of pregnenolone, dehydroepiandrosterone and their sulfate esters on learning and memory in cognitive aging. Brain Res Rev. 2001; 37(1-3): 301-312.
16. Daugherty DJ, Selvaraj V, Chechneva OV, Liu XB, Pleasure DE, Deng W. A TSPO ligand is protective in a mouse model of multiple sclerosis. EMBO Mol Med. 2013; 5(6): 891-903.
17. Naylor JC, Kilts JD, Hulette CM, Steffens DC, Blazer DG, Ervin JF, et al. Allopregnanolone levels are reduced in temporal cortex in patients with Alzheimer's disease compared to cognitively intact control subjects. Biochim Biophys Acta. 2010; 1801(8): 951-959.
18. Vallée M. Neurosteroids and potential therapeutics: focus on pregnenolone. J Steroid Biochem Mol Biol. 2016; 160: 78-87.
19. Razavi SR, Ghasemi N, Mardani M, Salehi H. Co-transplantation of human neurotrophic factor secreting cells and adipose-derived stem cells in rat model of multiple sclerosis. Cell J. 2018; 20(1): 46.
20. Torkildsen Ø, Brunborg L, Myhr K M, Bø L. The cuprizone model for demyelination. Acta Neurol Scand. 2008; 117: 72-76.
21. Paxinos G, Watson C. The rat brain in stereotaxic coordinates. 6th ed. Oxford: Academic Press; 2007: 62.
22. Hedayatpour A, Ragerdi I, Pasbakhsh P, Kafami L, Atlasi N, Mahabadi VP, et al. Promotion of remyelination by adipose mesenchymal stem cell transplantation in a cuprizone model of multiple sclerosis. Cell J. 2013; 15(2): 142-151.
23. Guan D, Li P, Zhang Q, Zhang W, Zhang D, Jiang J. An ultra-sensitive monoclonal antibody-based competitive enzyme immunoassay for aflatoxin M1 in milk and infant milk products. Food Chem. 2011; 125(4): 1359-1364.
24. Milo R, Miller A. Revised diagnostic criteria of multiple sclerosis. Autoimmun Rev. 2014; 13(4-5): 518-524.
25. Baecher-Allan C, Kaskow BJ, Weiner HL. Multiple sclerosis: mechanisms and immunotherapy. Neuron. 2018; 97(4): 742-768.
26. Namjooyan F, Ghanavati R, Majdinasab N, Jokari S, Janbozorgi M. Uses of complementary and alternative medicine in multiple sclerosis. J Tradit Complement Med. 2014; 4(3): 145-152.
27. Sen A, Lea-Currie YR, Sujkowska D, Franklin DM, Wilkison WO, Halvorsen YDC, et al. Adipogenic potential of human adipose derived stromal cells from multiple donors is heterogeneous. J Cell Biochem. 2001; 81(2): 312-319.
28. Skripuletz T, Gudi V, Hackstette D, Stangel M. De-and remyelination in the CNS white and grey matter induced by cuprizone: the old, the new, and the unexpected. Histol Histopathol. 2011; 26(12): 1585-1597.
29. Hiremath M, Saito Y, Knapp G, Ting JY, Suzuki K, Matsushima G. Microglial/macrophage accumulation during cuprizone-induced demyelination in C57BL/6 mice. J Neuroimmunol. 1998; 92(1-2): 38-49.
30. Franklin RJ. Remyelination in the CNS: from biology to therapy. Nat Rev Neurosci. 2008; 9(11): 839-855.
31. Ganji R, Razavi S, Ghasemi N, Mardani M. Improvement of remyelination in demyelinated corpus callosum using human adipose-derived stem cells (hADSCs) and pregnenolone in the cuprizone rat model of multiple sclerosis. J Mol Neurosci. 2020; 70(7): 1088-1099.
32. Ishii A, Fyffe-Maricich SL, Furusho M, Miller RH, Bansal R. ERK1/ERK2 MAPK signaling is required to increase myelin thickness independent of oligodendrocyte differentiation and initiation of myelination. J Neurosci. 2012; 32(26): 8855-8864.
33. Aharonowiz M, Einstein O, Fainstein N, Lassmann H, Reubinoff B, Ben-Hur T. Neuroprotective effect of transplanted human embryonic stem cell-derived neural precursors in an animal model of multiple sclerosis. PLoS One. 2008; 3(9): e3145.
34. Burt RK, Loh Y, Cohen B, Stefoski D, Balabanov R, Katsamakis G, et al. Autologous non-myeloablative haemopoietic stem cell transplantation in relapsing-remitting multiple sclerosis: a phase I/II study. Lancet Neurol. 2009; 8(3): 244-253.

Original Article

Aberrant DNA Methylation Status and mRNA Expression Level of *SMG1* Gene in Chronic Myeloid Leukemia: A Case-Control Study

Tahereh Hojjatipour, M.Sc.[1], Mahsa Sohani, M.Sc.[1], Amirhosein Maali, M.Sc.[2, 3], Shahrbano Rostami, Ph.D.[4*], Mehdi Azad, Ph.D.[5*]

1. Department of Hematology and Blood Transfusion, Students Research Center, School of Allied Medicine, Tehran University of Medical Sciences, Tehran, Iran
2. Department of Immunology, Pasteur Institute of Iran, Tehran, Iran
3. Department of Medical Biotechnology, School of Allied Medicine, Qazvin University of Medical Sciences, Qazvin, Iran
4. Hematologic Malignancies Research Center, Tehran University of Medical Sciences, Tehran, Iran
5. Department of Medical Laboratory Sciences, School of Paramedicine, Qazvin University of Medical Sciences, Qazvin, Iran

Corresponding Addresses: P.O.Box: 3419915315, Hematologic Malignancies Research Center, Tehran University of Medical Sciences, Tehran, Iran
P.O.Box: 1416634793, Department of Medical Laboratory Sciences, School of Paramedicine, Qazvin University of Medical Sciences, Qazvin, Iran
Emails: drostamy@yahoo.com, haematologicca@gmail.com

Received: 19/March/2022, Accepted: 08/June/2022

Abstract

Objective: Chronic myeloid leukemia (CML) is a myeloproliferative malignancy with different stages. Aberrant epigenetic modifications, such as DNA methylation, have been introduced as a signature for diverse cancers which also plays a crucial role in CML pathogenesis and development. Suppressor with morphogenetic effect on genitalia (*SMG1*) gene recently has been brought to the spotlight as a potent tumor suppressor gene that can be suppressed by tumors for further progress. The present study aims to investigate *SMG1* status in CML patients.

Materials and Methods: In this case-control study, peripheral blood from 30 patients with different phases of CML [new case (N)=10, complete molecular remission (CMR)=10, blastic phase (BP)=10] and 10 healthy subjects were collected. Methylation status and expression level of *SMG1* gene promoter was assessed by methylation-specific polymerase chain reaction (MSP) and quantitative reverse-transcription PCR, respectively.

Results: MSP results of *SMG1* gene promotor in the new case group were methylated (60% methylated, 30% hemimethylated and 10% unmethylated). All CMR and control group patients were unmethylated in the *SMG1* gene promoter. In the BP group, methylated *SMG1* promoter was seen (50% of patients had a methylated status and 50% had hemimethylated status). In comparison with the healthy subjects, expression level of *SMG1* in the new case group was decreased ($P<0.01$); in the CMR group and BP-CML groups, it was increased ($P<0.05$). No significant correlation between patients' hematological features and *SMG1* methylation was seen.

Conclusion: Our results demonstrated that aberrant methylation of *SMG1* occurred in CML patients and it had a significant association with *SMG1* expression. *SMG1* gene promoter showed diverse methylated status and subsequent expression levels in different phases of CML. These findings suggested possible participation of *SMG1* suppression in the CML pathogenesis.

Keywords: Chronic Myeloid Leukemia, DNA Methylation, Gene Expression, *SMG1*

Cell Journal(Yakhteh), Vol 24, No 12, December 2022, Pages: 757-763

Citation: **Hojjatipour T, Sohani M, Maali A, Rostami Sh, Azad M. Aberrant DNA methylation status and mRNA expression level of SMG1 gene in chronic myeloid leukemia: a case-control study. Cell J. 2022; 24(12): 757-763. doi: 10.22074/cellj.2022.8526.**

Introduction

Chronic myeloid leukemia (CML) is a myeloproliferative malignancy characterized by excessive myeloid clonal proliferation in hematopoietic tissues (1, 2). Clinically, CML is divided into three phases, including the chronic phase (CP), accelerated phase (AP) and blastic phase (BP) (3). CP, AP and BP are defined as less than 10%, more than 10% and more than 20% of myeloid blasts in the blood and bone marrow, respectively. CP is the prolonged phase of CML that might last several years; in contrast, BP is considered the terminal phase of CML. Almost all CML patients have acquired the Philadelphia chromosome (Ph) resulting from a reciprocal translocation between the long arm of chromosome 9 and the short arm of chromosome 22. The translocation results in the formation of the *BCR-ABL1* gene fusion whose oncoprotein product is assumed as the main responsible for CML pathogenesis (4). However, the initial mechanism involved in the pathogenic Ph formation is unclear (1). As well as the Ph chromosome, multiple cytogenetic abnormalities and epigenetic dysregulations are reported, especially in CML progressed phases, such as AP and BP (2).

Epigenetic modifications, including DNA methylation, histone modifications and microRNA expression, are inducible and reversible changes that play a crucial role in gene regulation and cell cycle control. DNA methylation occurs in CpG dinucleotides, which are highly located in gene promotors. DNA methyltransferase (*DNMT*) enzymes are responsible for the DNA methylation

process by adding a methyl (CH_3) group to the 5′ position of cytosines (5). DNA hypermethylation usually leads to gene silencing, while DNA hypomethylation results in gene expression. Alternatively, tumor cells, such as CML, recruit the upper mentioned capacity through desired gene expression or suppression for further development (1). For instance, hypermethylation of some tumor suppressor genes, including E-cadherin, glutathione peroxidase 3 (*GPX3*), death-associated protein kinase (*DAPK*), estrogen receptor (*ER*), *p15* and *p16* have been reported in CML (5-7). Transcription Factor AP-2 Alpha *(TFAP2A*) also functions as a tumor suppressor gene and plays a critical role in cancer cell sensitivity to chemotherapy. Significant hypermethylation of the *TFAP2A* gene is reported in the BP of CML (8, 9). Several significant transcription factors such as DNA-damage-inducible transcript 3 (*DDIT3*), Runt-related transcription factor 1 *(RUNX1)*, Signal transducer and activator of transcription 3 (*STAT3*) and stem cell leukemia (*SCL*) were also hypermethylated in CML patients, especially in the progressed phases (6, 10, 11). Since the related function of upper-mentioned genes are critical in DNA repair and cell cycle regulation, their aberrant silencing has a significant impact on CML development (12, 13). On the other hand, there is sufficient evidence on the side of DNA hypomethylation in CML. The overall DNA hypomethylation leading to genomic instability is assumed as one probable reason for CML blastic transformation. Furthermore, hypomethylation of tumor-associated antigens and some oncogenes such as preferentially expressed antigen of melanoma *(PRAME)* has been shown in CML (1, 14).

Suppressor with morphogenetic effect on genitalia (*SMG1*) is a member of the phosphoinositide 3-kinase-related kinases (PIKK) family. The primary role of *SMG1* is participation in the non-sense mediating mRNA decay (NMD) process to eliminate premature mRNAs (15). However, previous research have revealed tumor suppressor activity of *SMG1* in solid tumors and hematologic malignancies (16). Several studies demonstrated the hypermethylated *SMG1* promotor and subsequent downregulation in different cancers (17, 18). Specific epigenetic modifications pattern has been shown in different cancers. For example, distinct methylation patterns have been reported in different AML subclasses, which probably associated to the particular cytogenetic and molecular abnormality (19, 20). In this regard, although many aspects of epigenetic abnormality in CML have been investigated, to the best of our knowledge, there is no data regarding *SMG1* status in CML patients. The aim of this study was to investigate methylation status and expression level of the *SMG1* gene in CML patients and determine association of this result with different phases of CML.

Materials and Methods

Patients and samples

This case-control study was performed on 30 CML patients, including 10 N (newly diagnosed CML with chronic phase), 10 complete molecular response (CMR) patients and 10 BP (blastic phase of CML) patients, as well as 10 healthy control participants referred to Hematology, Oncology and Stem Cell Transplantation Research Center at Shariati Hospital, Tehran, Iran. CML diagnosis was confirmed genetically in all cases by detecting the *BCR/ABL1* gene fusion. All medical records of patients were collected. The Human Research Ethics Committee from Tehran University of Medical Sciences approved the current study (IR.TUMS.VCR.REC.1395.68). Written informed consent was taken from the all participants and those who refused to participate in study were substituted with new participants. Five milliliters of arterial blood were collected in the sterile condition via vacuum tubes containing K2-EDTA from all participants and transferred to the molecular laboratory.

DNA extraction and bisulfite modification

DNA was extracted using DNA extraction kit (Favorgen Biotech, Austria) as manufaturer's protocol. Yield and purity of DNA were determined using a NanoDrop spectrophotometer at 260/280 nm (NanoDrop ND-2000C Spectrophotometer, Thermo Fisher Scientific, USA). Then, DNA was treated with sodium bisulfite using Fast EpiTect Kit (Qiagen, USA). The treated DNA was resuspended in water and stored at -80˚C until the next steps.

Methylation-specific polymerase chain reaction

The treated DNA was prepared for methylation-specific polymerase chain reaction (MS-PCR) to investigate methylation status of the *SMG1* gene. The target DNA for PCR amplification was a 178 base pair segment of the 16p12.3 band, which was included in the CpG island of the *SMG1* promoter. The methylated (M) and unmethylated (U) primers of *SMG1* were designed with MethPrimer software.

MS-PCR method was performed using Taq DNA Polymerase Master Mix 2x (Ampliqon, Denmark). The PCR amplification was performed on the Applied Biosystems Veriti thermal (Applied Biosystems, USA). Each PCR tube contained 0.5 µl of forwarding methylated/un-methylated primers, 0.5 µl of reverse methylated/un-methylated primers, 10 µl of PCR master mix (2x), 8.5 µl of ddH_2O and 1 µl of bisulfite-treated DNA. The PCR was performed under the following condition: an initial pre-denaturation at 94˚C for 4 minutes, 35 cycles of PCR stages, including 94˚C for 30 seconds (denaturation), 62˚C for 30 seconds (annealing) and 72˚C for 30 seconds (extension), followed by a final extension of 5 minutes at 72˚C.

The PCR products were electrophoresed in a 2.5% agarose gel stained with DNA Safe Stain (Sinaclon, Iran, EP5083). Furthermore, for each MSP reaction a commercial methylated DNA (Qiagen Inc., cat. No. 59695) and a commercial unmethylated DNA (Qiagen Inc., cat. No. 59695) were used as methylated and unmethylated primer control, respectively. Distilled water was used as a non-template control in each set of PCR reactions.

RNA isolation and quantitative reverse transcription polymerase chain reaction

Total RNA was extracted using the TRIzol® Reagent (Thermo Fisher, USA). Yield and purity of RNA were determined using a NanoDrop spectrophotometer at 260/280 nm. cDNA was synthesized using the cDNA synthesis kit (Takara Bio Inc, Japan). The primers of the *SMG1* and *ABL* gene (reference gene) were extracted from the previous study (17). Accuracy and specificity of primers were checked using NCBI BLAST tool (HTTP://www.ncbi.nlm.nih.gov/tools/primer-blast/). The applied primers are shown in Table 1.

SMG1 expression levels were measured using the quantitative reverse-transcription PCR (qRT-PCR) with the SYBR® Premix Ex Taq™ II (Takara Bio Inc, Japan) kit in an ABI thermal cycler system. First, 10 µl of master mix (2x), 0.7 µl of each forward and reverse primers, 7 µl of ddH_2O and 2 µl of the cDNA were mixed. The reaction mixture was started with a primary denaturation at 95˚C for 30 seconds, then followed by 40 cycles including 95˚C for 5 seconds, 60˚C for 30 seconds and 72˚C for 30 seconds. Melting program was performed under the following condition: 95˚C for 15 seconds, 60˚C for 1 minute and 95˚C for 15 seconds. Relative expression level of *SMG1* mRNA in the test sample was calculated and normalized to the reference *ABL* mRNA transcript level, as an internal control gene. The equation: relative mRNA expression=$2^{-\Delta\Delta Ct}$ was used for calculation of mRNA expression in each sample (21).

Statistical analysis

Statistical analysis was calculated using SPSS 21.0 (IBM, USA) and JMP10.0 (SAS Institute Inc, USA). Chi-Square and contingency table test were carried out to compare the difference in methylation status between study groups. Kruskal Wallis and means comparisons test using Dunn method by Bonferroni correction, were carried out to compare the expression difference between each phase of CML and control group. Association of *SMG1* methylation status and the corresponding gene expression level was also done by Kruskal Wallis test via investigation of expression difference in various methylation statuses. Association between *SMG1* promoter methylation and hematologic parameters was analyzed using the Kruskal Wallis test with Post hoc tests. Pearson correlation was applied to assess the relationship between mRNA expression level and hematologic parameters. The graphs were drawn using JMP10.0 and GraphPad Prism 9.00 (GraphPad Software Inc, USA). For all analyses, the P values were two-tailed and a $P<0.05$ was considered statistically significant.

Results

SMG1 methylation status

Methylation status of the *SMG1* gene promotor was determined using bisulfite treatment and subsequent MS-PCR. The representative products of *SMG1* methylation for the U and M alleles are illustrated in Table 1. The subjects with a U allele alone are described as unmethylated, the subjects with an M allele alone are described as methylated, and the subject with both M and U alleles are described as the hemimethylated promoters.

All healthy subjects and CMR group participants were unmethylated in the *SMG1* gene promoter. The *SMG1* promoter was methylated in 60% of new case CML patients, while 30% and 10% of patients were hemimethylated and unmethylated in the *SMG1* gene promoter, respectively. In the BP group, 50% of patients were methylated and 50% were hemimethylated in the *SMG1* gene promoter. Therefore, BP and the new case group had hypermethylated gene promoters compared to the control group (P=<0.0001, Fig.1).

Table 1: Sequences of the primers used in this study

Techniques	Primer name	Primer sequences (5´-3´)	Product size (bp)
MS-PCR	*SMG1 M*	F: GCGTACGTGAATTTAAGGGTAC	178
		R: AACAAAAAATCTCCACTACTACGAC	
	SMG1 U	F: GGTGTATGTGAATTTAAGGGTATGT	178
		R: AACAAAAAATCTCCACTACTACAAC	
QR-PCR	SMG1 RNA	F: GGTGGCTCGATGTTACCCTC	106
		R: CTGCGTGAGCGAAGGTTTC	
	ABL RNA	F: TGGAGATAACACTCTAAGCATAACTAAAGG	124
		R: GATGTAGTTGCTTGGGACCCA	

M; Methylated primer, and U; Unmethylated primer, MS-PCR; Methylation-specific polymerase chain reaction, and QR-PCR; Quantitative reverse-transcription polymerase chain reaction.

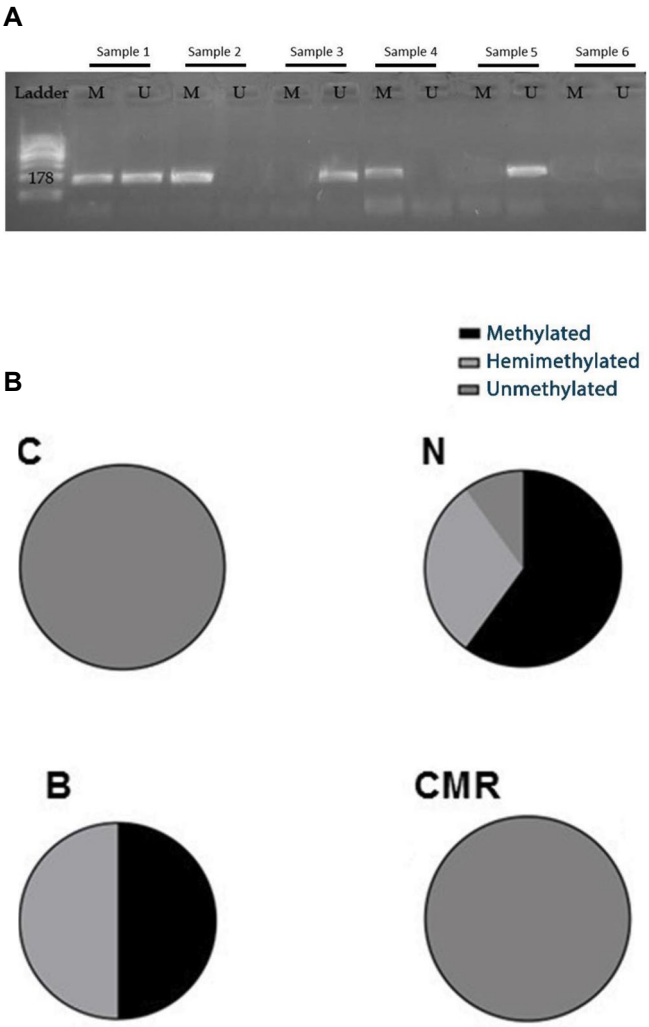

Fig.1: Methylation status of *SMG1* in CML. **A.** Representative gel electrophoresis of PCR products for unmethylated (U) and methylated (M) alleles of *SMG1* in the hemimethylated sample (sample 1), M sample (sample 2), U sample (sample 3), negative control (sample 6), as well as unmethylated primer control (sample 5), and methylated primer control (sample 4). **B.** The pie chart represents proportion (%) of the *SMG1* methylation status in different groups of the current study. CML; Chronic myeloid leukemia, PCR; Polymerase chain reaction, BP; Blastic phase, CMR; Complete molecular response, N; New case, and C; Control.

Baseline and demographic features of patients and healthy subjects are represented in Table 2. There was no significant association between the methylation status of the *SMG1* gene promoter and the hematologic parameters, including hemoglobin level, platelet count and WBC count (Table 3).

Expression level of *SMG1*

qRT-PCR was performed to determine expression level of *SMG1*. Expression level of *SMG1* in the new case group was decreased compared to the control group (P=0.0295). Expression level of *SMG1* in the CMR group was significantly higher than the control group (P=0.04). On the other hand, expression level in the BP group was decreased compared to the control group (P=0.0028). Expression level of *SMG1* in BP group was lower than the new case group (P=0.047). The highest expression level was seen in the CMR group, while the lowest expression level was observed in the BP group (Fig.2).

Table 2: Baseline and demographic features of patients and healthy subjects

Property	CML patients (n=30)	Healthy control (n=10)
Gender	Male=12 (40%)	Male=5 (50%)
	Female=18 (60%)	Female=5 (50%)
Age (Y)	30.5 ± 14.1	28 ± 5.1
WBC count ($\times 10^9$/L)	60 ± 10.2	7.5 ± 1.4
Platelet count ($\times 10^9$/L)	3440 ± 227.499	312 ± 49
Hemoglobin (g/dL)	11.26 ± 2.3	13.6 ± 2.8

CML; Chronic myeloid leukemia and WBC; White blood cell. Data are presented as mean ± SD.

Table 3: Association of methylation as well as correlation of *SMG1* gene expression with hematologic parameters. No significant data was seen

Index	P value	
	Methylation status	mRNA expression (co-efficiency)
WBC count	0.6250	0.2771 (-0.289)
Platelet count	0.5738	0.9424 (0.02)
Hemoglobin	0.2898	0.5883 (0.147)

WBC; White blood cell.

Association of *SMG1* expression and methylation status

Statistical analysis showed that mRNA expression of *SMG1* gene promotor from CML patients negatively associated with methylation status of promoter of this gene (P<0.0001). Methylated samples from new case and blastic groups showed the lowest expression levels, while the unmethylated samples from different study groups had the highest expression level. Hemimethylated samples from the BP or new case groups represented an intermediate expression level, compared to methylated and unmethylated samples.

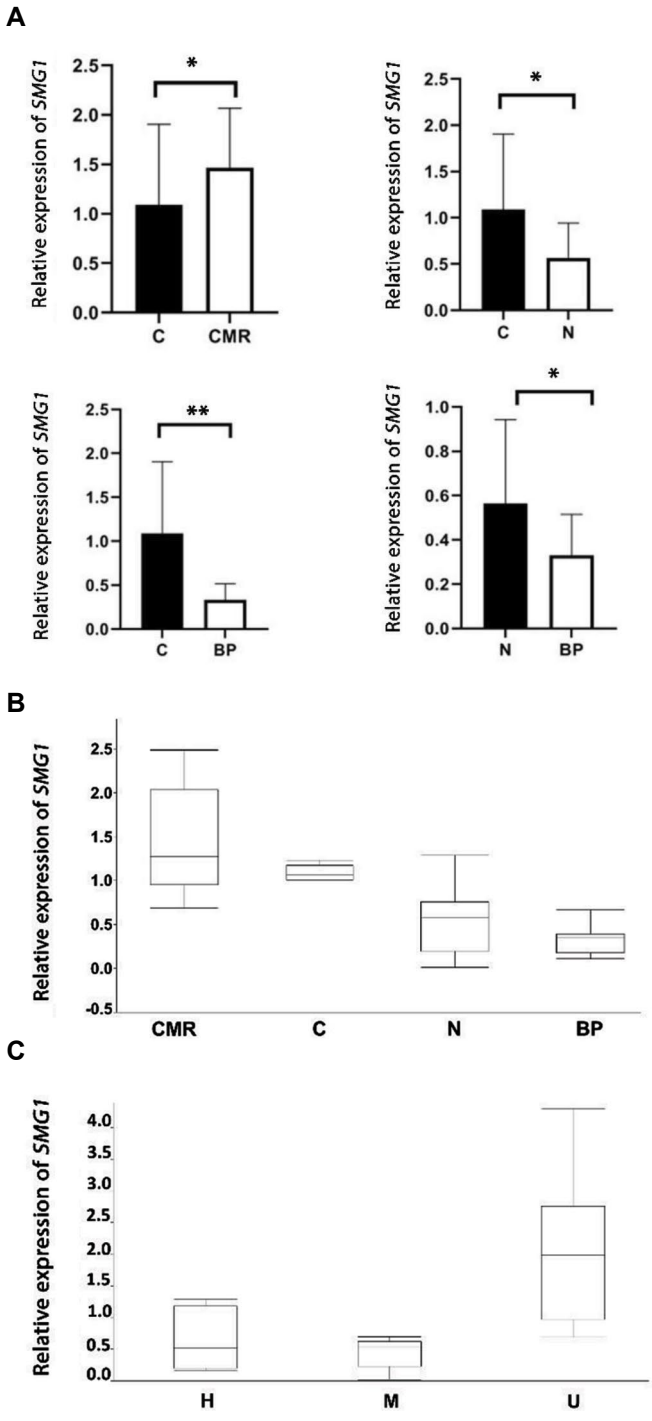

Fig.2: Relative mRNA expression level of the *SMG1* gene CML. **A.** Adual comparison of different groups, **B.** The box plot representations of different groups, and **C.** The box plot representations of different status. CML; Chronic myeloid leukemia, BP; Blastic phase, CMR; Complete molecular response, N; New case, C; Control; H; Hemimethylated, M; Methylated, and U; Unmethylated, *; P<0.05, and **; P<0.01.

Discussion

Epigenetic modifications have recently drawn important attention in the field of cancer etiopathology (22). In the current study, we were interested in the impact of possible aberrant methylated *SMG1* promotors on CML pathogenesis. A bulk of studies have focused on the role of aberrant DNA methylation in CML propagation and subsequent acquired resistance to therapy (10, 23).

SMG1 is a well-known member of the phosphatidylinositol-3 kinase-related kinases (PIKK) family which encompasses important regulating factors, such as mammalian target of rapamycin *(mTOR*) and ataxia telangiectasia mutated (*ATM*) (24). While contribution of *SMG1* in NMD process are well-established, a novel tumor suppressor activity of *SMG1* has been brought to the spotlight (25). *SMG1* activities are essential for genome maintenance and telomere integrity in response to radiation, hypoxia and stress. Preservation from tumor necrosis factor-α (TNF-α)-dependent apoptosis, lifespan adjustment, p53 activation and regulation of diverse genes are some critical anti-tumor activities of *SMG1* in normal cells. Furthermore, DNA damage response (DDR) process is highly dependent on SMG1 activity to protect cells from genetic instability (15, 26-29). In this regard, major research has recently been focused on *SMG1* dysregulation in diverse cancer development. Gubanova et al. (30) revealed a significant reduction in p53 activity in response to radiation in *SMG1*-absent osteosarcoma cell line compared to *SMG1*-wildtype cells. Researchers also demonstrated a deformed response following exposure to genotoxic stress in the cells with loss of *SMG1* activity. According to the multiple studies, complete loss of *SMG1* activity is embryonically lethal; however, deficient mice or *SMG1* haploinsufficiency potently develop inflammation and cancers, especially hematologic malignancy compared to the normal cells. Wong et al. (31) represented *SMG1* mutant variants that lead to the dysfunctional activity of translational proteins as potent pancreatic cancer susceptibility genes. *SMG1* downregulation was reported in hepatocellular carcinoma patients, especially in the end stage disease. Additionally, researchers suggested *SMG1* downregulation as a favorable biomarker for the hepatocellular carcinoma prognosis (32). Hypermethylation and subsequent downregulation of *SMG1* gene promotor have been shown in head and neck squamous cell carcinoma and acute myeloblastic leukemia (AML) (16, 17). It was recently revealed that *SMG1* expression was decreased in chronic lymphoblastic leukemia (CLL) patients, which might be exerted through aberrant promoter hypermethylation (18). Our results, in accordance with these findings, revealed a significant hypermethylation of *SMG1* promotor and subsequent downregulation in CML patients compared to the healthy controls and CMR-CML patients.

Based on the findings of this study, hypermethylation of *SMG1* might play a prognostic role in CML pathogenesis and blastic transformation. Although all CML patients carry similar translocation, they have remarkable clinical heterogeneity. Accumulation of aberrant DNA methylation might associate with clinical heterogeneity and further CP transformation to the BP-CML (8). In our study, both the control and CMR groups showed an unmethylated pattern; however, the expression level of *SMG1* in the CMR group was higher than the control group. While the *SMG1* promoter in the new case group

and BP group were hypermethylated, the BP group had lowest expression level in our study.

Regarding the crucial tumor suppressor activity of *SMG1*, these data suggested that as well as the methylation, other mechanisms participate in *SMG1* expression modulation. In this regard, it has recently been demonstrated that an upregulated microRNA (miR)-18a in nasopharyngeal carcinoma correlated with larger tumor size and further disease propagation. The oncogenic impact of miR-18a is exerted by *SMG1* suppression, which is highly downregulated in the final stages of cancer (33). Furthermore, a devastating role of miR-32 upregulation in ovarian cancer was shown, whose oncogenic role was also applied by suppressing *SMG1* expression (34). In pancreatic cancer, tumor suppressor activity of *SMG1* was suppressed by miR-192 and miR-215, whose downregulation led to the tumor proliferation decline (35). Ectopic expression of miR-585, which was reported to be downregulated in non-small cell lung cancer carcinoma, exerts a tumor suppressor activity by targeting *SMG1* (36). Besides the microRNAs, the potential impact of long noncoding RNAs (lncRNAs) on *SMG1* regulation has recently been shown. lncRNA MAGI2-AS3 exerted tumor suppresser activity in HCC, and its overexpression could limit tumor growth through several mechanisms, including *SMG1* higher expression (37).

Altogether, a significant decline in *SMG1* activity is essential for cancer development that aligns with the reversible epigenetic modifications and provides a brilliant opportunity for cancer treatment (16). It has been demonstrated that CML treating drugs like Imatinib had an indirect effect on methylation status that might recruit candidate genes for anti-tumor activity, such as *SMG1* for boosting treatment response (23). Zhang et al. (38) demonstrated that hepatic cancer cell line treatment with AZD5369, a post-translational modifier agent, induced *SMG1* activation and cancer growth suppression. These findings suggested that *SMG1* was one of the breakthrough targets in cancer therapy. Furthermore, AML cells treatment with Decitabine, a demethylating agent, showed treatment response, including tumor growth inhibition and apoptosis of leukemic cells. Knockdown of the *SMG1* gene destroyed the therapeutic activity of Decitabine, indicating the *SMG1*-dependence role of Decitabine in cancer treatment (17). As a histone modifier agent, Curcumin was is also treated with ovarian cancer and showed therapeutic advantage due to *SMG1* mediating pathways (39). As a result, it is not beyond the expectation that reviving *SMG1* anti-tumor activity with demethylating agents or other regulating ways in CML patients potentially exert treatment advantages. Further research is needed to reach a comprehensive overview of diverse *SMG1* targeting pathways and their possible effect on cancer therapy.

Conclusion

To the best of our knowledge, our results demonstrated for the first time that hypermethylation of the *SMG1* gene is a common circumstance in CML. Furthermore, there is a significant association between methylation status of *SMG1* and its expression. The current study provided an insight into the understanding of *SMG1* hypermethylation status in CML progress, as a possible blastic transformation prognosis or anti-tumor treatment. Moreover, regarding the outstanding anti-tumor activity of *SMG1*, other *SMG1* regulatory pathways have the potential to be modulated for cancer therapy. However, further research is needed to determine the role of *SMG1*, especially *SMG1* hypermethylation, in the development, prognosis and treatment of CML.

Acknowledgments

The study has been supported by the Tehran University of Medical Science and Health Services (Grant number was 94-03-31-29963). The authors declare no conflict of interest.

Authors' Contributions

T.H.; Participated in data collecting and performing all experiments. M.S.; Participated for data collecting and analyzing. A.M.; Participated to qRT-PCR assay performance and data analysis. Sh.R., M.A.; Supervised all steps of study and coordinated experiment. All authors read and approved the final manuscript.

References

1. Roman-Gomez J, Jimenez-Velasco A, Agirre X, Castillejo JA, Navarro G, Jose-Eneriz ES, et al. Epigenetic regulation of PRAME gene in chronic myeloid leukemia. Leuk Res. 2007; 31(11): 1521-1528.
2. Kamachi K, Ureshino H, Watanabe T, Yoshida N, Yamamoto Y, Kurahashi Y, et al. Targeting DNMT1 by demethylating agent OR-2100 increases tyrosine kinase inhibitors-sensitivity and depletes leukemic stem cells in chronic myeloid leukemia. Cancer Lett. 2022; 526: 273-283
3. How J, Venkataraman V, Hobbs GS. Blast and accelerated phase CML: room for improvement. Hematology Am Soc Hematol Educ Program. 2021; 2021(1): 122-128.
4. Calabretta B, Perrotti D. The biology of CML blast crisis. Blood. 2004; 103(11): 4010-4022.
5. Celik S, Akcora D, Ozkan T, Varol N, Aydos S, Sunguroglu A. Methylation analysis of the DAPK1 gene in imatinib-resistant chronic myeloid leukemia patients. Oncol Lett. 2015; 9(1): 399-404.
6. Wang YL, Qian J, Lin J, Yao DM, Qian Z, Zhu ZH, et al. Methylation status of DDIT3 gene in chronic myeloid leukemia. J Exp Clin Cancer Res. 2010; 29(1): 54.
7. Yao DM, Zhou JD, Zhang YY, Yang L, Wen XM, Yang J, et al. GPX3 promoter is methylated in chronic myeloid leukemia. Int J Clin Exp Pathol. 2015; 8(6): 6450-6457.
8. Jelinek J, Gharibyan V, Estecio MR, Kondo K, He R, Chung W, et al. Aberrant DNA methylation is associated with disease progression, resistance to imatinib and shortened survival in chronic myelogenous leukemia. PLoS One. 2011; 6(7): e22110.
9. Dunwell T, Hesson L, Rauch TA, Wang L, Clark RE, Dallol A, et al. A genome-wide screen identifies frequently methylated genes in haematological and epithelial cancers. Mol Cancer. 2010; 9: 44.
10. Amabile G, Di Ruscio A, Müller F, Welner RS, Yang H, Ebralidze AK, et al. Dissecting the role of aberrant DNA methylation in human leukaemia. Nat Commun. 2015; 6: 7091.
11. Annamaneni S, Kagita S, Gorre M, Digumarti RR, Satti V, Battini MR. Methylation status of CEBPA gene promoter in chronic myeloid leukemia. Hematology. 2014; 19(1): 42-44.
12. Al-Jamal HA, Jusoh SA, Yong AC, Asan JM, Hassan R, Johan MF. Silencing of suppressor of cytokine signaling-3 due to methylation results in phosphorylation of STAT3 in imatinib resistant BCR-ABL positive chronic myeloid leukemia cells. Asian Pac J Cancer Prev.

2014; 15(11): 4555-4561.
13. Alipour S, Sakhinia E, Khabbazi A, Samadi N, Babaloo Z, Azad M, et al. Methylation status of interleukin-6 gene promoter in patients with Behçet's disease. Reumatol Clin (Engl Ed). 2020; 16(3): 229-234.
14. Roman-Gomez J, Jimenez-Velasco A, Agirre X, Castillejo JA, Navarro G, San Jose-Eneriz E, et al. Repetitive DNA hypomethylation in the advanced phase of chronic myeloid leukemia. Leuk Res. 2008; 32(3): 487-490.
15. Yamashita A, Ohnishi T, Kashima I, Taya Y, Ohno S. Human SMG-1, a novel phosphatidylinositol 3-kinase-related protein kinase, associates with components of the mRNA surveillance complex and is involved in the regulation of nonsense-mediated mRNA decay. Genes Dev. 2001; 15(17): 2215-2228.
16. Gubanova E, Brown B, Ivanov SV, Helleday T, Mills GB, Yarbrough WG, et al. Downregulation of SMG-1 in HPV-positive head and neck squamous cell carcinoma due to promoter hypermethylation correlates with improved survival. Clin Cancer Res. 2012; 18(5): 1257-1267.
17. Du Y, Lu F, Li P, Ye J, Ji M, Ma D, et al. SMG1 acts as a novel potential tumor suppressor with epigenetic inactivation in acute myeloid leukemia. Int J Mol Sci. 2014; 15(9): 17065-17076.
18. Rebeiro P, James A, Ling S, Caxeiro N, Lee CS, Roberts T. The role of SMG1 expression in B cell lymphoproliferative disease. Pathology, 2016; 48(1): S74.
19. Figueroa ME, Lugthart S, Li Y, Erpelinck-Verschueren C, Deng X, Christos PJ, et al. DNA methylation signatures identify biologically distinct subtypes in acute myeloid leukemia. Cancer Cell. 2010; 17(1): 13-27.
20. Akalin A, Garrett-Bakelman FE, Kormaksson M, Busuttil J, Zhang L, Khrebtukova I, et al. Base-pair resolution DNA methylation sequencing reveals profoundly divergent epigenetic landscapes in acute myeloid leukemia. PLoS Genet. 2012; 8(6): e1002781.
21. Aslani S, Mahmoudi M, Garshasbi M, Jamshidi AR, Karami J, Nicknam MH. Evaluation of DNMT1 gene expression profile and methylation of its promoter region in patients with ankylosing spondylitis. Clin Rheumatol. 2016; 35(11): 2723-2731.
22. Kanwal R, Gupta S. Epigenetic modifications in cancer. Clin Genet. 2012; 81(4): 303-311.
23. Mencalha AL, Corrêa S, Salles D, Du Rocher B, Santiago MF, Abdelhay E. Inhibition of STAT3-interacting protein 1 (STATIP1) promotes STAT3 transcriptional up-regulation and imatinib mesylate resistance in the chronic myeloid leukemia. BMC Cancer. 2014; 14: 866.
24. Lloyd JP, Davies B. SMG1 is an ancient nonsense-mediated mRNA decay effector. Plant J. 2013; 76(5): 800-810.
25. McIlwain DR, Pan Q, Reilly PT, Elia AJ, McCracken S, Wakeham AC, et al. Smg1 is required for embryogenesis and regulates diverse genes via alternative splicing coupled to nonsense-mediated mRNA decay. Proc Natl Acad Sci USA. 2010; 107(27): 12186-12191.
26. Horejsí Z, Takai H, Adelman CA, Collis SJ, Flynn H, Maslen S, et al. CK2 phospho-dependent binding of R2TP complex to TEL2 is essential for mTOR and SMG1 stability. Mol Cell. 2010; 39(6): 839-850.
27. González-Estévez C, Felix DA, Smith MD, Paps J, Morley SJ, James V, et al. SMG-1 and mTORC1 act antagonistically to regulate response to injury and growth in planarians. PLoS Genet. 2012; 8(3): e1002619.
28. Chen RQ, Yang QK, Chen YL, Oliveira VA, Dalton WS, Fearns C, et al. Kinome siRNA screen identifies SMG-1 as a negative regulator of hypoxia-inducible factor-1alpha in hypoxia. J Biol Chem. 2009; 284(25): 16752-16758.
29. Cheung HH, St Jean M, Beug ST, Lejmi-Mrad R, LaCasse E, Baird SD, et al. SMG1 and NIK regulate apoptosis induced by Smac mimetic compounds. Cell Death Dis. 2011; 2(4): e146.
30. Gubanova E, Issaeva N, Gokturk C, Djureinovic T, Helleday T. SMG-1 suppresses CDK2 and tumor growth by regulating both the p53 and Cdc25A signaling pathways. Cell Cycle. 2013; 12(24): 3770-3780.
31. Wong C, Chen F, Alirezaie N, Wang Y, Cuggia A, Borgida A, et al. A region-based gene association study combined with a leave-one-out sensitivity analysis identifies SMG1 as a pancreatic cancer susceptibility gene. PLoS Genet. 2019; 15(8): e1008344.
32. Han LL, Nan HC, Tian T, Guo H, Hu TH, Wang WJ, et al. Expression and significance of the novel tumor-suppressor gene SMG-1 in hepatocellular carcinoma. Oncol Rep. 2014; 31(6): 2569-2578.
33. Mai S, Xiao R, Shi L, Zhou X, Yang T, Zhang M, et al. MicroRNA-18a promotes cancer progression through SMG1 suppression and mTOR pathway activation in nasopharyngeal carcinoma. Cell Death Dis. 2019; 10(11): 819.
34. Zeng S, Liu S, Feng J, Gao J, Xue F. MicroRNA-32 promotes ovarian cancer cell proliferation and motility by targeting SMG1. Oncol Lett. 2020; 20(1): 733-741.
35. Zhang X, Peng Y, Huang Y, Yang M, Yan R, Zhao Y, et al. SMG-1 inhibition by miR-192/-215 causes epithelial-mesenchymal transition in gastric carcinogenesis via activation of Wnt signaling. Cancer Med. 2018; 7(1): 146-156.
36. Ding X, Yang Y, Sun Y, Xu W, Su B, Zhou X. MicroRNA-585 acts as a tumor suppressor in non-small-cell lung cancer by targeting hSMG-1. Clin Transl Oncol. 2017; 19(5): 546-552.
37. Yin Z, Ma T, Yan J, Shi N, Zhang C, Lu X, et al. LncRNA MAGI2-AS3 inhibits hepatocellular carcinoma cell proliferation and migration by targeting the miR-374b-5p/SMG1 signaling pathway. J Cell Physiol. 2019; 234(10): 18825-18836.
38. Zhang Y, Zheng Y, Faheem A, Sun T, Li C, Li Z, et al. A novel AKT inhibitor, AZD5363, inhibits phosphorylation of AKT downstream molecules, and activates phosphorylation of mTOR and SMG-1 dependent on the liver cancer cell type. Oncol Lett. 2016; 11(3): 1685-1692.
39. Sun S, Fang H. Curcumin inhibits ovarian cancer progression by regulating circ-PLEKHM3/miR-320a/SMG1 axis. J Ovarian Res. 2021; 14(1): 158.

Original Article

Generation and Differentiation of Induced Pluripotent Stem Cells from Mononuclear Cells in An Age-Related Macular Degeneration Patient

Tongmiao Wang, M.Sc.[1, 2, 3#], Jingwen Liu, M.Sc.[1, 2, 3#], Jianhua Chen, M.B.B.S.[1, 2, 3, 4*], Bo Qin, M.D., Ph.D.[1, 2, 3, 4*]

1. Shenzhen Aier Eye Hospital, Shenzhen, China
2. Aier Eye Hospital, Jinan University, Shenzhen, China
3. Shenzhen Aier Ophthalmic Technology Institute, Shenzhen, China
4. Aier Eye Hospital Group, Changsha, China

 # These authors equally contributed to this work.

Corresponding Address: Shenzhen Aier Eye Hospital, Shenzhen, China
Emails: 15807910036@139.com, qinbozf@126.com

Received: 11/July/2022, Accepted: 02/November/2022

Abstract

Objective: We aimed to generate induced pluripotent stem cells (iPSCs)-derived retinal pigmented epithelium (RPE) cells from peripheral blood mononuclear cells (PBMCs) and age-related macular degeneration (AMD) patient to provide potential cell sources for both basic scientific research and clinical application.

Materials and Methods: In this experimental study, PBMCs were isolated from the whole blood of a 70-year-old female patient with AMD and reprogrammed into iPSCs by transfection of Sendai virus that contained Yamanaka factors (OCT4, SOX2, KLF4, and c-MYC). Flow cytometry, real-time quantitative polymerase chain reaction (qPCR), karyotype analysis, embryoid body (EB) formation, and teratoma detection were performed to confirm that AMD-iPSCs exhibited full pluripotency and maintained a normal karyotype after reprogramming. AMD-iPSCs were induced into RPE cells by stepwise induced differentiation and specific markers of RPE cells examined by immunofluorescence and flow cytometry.

Results: The iPSC colonies started to form on three weeks post-infection. AMD-iPSCs exhibited typical morphology including roundness, a large nucleus, sparse cytoplasm, and conspicuous nucleoli. QPCR data showed that AMD-iPSCs expressed pluripotency markers (endo-*OCT4*, endo-*SOX2, NANOG* and *REX1*). Flow cytometry indicated 99.7% of generated iPSCs was TRA-1-60 positive. Methylation sequencing showed that the regions of OCT4 and NANOG promoter were demethylated in iPSCs. EBs and teratomas formation assay showed that iPSCs had strong differentiation potential and pluripotency. After a series of inductions with differentiation mediums, a monolayer of AMD-iPSC-RPE cells was observed on day 50. The AMD-iPSC-RPEs highly expressed specific RPE markers (MITF, ZO-1, Bestrophin, and PMEL17).

Conclusion: A high quality iPSCs could be established from the PBMCs obtained from elderly AMD patient. The AMD-iPSC displayed complete pluripotency, enabling for scientific study, disease modeling, pharmacological testing, and therapeutic applications in personalized medicine. Collectively, we successfully differentiated the iPSCs into RPE with native RPE characteristics, which might provide potential regenerative treatments for AMD patients.

Keywords: Age-Related Macular Degeneration, Differentiation, Induced Pluripotent Stem Cell, Reprogramming, Retinal Pigment Epithelium

Cell Journal(Yakhteh), Vol 24, No 12, December 2022, Pages: 764-773

Citation: **Wang T, Liu J, Chen J, Qin B. Generation and differentiation of induced pluripotent stem cells from mononuclear cells in an age-related macular degeneration patient. Cell J. 2022; 24(12): 764-773. doi: 10.22074/CELLJ.2022.557559.1072.**

Introduction

Induced pluripotent stem cells (iPSCs) as a type of postnatal stem cell, have self-renewal ability and the potential to differentiate into several kinds of mature cells under artificial induction (1-3), which makes iPSCs technology an important method for disease modeling, drug research and organ regeneration (3). IPSC was first successfully generated and named by Shinya Yamanaka, utilizing retroviral vectors to introduce four transcription factors (OCT4, SOX2, KLF4, and c-MYC) and reprogram somatic cells into a pluripotent state (4). Human iPSCs have characteristics and phenotypes that are comparable to human embryonic stem cells (ESCs), such as the ability to multiply indefinitely and differentiate into various cells for multiple applications (3). Disease modeling with patient iPSCs is one of the most practical uses. *In vitro* iPSC derived cells provide identical genetic background. With the same pluripotency as ESCs, iPSCs can be more easily obtained while avoiding ethical and legal problems. Aside from fundamental embryology research, iPSC research has sparked widespread interest in the following potential applications: i. Regenerative medicine, including disease pathology elucidation and drug development research employing iPSC disease models, and ii. Medicinal therapies (3, 5).

The idea behind the generation of iPSCs is simple that ectopically express a cocktail of stem cell reprogramming factors and allow for cells to de-differentiate (1, 3). However, deciding which methodology to use could be challenging. For instance, synthetic mRNA-based reprogramming with high effectiveness was reported.

Because mRNA is translated into protein in the cytoplasm rather than the nucleus, there is less likelihood of undesired genetic changes. This method appears to be fast and effective, but the major disadvantages is that mRNA degrades in a couple of days. As a result, effective reprogramming necessitates repeated transfection (6). Although transduction of lentivirus or retrovirus encoding defined transcriptional factors can generate human and mouse iPSCs, the lentiviral reprogramming approach has a potential drawback in which the reprogramming factors are frequently reactivated when iPSCs differentiate into various lineages leading to tumor formation (7). Thus, for both fundamental research and potential clinical applications, effective and safe techniques for iPSC generation must be developed which produce pluripotency without transgene reactivation, viral integration, or genetic changes.

The Sendai virus (SeV), an RNA virus with no risk of modifying the host genome, is an effective way to generate safe iPSC. Human iPSCs infected with the Sendai virus displayed pluripotency genes and exhibited demethylation, a hallmark of reprogrammed cells. During cell division, SeV-derived transgenes would be reduced (8). Thus, Sendai virus is an effective strategy for producing safe iPSC.

There are several essential assays for assessing the characterizations of iPSC (1, 3, 9): i. To ensure that each iPSC line created the parental cell from which it was reprogrammed, the iPSCs were validated using short tandem repeat (STR) profiling, ii. G-band karyotyping and qPCR-based profiling for genomic hotspot areas are typically modified during reprogramming were used to examine genomic integrity in iPSCs, iii. The pluripotency was further validated by evaluating their capacity to produce embryoid bodies (EBs), develop into each of the three germ layers, and develop cortical neurons, iv. Another important method for assessing pluripotency of iPSCs is a teratoma experiment in which iPSCs are implanted into immune-deficient mice and detect their ability to develop teratomas, and v. The DNA methylation status in the iPSCs marker gene loci should be assessed.

Age-related macular degeneration (AMD) is one of the primary causes of blindness in people over the age of 50, which accounts for 7-8% of all blindness globally with an estimated 200 million people worldwide in 2020 and 288 million people by 2040 (10, 11). AMD is a multifactorial late-onset eye disease characterized by progressive degeneration of the retinal pigment epithelial complex and subsequent photoreceptor cell death, particularly in the macular area of the retina, culminating in permanent central vision loss and reduced quality of life (10). Clinically, AMD can be divided into two types, neovascular (wet) and non-neovascular (dry). Existing treatments for wet AMD, such as intravitreal injections of anti-vascular endothelial growth factor (anti-VEGF), photocoagulation, or a combination of the two, have relatively limited impact in terms of functional and morphological improvement that simply serve to stabilize the illness (12). Dry AMD, on the other hand, is resistant to existing therapies, and there are presently no successful treatments that could reverse it despite the fact that neuroprotective medicines and visual cycle modulators have been used (13).

AMD is initiated by degeneration and damage of the retinal pigmented epithelium (RPE) in the macula, which is caused by a variety of mechanisms that remain uncovered (14). The RPE is a single sheet of post-mitotic cells that forms the outer blood-retinal barrier (BRB) at the boundary between the choriocapillaris and the sensory retina (15). By releasing immunosuppressive substances, the RPE layer is responsible for the eye's immune-privileged status (16). The most important function of RPE layer include regulating the transport of ions, nutrients, water, and waste products to the choroidal vasculature through the Bruch's membrane, phagocytosis of the photoreceptor's outer segment, re-isomerization of all transretinal into 11-cis-retinal, and finally, maintaining the integrity of the RPE-retina structure through directional secretion of its essential components (15). RPE cell dysfunction is an early and critical event in the molecular pathways that leads to gradual irreversible photoreceptor impairment and clinically relevant AMD symptoms (14). However, due to the limitations of existing disease models, the pathophysiology of this disease, involving a complex combination of metabolic, functional, genetic, and environmental variables, remains unknown. Thus, no effective therapy strategy is currently available.

As researchers successfully induced iPSCs into photoreceptor-like cells and RPE-like cells *in vitro* (17, 18), and further proved its feasibility of visual improvement after transplantation on patients with retinal degeneration (19), patient-derived iPSC-RPE cells have been playing an important role in disease modeling, drug testing and even clinical application of AMD in recent years (20). In this study, we aimed to assess the generation and differentiation of iPSCs from peripheral blood mononuclear cells (PBMCs) of a 70-year-old female patient with AMD, which could provide choices for the establishment of *in vitro* AMD model, and potentially a prospective therapy for AMD.

Materials and Method

Primary culture of PBMCs

In this experimental study, we obtained 10 ml fresh venous blood from a 70-year-old AMD patient in Shenzhen Aier Eye Hospital. PBMCs were isolated from blood by Ficoll density gradient. Briefly, blood were diluted by 30 ml phosphate-buffered saline (PBS) buffer and carefully layered on the top of 15 ml of Ficoll-Paque (Thermo Fisher, USA) in a 50 ml tube. The tube was centrifuged at 400×g for 30 minutes at room temperature. The mononuclear cell layer was transferred to a new 50 ml tube. PBMCs were washed by PBS buffer twice.

Cells were cultured subsequently in X-VIVO™ 15 Serum-free Hematopoietic Cell Medium (Lonza,

Switzerland) supplemented with 1% penicillin/streptomycin. The patient provided informed consent. The protocol of the present experimental study was approved by the Ethical Committee of Shenzhen Aier Eye Hospital (#2020-002-01).

Reprogramming PBMCs to iPSCs

We generated human iPSCs from PBMCs by using CytoTune®-iPS 2.0 Sendai Reprogramming Kit (Life Technologies, USA). The cells were placed into a 6-well plate coated with Matrigel (BD Biosciences, USA) three days after being inoculated with OCT4, SOX2, KLF4, and c-MYC. On the seventh day after the transduction, half of the medium was replaced with Essential 8™ Medium (Life Technologies, USA). Daily replacement of the Essential 8™ Medium began on day 8. The formation of iPSC colonies was observed about 3-4 weeks afterward, and then the iPSCs were collected, purified and amplified. All cells were cultured in a humidified atmosphere that contained 5% CO_2 at 37˚C.

Reverse transcription polymerase chain reaction and real-time quantitative polymerase chain reaction

Genomic DNA was isolated from iPSCs using Wizard® Genomic DNA Purification kit (Promega, USA). Total RNA isolation was performed with TRIzol method (Sigma-Aldrich, USA), and cDNA synthesized from 1 μg of RNA using the M-MLV Reverse Transcriptase Kit (Promega, USA) according to the manufacturer's instructions. Real-time quantitative polymerase chain reaction (qPCR) was performed with a SYBR® Premix Ex Taq™ II Kit (Takara, Japan) and ABI™ 7500 Real Time System. Primers were used as previously reported (21). Relative transcription levels were determined by using the $2^{-\Delta\Delta CT}$ analysis method.

Teratoma formation assay

Cells were collected by EDTA and suspended in Dulbeccos Phosphate Buffered Saline. Hamilton syringe was used to inject 20 μl (1×10^6 cells) of cell suspension into severe combined immunodeficiency (SCID) mice. Eight weeks after injection, the mice were anesthetized and sacrificed, and teratomas were dissected, fixed, sectioned and stained with hematoxylin/eosin for further analysis. The National Institutes of Health standards for the human use of laboratory animals was applied to the care and maintenance of experimental animals.

Karyotype analysis

Eighty-five percent confluent iPSCs were treated for 2 hours with Karyo MAX Colcemid and 30 minutes with 0.1 M KCl at 37˚C, harvested and fixed with methanol:glacial acetic acid (3:1). Cells were then centrifuged, fixed, resuspended, dropped on a slide and dried naturally. The metaphase chromosome number from individual nuclei was counted microscopically after staining the cells with Giemsa for 1 hour (Axio Imager Z2, USA, Zeiss) and then analyzed by MetaClient 2.0.1. software.

Mycoplasma detection

MycoAlert Mycoplasma Detection Kit (Lonza, USA) was used for routine detection of mycoplasma contamination according to the manufacturer's instructions. Briefly, 100 μl of culture supernatant was transferred to a 1.5 ml tube. MycoAlert® Reagent (100 μl) was added to supernatant. Luminescence was measured after 5 minutes incubation (reading A). MycoAlert® (100 μl) Substrate was added to supernatant. Luminescence was measured after 10 minutes incubation (reading B). The ratio of reading B/reading A was calculated. Mycoplasma detection was performed before and after tetratomic formation assay to make sure free of mycoplasma contamination.

Differentiation of iPSCs into RPE

The procedure of differentiation of iPSCs into RPE cells were reported previously with slightly modification (22, 23). Confluent iPSCs were pretreated with mTeSR1 (Stem Cell, Canada) and 10 μM Y27632 (Sigma-Aldrich, USA) for 30 minutes, dissociated into single cells by Accutase (Sigma-Aldrich, USA), plated on Matrigel-coated 6-well plates at a density of 4×10^5 cells/ml on day 0 and cultured in D0 medium. The medium was changed on day 3 and half-changed every three days afterward with the components listed in Table 1 accordingly. On day 21, cells were plated on Matrigel-coated 12-well plates and cultured in D15/D18 medium. On day 24, 10% KSRm was used as medium and changed every other day until pebble-shaped RPE cells were observed. Cells were digested with 1 mg/ml Dispase (Sigma-Aldrich, USA), scraped and cultured in EB suspension medium that contained high-glucose DMEM supplemented with 20% FBS (Gibco, USA), 0.1 mM NEAA (Life Technologies, USA), 2 mM GlutaMax (Lifem Technologies, USA) and 0.1 mM β-mercaptoethanol (Sigma-Aldrich, USA) for 8 days and subsequently in EB adherent medium (DMEM/High Glucose+10% FBS+0.1 mM NEAA+2 mM GlutaMax) for 8 days.

Flow cytometry

Cells were harvested, centrifuged, fixed in 4% PFA and incubated with anti-TRA-1-60 primary antibody (1:1000, Abcam, USA), anti-MITF primary antibody (1:1000, Abcam, USA), anti-Pmel17 primary antibody (1:1000, Abcam, USA) followed by goat anti-mouse IgG secondary antibody (1:5000, Thermo Scientific, USA). Cells were analyzed on a flow cytometer (BD Biosciences, USA), and processed using FACSDiva and Weasel software.

Table 1: Mediums used for differentiation

Medium	Component
D0 medium	DMEM/F12 (Gibco, USA)+20% KSR (Gibco, USA)+0.1 mM NEAA (Life Technologies, USA)+2 mM Glutamax (Life Technologies, USA)+0.1 mM 2-Mercaptoethanol (Thermo Fisher, USA)+10 μM Y27632 (Sigma-Aldrich, USA)+100 ng/ml DKK-1 (R&D, USA)+500 ng/ml Lefty-A (R&D, USA)
D3 medium	G-MEM (1×, Gibco, USA)+20% KSR (Gibco, USA)+0.1 mM NEAA (Life Technologies, USA)+1×Penicillin-Streptomycin (Thermo Fisher, USA)+0.1 mM 2-Mercaptoethanol (Thermo Fisher, USA)+10 μM Y27632 (Sigma-Aldrich, USA)+100 ng/ml DKK-1 (R&D, USA)+500 ng/ml Lefty-A (R&D, USA)+1 mM Pyruvate (Sigma-Aldrich, USA)
D6/9/12 medium	G-MEM (1×, Gibco, USA)+15% KSR (Gibco, USA)+0.1 mM NEAA (Life Technologies, USA)+1×Penicillin-Streptomycin (Thermo Fisher, USA)+0.1 mM 2- Mercaptoethanol (Thermo Fisher, USA) +10 μM Y27632 (Sigma-Aldrich, USA)+100 ng/ml DKK-1 (R&D, USA)+500 ng/ml Lefty-A+1mM Pyruvate (Sigma-Aldrich, USA)
D15/18 medium	G-MEM (1×, Gibco, USA)+10% KSR (Gibco, USA)+0.1 mM NEAA (Life Technologies, USA)+1×Penicillin-Streptomycin (Thermo Fisher, USA) +0.1 mM 2- Mercaptoethanol (Thermo Fisher, USA)+100 ng/ml DKK-1 (R&D, USA)+500 ng/ml Lefty-A+1mM Pyruvate (Sigma-Aldrich, USA)
10% KSRm	G-MEM (1×, Gibco, USA)+10% KSR (Gibco, USA)+0.1 mM NEAA (Life Technologies, USA)+1×Penicillin-Streptomycin (Thermo Fisher, USA)+0.1 mM 2-Mercaptoethanol (Thermo Fisher, USA) +1 mM Pyruvate (Sigma-Aldrich, USA)

Immunofluorescence

The cells were fixed for 15 minutes at room temperature in 4% paraformaldehyde (Sigma, USA), blocked for 1 hour with 5% fetal bovine serum, and then incubated overnight in blocking buffer containing the primary antibodies: anti-Bestrophin (1:200; Abcam, USA), anti-ZO-1 (1:100; Thermo Fisher, USA), anti-MITF (1:200; Proteintech, USA), and anti-Pmel17 (1:200; Abcam, USA). Nuclei were counterstained with DAPI after 1 hour of incubation with fluorescently labeled secondary antibodies at room temperature in the dark. The Axiovert 200 fluorescent microscope (Zeiss) and Adobe Photoshop software were used to capture the images (Adobe Systems).

Statistical analysis

We applied GraphPad PrismVer. 8.01 (GraphPad Software Inc., La Jolla, CA) to conduct the statistical analysis. Student's t test were used to evaluate the differences between two comparison groups. One-way ANOVA was used for multiple-group comparisons.

Results

Generation of iPSCs from PBMCs

To generate iPSCs, we first isolated the PBMCs from patient's venous blood. About 10 ml fresh venous blood was obtained from an AMD patient in Shenzhen Aier Eye Hospital. PBMCs were isolated from blood by Ficoll density gradient (see Materials and Method). Next, cells were washed by PBS and cultured subsequently in X-VIVO™ 15 medium for 2 days. Then, PBMCs were infected with sendai virus containing Yamanaka factors (OCT4, SOX2, KLF4 and c-MYC). Three to four weeks after infection, the iPSC-like colonies started to form (Fig.1). Inside a colony, iPSCs had the following morphological characteristics: roundness, a large nucleus, sparse cytoplasm, and conspicuous nucleoli. The central section of the colony became more compact than the periphery as it expands. We selected the colonies that displayed a typical morphology of iPSCs which were in a round or oval shape with large nuclear/cytoplasmic ratio, and plated them into 24-well plates coated with Matrigel.

Characterization of iPSCs

Next, we assessed characterizations of iPSCs. Expression of pluripotency associated stem cell markers (endo-*OCT4*, endo-*SOX2*, *NANOG* and *REX1*) in iPSCs were analyzed by qPCR (Fig.2A). As a positive control, we employed human embryonic stem cell line H9 (ESC cell) and PBMC as a negative control. We found that both iPSC and ESC expressed significance higher of pluripotency associated stem cell markers. IPSCs expressed higher endo-SOX2 and REX1 than that of ESCs. Then we measured the expression of TRA-1-60 (Podocalyxin), a commonly positive indicator of pluripotent human stem cell (24), by flow cytometry. Our data showed that 99.7% of generated iPSCs was TRA-1-60 positive (Fig.2B). Furthermore, karyotyping analysis showed that the iPSCs had normal karyotypes according to the standard G-banding results (Fig.2C). In addition, we analyzed the expression of exogenous genes (*OCT4, KLF4, c-MYC* and *SEV)* by RT-PCR. Figure 2D showed that AMD-derived iPSCs expressed no exogenous *OCT4, KLF4, c-MYC* or *SEV,* indicating that SeV-derived transgenes that had been reduced or lost and we generated genome integration-free iPSCs.

Reprogramming of methylated sites of genome is a signature of pluripotent cells (25). Thus, we performed basalt genome sequencing to examine the methylation statuses of CpG dinucleotides in the OCT4 and NANOG promoter regions. Unlike PBMCs, the OCT4 and NANOG promoter regions were shown to be demethylated in iPSCs (Fig.2E).

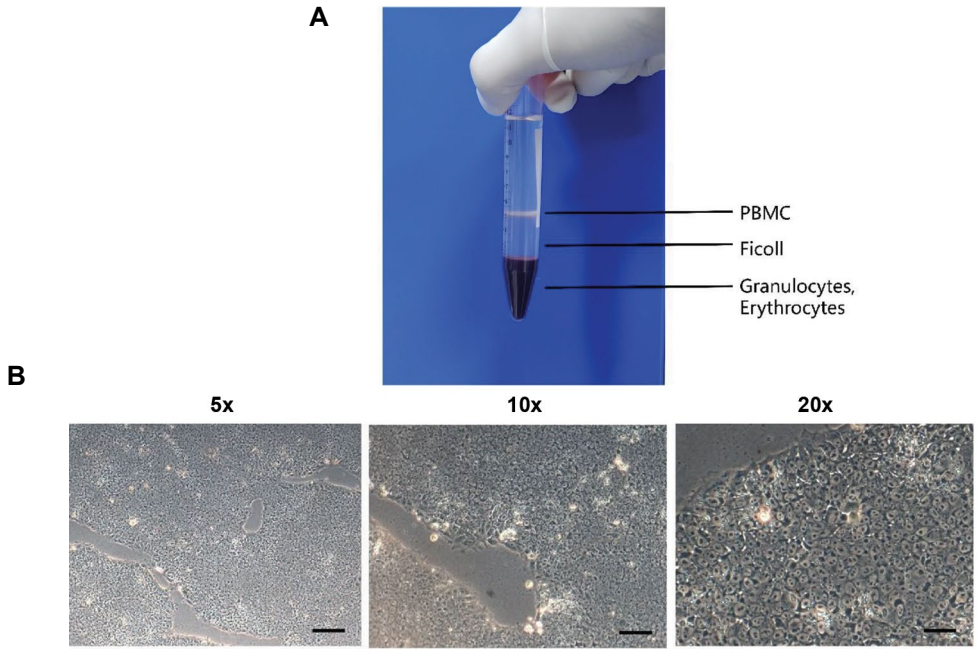

Fig.1: Generation of iPSCs from PBMCs. **A.** PBMCs were isolated from blood by Ficoll density gradient. **B.** The morphology of generated iPSCs from PBMCs from an AMD patient (scale bars: 200 µm, 100 µm and 50 µm from left to right respectively). iPSCs; Induced pluripotent stem cells, PBMCs; Peripheral blood mononuclear cells, and AMD; Age-related macular degeneration.

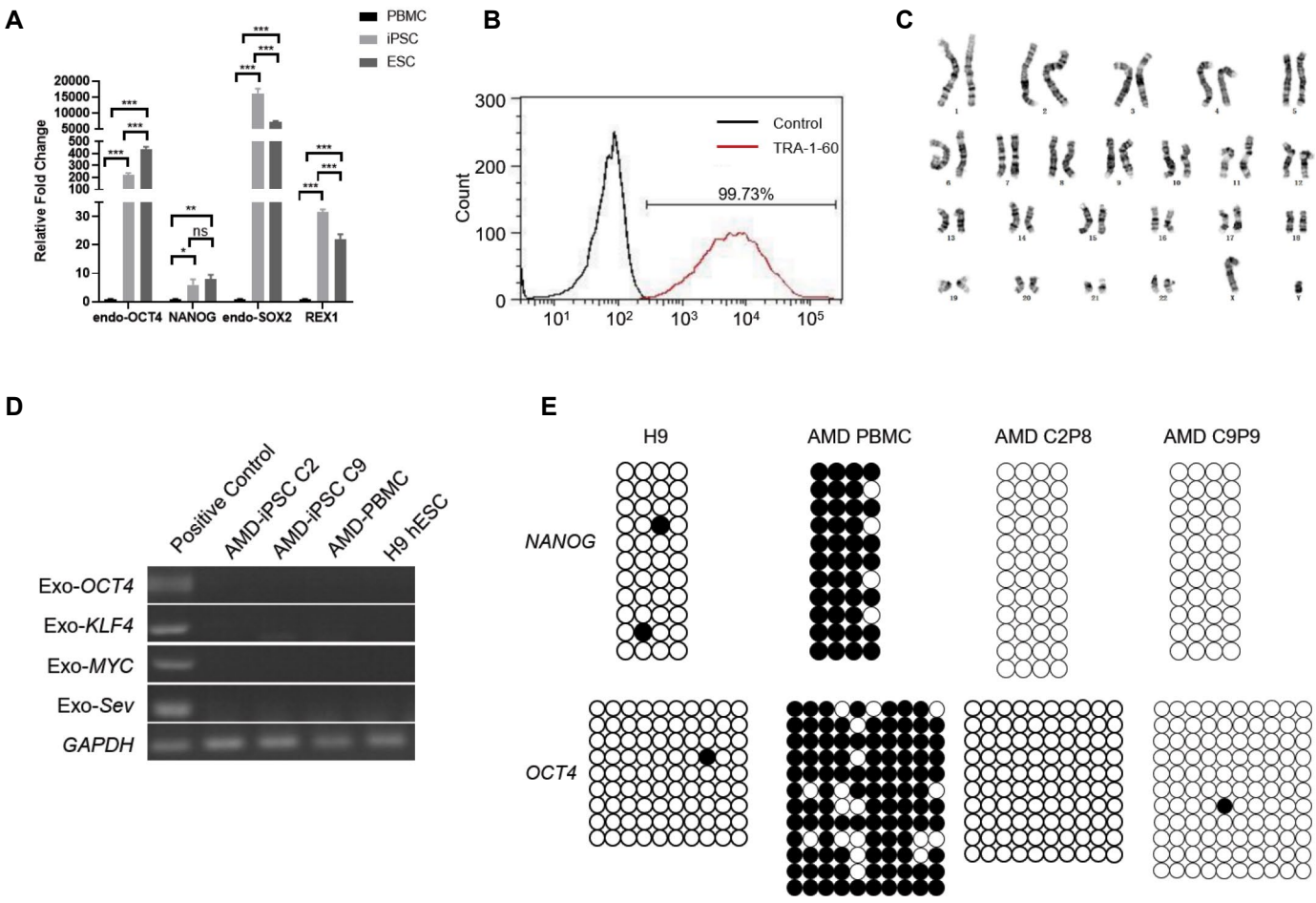

Fig.2: Characterization of iPSCs derived from PBMCs (all experiments were performed at least three times). **A.** Expression of pluripotency markers between iPSCs, embryonic stem cell line H9 and PBMCs analyzed by qPCR. P values were determined by one-way ANOVA. Error bars indicated SEM. **B.** Flow cytometry analysis confirmed the expression of TRA-1-60 in iPSCs. **C.** Images for karyotyping of iPSCs. **D.** RT-PCR of exogenous genes of iPSCs, PBMCs, H9. PBMCs infected by Sendai virus as positive control. **E.** Methylation analysis of OCT4 and NANOG promoter regions in iPSCs, H9 and PBMCs (black circles represent methylated, white circles represent unmethylated). iPSCs; Induced pluripotent stem cells, PBMCs; Peripheral blood mononuclear cells, qPCR; Real-time quantitative polymerase chain reaction, SEM; Standard error of mean, RT-PCR; Reverse transcription polymerase chain reaction, Ns; Not significant, *; P<0.05, **; P<0.01, and ***; P<0.001.

The differentiation potential and pluripotency of iPSCs was analyzed by EB culture *in vitro*. It is reported that EBs are three-dimensional cell aggregates composed of the three developmental germ layers (5). Our data showed that iPSCs were able to generate EBs *in vitro* (Fig.3A) and had the ability to differentiate into 3 germ layer-derived cell types. To confirm the expression of germ layer-specific gene markers, qPCR analysis were performed. Our data showed the EBs expressed ectoderm (Pax6), mesoderm (Tbx1, Tbxt) and endoderm (Afp, Gata4, Sox17) markers (Fig.3B). We further determined the pluripotency of iPSCs by teratoma formation *in vivo*. iPSCs were collected and injected subcutaneously into SCID mice, 8 weeks after injection, the mice were anesthetized and sacrificed, and teratomas subjected to histological examination. Figure 3C depicted the existence of a set of representative tissues derived from the three embryonic germ layers. Taken together, our data indicated that AMD-iPSCs had complete differentiation potential and pluripotency.

Differentiation of iPSCs into RPE cells

After successfully generation of AMD patient derived iPSCs, we next differentiate the iPSCs into RPE cells (22, 23). The time points in this procedure presented in Figure 4 and Materials and Method. The differentiation procedure began with iPSC colonies plated on D0 media (Fig.4A) and then removed to be cultured in suspension on day 21 (Fig.4B, C). On day 50, a monolayer of pigmented cells with a cobblestone appearance that could be purified and expanded. We observed the formation of pigmented cells with cobblestone morphology (Fig.4D). Importantly, immunofluorescence revealed that these pigmented cells expressed RPE hallmark proteins such as MITF, ZO-1, Bestrophin, and PMEL17 (Fig.5A). Flow cytometry revealed that these RPE-like cells were positive for RPE-specific markers, including MITF (75.3% positive) and PMEL17 (83.3% positive) (Fig.5B). Taken together, these findings implied that pigmented pebble-shaped cells generated from iPSCs shared the expression characteristics of native RPE.

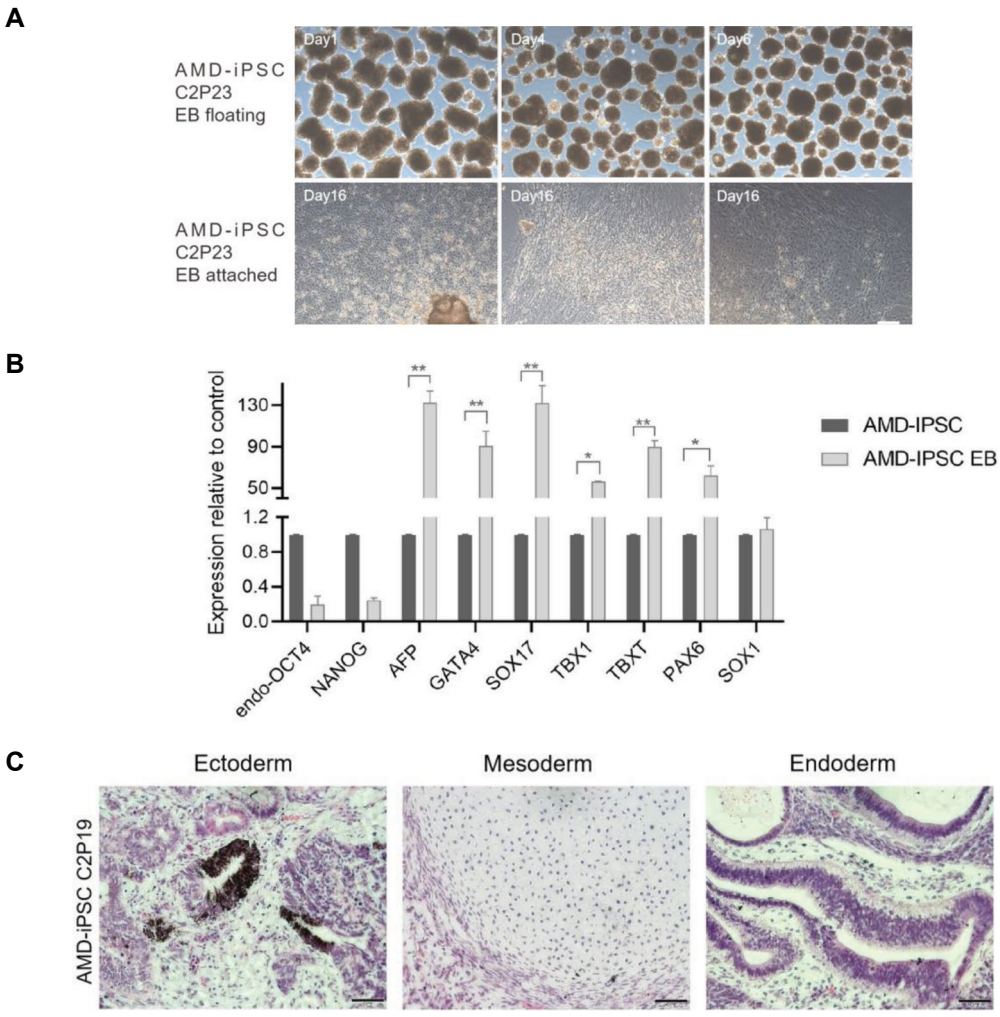

Fig.3: *In vitro* and *in vivo* differentiation of iPSCs. **A.** EBs derived from iPSCs (scale bars: 200 µm). C2P23 indicated the clone #2 passage 23. **B.** QPCR showed the different expression level of 3 germ layer markers in EBs and undifferentiated iPSCs. P values were determined by the student's t test. Error bars indicated SEM. The differences of expression level of *OCT4, NANOG* and *SOX1* between the two groups were not significant. **C.** Histological examination of teratomas (8 weeks post-injection into SCID mice). *; P<0.05, **; P<0.01, iPSCs; Induced pluripotent stem cells, qPCR; Real-time quantitative polymerase chain reaction, EB; Embryoid bodies, and SEM; Standard error of mean.

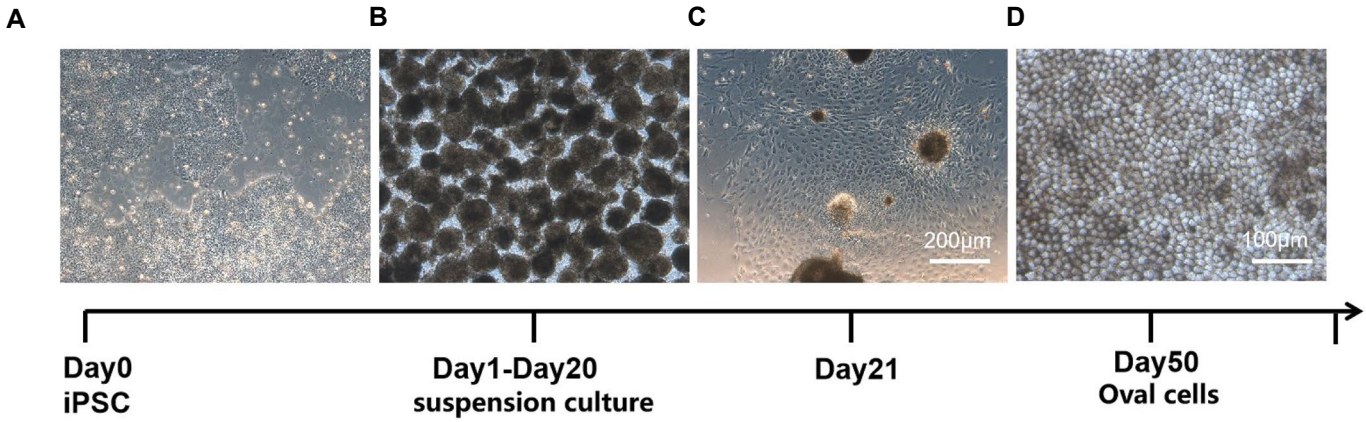

Fig.4: Differentiation of iPSCs into RPE cells. **A.** The differentiation process began with colonies of iPSCs plated initially on D0 medium and **B, C.** Subsequently detached to be cultured in suspension on day 21. **D.** A monolayer of pigmented cells with a cobblestone appearance that can be further purified and expanded appeared on day 50 (scale bars: A, B, C: 200 µm, D: 100 µm).

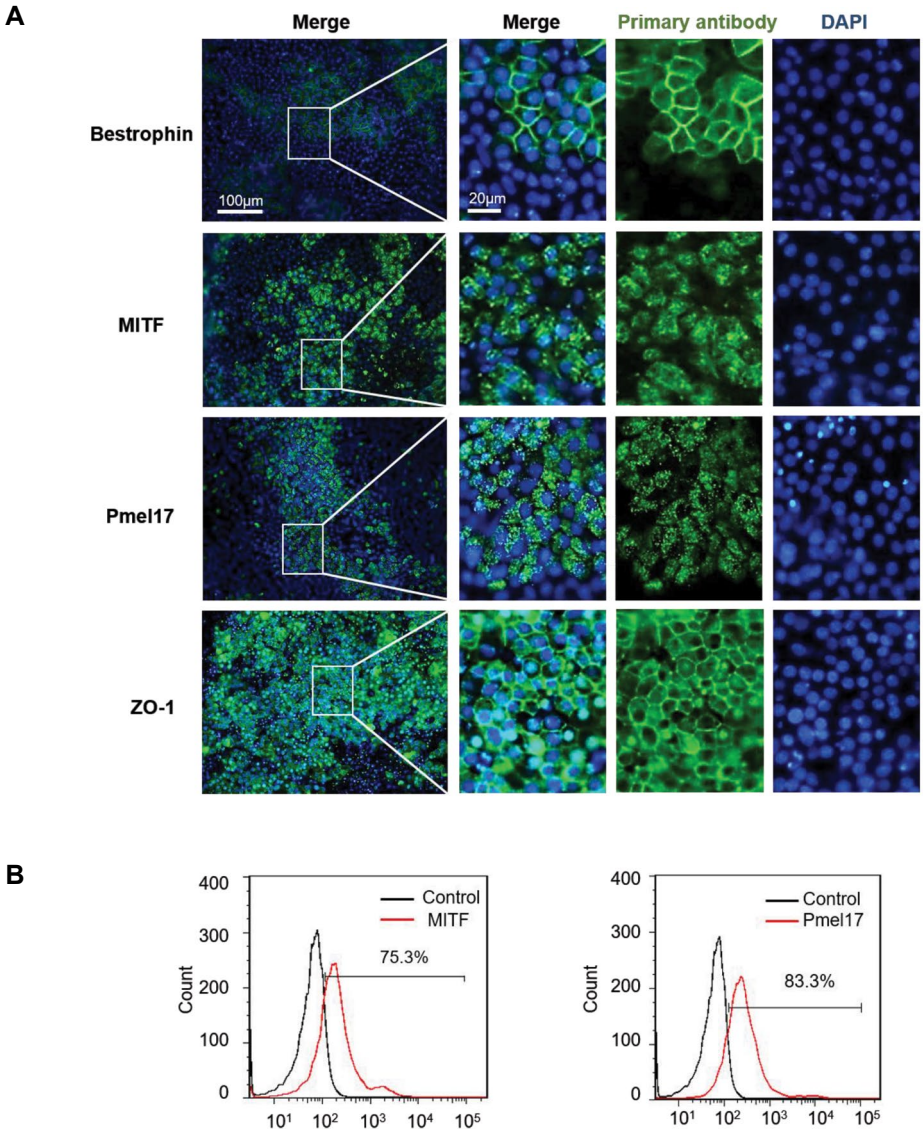

Fig.5: Characterization of iPSC-derived RPE cells. **A.** Expression of RPE-specific proteins in iPSC-derived RPE cells indicated by immunofluorescence. **B.** Flow cytometry results showed that the isolated iPSC-derived RPE cells were positive for MITF and PMEL17. iPSC; Induced pluripotent stem cells and RPE; Retinal pigmented epithelium.

Discussion

Cell therapy provides an unlimited source of cells for cell transplantation research (26). Retinal cell transplantation, which differs from stem cell transplantation, is now a promising treatment approach in ophthalmology. A variety of cell types are now being explored for clinical cell therapies in AMD, especially in dry AMD. The RPE cell is the most prevalent target for cell treatment in AMD trials among all retinal cells (10). The most difficult task confronting cell therapists in the treatment of AMD is deciding which cells to use and how to generate bonfire RPE cells (27). ESC was once believed to be the promising source in cell transplantation and cell therapy (28), but there are certain limitations in clinical application due to ethics issue and allogeneic immune rejection. With similar characteristics to ESCs, iPSCs are easier to obtain, with less concern of ethical and rejection problem, and thus have become a novel alternative in therapeutic cell research (29). Importantly, the researchers genetically evaluated the iPSC-derived RPE cells in animal models and discovered no alterations associated with possible tumor formation (30). Here, we produced iPSC-RPE that is highly similar to natural RPE using clinical-grade iPSC derived from PBMC from a 70-year-old AMD patient, providing a potential cell source and tools for fundamental science and clinical application.

The generation of safe iPSCs is essential for clinical application of iPSC-RPE cells. The reprogramming factors were previously delivered via retroviral and lentiviral delivery techniques to produce iPSCs. This caused concerns that the delivery techniques would result in insertional inactivation of tumor suppressor genes and/or insertional activation of oncogenes, as well as that the reprogramming factors' constitutive expression would change iPSC features and differentiation potentials. This necessitated the use of transient, integration-free delivery methods such as viral delivery/transient transfection methods with Sendai virus, adenovirus, episomal plasmids, minicircle plasmids, mini-intronic plasmids, PiggyBac transposons, synthetic modified mRNAs, or miRNAs (8, 31, 32). Sendai virus, episomal DNAs, and synthetic mRNAs are among the most widely utilized methods in fundamental and clinical research to generate integration-free iPSCs (33). For generating clinical-grade iPSCs, episomal plasmids and Sendai virus have been the tools of choice, and Sendai virus method had the highest overall reprogramming rate that is a reliable and effective approach with a complete clearance of viral sequences at higher cell passages (31, 34, 35). Thus, the iPSCs we generated in this study is a promising cell source for both basic scientific research and clinical application.

Indeed, iPSCs offer new hope against eye diseases. Nakano et al. developed a methodology for the generation of self-organizing optic cups containing photoreceptors, retinal neurons, and Muller glial cells using hESCs and iPSCs, drawing on previous research into retinal differentiation pathways *in vitro* (36, 37). Many studies have reported the methodologies and protocols for iPSC-RPEs, some modern protocols have combined two-dimensional and three-dimensional culture, preferring to produce optic vesicles and cups at an adherent stage before committing cells to long-term three-dimensional differentiation (38, 39). These protocols are advantageous since they require a high level of inspection when removing retinal tissue from a monolayer of cells and reduce intra- and inter-culture variability (40). Three-dimensional protocols are advantageous because they precisely mimic retinal microarchitecture, produce a high proportion of retinal cells, and enable self-organization to mature ocular tissue with excellent fidelity to human eye development (39). These techniques, however, are unfavorable because of the formation of ectopic retinal cells and aberrant structures in culture, the loss of inner cell types due to prolonged culture durations, and higher variability across vesicles. Thus, more effort is required to develop an effective and practical protocol in the future.

One of limitation of this study is that we did not perform whole exome sequencing (WES) to screen whether the PBMC from an elderly individual contained potential oncogenic mutation, although PBMCs are less likely harboring somatic mutations. Another limitation is that we did not test this protocol with fibroblast cells from the patient. Since AMD is one of the leading causes of blindness in elderly people, it usually firstly disturbs people in their 50s and 60s. Thus, future studies should optimize the protocol for the production of iPSCs from senior citizens at high risk for developing AMD.

Conclusion

We successfully established and validated a high grade AMD-iPSC-line utilizing PBMCs from an AMD patient. The AMD-iPSCs retained pluripotency with standard marker, allowing for disease modeling, drug testing, and therapeutic applications. Collectively, we successfully differentiated the AMD-iPSCs into RPE cells with native RPE characteristics, which might provide potential regenerative treatments for AMD patients.

Acknowledgments

This study was supported by the Science and Technology Innovation Program of Hunan Province (Grant No. 2020SK50107), the Science Research Foundation of Shenzhen Aier Eye Hospital (SZAE2020B04), the Science Research Grant of Aier Eye Hospital Group (AM2001D2, AF2001D9, AM2101D1) and the Guangdong Basic and Applied Basic Research Foundation (Grant No. 2022A1515010742). We thank Cell Inspire

Biotechnology Co., Ltd. (CIB), Shenzhen, for their kind technical assistance. The authors declare there is no conflict of interest in this study.

Authors' Contributions

J.C., B.Q.; Contributed to conception and design. T.W., J.L.; Contributed to experimental work, statistical analysis, drafted and critically revised the manuscript. T.W., J.L., B.Q.; Contributed extensively in interpretation of data. All authors read and approved the final manuscript.

References

1. Okita K, Ichisaka T, Yamanaka S. Generation of germline-competent induced pluripotent stem cells. Nature. 2007; 448(7151): 313-317.
2. Takebe T, Sekine K, Enomura M, Koike H, Kimura M, Ogaeri T, et al. Vascularized and functional human liver from an iPSC-derived organ bud transplant. Nature. 2013; 499(7459): 481-484.
3. Rowe RG, Daley GQ. Induced pluripotent stem cells in disease modelling and drug discovery. Nat Rev Genet. 2019; 20(7): 377-388.
4. Takahashi K, Tanabe K, Ohnuki M, Narita M, Ichisaka T, Tomoda K, et al. Induction of pluripotent stem cells from adult human fibroblasts by defined factors. Cell. 2007; 131(5): 861-872.
5. Wiegand C, Banerjee I. Recent advances in the applications of iPSC technology. Curr Opin Biotechnol. 2019; 60: 250-258.
6. Warren L, Manos PD, Ahfeldt T, Loh YH, Li H, Lau F, et al. Highly efficient reprogramming to pluripotency and directed differentiation of human cells with synthetic modified mRNA. Cell Stem Cell. 2010; 7(5): 618-630.
7. Itakura G, Kawabata S, Ando M, Nishiyama Y, Sugai K, Ozaki M, et al. Fail-safe system against potential tumorigenicity after transplantation of iPSC derivatives. Stem Cell Reports. 2017; 8(3): 673-684.
8. Stadtfeld M, Nagaya M, Utikal J, Weir G, Hochedlinger K. Induced pluripotent stem cells generated without viral integration. Science. 2008; 322(5903): 945-949.
9. Jakubosky D, D'Antonio M, Bonder MJ, Smail C, Donovan MKR, Young Greenwald WW, et al. Properties of structural variants and short tandem repeats associated with gene expression and complex traits. Nat Commun. 2020; 11(1): 2927.
10. Zarbin M, Sugino I, Townes-Anderson E. Concise review: update on retinal pigment epithelium transplantation for age-related macular degeneration. Stem Cells Transl Med. 2019; 8(5): 466-477.
11. Wong WL, Su X, Li X, Cheung CM, Klein R, Cheng CY, et al. Global prevalence of age-related macular degeneration and disease burden projection for 2020 and 2040: a systematic review and meta-analysis. Lancet Glob Health. 2014; 2(2): e106-e116.
12. Mettu PS, Allingham MJ, Cousins SW. Incomplete response to Anti-VEGF therapy in neovascular AMD: Exploring disease mechanisms and therapeutic opportunities. Prog Retin Eye Res. 2021; 82: 100906.
13. Cabral de Guimaraes TA, Daich Varela M, Georgiou M, Michaelides M. Treatments for dry age-related macular degeneration: therapeutic avenues, clinical trials and future directions. Br J Ophthalmol. 2022; 106(3): 297-304.
14. Fisher CR, Ferrington DA. Perspective on AMD pathobiology: a bioenergetic crisis in the RPE. Invest Ophthalmol Vis Sci. 2018; 59(4): AMD41-AMD47.
15. Boulton M, Dayhaw-Barker P. The role of the retinal pigment epithelium: topographical variation and ageing changes. Eye (Lond). 2001; 15(Pt 3): 384-389.
16. Simó R, Villarroel M, Corraliza L, Hernández C, Garcia-Ramírez M. The retinal pigment epithelium: something more than a constituent of the blood-retinal barrier--implications for the pathogenesis of diabetic retinopathy. J Biomed Biotechnol. 2010; 2010: 190724.
17. Buchholz DE, Hikita ST, Rowland TJ, Friedrich AM, Hinman CR, Johnson LV, et al. Derivation of functional retinal pigmented epithelium from induced pluripotent stem cells. Stem Cells. 2009; 27(10): 2427-2434.
18. Tucker BA, Mullins RF, Streb LM, Anfinson K, Eyestone ME, Kaalberg E, et al. Patient-specific iPSC-derived photoreceptor precursor cells as a means to investigate retinitis pigmentosa. Elife. 2013; 2: e00824.
19. Mandai M, Watanabe A, Kurimoto Y, Hirami Y, Morinaga C, Daimon T, et al. Autologous Induced Stem-Cell-Derived Retinal Cells for Macular Degeneration. N Engl J Med. 2017; 376(11): 1038-1046.
20. Smith EN, D'Antonio-Chronowska A, Greenwald WW, Borja V, Aguiar LR, Pogue R, et al. Human iPSC-derived retinal pigment epithelium: a model system for prioritizing and functionally characterizing causal variants at AMD risk loci. Stem Cell Reports. 2019; 12(6): 1342-1353.
21. Sanchez LM, Montero-Sanchez A, Ponte-Zuñiga B, de la Cerda B, Bhattacharya SS, Diaz-Corrales FJ. Generation of a human iPS cell line (CABi003-A) from a patient with age-related macular degeneration carrying the CFH Y402H polymorphism. Stem Cell Res. 2019; 38: 101473.
22. Brandl C, Zimmermann SJ, Milenkovic VM, Rosendahl SM, Grassmann F, Milenkovic A, et al. In-depth characterisation of retinal pigment epithelium (RPE) cells derived from human induced pluripotent stem cells (hiPSC). Neuromolecular Med. 2014; 16(3): 551-564.
23. D'Antonio-Chronowska A, D'Antonio M, Frazer KA. In vitro differentiation of human iPSC-derived retinal pigment epithelium cells (iPSC-RPE). Bio Protoc. 2019; 9(24): e3469.
24. Schopperle WM, DeWolf WC. The TRA-1-60 and TRA-1-81 human pluripotent stem cell markers are expressed on podocalyxin in embryonal carcinoma. Stem Cells. 2007; 25(3): 723-730.
25. Ruiz S, Diep D, Gore A, Panopoulos AD, Montserrat N, Plongthongkum N, et al. Identification of a specific reprogramming-associated epigenetic signature in human induced pluripotent stem cells. Proc Natl Acad Sci USA. 2012; 109(40): 16196-16201.
26. Glicksman MA. Induced pluripotent stem cells: the most versatile source for stem cell therapy. Clin Ther. 2018; 40(7): 1060-1065.
27. Buchholz DE, Pennington BO, Croze RH, Hinman CR, Coffey PJ, Clegg DO. Rapid and efficient directed differentiation of human pluripotent stem cells into retinal pigmented epithelium. Stem Cells Transl Med. 2013; 2(5): 384-393.
28. Lalu MM, McIntyre L, Pugliese C, Fergusson D, Winston BW, Marshall JC, et al. Safety of cell therapy with mesenchymal stromal cells (SafeCell): a systematic review and meta-analysis of clinical trials. PLoS One. 2012; 7(10): e47559.
29. Shi Y, Inoue H, Wu JC, Yamanaka S. Induced pluripotent stem cell technology: a decade of progress. Nat Rev Drug Discov. 2017; 16(2): 115-130.
30. Zhang H, Su B, Jiao L, Xu ZH, Zhang CJ, Nie J, et al. Transplantation of GMP-grade human iPSC-derived retinal pigment epithelial cells in rodent model: the first pre-clinical study for safety and efficacy in China. Ann Transl Med. 2021; 9(3): 245.
31. Ban H, Nishishita N, Fusaki N, Tabata T, Saeki K, Shikamura M, et al. Efficient generation of transgene-free human induced pluripotent stem cells (iPSCs) by temperature-sensitive Sendai virus vectors. Proc Natl Acad Sci USA. 2011; 108(34): 14234-14239.
32. Attwood SW, Edel MJ. iPS-cell technology and the problem of genetic instability-can it ever be safe for clinical use? J Clin Med. 2019; 8(3): 288.
33. Schlaeger TM, Daheron L, Brickler TR, Entwisle S, Chan K, Cianci A, et al. A comparison of non-integrating reprogramming methods. Nat Biotechnol. 2015; 33(1): 58-63.
34. Ye H, Wang Q. Efficient generation of non-integration and feeder-free induced pluripotent stem cells from human peripheral blood cells by sendai virus. Cell Physiol Biochem. 2018; 50(4): 1318-1331
35. Macarthur CC, Fontes A, Ravinder N, Kuninger D, Kaur J, Bailey M, et al. Generation of human-induced pluripotent stem

cells by a nonintegrating RNA Sendai virus vector in feeder-free or xeno-free conditions. Stem Cells Int. 2012; 2012: 564612.
36. Nakano T, Ando S, Takata N, Kawada M, Muguruma K, Sekiguchi K, et al. Self-formation of optic cups and storable stratified neural retina from human ESCs. Cell Stem Cell. 2012; 10(6): 771-785.
37. Meyer JS, Howden SE, Wallace KA, Verhoeven AD, Wright LS, Capowski EE, et al. Optic vesicle-like structures derived from human pluripotent stem cells facilitate a customized approach to retinal disease treatment. Stem Cells. 2011; 29(8): 1206-1218.
38. Achberger K, Haderspeck JC, Kleger A, Liebau S. Stem cell-based retina models. Adv Drug Deliv Rev. 2019; 140: 33-50.
39. Lowe A, Harris R, Bhansali P, Cvekl A, Liu W. Intercellular adhesion-dependent cell survival and ROCK-regulated actomyosin-driven forces mediate self-formation of a retinal organoid. Stem Cell Reports. 2016; 6(5): 743-756.
40. Capowski EE, Samimi K, Mayerl SJ, Phillips MJ, Pinilla I, Howden SE, et al. Reproducibility and staging of 3D human retinal organoids across multiple pluripotent stem cell lines. Development. 2019; 146(1): dev171686.

Short Communication

Androgen Receptor Blockade Using Enzalutamide Suppresses Long Non-Coding RNA *ARLNC1* in Prostate Cancer Cells

Günel Huseynova, M.Sc.[1], Emre Özgür, Ph.D.[2], Sema Bilgiç Gazioğlu, Ph.D.[3], Ebru Esin Yörüker, Ph.D.[2], Ugur Gezer, Ph.D.[2]*

1. Institute of Health Sciences, Istanbul University, Istanbul, Turkey
2. Department of Basic Oncology, Istanbul University Oncology Institute, Istanbul, Turkey
3. Department of Immunology, Istanbul University Aziz Sancar Institute of Experimental 7 Medicine, Istanbul, Turkey

**Corresponding Address: Department of Basic Oncology, Istanbul University Oncology Institute, Istanbul, Turkey*
Email: ugurd@istanbul.edu.tr

Received: 30/March/2022, Accepted: 19/July/2022

Abstract

Prostate cancer (PCa) is a common malignant disease with high mortality rates that develops and progresses in an androgen-dependent way. In recent years, RNA sequencing enabled identification of many PCa-related long non-coding RNAs including androgen receptor-regulated long non-coding RNA 1 (*ARLNC1*) and prostate cancer-associated transcript 1 (*PCAT1*). In the present study, our goal was to illuminate expression changes of *ARLNC1* and *PCAT1* in the context of androgen stimulation or androgen receptor (AR) blockade with respect to AR expression status. In this experimental study, LNCaP cells and higher AR-expressing LNCaP-AR++ cells were used as cell models. Cells were treated with dihydrotestosterone (DHT) as an androgen stimulator and/or enzalutamide as an AR inhibitor. Cell viability was assessed using annexin V and propidium iodide (PI) staining in flow cytometry. Androgen stimulation prompted baseline *ARLNC1* levels by 53.5-fold in the LNCaP cells (P=0.01) and by 25-fold in the LNCAP-AR+ cells (P=0.18). AR inhibition by enzalutamide reduced baseline *ARLNC1* in LNCaP-AR++ cells by 2-fold (P=0.01), but to a lesser extent in LNCaP cells. Co-treatment of cells with DHT and enzalutamide led to a remarkable decrease in the DHT effect on *ARLNC1* expression. No specific effect of androgen stimulation or AR blockade on *PCAT1* expression was detected. Our results revealed that the extent of induction of *ARLNC1* by androgen is modulated by receptor expression status. In addition, we determined that AR blockade, via enzalutamide, effectively suppresses *ARLNC1* both at baseline and after induction by DHT.

Keywords: Androgen, Androgen Receptor, Enzalutamide, Long Non-Coding RNAs, Prostate Cancer

Cell Journal(Yakhteh), Vol 24, No 12, December 2022, Pages: 774-778

Citation: Huseynova G, Özgür E, Bilgiç Gazioğlu S, Esin Yörüker E, Gezer U. Androgen receptor blockade using enzalutamide suppresses long non-coding RNA ARLNC1 in prostate cancer cells. Cell J. 2022; 24(12): 774-778. doi: 10.22074/CELLJ.2022.557563.1076.

Prostate cancer (PCa) is the second most common malignancy in men with an incidence of approximately 36 cases per 100,000 worldwide and in Turkey (1). In most of patients diagnosed with PCa, the disease is locally confined to the prostate and does not affect their natural life expectancy following the appropriate treatment options. However, in some patients, the disease may progress and metastasize to other sites outside the prostate, significantly shortening life expectancy. Indeed, 5-year survival in patients with metastatic PCa is only around 30% (2). Although many molecular/epigenetic alterations occur in the development and progression of PCa, the most fundamental component of prostate carcinogenesis is the androgen receptor (AR) pathway, as development and progression of PCa is androgen-dependent (3). Thus, suppressing androgen pathway by surgical or medical castration is the path to treatment of the disease. A higher response rate is achieved with androgen deprivation in the majority of patients. However, due to the increased receptor expression or emergence of mutations leading to resistance of the receptor to inhibitors, many patients with metastatic disease progress to castration-resistant PCa (CRPCa) (4). Recently, the second-generation of AR inhibitor, enzalutamide, has been established as a treatment option in patients with metastatic CRPCa (5).

Identification and characterization of non-coding RNAs have been some of the major advancements in molecular cell biology in the last two decades (6). Non-coding RNAs include a wide range of RNA types, among which long non-coding RNAs (lncRNAs), with a diverse variety and uncharacterized biologic functions, constitute a significant sub-group. So far characterized lncRNAs have been shown to be implicated in the regulation of many molecular and cellular events such as gene expression and chromatin regulation, epigenetic regulation, genomic imprinting, differentiation, cell growth and death (7). High-throughput RNA sequencing (RNA-seq) studies have enabled identification of oncogenic and tumor-suppressing lncRNAs that contribute to the pathogenesis of PCa, as with other cancers.

Androgen receptor-regulated long non-coding RNA 1 (*ARLNC1*) is a recently identified cancer-related lncRNA and it has been shown to be associated with AR signaling in PCa. *ARLNC1* and AR protein mutually regulate each other, because *ARLNC1* is induced by AR, whereas *ARLNC1* stabilizes AR transcript via RNA-RNA interaction (8). Prostate cancer-associated transcript (*PCAT1*) is a PCa-overexpressed lncRNA and it has been shown to induce proliferation of PCa cells in a c-Myc-dependent way (9, 10). Herein, we intended to elucidate *ARLNC1* and *PCAT1* expression changes in the context of androgen stimulation or AR blockade with respect to AR expression status, where two cell lines (LNCaP and LNCaP-AR^{++}) were employed as cellular models with differential AR expression.

In the present experimental study, we used the LNCaP and LNCaP-AR^{++} PCa cell lines. LNCaP cells were obtained from a lymph node metastasis of the patient with prostate adenocarcinoma in 1977 that expressed AR and thus was androgen-sensitive (11). The LNCaP-AR^{++} cell line is genetically engineered from ancestral LNCaP cells and expresses more AR (5). The LNCaP cell line (ATCC# CRL-1740) was previously acquired from the American Type Culture Collection. The AR^{++} cell line was attentively provided by Memorial Sloan Kettering Cancer Center (New York, USA). Standard cell culture protocols were followed to handle the cells. LNCaP and LNCaP-AR^{++} cells were grown in standard growth conditions (5% CO_2, 95% humidity at 37˚C) with RPMI, as the growth medium with added fetal bovine serum (FBS, 10%, Biochrom, Germany) and antibiotics (1% penicillin and streptomycin).

For androgen stimulation in PCa cells, we used dihydrotestosterone (DHT), as a potent agonist of ARs that binds to tissue ARs more strongly than its precursor testosterone, thus harboring a more pronounced androgenic effect at lower concentrations (12). A stock solution (100 mM) was prepared by dissolving DHT in ethanol and stored at -20˚C in aliquots. Enzalutamide, a non-steroidal anti-androgen currently used in the treatment of metastatic CRPCa, was used as an AR inhibitor and it was kindly provided by Aztellas. Enzalutamide was dissolved in dimethyl sulfoxide (DMSO) and stored at -20˚C as 1 mM stocks. Enzalutamide acts in multiple ways either by blocking the binding of androgens to the AR and transition of active AR into the nucleus or by preventing AR binding to its binding sites in DNA (5).

Before treating cells with DHT and/or enzalutamide, serum growth hormones were removed from FBS using charcoal treatment, as described previously (13). For DHT and/or enzalutamide administration, approximately 200000 cells were plated into each well of six-well Petri dishes and they were kept in hormone-free medium conditions for 24 hours. The cells were then further cultured for 24 hours in a complete medium containing 10 nM DHT (14) and/or 10 µM enzalutamide (15). We considered induction and suppression of prostate-specific antigen (PSA) expression, as proof of effective androgen stimulation by DHT or AR inhibition by enzalutamide, respectively (data not shown).

For assessing effect of AR blockade on the viability of cells, we utilized annexin V and propidium iodide (PI) staining assay using the Annexin V Apoptosis Detection Kit (Thermo Fisher Scientific, USA) in the flow cytofluorimetric analysis. Annexin V staining is aimed to detect cellular apoptosis, whereas PI detects necrotic or late apoptotic cells that lose membrane integrity. In brief, the cells were harvested and adjusted to 1×10^6 cells/100 µl in appropriate tubes. After several wash steps, the cells were resuspended in 100 µl of 1x annexin V binding buffer, followed by adding 5 µl annexin V-FITC and 1 µl PI from 100 µg/ml stock. Subsequently, they were incubated in dark (15 minutes). Fluorescence measurement was performed with a FACSCalibur® flow cytometer (BD Biosciences, USA) and analyzed using the CellQuest software. The generated data were illustrated in two-dimensional dot plots in which PI was displayed versus annexin V-FICT. The Q2-3 in the plots represented (Fig.1) viable cells that were not stained with either probe; Q2-4 included early apoptotic cells that were only positive for annexin V; in Q2-2, late apoptotic cells were compromised and they were positive for both dyes, while the cells in Q2-1 were necrotic/dead cells and only stained with PI.

Expression of the target molecules was determined using reverse transcription-quantitative polymerase chain reaction (RT-qPCR). For this, total RNA was isolated from the cells using a commercially available RNA isolation solution (Life Technologies, USA) according to the instructions. Integrity and purity of the RNA were checked using electrophoresis and spectrophotometrically. RNA was used as a template to synthesize complementary DNA (cDNA) according to the instructions of the kit (Life Technologies, USA), which was then used as a template in qRT-PCR. The assay included the primer sets displayed in Table 1 and the SYBR Green dye (Life Technologies, USA) for fluorescence detection. The PCR protocol included initial denaturation of 10 minutes and 40 cycles of amplification according to the instructions of the SYBR Green assay kit and run in a LightCycler 480 PCR device (Roche Diagnostics, Germany). Expressions of *ARLNC1* and *PCAT1* in the PCa cells were determined semi-quantitatively using the housekeeping gene *GAPDH*, as the internal control, and their relative expression was calculated using the $2^{-\Delta\Delta cCt}$ method.

Outcomes of the three independent qRT-PCR measurements were used for inter-group comparisons. Changes relative to baseline levels in the control cells were expressed as 'fold changes,' and mean values were statistically compared using an independent sample t test between test groups.

Table 1: The utilized primer sequences

Gene	Primer sequences (5′-3′)	Reference
ARLNC1	F: CCTTGTCCACTGGAACTCGT R: TATAACCTTGGGGGCCATGA	(8)
PCAT1	F: TGAGAAGAGAAATCTATTGGAACC R: GGTTTGTCTCCGCTGCTTTA	(9)
PSA	F: TGAACCAGAGGAGTTCTTGAC R: CCCAGAATCACCCGAGCAG	(16)
AR	F: TATCCCAGTCCCACTTGTGTC R: CTTGTGCATGCGGTACTCATTG	(17)
GAPDH	F: AGCCACATCGCTCAGACAC R: GCCCAATACGACCAAATCC	(18)

Outcomes of the three independent qRT-PCR measurements were used for inter-group comparisons. Changes relative to baseline levels in the control cells were expressed as 'fold changes,' and mean values were statistically compared using an independent sample t test between test groups.

Viability of the PCa cells treated with DHT or enzalutamide was investigated using annexin V/PI counterstaining (Fig.1). DHT strongly induced cell proliferation in the both LNCaP (92%) and LNCaP-AR^{++} cells (95.4%) (P=0.01). In the enzalutamide-treated LNCaP cells, proportion of the late apoptotic cells was increased from 6.4% to 9.4%, while in the LNCaP-AR^{++} cells it was increased from 10.8% to 13%. In the cells co-treated with DHT and enzalutamide, DHT effect was dominant in the viability of the cells.

We validated the elevated AR expression in LNCaP-AR^{++} cells compared to the parental LNCaP cells, because these cells have been artificially engineered to express higher AR (5). Figure 2A depicts 4.6-fold higher AR expression in the LNCaP-AR^{++} than the LNCaP cells (P=0.02), providing further evidence of the AR-regulation of *ARLNC1*. Similar to AR, baseline *ARLNC1* expression was 1.7-fold higher in the LNCaP-AR^{++}, rather than the LNCaP cells, whereas *PCAT1* molecules had the opposite expression pattern with 3.8-fold lower expression in the LNCaP-AR^{++} cells than the LNCaP cells.

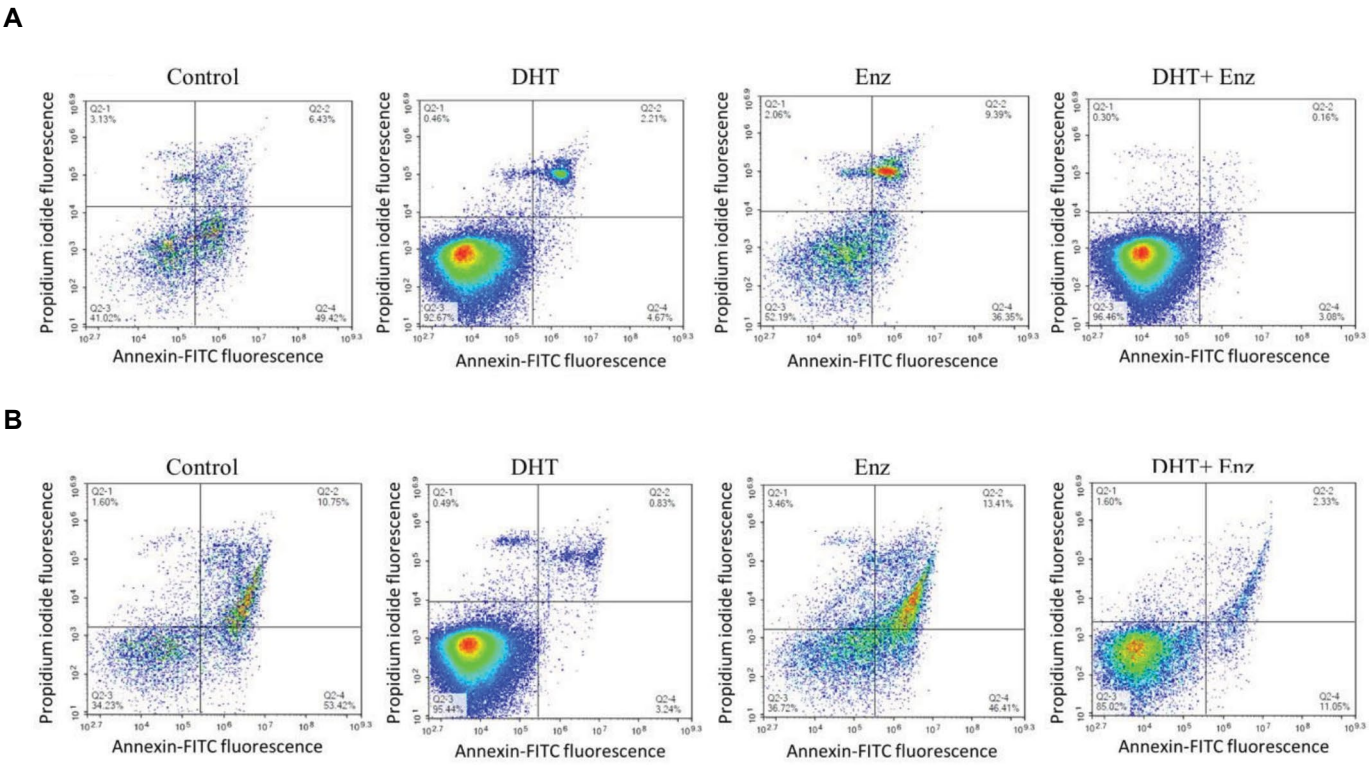

Fig.1: Cell viability assessment in PCa cells by flow cytometry. Approximately 200,000 cells were plated and kept in hormone-free medium conditions for 24 hours. The cells were then further cultured for 24 hours in a complete medium containing 10 nM dihydrotestosterone and/or 10 µM enzalutamide. After treatment, the cells were collected and washed, followed by staining with annexin V-FITC and propidium iodide. Following the measurement of fluorescence from cells, propidium iodide (y-axis) was plotted against annexin V-FITC (x-axis). The cells in Q2-3 plots included viable cells stained with neither PI nor FITC; the cells in Q2-4 were apoptotic cells and annexin-positive; Q2-2 illustrates late apoptotic cells that were stained with both dyes, and the cells in Q2-1 were dead cells, which were positive for propidium iodide only. **A**. LNCaP cells and **B**. LNCaP-AR^{++} cells. DHT; dihydrotestosterone and Enz; Enzalutamide.

Neither androgen stimulation nor AR blockade increased *PCAT1* expression. However, *PCAT1* expression levels were lower in the all experimental conditions compared to the levels in the control cells (Fig.2C). Thus, no specific conclusions could be drawn on the effect of androgen stimulation or AR inhibition on *PCAT1* expression.

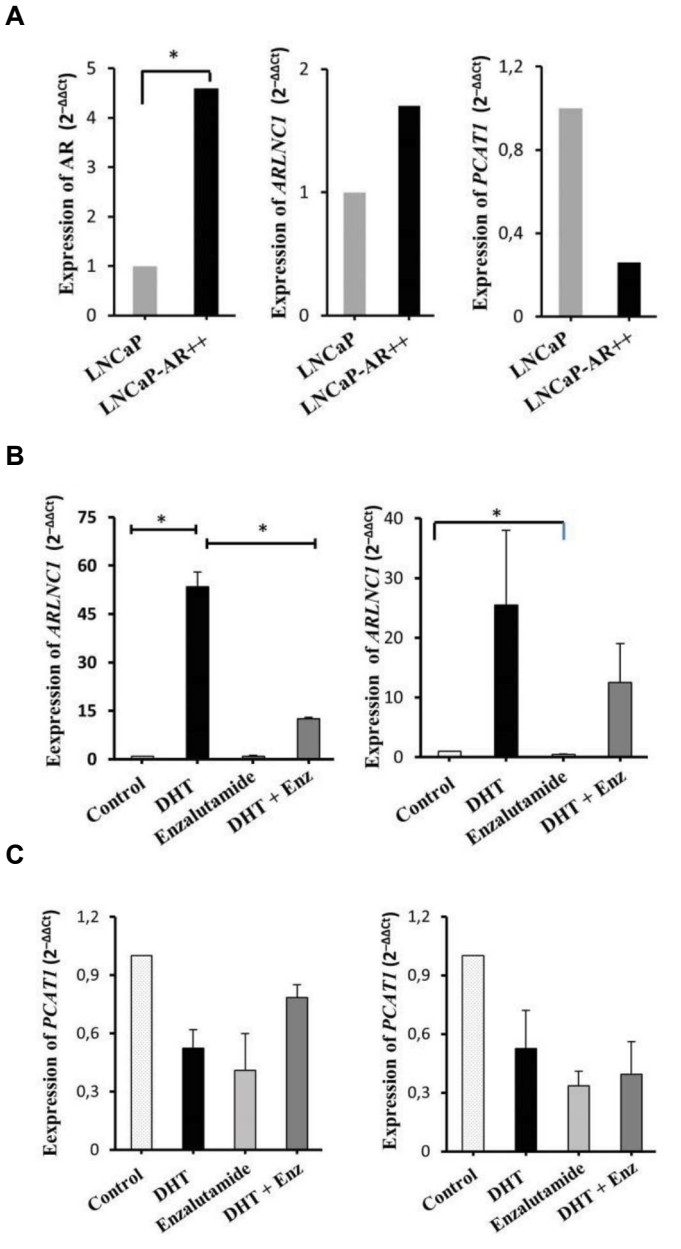

Fig.2: Expression analyses of androgen receptor, *ARLNC1* and *PCAT1* in prostate cancer cells. Total RNA was isolated from the cells treated with dihydrotestosterone and/or enzalutamide and it was used for complementary DNA (cDNA) synthesis. cDNA was then employed as a template in reverse transcription-quantitative polymerase chain reaction (RT-qPCR). Expression levels of *ARLNC1* and *PCAT1* was determined semi-quantitatively with *GAPDH*, as the internal control. Their relative expression levels were calculated using the $2^{-\Delta\Delta Ct}$ method. **A**. Baseline relative expression of androgen receptor, *ARLNC1* and *PCAT1* in the LNCaP cells and LNCaP-AR^{++} cells. **B**. Relative *ARNC1* expression in the control cells, dihydrotestosterone- and /or enzalutamide-treated cells (left: the LNCAP cells, right: the LNCaP-AR^{++} cells). **C**. *PCAT1* expression in the control cells, dihydrotestosterone- and/or enzalutamide-treated cells (left: the LNCAP cells, right: the LNCaP-AR^{++} cells). Bar graphs show mean values and standard deviations. * indicates statistical significance. The independent sample t-test was used to investigate statistical differences between the test groups.

Present study aimed to interrogate *ARLNC1* and *PCAT1* expression changes in the context of androgen stimulation or AR blockade with respect to AR expression status. Differential AR expression status was accomplished by the utilizing two cell lines (LNCaP and LNCaP-AR^{++}) which express AR in various extent (5). We validated higher AR expression in LNCaP-AR^{++} cells which were also shown to expresses higher *ARLNC1* at baseline than parental LNCaP cells. Interestingly, the extent of *ARLNC1* induction by androgen stimulation was lower in the LNCaP-AR^{+} cells than in LNCaP cells (25-fold vs. 53.5-fold, respectively). In contrast to this, AR blockade reduced basal *ARLNC1* expression stronger in the LNCaP-AR^{++} cells, and attenuated the DHT effect on *ARLNC1* expression in both cell types remarkably. Our findings showed that AR inhibition had no suppressive effect on the DHT-stimulated cell proliferation in cells co-treated with DHT and enzalutamide, whereas DHT-stimulated *ARLNC1* was effectively suppressed by enzalutamide. This indicated the prompt responsiveness of *ARLNC1* to AR blockade. Thus, enzalutamide, which is currently used in CRPCa (19), may be beneficial in targeting *ARLNC1,* a potential therapeutic target in the progression of AR-positive castration-sensitive PCa (8).

In contrast to *ARLNC1, PCAT1* expression was affected neither by androgen stimulation nor AR blockade in a specific way, and lower in the all experimental conditions compared to the levels in the control cells. Although *PCAT1* has been identified as a PCa-related lncRNA (9), recent data indicated that it was not specific to PCa because *PCAT1* has been found to be overexpressed in different types of cancer. It was also implicated in several processes such as cell proliferation, invasion, metastasis, apoptosis, cell cycle and chemoresistance (20). Our finding that *PCAT1* was not up-regulated by androgen stimulation supported the notion that *PCAT1* acted independently on the AR pathway in the carcinogenesis of PCa.

Our findings revealed that the extent of androgen stimulation of *ARLNC1* varies according to its baseline cellular levels and it may be modulated by AR expression status in PCa cells. *PCAT1*, de-regulated in many cancer types, seems not to be regulated by androgens. We also demonstrated that AR blockade via enzalutamide effectively suppressed baseline *ARLNC1* expression in LNCaP-AR^{++} cells and remarkably reduced the DHT-stimulated *ARLNC1* expression in the both cell types. Our study possesses some limitations including lack of mechanistic work for elucidating the mechanism of *ARLNC1* suppression by enzalutamide and clinical implications of this in the management of patients.

Acknowledgements

The present work is part of M.Sc thesis of Günel Hüseynova and supported by the Scientific Research Coordination Unit of Istanbul University (Istanbul, Turkey; Project No. 37110). We state that there is no conflict of interest.

Authors' Contributions

U.G.; Were responsible for overall supervision. G.H., E.E.Y., U.G.; Contributed to conception and design. G.H., E.Ö., S.B.G.; Contributed to the all experimental works, data and statistical analysis, as well as interpretation of data. G.H.; Drafted the manuscript, which was revised by U.G. All authors read and approved the final manuscript.

References

1. Siegel RL, Miller KD, Jemal A. Cancer statistics, 2018. CA Cancer J Clin. 2018; 68 (1): 7-30.
2. Damodaran S, Kyriakopoulos CE, Jarrard DF. Newly diagnosed metastatic prostate cancer: has the paradigm changed? Urol Clin North Am. 2017; 44(4): 611-621.
3. Ichikawa T, Suzuki H, Ueda T, Komiya A, Imamoto T, Kojima S. Hormone treatment for prostate cancer: current issues and future directions. Cancer Chemother Pharmacol. 2005; 56 Suppl 1: 58-63.
4. Chandrasekar T, Yang JC, Gao AC, Evans CP. Mechanisms of resistance in castration-resistant prostate cancer (CRPC). Transl Androl Urol. 2015; 4(3): 365-380.
5. Tran C, Ouk S, Clegg NJ, Chen Y, Watson PA, Arora V, et al. Development of a second generation antiandrogen for treatment of advanced prostate cancer. Science. 2009; 324(5928): 787-790.
6. Washietl S, Pedersen JS, Korbel JO, Stocsits C, Gruber AR, Hackermüller J, et al. Structured RNAs in the ENCODE selected regions of the human genome. Genome Res. 2007; 17(6): 852-864.
7. Statello L, Guo CJ, Chen LL, Huarte M. Gene regulation by long noncoding RNAs and its biological functions. Nat Rev Mol Cell Biol. 2021; 22(2): 96-118.
8. Zhang Y, Pitchiaya S, Cieślik M, Niknafs YS, Tien JC, Hosono Y, et al. Analysis of the androgen receptor-regulated lncRNA landscape identifies a role for ARLNC1 in prostate cancer progression. Nat Genet. 2018; 50(6): 814-824.
9. Prensner JR, Iyer MK, Balbin OA, Dhanasekaran SM, Cao Q, Brenner JC, et al. Transcriptome sequencing across a prostate cancer cohort identifies PCAT-1, an unannotated lincRNA implicated in disease progression. Nat Biotechnol. 2011; 29(8): 742-749.
10. Prensner JR, Chen W, Han S, Iyer MK, Cao Q, Kothari V, et al. The long non-coding RNA PCAT-1 promotes prostate cancer cell proliferation through cMyc. Neoplasia. 2014; 16(11): 900-908.
11. Horoszewicz JS, Leong SS, Kawinski E, Karr JP, Rosenthal H, Chu TM, et al. LNCaP model of human prostatic carcinoma. Cancer Res. 1983; 43(4): 1809-1818.
12. Liu L, Wu L, Gao A, Zhang Q, Lv H, Xu L, et al. The influence of dihydrotestosterone on the development of graves' disease in female BALB/c mice. Thyroid. 2016; 26(3): 449-457.
13. Özgür E, Celik AI, Darendeliler E, Gezer U. PCA3 silencing sensitizes prostate cancer cells to enzalutamide-mediated androgen receptor blockade. Anticancer Res. 2017; 37(7): 3631-3637.
14. Hay CW, Watt K, Hunter I, Lavery DN, MacKenzie A, McEwan IJ. Negative regulation of the androgen receptor gene through a primate-specific androgen response element present in the 5' UTR. Horm Cancer. 2014; 5(5): 299-311.
15. Yuan F, Hankey W, Wu D, Wang H, Somarelli J, Armstrong AJ, et al. Molecular determinants for enzalutamide-induced transcription in prostate cancer. Nucleic Acids Res. 2019; 47(19): 10104-10114.
16. Laiseca JE, Ladelfa MF, Cotignola J, Peche LY, Pascucci FA, Castaño BA, et al. Functional interaction between co-expressed MAGE-A proteins. PLoS One. 2017; 12(5): e0178370.
17. Hay CW, Watt K, Hunter I, Lavery DN, MacKenzie A, McEwan IJ. Negative regulation of the androgen receptor gene through a primate-specific androgen response element present in the 5' UTR. Horm Cancer. 2014; 5(5): 299-311.
18. Arenas-Hernandez M, Vega-Sanchez R. Housekeeping gene expression stability in reproductive tissues after mitogen stimulation. BMC Res Notes. 2013; 6: 285.
19. Scott LJ. Enzalutamide: a review in castration-resistant prostate cancer affiliations expand. Drugs. 2018; 78(18): 1913-1924.
20. Liang C, Qi Z, Ge H, Liang C, Zhang Y, Wang Z, et al. Long noncoding RNA PCAT-1 in human cancers: a meta-analysis. Clin Chim Acta. 2018; 480: 47-55.

Correction

Inhibition of miR-200b Promotes Angiogenesis in Endothelial Cells by Activating The Notch Pathway

Tie-Ying Qiu, M.M.[1], Jin Huang, M.D.[1], Li-Ping Wang, M.M.[1], Bi-Song Zhu, M.D.[2]*

1. Clinical Nursing Teaching and Research Section of The Second Xiangya Hospital, Changsha 410011, P.R. China
2. Organ Transplant Center, Xiangya Hospital, Central South University, Changsha 410008, P.R. China

Corresponding AAddress: Organ Transplant Center, Xiangya Hospital, Central South University, Changsha 410008, P.R. China
Email: 277364307@qq.com

In this article which was published in Cell J, Vol 23, No 1, Spring 2021, on pages 51-60, the authors discovered that Figures 1B, 2D, 2F, 5B, and 5D some errors that occurred accidentally during figure organization in this article. The figures below have been corrected.

The authors would like to apologies for any inconvenience caused.

Citation: Qiu TY, Huang J, Wang LP, Zhu BS. Inhibition of miR-200b promotes angiogenesis in endothelial cells by activating the notch pathway. Cell J. 2022; 24(12): 779-781. doi: 10.22074/cellj.2022.697065.

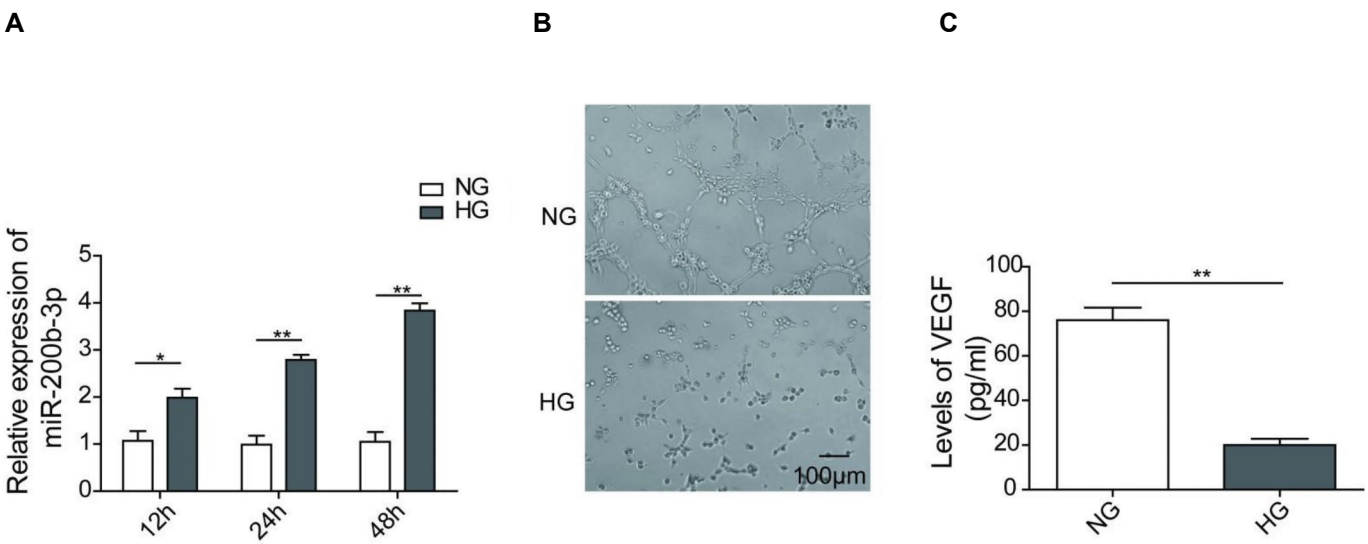

Fig.1: The high-glucose treatment induced the expression of miR-200b and impaired angiogenesis. **A.** Quantification of miR-200b by realtime PCR in Human umbilical vein endothelial cell (HUVECs) grown in normal glucose (NG) or high-glucose (HG) conditions for 12, 24, and 48 hours. U6 was used as an internal control for normalization. **B.** Representative images of HUVECs under different conditions during the in vitro angiogenesis assay. **C.** Quantification of secreted Vascular Endothelial Growth Factor (VEGF) from HUVECs, as determined by enzyme-linked immunosorbent assay (ELISA) after the indicated treatment (n=3). *; P<0.05, **; P<0.01, and H; Hour.

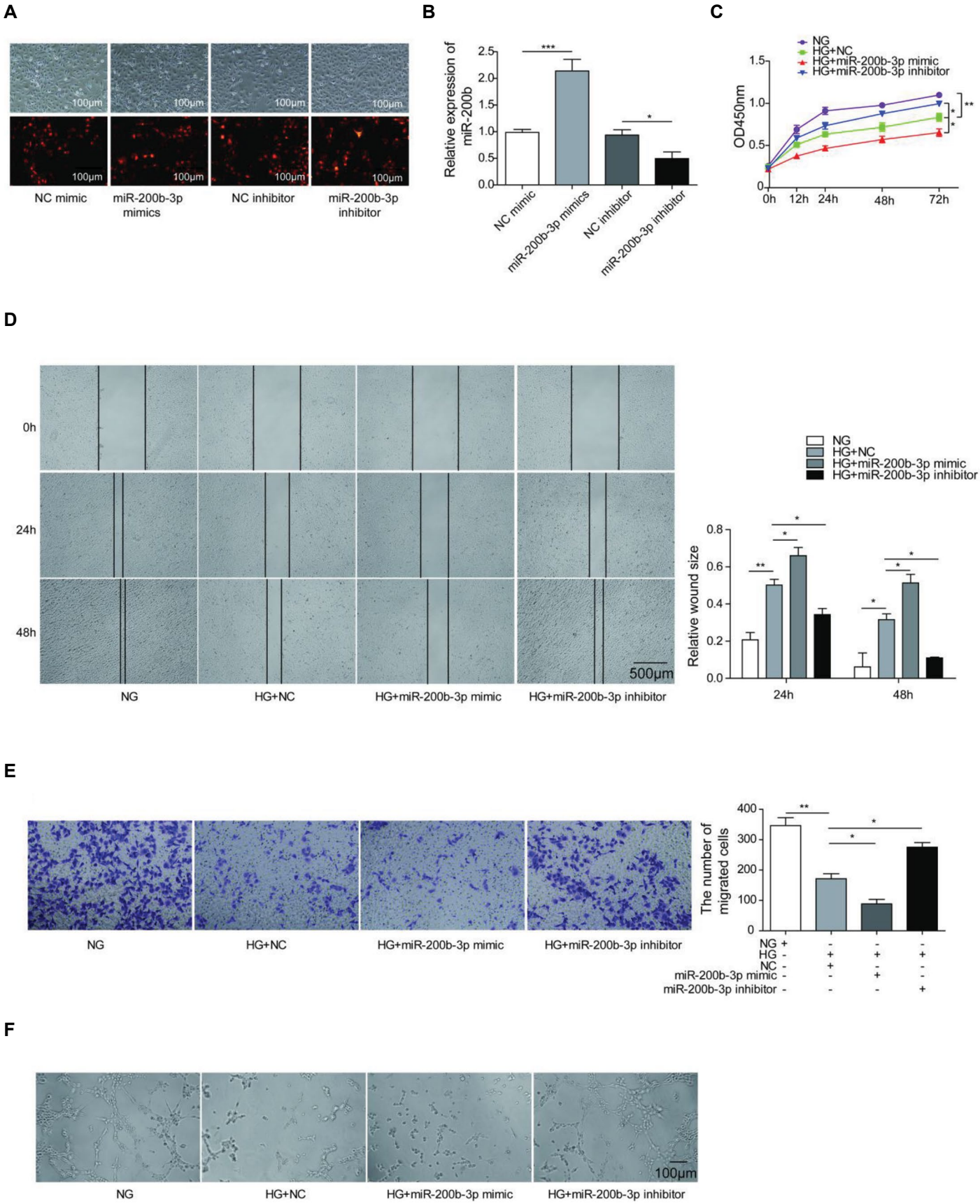

Fig.2: miR-200b affected the angiogenesis ability of human umbilical vein endothelial cell (HUVECs). The HUVECs cells were transfected with NC mimic, miR200b mimics, NC inhibitor, miR-200b inhibitor, and miR-200b transfection efficiency were analyzed by **A.** IF imaging and **B.** Real-time PCR. **C.** Quantification of HUVEC viability after the indicated treatment, as determined by CCK-8 assays. **D.** Representative images of HUVECs after the indicated treatments during the wound healing assay. **E.** Typical images and quantification of HUVECs with different treatments during the migration assay. **F.** Representative images of HUVECs under different conditions during the *in vitro* angiogenesis assay (n=3). NG; Normal glucose, HG; high-glucose, PCR; Polymerase chain reaction, *; P<0.05, and **; P<0.01.

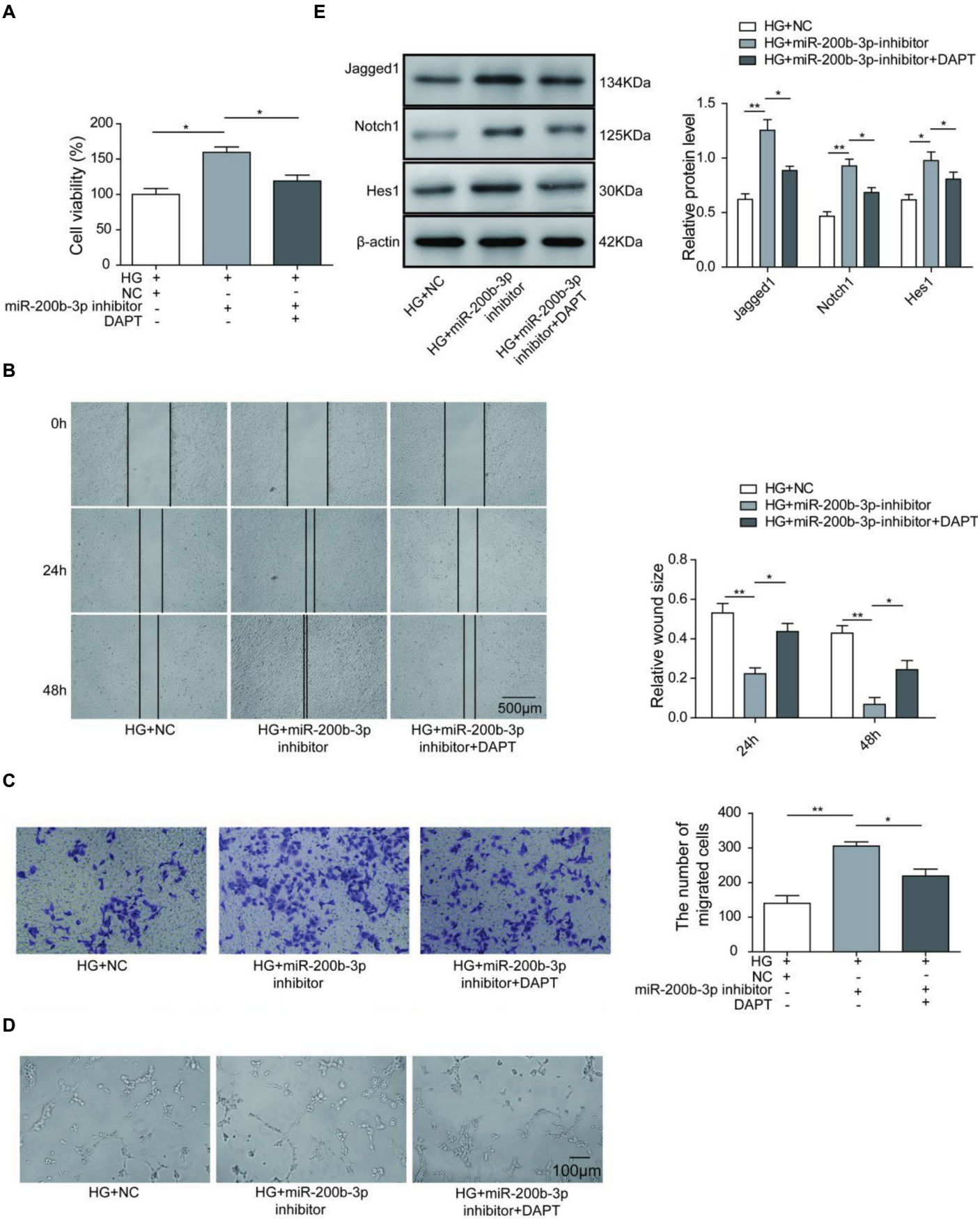

Fig.5: miR-200b affected angiogenesis by regulating Notch1. **A.** Quantification of human umbilical vein endothelial cell (HUVEC) viability was measured by CCK-8 assay after the indicated treatments**. B.** Representative images of HUVECs after the indicated treatments during the wound healing assay. **C.** Typical images and quantification of HUVECs with different treatments during the migration assay. **D.** Representative images of HUVECs under different conditions during *in vitro* angiogenesis assays. **E.** Representative images and quantification of Notch pathway protein expression in HUVECs (n=3). NG; Normal glucose, HG; High-glucose, *; P<0.05, and **; P<0.0**1.**

Advisory Board of Cell Journal(Yakhteh)
Vol 24, No 1-12, 2022

A

Abbaspanah B

Adnan M

Afzaljavan F

Ahmadi AH

Ajami M

Ali FM

Alizadeh A

Arab Najafi SM

Arasteh A

Asgari AR

Ashrafmansouri SS

Atashi A

Atlasi MA

Azad M

Azimian H

Azizi H

Azizidoost Sh

B

Babaei Abraki Sh

Bahadori MH

Baheiraei N

Bahramy S

Bandehpour M

Barekat M

Bathaei Z

Bayat M

Behzadi P

Beigi M

Bidkhori HR

C

Celick S

Cheraghi R

Carone D

D

Dalman A

Darbandi M

Dayer D

E

Ebrahimi S

Entezam M

Eskandari N

F

Faghihloo E

Falak R

Fardid R

Fardid R

Forootan SF

G

Ghadimi K

Ghaheri A

Ghanbari A

Ghasemi H

Ghazaey S

Ghezelbash B

Gourabi H

Govahi M

H

Haghiralsadat F

Hajebrahimi Z

Hajizadeh E

Halvaei I

Hashemi M

Hesaraki M

Hezavehei M

Hosseini S

I

Iranloo Rahatloo K

J

Jafari Sani M

Jafarian A

Javeri A

K

Karimian M

Kaushik NK

Kazemi A

Kazemi B

Kazemi M

Keshavarz H

Khamisipour GhR

Khazaei M

Khochbin S

Khorsandi L

Khoshzaban A

Kode J

Koruji M

M

Maghami P

Mansory K

Marzouni ET

Mehrabi S

Index by Authors in Cell Journal(Yakhteh)
Vol 24, No 1-12, 2022

Index by Authors in Cell Journal(Yakhteh)
Vol 24, No 1-12, 2022